Mathematical Modelling to Control Psoriatic Inflammation Introducing Stem Cell Therapy

Thesis Submitted to
Jadavpur University in Fulfillment of the Requirements
for the Degree of *Doctor of Philosophy* in *Science*

Submitted by
Subhankar Kushary
Registration No.: SMATH1100822

Centre for Mathematical Biology and Ecology,
Department of Mathematics, Jadavpur University,
Kolkata-700032, West Bengal, India

September, 2025

যাদবপুর বিশ্ববিদ্যালয়

FACULTY OF SCIENCE
DEPARTMENT OF MATHEMATICS

JADAVPUR UNIVERSITY
Kolkata - 700 032, India
Telephone : 91 (33) 2457 2269

CERTIFICATE FROM THE SUPERVISOR(S)

This is to certify that the thesis entitled **"Mathematical Modelling to Control Psoriatic Inflammation Introducing Stem Cell Therapy"** Submitted by Sri **Subhankar Kushary** (Index No.: **8/22/Maths./27**, Reg. No.: **SMATH1100822**), who got his name registered on **09/02/2022** for the award of **Ph.D. (Science)** Degree of Jadavpur University, is absolutely based upon his own work under the supervision of **Dr. Priti Kumar Roy** and **Dr. Amit Chakraborty** and that neither this thesis nor any part of it has been submitted for either any degree / diploma or any other academic award anywhere before.

Priti Kumar Roy

Signature of the Supervisor
(With Seal)

Date: 08/10/2025

Prof. (Dr.) Priti Kumar Roy
Professor
Department of Mathematics
Jadavpur University
Kolkata-700 032, West Bengal

Amit Chakraborty

Signature of the Co-Supervisor
(With Seal)

Date: 08/10/2025

Prof (Dr) Amit Chakraborty
Professor
Department of Mathematics
Sikkim University

I dedicate my thesis to my Grandfather,
"Late Amalendu Kushary",
my Father, ***Sri Jiban Kushary,*** *and*
my Mother, ***Smt. Subhra Kushary.***

Title: **"Mathematical Modelling to Control Psoriatic Inflammation Introducing Stem Cell Therapy"**
Submitted by: **Subhankar Kushary,** Index No.: **8/22/Maths./27,** Reg. No.: **SMATH1100822**

Abstract

Stem cell therapy is gaining attention in autoimmune disease treatment and is emerging as a promising field of regenerative medicine. Psoriasis, a chronic autoimmune skin disorder, remains a major challenge due to its complex immune pathways and multifactorial nature. Existing therapies often provide only temporary relief, with relapse occurring after discontinuation, and complete remission is rarely achieved. This thesis studies the progression and control of psoriasis from mathematical points of view through modelling. The aim is to understand the underlying biological mechanisms and to evaluate the effects of control strategies, mainly biologic drugs and stem cell-based therapies. Special focus is given to stem cell therapy as a possible future alternative where conventional approaches fail. Each chapter combines theoretical analysis with numerical simulations to maintain biological relevance and clinical applicability. Methods such as optimal control theory and impulsive differential equations are applied to design and evaluate different control interventions. The overall goal is to provide a mathematical framework that may guide the development of more effective treatment strategies for psoriasis in the future.

Chapter wise Contributions

- ***Chapter 2*** provides a nonlinear ODE-based model including Th_1, Th_{17} cells, keratinocytes, and mesenchymal stem cells (MSCs). The effects of pulsed MSC transplantation are studied, showing their potential in immune modulation.
- ***Chapter 3*** introduces simplified mathematical model with T cells, dendritic cells, keratinocytes, and MSCs. The role of anti–TNF-α biologics is examined introducing optimal control. Further, pulsed MSC therapy is introduced as an adjunct in resistant cases, demonstrating the combined therapeutic benefits of the biologic TNF-α inhibitor and MSCs.
- ***Chapter 4*** extends the model of Chapter 3 to fractional-order systems to include the memory effects. Three operators, namely Caputo, Caputo–Fabrizio, and Atangana–Baleanu–Caputo operators, are used for the fractional-order models. Theoretical analysis is carried out for the ABC operator with a non-singular Mittag-Leffler kernel, and biologic control strategies are tested using the Forward-Backward Sweep Method with respect to all considered fractional operators.
- ***Chapter 5*** incorporates two intracellular time delays in T cell–dendritic cell interactions. Hopf bifurcation analysis is carried out, and a dual-biologic strategy (TNF-α and IL-17 inhibitors) is proposed to regulate oscillatory disease behavior, highlighting the role of delayed immune signaling.
- ***Chapter 6*** provides a model with stem cell maturation stages and uses impulsive differential equations to study the effect of stem cell administrations. The results show that periodic impulses, given at proper intervals, can control T cell and keratinocyte over-activity effectively.
- ***Chapter 7*** integrates five key cytokines with T cells, dendritic cells, keratinocytes, and stem cells with differentiation lineages. Quasi-steady-state approximations simplify cytokine interactions. Hopf bifurcation analysis and numerical simulations confirm that impulsive stem cell therapy can restore cytokine balance and control keratinocyte overgrowth.
- ***Chapter 8*** outlines future directions of research and presents a model as part of ongoing work.

Signature of the Supervisor
(With Seal)
Date: 08.10.2025

Prof. (Dr.) Priti Kumar Roy
Professor
Department of Mathematics
Jadavpur University
Kolkata-700 032, West Bengal

Signature of the Co-Supervisor
(With Seal)
Date: 08/10/2025

Prof (Dr) Amit Chakraborty
Professor
Department of Mathematics
Sikkim University

Acknowledgements

I am deeply grateful to many individuals whose support, guidance, encouragement, sometimes constructive criticism, and friendly advice have made this research journey possible. At the end of my Ph.D. journey, it is my pleasure to express my sincere thanks to all those who contributed in many ways to the successful completion of this study and made it an experience I will never forget.

While writing this acknowledgement for my thesis, I do feel emotional. First and foremost, I would like to express my heartfelt gratitude to my supervisor, ***Prof. Priti Kumar Roy****, for his invaluable guidance and endless love and support throughout my research journey. It would be impossible at all to carry out and accomplish this research work and achieve the Ph.D. degree without him. I have faced many challenges in my career before and during this journey, but thanks to Prof. Roy. He is the person who taught me to stand tall and strong in every tough situation. His enthusiasm for research, dedication, and insightful feedback have been a constant source of inspiration. His tough personality has helped me grow both academically and personally. Firstly, he motivated me and then guided the overall structure of the study, which I have followed, and I started investigating and exploring fundamental knowledge and ideas in my research. His availability and willingness to provide thoughtful advice made my research journey much smoother. I would also like to extend my sincere thanks to Mrs. Roy, who has supported me with motherly care and affection throughout my doctoral journey.*

Also, I would like to convey my sincere admiration to my co-supervisor, ***Prof. Amit Chakraborty****, for his guidance and encouragement throughout this journey. Although his university is far away from my work city, his suggestions and feedback during the meetings have been instrumental in shaping the direction of this research.*

I would further like to extend my thanks and deepest appreciation to Prof. Xianbing Cao (School of Mathematics and Statistics, Beijing Technology and Business University, China), Prof. David Greenhalgh (Department of Mathematics and Statistics, University of Strathclyde, UK), Prof. Stacey R. Smith? (Dept. of Mathematics and Faculty of Medicine, University of Ottawa, Canada), Prof. Oluwole Daniel Makinde (Faculty of Military Science, Stellenbosch University, South Africa), and Prof. Xue-Zhi Li (College of Statistics and Mathematics, Henan Finance University, China). Working with them as co-authors has been a truly enriching experience, and our interactions have deepened my understanding of research and broadened my academic perspective.

It has been a great privilege to spend several formative years in the Department of Mathematics at Jadavpur University. I have started my journey at this university as a postgraduate student. After completing the Master of Science degree, I got the opportunity to be admitted further to the Ph.D. program at this university. This has been a long journey, and I think it will always be one of the best memories of my life. I would like to express my heartiest gratitude to all of the respected teachers and official staff in my department for making those times like a joyful ride. I am also thankful to the members of my doctoral committee, Prof. Nandadulal Bairagi and my current departmental head, Prof. Subhas Chandra Mandal, for their constructive and valuable feedback, which significantly enriched the quality of this work.

My heartfelt thanks to my fellow lab mates—Sanju, Mosaraf, Tushar, Tarun, Amit Da, Homagnic, and Satyajit—for their companionship and for making this journey a truly memorable and joyful experience. Especially, I want to convey my love and affection to my dearest Tushar, who has been not only my co-author in several works but also a constant source of enthusiasm and motivation in research. My dearest friend Sanju and other lab mates also supported me a lot in many ways. My acknowledgement would be incomplete without a special mention of my immediate lab seniors, Dr. Salil Ghosh and Dr. Amit Kumar Roy, for their love, guidance, and support. I am deeply grateful to them for addressing all my research queries, their patience, and the invaluable time they shared with me throughout this journey. They not only assisted me in shaping this thesis but were always available whenever I needed help. I would also like to acknowledge some of my respected seniors—Dr. Amar Nath Chatterjee, Dr. Jayanta Mondal, Dr. Fahad Al Basir, Dr. Biplab Sinha Mahapatra, Dr. Shubhankar Saha, and Dr. Jahangir Chowdhury—for instilling in me the discipline and dedication required in research and for offering thoughtful advice along the way. I am also sincerely thankful to my best friend, Mr. Chayan Maitra, for his constant love, support, and continuous motivation over the last twelve years.

The journey began at Sodepur High School (H.S.), a cherished part of my memory where I grew up with dear friends and caring teachers. Their love and encouragement inspired me to pursue my long journey in higher education. I am especially indebted to my school teacher, Mr. Falguni Dandapat, for his continued love, affection, and unwavering support to this day.

Most importantly, none of this would have been possible without the support of my family. Their contribution to both my Ph.D. journey and my life is beyond words. I wish to express my deepest gratitude to my parents, Sri Jiban Kushary and Smt. Subhra Kushary. My father laid the foundation of my academic character, inspiring me from childhood with the joy of learning and the deep respect of recognition. His honesty and integrity inspire me every day. My mother, with her gentle love and constant care, has been a source of comfort and strength. Words fall short in expressing my appreciation for all they have done; I truly believe their blessings will continue to guide me through every challenge ahead. A very special note of thanks goes to my soulmate, Miss Adrita Choudhury. No matter the situation, from the highest points of achievement to the most difficult moments, her support, patience, and encouragement have been my greatest source of strength.

Finally, I would like to thank the Swami Vivekananda Merit Cum Means Scholarship for providing financial support during my research period. I am also grateful to the anonymous referees of the journals for their prompt and constructive feedback, which greatly helped improve my work.

This thesis is the result of collective effort and support. To all who have helped me along the way, I am truly grateful. I also apologize to anyone I may have unintentionally missed mentioning here.

Subhankar Kushary

September, 2025

(SUBHANKAR KUSHARY)

Contents

ACRONYMES AND ABBREVIATIONS

t	time
$\mathbb{R}$	Real line
$\mathbb{R}^n$	n-dimensional euclidean space
WHO	World Health Organization
FDA	Food and Drug Administration
EU	European Union
UC-MSCs	Umbilical cord derived mesenchymal stem cells
hAT-MSCs	Human amnion mesenchymal stem cells
ADSC-CM	Adipose derived stem cell in conditioned medium
AD-MSCs	Adipose derived mesenchymal stem cells
hBM-MSCs	Human bone marrow mesenchymal stem cells
TNF-α	Tumor necrosis factor alpha
TGF-β	Transforming growth factor beta
IFN-γ	Interferon gamma
IL-4	Interleukin 4
IL-10	Interleukin 10
IL-12	Interleukin 12
IL-17	Interleukin 17
IL-21	Interleukin 21
IL-22	Interleukin 22
IL-23	Interleukin 23
PASI	Psoriasis area and severity index
ODEs	Ordinary Differential Equations
FDEs	Fractional Differential Equations
DDEs	Delay Differential Equations
R-H criterion	Routh Hurwitz criterion
FBSM	Forward-Backward Sweep Method

Chapter 1

Introduction

"Psoriasis has a significant impact on quality of life and is associated with a range of physical and psychological comorbidities. It is a serious global problem that needs more awareness, advocacy, and coordinated care."

$\sim$ World Health Organization, Global Report on Psoriasis (2016) □

1.1 Psoriasis: History of the Disease

[1]Psoriasis is a chronic immune-mediated skin disorder with a history dating back to ancient times. Early descriptions by Hippocrates often confused it with other skin conditions like leprosy due to overlapping symptoms. The disease was formally named in the 19th century by Ferdinand von Hebra, who distinguished it as a non-contagious condition. Initially thought to be a disorder of excessive skin cell growth, psoriasis is now understood as an autoimmune condition involving immune cells and pro-inflammatory cytokines. Treatments have evolved from coal tar and phototherapy to systemic drugs and, more recently, biologics targeting immune pathways. Today, psoriasis is recognized as a complex, systemic disease with physical and psychological impacts, and while treatment options have advanced, a complete cure remains out of reach. However, stem cell based therapies are under investigation for their potential to restore immune tolerance and modulate chronic inflammation, offering a promising avenue for long-term remission in psoriasis patients [1].

1.2 The Epidemiology of Psoriasis

Psoriasis is a chronic, multifactorial, immune-mediated inflammatory skin disorder that imposes a significant global health burden, transcending geographic, racial, and socioeconomic boundaries. It is clinically characterized by raised, erythematous, scaly plaques that most commonly appear on the elbows, knees, scalp, back, face, palms, and soles of the feet. Affected individuals often experience symptoms such as dryness, pruritus, erythema, and thick

[1]*Information given/listed in this chapter are collected from several web links and peer-reviewed journals (cited here).*

scaling, which may lead to painful fissures and bleeding. Beyond its visible dermatological manifestations, psoriasis is associated with systemic comorbidities as well as considerable psychosocial distress. The in-depth overview and the important features of the disease psoriasis are organized as follows.

- **Global Prevalence:** Psoriasis affects approximately 2–3% of the global population, although prevalence estimates vary by country [2]. It is estimated that more than 125 million people worldwide live with psoriasis, making it one of the most prevalent autoimmune conditions globally. The incidence of psoriasis appears to be rising in certain parts of the world, potentially due to increasing awareness, improved diagnostics, urbanization, and environmental changes [3, 4].

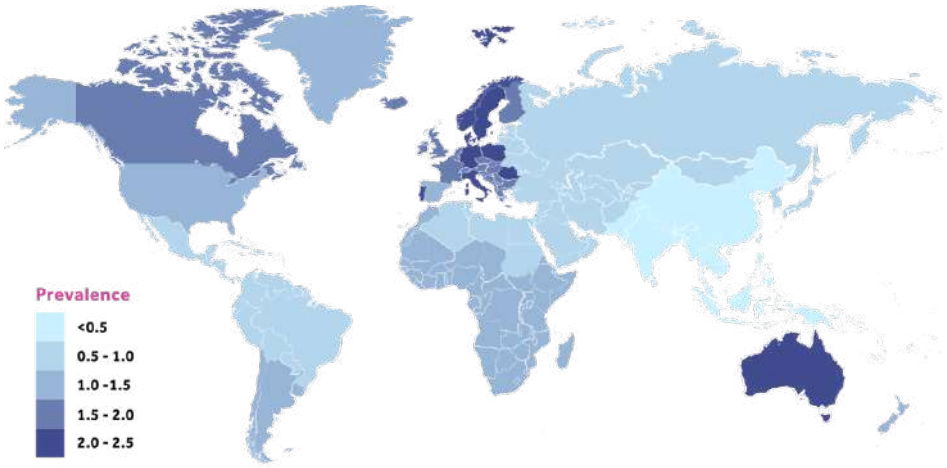

Figure 1.1: Worldwide Psoriasis Update (2020): Geographical distribution of psoriasis prevalence, highlighting regional variations across continents.

- **Geographic Distribution:** The distribution of psoriasis exhibits marked geographic heterogeneity. High-prevalence regions include Northern and Western Europe, North America, and Australia, where rates often exceed 4% of the population [2]. In contrast, lower prevalence is reported in East Asia, Sub-Saharan Africa, and certain parts of Latin America, sometimes falling below 1% [5]. Genetic predisposition, environmental exposures, and variations in health systems contribute to these disparities.

- **Clinical Spectrum:** Psoriasis manifests in multiple clinical forms, including plaque psoriasis (the most common), guttate, pustular, erythrodermic, and inverse variants [6]. Disease severity also varies widely—from localized plaques with minimal symptoms to extensive, debilitating skin involvement. The condition frequently coexists with comorbidities such as psoriatic arthritis, cardiovascular disease, metabolic syndrome, and depression, further complicating its clinical management [7].

- **Endeavors Toward Eradication:** Psoriasis is currently incurable, though significant progress has been made in disease management and policy recognition. The World

Health Organization (WHO) adopted a resolution in 2014 to improve access to care and reduce stigma associated with psoriasis [8]. Advances in biologic therapies and stem cell-based therapy have revolutionized treatment paradigms, offering symptom remission and improved quality of life in many cases [9].

1.3 Types of Psoriasis

Psoriasis encompasses a spectrum of clinical phenotypes, each with distinct morphological features, distribution patterns, and severities. The major types include:

- **Plaque Psoriasis (Psoriasis Vulgaris):** Plaque psoriasis is the most prevalent form, accounting for approximately 80–90% of all cases. It presents as well-demarcated, erythematous plaques covered with silvery-white scales, typically found on extensor surfaces such as the elbows, knees, scalp, and lower back. Lesions may be asymptomatic or accompanied by itching, burning, or pain.

- **Guttate Psoriasis:** Guttate psoriasis commonly affects children and young adults and is often triggered by streptococcal throat infections. It appears as numerous small, droplet-shaped, pink papules on the trunk and proximal extremities. This form may resolve spontaneously or evolve into chronic plaque psoriasis.

- **Erythrodermic Psoriasis:** This is a rare but severe form, accounting for less than 3% of psoriasis cases. It manifests as widespread erythema and scaling covering most of the body surface area. Erythrodermic psoriasis may be accompanied by systemic symptoms such as fever, chills, dehydration, and electrolyte imbalance. It requires immediate medical attention due to risks of complications including cardiac failure and infection.

- **Inverse Psoriasis (Flexural Psoriasis):** Inverse psoriasis occurs in intertriginous areas such as the axillae, groin, inframammary folds, and genital region. Lesions are typically smooth, shiny, and erythematous, lacking the characteristic scaling due to the moist environment. It is often misdiagnosed as a fungal or bacterial infection.

- **Pustular Psoriasis:** Pustular psoriasis is characterized by sterile pustules on an erythematous base. It may be localized (e.g., palmoplantar pustulosis) or generalized (generalized pustular psoriasis, GPP), the latter being a severe, potentially life-threatening condition often requiring hospitalization. GPP may be associated with fever, malaise, and leukocytosis.

- **Psoriatic Arthritis (PsA):** PsA is a chronic inflammatory arthropathy associated with psoriasis, occurring in approximately 20–30% of patients. It can affect peripheral joints, axial skeleton, and entheses. If left untreated, PsA may lead to joint damage and functional impairment. Early diagnosis and treatment are crucial for preventing long-term disability.

1.4 Etiology of Psoriasis

Psoriasis is a complex, multifactorial disease arising from the interplay of genetic predisposition, immune system dysregulation, and environmental triggers. Its pathogenesis is not attributed to a single cause but rather a cascade of interacting biological and external factors that initiate and perpetuate the inflammatory cycle characteristic of the condition.

1.4.1 Immunological Factors

Psoriasis is primarily driven by immune dysregulation, particularly involving the innate and adaptive immune systems. Activation of dendritic cells and macrophages leads to the release of pro-inflammatory cytokines (e.g., TNF-α, IL-12, IL-23), which stimulate naïve T cells to differentiate into Th_1, Th_{17}, and many more cells. These effector T cells infiltrate the skin and secrete cytokines such as IL-17A, IL-22, and IFN-γ, promoting keratinocyte hyperproliferation and sustaining inflammation [9].

1.4.2 Immune System Dysregulation

The development of psoriasis is caused by multiple interrelated factors, including keratinocyte hyper-proliferation, abnormal differentiation, and a dysregulated crosstalk between T cells and dendritic cells through the secretion of inflammatory cytokines [10]. This interaction also promotes the recruitment and infiltration of several inflammatory cells into the epidermal layer. A hallmark of this immune dysfunction is the hyper-activation of helper T cells, which secrete excessive inflammatory cytokines [11]. These cytokines orchestrate a cascade of autoimmune responses that target keratinocytes. The synergistic action of these mediators sustains chronic inflammation and contributes significantly to disease development and persistence [12].

(i) Role of T Cells and Dendritic Cells

T cells and dendritic cells (DCs) play central roles in the initiation and maintenance of psoriatic inflammation. The disease is initiated when plasmacytoid dendritic cells (pDCs) become activated in response to skin injury or other environmental triggers, leading to the production of type I interferons [13]. These cytokines stimulate myeloid dendritic cells (mDCs), which subsequently migrate to lymph nodes where they activate naïve T cells. Upon activation, T cells differentiate into effector subsets such as Th_1, Th_{17}, and Th_{22}, which then home to the skin and secrete pro-inflammatory cytokines, including IFN-γ, TNF-α, IL-17, and IL-22 [14]. These cytokines act on keratinocytes and other skin-resident cells, promoting hyper-proliferation, altered differentiation, and further production of chemokines that recruit additional immune cells to the site of inflammation. Dendritic cells also contribute to the maintenance of the inflammatory environment by presenting self-antigens and continuously activating auto-reactive T cells. In psoriatic lesions, DCs express high levels of co-stimulatory molecules and cytokines such as IL-23 and IL-12, which are critical for the expansion and survival of pathogenic Th_1 and Th_{17} cells, respectively [11]. The continuous interplay between T cells and dendritic cells establishes a self-perpetuating inflammatory loop. This

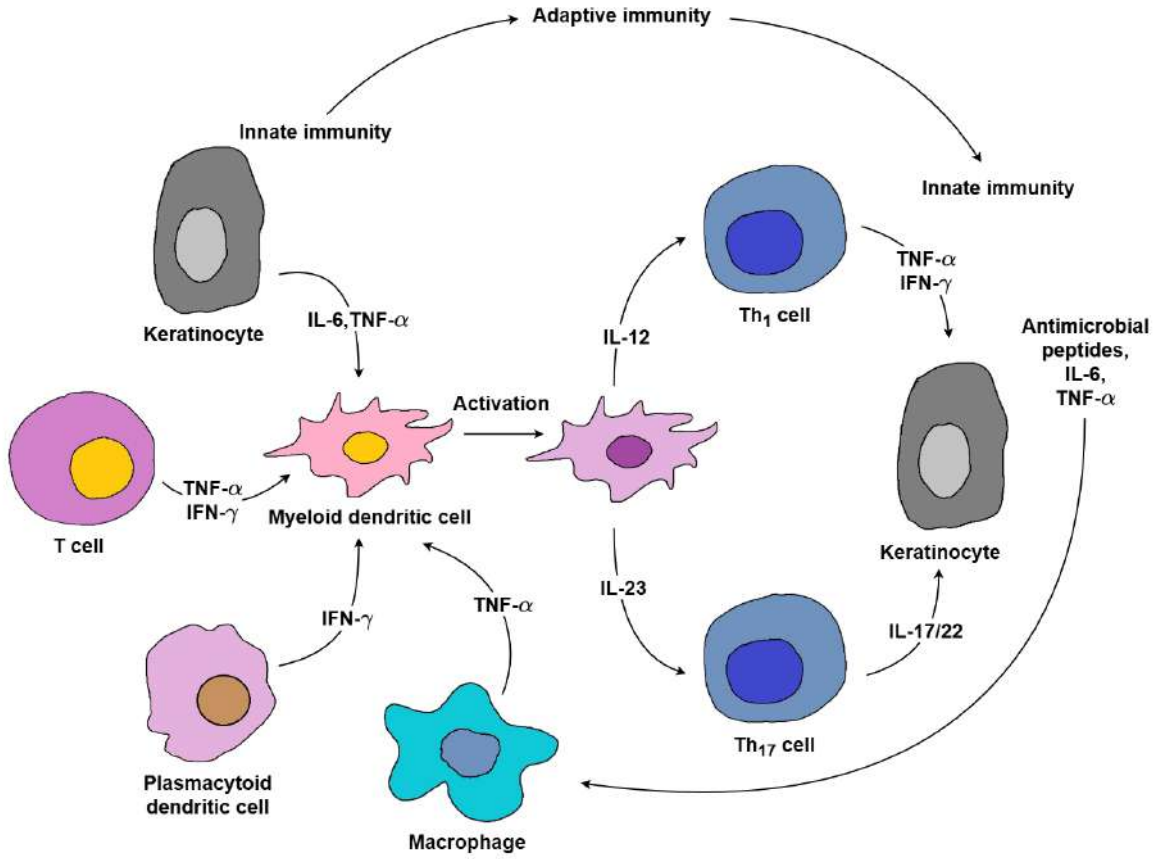

Figure 1.2: Diagrammatic representation of the initial trigger of psoriasis involving immune cell activation and differentiation. The figure illustrates the role of dendritic cells, macrophage T cell subsets (Th_1, Th_{17}), natural killer cells and their interactions with keratinocytes, alongside the key cytokines (e.g., TNF-α, IL-12, IL-23, IL-17, IL-22) that orchestrate the inflammatory cascade characteristic of psoriatic pathogenesis.

cellular crosstalk not only amplifies the local immune response but also disrupts epidermal homeostasis, making both cell types key therapeutic targets in modern biologic treatments for psoriasis.

(ii) Role of Keratinocytes

Keratinocytes are essential for keeping the body safe from environmental hazards and are also involved in the healing of wounds under normal homeostatic conditions. Keratins, which are naturally present in keratinocytes, are crucial in cytokine synthesis in the epidermis [15]. However, in psoriatic inflammation, keratinocytes are not only passive targets but active participants. Upon stimulation by cytokines such as IL-17 and TNF-α, keratinocytes produce chemokines (e.g., CCL20, CXCL1, CXCL8) that recruit additional immune cells to the epidermis. They also release antimicrobial peptides (AMPs), including LL-37, which can

complex with self-DNA or RNA to further activate plasmacytoid dendritic cells via TLR7/9 pathways. This interaction between immune cells and keratinocytes perpetuates the psoriatic lesion, resulting in abnormal differentiation, proliferation, and a chronic inflammatory microenvironment [5, 9].

1.5 Treatment Options of Psoriasis So Far

The treatment of psoriasis has evolved significantly over recent decades, reflecting a deeper understanding of the disease's immunopathogenesis. Current therapeutic strategies aim to reduce inflammation, control keratinocyte hyperproliferation, and restore skin homeostasis.

1. **Phototherapy:** Ultraviolet (UV) phototherapy, particularly narrowband UVB and psoralen plus UVA (PUVA) are effective for moderate to severe psoriasis. Phototherapy acts by inducing T cell apoptosis, reducing cytokine production, and promoting keratinocyte differentiation [16].

2. **Systemic Therapies:** Patients with widespread or refractory disease may require systemic treatment. Traditional systemic agents include methotrexate, cyclosporine, and acitretin. These treatments are effective but associated with potential long-term toxicity and require close monitoring [17].

3. **Topical Therapies:** For mild to moderate psoriasis, topical treatments are typically the first line of intervention. These include corticosteroids, vitamin D analogs (such as calcipotriol), coal tar preparations, and topical retinoids [18]. Topical corticosteroids remain the most commonly prescribed agents due to their anti-inflammatory and immunosuppressive properties.

4. **Biologic Therapies:** Biologic drugs have revolutionized the management of moderate to severe psoriasis by specifically targeting key components of the immune system. These agents include TNF-α inhibitors (e.g., etanercept, adalimumab), IL-12/23 inhibitors (e.g., ustekinumab), IL-17 inhibitors (e.g., secukinumab), and IL-23 inhibitors (e.g., guselkumab) [19]. Biologics have shown superior efficacy and safety profiles compared to conventional systemic therapies, though their high cost and risk of immunosuppression are considerations.

5. **Stem Cell Therapies:** Stem cell-based therapies are the emerging treatment options currently under investigation for their potential to restore immune tolerance and modulate chronic inflammatory response. These therapies offer a promising avenue for achieving long-term remission in psoriatic patients, potentially complete eradication of psoriasis so far [1]. At present, stem cells are routinely harvested and preserved in stem cell banks by various organizations during the childbirth process, enabling their potential application in the future treatment of several autoimmune diseases, including psoriasis.

1.6 Stem Cells: A Short Review

Stem cells are undifferentiated cells characterized by their ability to self-renew and differentiate into specialized cell types. They serve as a fundamental component in tissue development, regeneration, and repair. Broadly, stem cells are categorized based on their origin and potency.

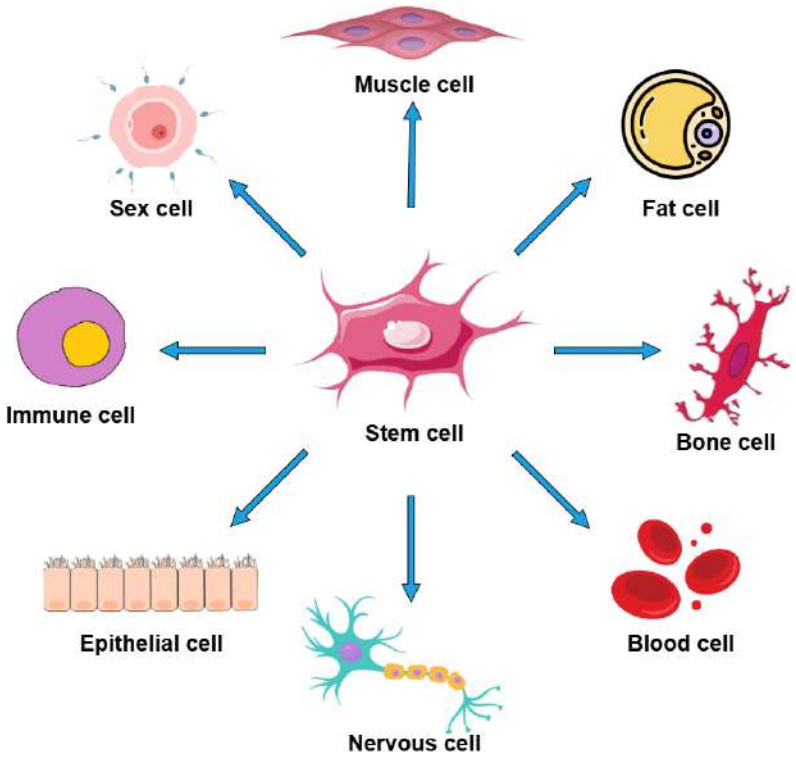

Figure 1.3: Stem cells have the ability to differentiate into various specialized cell types, contributing to tissue regeneration and repair.

1.6.1 Mesenchymal Stem Cells (MSCs)

MSCs are a type of adult stem cell found in bone marrow, adipose tissue, umbilical cord, and dermis. They exhibit immunomodulatory properties and are capable of differentiating into mesodermal lineages such as osteoblasts, adipocytes, and chondrocytes [20]. MSCs secrete anti-inflammatory cytokines, promote tissue regeneration, and suppress pathological immune responses, making them promising candidates for treating immune-mediated disorders like psoriasis [21, 22].

1.7 Mathematical Methods and Their Applications

This section presents key mathematical techniques commonly employed to investigate the dynamical behavior of systems. The qualitative methods discussed herein have been applied to analyze various models proposed throughout this thesis.

Equilibrium Analysis

Consider a discrete-time autonomous system described by the first-order difference equation:

$$X_{t+1} = f(X_t), \quad \text{or} \quad X \to f(X), \tag{1.7.1}$$

where $X = (X^1, X^2, \ldots, X^n) \in \mathbb{R}^n$, $f = (f^1, f^2, \ldots, f^n) \in \mathbb{R}^n$, and $f : \mathbb{R}^n \to \mathbb{R}^n$. Here, X_t denotes the state of the system at discrete time $t \in \mathbb{T}$ with initial condition

$$X_{t=0} = X_0 = (X_0^1, X_0^2, \ldots, X_0^n).$$

Definition 1.7.1 *A point $X^* \in \mathbb{R}^n$ is called an equilibrium point (or fixed point or critical point) of the system (1.7.1) if it satisfies $f(X^*) = X^*$.*

To understand the behavior of the system near its equilibrium points, we analyze the stability properties of these points.

Local Stability

Local stability analysis plays a fundamental role in applied mathematics and control theory, particularly in mathematical biology [23, 24]. The stability of an equilibrium point determines whether nearby trajectories remain close or diverge from it.

Definition 1.7.2 *The equilibrium point X^* of system (1.7.1) is said to be locally stable if for every $\epsilon > 0$, there exists a $\delta > 0$ such that*

$$\|f^n(X_0) - X^*\| < \epsilon \quad \textit{whenever} \quad \|X_0 - X^*\| < \delta. \tag{1.7.2}$$

That is if a solution starts sufficiently close to X^*, it remains close for all future times.

Definition 1.7.3 *If an equilibrium point X^* is not stable, then it is called an unstable fixed point.*

Definition 1.7.4 *An equilibrium point X^* is said to be locally asymptotically stable if it is locally stable and there exists $\delta > 0$ such that*

$$\lim_{n\to\infty} f^n(X_0) = X^* \quad \textit{whenever} \quad \|X_0 - X^*\| < \delta. \tag{1.7.3}$$

Let X be any solution near the fixed point X^* and let $\lambda = (\lambda_1, \lambda_2, \ldots, \lambda_n)$ denote a small perturbation, such that:

$$X = X^* + \lambda, \qquad \lambda_{n+1} = N\lambda_n, \tag{1.7.4}$$

where

$$N = \left[\frac{\partial f_i}{\partial X_j}\right]_{X=X^*}, (i, j = 1, 2, \ldots n)$$

is the Jacobian matrix of f evaluated at X^*. The system (1.7.4) is the linearization of the nonlinear system (1.7.1) at X^*.

Let λ_0 be the initial perturbation, then: $\lambda_n = N^n \lambda_0$. The local behavior near the fixed point is determined by the eigenvalues of N. Let ξ be an eigenvalue of N corresponding to an eigenvector v, then the characteristic equation is:

$$\det(N - \xi I) = p_0 \xi^n + p_1 \xi^{n-1} + \ldots + p_n, \quad p_0 \neq 0. \tag{1.7.5}$$

Stability Criterion: The equilibrium point X^* is locally asymptotically stable if and only if all eigenvalues of N lie inside the unit circle in the complex plane [25].

Global Stability

Global stability examines the system's behavior from arbitrary initial conditions. One of the most effective tools for establishing global stability is Lyapunov's stability theory. Consider a continuous-time dynamical system:

$$\dot{x} = F(x), \quad F : \mathbb{R}^n \to \mathbb{R}^n, \tag{1.7.6}$$

with equilibrium point $x = 0$.

Definition 1.7.5 *A scalar function $V : \mathbb{R}^n \to \mathbb{R}$ is called a Lyapunov function for system (1.7.6) if:*

- *V is continuously differentiable,*
- *V is locally positive definite, i.e., $V(x) > 0$ for all $x \neq 0$ and $V(0) = 0$,*
- *the derivative along trajectories, $\dot{V}(x) = \nabla V \cdot F(x)$, is locally negative definite.*

Definition 1.7.6 *The equilibrium point $x = 0$ of system (1.7.6) is globally asymptotically stable if:*

- *$V(x)$ is globally positive definite and radially unbounded,*
- *$\dot{V}(x) < 0$ for all $x \in \mathbb{R}^n \setminus \{0\}$.*

Application of Stability Analysis

Throughout this thesis, we studied the stability of equilibrium points for the proposed models. A locally stable equilibrium means that after a small perturbation, the system returns to its original state. In autoimmune diseases like psoriasis, this represents a stable diseased state, where minor immune fluctuations do not alter the overall system behavior. Global stability, on the other hand, shows whether the system will converge to an equilibrium point regardless

of the initial conditions. A globally stable diseased state reflects a self-sustaining pathological condition.

Remark: Global stability implies local stability, but not vice versa. While local stability ensures convergence to the equilibrium from nearby initial conditions, global stability ensures convergence from any initial state in the entire domain. However, practical application is often limited by the difficulty in constructing suitable Lyapunov functions.

Bifurcation Analysis

Bifurcation analysis is a powerful tool in the study of dynamical systems. It investigates the qualitative or topological changes in the behavior of solutions as a parameter of the system is varied. Bifurcation occurs when a small, smooth variation in one or more system parameters (called *bifurcation parameters*) causes a sudden change in the long-term behavior of the system. It can arise in both continuous and discrete systems. The most commonly studied types of bifurcations in continuous systems are Saddle-node bifurcation, Transcritical bifurcation, Pitchfork bifurcation, and Hopf bifurcation.

Consider the following continuous dynamical system defined by an autonomous ODE:

$$\dot{x} = f(x, \lambda), \quad f : \mathbb{R}^n \times \mathbb{R} \to \mathbb{R}^n, \tag{1.7.7}$$

where $\lambda \in \mathbb{R}$ is a bifurcation parameter, and $x \in \mathbb{R}^n$ is the state variable. Let (x_0, λ_0) be an equilibrium point of the system (1.7.7), and let $df_{(x_0,\lambda_0)}$ denote the Jacobian matrix evaluated at that point.

Definition 1.7.7 *A bifurcation occurs at the fixed point (x_0, λ_0) if the Jacobian matrix $df_{(x_0,\lambda_0)}$ has at least one eigenvalue with real part equal to zero.*

Definition 1.7.8 *A Hopf bifurcation occurs when a pair of complex conjugate eigenvalues of the Jacobian matrix crosses the imaginary axis, causing the system transit from a stable fixed point to a periodic orbit (or vice versa).*

The following theorem, adapted from Hale et al. [26], provides a criterion for the occurrence of a Hopf bifurcation.

Theorem 1.7.1 (Hopf Bifurcation Theorem) *Suppose that all eigenvalues of the Jacobian matrix $df_{(x_0,\lambda_0)}$ evaluated at the equilibrium point (x_0, λ_0) have negative real parts, except for a conjugate pair of purely imaginary eigenvalues $\pm i\beta$ with $\beta \neq 0$. Then a Hopf bifurcation occurs if, as the parameter λ varies, this pair of eigenvalues crosses the imaginary axis, leading to the birth (or disappearance) of a stable or unstable periodic orbit.*

Application of Hopf Bifurcation

Hopf bifurcation theory has been employed to analyze the transition from steady-state behavior to oscillatory dynamics. Parameter-influenced Hopf bifurcation within a deterministic framework, demonstrating how variations in certain model parameters can induce or eliminate periodic behavior of the equilibrium through change in the stability. Delay-induced Hopf bifurcation is also analyzed, where the inclusion of time delay leads to the emergence of periodic solutions due to a loss of stability in the equilibrium state.

Preliminaries of Fractional Calculus

Definition 1.7.9 *[27] Let $f(t)$ be a function that is n-times continuously differentiable on the interval $[0,T]$, where $n = \lceil \lambda \rceil$ is the smallest integer greater than or equal to the fractional order $\lambda > 0$. The Caputo fractional derivative of order λ, denoted by ${}^{C}D_t^{\lambda} f(t)$, is defined as:*

$$ {}^{C}\mathcal{D}_t^{\lambda}[f(t)] = \begin{cases} \dfrac{1}{\Gamma(n-\lambda)} \displaystyle\int_0^t \frac{f^{(n)}(s)}{(t-s)^{\lambda-n+1}}\, ds, & n-1 < \lambda < n, \\ \dfrac{d^n f(t)}{dt^n}, & \lambda = n \in \mathbb{N}, \end{cases} $$

where $\Gamma(\cdot)$ denotes the Gamma function.

Definition 1.7.10 *[28] Let $f(t) \in C^1([0,T])$ be a continuously differentiable function on the interval $[0,T]$, and let $\zeta \in (0,1)$ be the fractional order. The Caputo–Fabrizio fractional derivative of order ζ, is defined as follows:*

$$ {}^{CF}\mathcal{D}_t^{\zeta}[f(t)] = \frac{N(\zeta)}{1-\zeta} \int_0^t f'(s) \exp\left[-\zeta \frac{t-s}{1-\zeta}\right] ds, t > 0, $$

where $N(\zeta)$ is a normalization constant such that $N(0) = N(1) = 1$.

Definition 1.7.11 *[29] Consider a real-valued function $f : [0,T] \to \mathbb{R}$ such that $f \in \mathcal{H}^1(0,t)$, where $\mathcal{H}^1(0,t)$ denotes the Sobolev space of functions with square-integrable first derivatives:*

$$ \mathcal{H}^1(0,t) = \left\{ f \in L^2(0,t) \mid f' \in L^2(0,t) \right\}. $$

The Atangana-Baleanu fractional derivative in the Caputo sense of order $\alpha \in [0,1)$ is defined by

$$ {}^{ABC}\mathcal{D}_t^{\alpha}[f(t)] = \frac{\mathbf{B}(\alpha)}{1-\alpha} \int_0^t f'(s) \mathbf{E}_{\alpha}\left[-\frac{\alpha}{1-\alpha}(t-s)^{\alpha}\right] ds, $$

where $\mathbf{E}_{\alpha}(\cdot)$ is the one-parameter Mittag-Leffler function and the normalizing function $\mathbf{B}(\alpha)$ is given by

$$ \mathbf{B}(\alpha) = 1 - \alpha + \frac{\alpha}{\Gamma(\alpha)}. $$

Definition 1.7.12 *[29] Let $f \in \mathcal{H}^1(0,t)$, and $\alpha \in [0,1]$. The Atangana-Baleanu-Caputo fractional integral operator of order α is defined as*

$$ {}^{ABC}I_t^{\alpha}[f(t)] = \frac{1-\alpha}{\mathbf{B}(\alpha)} f(t) + \frac{\alpha}{\mathbf{B}(\alpha)\Gamma(\alpha)} \int_0^t f(s)(t-s)^{\alpha-1} ds. $$

Application of Fractionalized Model

The progression of autoimmune diseases like psoriasis depends not only on the current state but also on the history of cellular interactions. Memory effects and multiscale immune responses play an important role in triggering disease expression. To capture these non-local

features, fractional-order models are useful. Unlike classical integer-order systems, they provide a stronger framework to represent memory and hereditary properties in biological systems.

Delay Differential Equations (DDEs)

A delay differential equation (DDE) is a type of differential equation where the derivative of the state variable at time t depends not only on its current value but also on its values at earlier times. These delays often represent maturation, reaction, or transmission times in various systems.

The general form of a DDE is:

$$\frac{dx(t)}{dt} = f(x(t), x(t-\tau_1), x(t-\tau_2), \ldots, x(t-\tau_n)), \tag{1.7.8}$$

where $x(t)$ is the state variable and τ_i are constant time delays. The function f governs how both present and past states influence the system's evolution.

Example: Consider a logistic population model with delayed feedback:

$$\frac{dX(t)}{dt} = \nu X(t)\left(1 - \frac{X(t-\tau)}{K}\right),$$

where $X(t)$ is the population at time t, ν is the intrinsic growth rate, K is the carrying capacity, and τ is the time delay representing maturation time. The delay τ affects how past population sizes influence current growth.

Linearization Around Equilibrium

Assume $x = 0$ is a steady state of a DDE of the form:

$$\dot{x}(t) = g(x(t), x(t-\tau)),$$

with $g(0,0) = 0$. The linearized system near $x = 0$ is:

$$\dot{x}(t) = \sigma_1 x(t) + \sigma_2 x(t-\tau),$$

where $\sigma_1 = g_x(0,0)$ and $\sigma_2 = g_y(0,0)$. Substituting $x(t) = e^{\lambda t}$ yields the characteristic equation:

$$\lambda = \sigma_1 + \sigma_2 e^{-\lambda\tau}.$$

This transcendental equation generally has infinitely many roots, which determine the stability and oscillatory nature of the equilibrium. Only finitely many roots lie to the right of any vertical line in the complex plane and all roots satisfy $\alpha < |\sigma_1| + |\sigma_2|$, where $\lambda = \alpha + i\beta$.

Application of Delayed Model

Mathematical models with delay differential equations (DDEs) are increasingly used to study biological systems where time delays are crucial [30]. Such models capture the lags in processes like signal transmission and cell interactions through cytokine feedback. Recent studies show that DDE-based models provide more accurate insights describing dynamics of different diseases [31, 32]. Incorporating delays therefore enhances the biological realism of models and improves understanding of disease progression and treatment. In this thesis, Chapter 5 focuses on the role of immune-mediated delays in psoriatic inflammation.

Optimal Control Theory

Optimal control theory is a mathematical framework used to determine a control policy that optimizes a given performance criterion for a dynamical system. The goal is to find time-dependent profiles of the control variable that optimize a certain objective, often subject to system dynamics governed by differential equations. Consider a system governed by ODE:

$$\frac{dX(t)}{dt} = f(X(t)), \quad X(0) = X_0, \tag{1.7.9}$$

where $X_0 \in \mathbb{R}^n$ is the initial state and $f : \mathbb{R}^n \to \mathbb{R}^n$ is a function that governs the system's evolution. The function $X : [0, \infty) \to \mathbb{R}^n$ denotes the state trajectory over time. Now, assume the system is influenced by control parameters $u \in U \subset \mathbb{R}^n$. The function f is redefined as:$f : \mathbb{R}^n \times U \to \mathbb{R}^n$, and the controlled system becomes:

$$\frac{dX(t)}{dt} = f(X(t), u), \quad X(0) = X_0. \tag{1.7.10}$$

To capture time-dependent control, we define a measurable control function $\vartheta : [0, \infty) \to U$ that assigns different control values over time:

$$\vartheta(t) = \begin{cases} u_1, & 0 \le t \le t_1, \\ u_2, & t_1 < t \le t_2, \\ u_3, & t_2 < t \le t_3, \\ \vdots \end{cases}$$

where $0 < t_1 < t_2 < t_3 < \dots$ and $u_i \in U$ for all i.

The control system now takes the form:

$$\frac{dX(t)}{dt} = f(X(t), \vartheta(t)), \quad X(0) = X_0. \tag{1.7.11}$$

For each admissible control $\vartheta(t)$, the solution $X(\cdot)$ describes the state trajectory over time. The set of all admissible controls is denoted as:

$$\mathcal{L} = \left\{ \vartheta : [0, \infty) \to U \;\middle|\; \vartheta(\cdot) \text{ is Lebesgue measurable} \right\}.$$

Given a control $\vartheta(\cdot) \in \mathcal{L}$, we define the performance of the system via an objective (cost) functional:

$$J[\vartheta(\cdot)] = \int_{t_s}^{t_f} \rho(X(t), \vartheta(t))\, dt + G(X(t_f)), \tag{1.7.12}$$

where $\rho : \mathbb{R}^n \times U \to \mathbb{R}$ is the running payoff function, $G : \mathbb{R}^n \to \mathbb{R}$ is the terminal payoff function, t_s and t_f denote the start and end times for the control action.

The main objective of optimal control theory is to determine an optimal control $\vartheta^*(\cdot) \in \mathcal{L}$ that minimizes (or maximizes) the objective functional:

$$J[\vartheta^*(\cdot)] \leq (\text{or } \geq) J[\vartheta(\cdot)], \quad \forall\, \vartheta(\cdot) \in \mathcal{L}.$$

Such a control $\vartheta^*(\cdot)$ is called an **optimal control**, and the corresponding trajectory $X^*(\cdot)$ is the optimal state evolution of the system.

Application of Optimal Control

Optimal control is a useful mathematical tool for designing treatment strategies using model systems analysis. It plays an important role in addressing issues like drug resistance in long-term treatments by helping to plan better therapies and analyze their cost-effectiveness. Pontryagin's Principle [33] provides the necessary conditions for deriving such strategies. In this thesis, we use time-dependent control strategies for psoriasis and apply Pontryagin's framework to design optimal protocols for biologic therapies targeting TNF-α, IL-17, and IL-23, with the goal of achieving effective and balanced treatment outcomes.

Impulsive Differential Equations

Impulsive differential equations (IDEs) describe dynamical systems where abrupt changes (impulses) occur at specific moments in time. Consideration of IDEs are useful for capturing phenomena where state variables evolve continuously but also experience sudden shifts, such as in population dynamics, epidemiology, economics, and control theory.

The theory of impulsive differential equations was first introduced by Myshkis et al. [34], with significant developments made by Lakshmikantham et al. [24] and Smith et al. [35]. A typical IDE system includes three main components: (i) A continuous-time differential equation governing system behavior between impulses, (ii) An impulsive jump equation that models sudden changes, and (iii) A jump criterion that specifies the moments of impulses. The general form of an impulsive differential system is:

$$\begin{aligned} \frac{dX(t)}{dt} &= f(t, X(t)), \quad t \neq \tau_k, \\ \Delta X(\tau_k) &= I_k(X(\tau_k)), \quad k = 1, 2, \ldots, m. \end{aligned} \tag{1.7.13}$$

where τ_k are fixed impulse times, and $\Delta X(\tau_k) = X(\tau_k^+) - X(\tau_k^-)$ denotes the jump in the state variable at $t = \tau_k$. The limits are defined as:

$$X(\tau_k^+) = \lim_{h \to 0^+} X(\tau_k + h), \quad X(\tau_k^-) = \lim_{h \to 0^-} X(\tau_k + h).$$

A parameterized version of the impulsive model takes the form:

$$\begin{aligned} \frac{dX(t)}{dt} &= f(t, X(t)), \quad t \neq \tau_k, \\ X(\tau_k^+) &= \alpha X(\tau_k^-) + \beta, \quad k = 1, 2, \ldots, m. \end{aligned} \tag{1.7.14}$$

where $\alpha, \beta \in \mathbb{R}$, with $\alpha \neq 0$, and $X(0) = X_0$ is the initial condition.

Application of Impulsive Control

The impulsive control approach models treatments given at discrete time intervals, such as drug injections or stem-cell transplantation. Unlike continuous control, it captures the sudden and periodic effects of therapy on disease dynamics. In psoriasis, where treatments are often delivered in pulses, this method better represents real clinical interventions and their long-term effects. In this thesis, we apply impulsive control at discrete intervals and study the impact of both biologic cytokine inhibitors and stem cell therapy on the dynamics of psoriatic inflammation.

Floquet Theory

Floquet theory provides a powerful framework to analyze the stability of solutions to linear differential equations with periodic coefficients. It is particularly applicable to the study of periodic dynamical systems arising in physics, biology, engineering, and control theory.

Consider a linear system of differential equations of the form:

$$\dot{x}(t) = A(t)x(t), \tag{1.7.15}$$

where $x(t) \in \mathbb{R}^n$ and $A(t)$ is a continuous, T-periodic matrix, i.e., $A(t+T) = A(t)$ for all $t \in \mathbb{R}$ and some fixed $T > 0$.

Theorem 1.7.2 (Floquet's Theorem) *Let $A(t)$ be a continuous T-periodic matrix. Then the fundamental matrix solution $\Phi(t)$ of (1.7.15) can be written as:*

$$\Phi(t) = P(t)e^{Rt},$$

where $P(t)$ is a nonsingular, T-periodic matrix function, and R is a constant matrix.

This result implies that the behavior of the system can be decomposed into a periodic part and an exponential part. The eigenvalues of the monodromy matrix $\Phi(T)$, also known as Floquet multipliers, determine the stability of the periodic system. Let μ_i be the Floquet multipliers (eigenvalues of $\Phi(T)$). The trivial solution $x = 0$ of the system (1.7.15) is:

1. **Asymptotically stable** if all $|\mu_i| < 1$,
2. **Stable** (but not asymptotically) if all $|\mu_i| \leq 1$ and those with modulus 1 are simple,
3. **Unstable** if any $|\mu_i| > 1$.

Stability of periodic solutions in nonlinear systems

Using linearization techniques, the stability of periodic orbits in nonlinear systems can be determined. This theory is commonly applied to the linearized variational equations around a periodic orbit in nonlinear systems. Consider a nonlinear system:

$$\frac{d\mathbf{x}}{dt} = \mathbf{f}(t, \mathbf{x}), \quad \mathbf{f}(t+T, \mathbf{x}) = \mathbf{f}(t, \mathbf{x}), \tag{1.7.16}$$

and suppose $\mathbf{x}_p(t)$ is a T-periodic solution. The linear variational equation along $\mathbf{x}_p(t)$ is given by:

$$\frac{d\xi}{dt} = D_{\mathbf{x}}\mathbf{f}(t, \mathbf{x}_p(t))\,\xi. \tag{1.7.17}$$

Floquet's theory is then used to analyze the stability of the periodic orbit $\mathbf{x}_p(t)$ by examining the Floquet multipliers of the monodromy matrix associated with the variational system.

Application of Floquet's Theory

Floquet's theory is a mathematical tool used to check the stability of periodic solutions in dynamical systems. It helps us understand whether small changes around a periodic state will die out or increase with time. In biological models, especially those with impulsive effects, this theory is very useful to study repeated treatments and recurring disease patterns. In this thesis, we use Floquet's theory [36] to analyze the periodic behavior of stem cell-based therapy given impulsively.

1.8 Motivation of the Study

To lay the foundation for this thesis, it is important to recognize the contributions of earlier studies that explored the biological mechanisms of psoriasis. These studies have provided valuable insights and motivated the development of mathematical models to better explain disease progression. Early attempts, such as those by Savill *et al.* [37], Diffey [38], and Laptev and Nikulin [39], highlighted processes ranging from nitric oxide signaling to epidermal mitotic activity. Later works, including Datta *et al.* [40], Zhang *et al.* [41], Oza *et al.* [42], and Roy *et al.* [43], further advanced this field of research by integrating immune cell regulation, cytokine signaling, and biologic therapies. These contributions form the basis for further mathematical exploration of psoriasis.

In recent years, stem cell-based therapies have gained attention as a potential alternative for treating autoimmune diseases like psoriasis. Mesenchymal stem cells (MSCs), in particular, show strong immunomodulatory effects by suppressing pro-inflammatory cytokines (e.g., TNF-α, IL-23, IL-17) while promoting anti-inflammatory cytokines (e.g., IL-4, IL-10, TGF-β) [44, 45]. Several clinical studies and case reports [46, 47, 48, 49, 50] have demonstrated the safety and therapeutic potential of MSCs in psoriasis patients, often with long-term remission and minimal side effects. However, despite this growing evidence, their integration into mathematical models remains largely unexplored.

From a clinical perspective, current biologic therapies are effective but costly, and re-

lapse often occurs after treatment discontinuation [51]. In contrast, stem cell therapy offers a regenerative and potentially longer-lasting approach, but its mechanisms and long-term effects require systematic theoretical and clinical study. A mathematical framework incorporating stem cell dynamics can provide predictive insights into disease regulation, compare therapeutic strategies, and guide future clinical applications.

Based on these gaps, this thesis is motivated by the need to extend existing mathematical models of psoriasis by integrating stem cell therapy, cytokine regulation, and advanced modeling techniques. In particular, we focus on fractional-order systems to capture memory effects, delay differential equations to model immune-mediated time lags, and optimal and impulsive control approaches to design effective treatment strategies. Through these contributions, the thesis aims to advance the theoretical understanding of psoriatic inflammation and support the development of more effective therapeutic interventions.

1.9 Objective of the Thesis

Throughout the thesis, our key objectives are

1. Develop mathematical models describing the progression of psoriatic inflammation in the epidermal layer through various biological avenues.

2. Examine the crosstalk between stem cells and immune cells in psoriasis and its role in modulating keratinocyte overgrowth.

3. Explore stem cell-based treatments mathematically, incorporating multilineage differentiation, predict key parameters associated with important biological feathers and cytokine levels in psoriatic inflammation post-treatment.

4. Analyze the mathematical model both analytically and numerically to investigate the important cell dynamics that can contribute to treatment progression.

5. Comparison between the effects of biologic inhibitor drugs and stem cell-based therapies, as well as the impacts of combined treatment strategies.

6. Determine the optimal drug dosage and dosing intervals for clinical treatment, identify threshold values for effective therapy using control theoretic approaches and modified impulse theory, ensuring efficacy and improved predictions.

1.10 Outline of the Thesis

This thesis investigates the immunopathological mechanisms and therapeutic strategies for psoriasis through mathematical modeling, with a focus on stem cell-based interventions and cytokine dynamics. Each chapter builds upon the previous, progressing from classical models to advanced fractional and delay-based systems, and exploring optimal control, and impulsive control strategies.

- In *Chapter 2*, we have formulated a nonlinear ODE-based mathematical model for the disease psoriasis considering populations: Th_1, Th_{17} cells, keratinocytes, and mesenchymal stem cells (MSCs). The impact of pulsed umbilical cord-derived MSC (UC-MSC) transplantation is studied both analytically and numerically, providing insights into stem cell-based immune modulation in psoriasis.

- Expanding on this, *Chapter 3* presents a simplified but control-oriented model incorporating T cells (ignoring the subtypes), dendritic cells, keratinocytes, and MSCs. The efficacy of anti TNF-α biologics is explored using optimal control theory. In scenarios of treatment resistance, pulsed stem cell therapy is introduced as an adjunct. The combined therapeutic impact of biologics and MSCs is demonstrated, establishing a bridge between cell replacement therapy and cytokine inhibition.

- In *Chapter 4*, the previous ODE-based continuous model is extended to fractionalized systems using three different kernel functions, namely, Caputo, Caputo-Fabrizio, and Atangana-Baleanu-Caputo operators, to incorporate memory effects. Stability analysis is conducted via the Banach fixed-point theorem. Optimal control strategies involving TNF-α and IL-23 inhibitors are applied using the Forward-Backward Sweep Method (FBSM), highlighting how memory-based dynamics can inform long-term treatment outcomes.

- *Chapter 5* advances the model further by incorporating two immune-mediated intracellular time delays into the system introduced in *Chapter 3*. These delays reflect cytokine signaling lags in T cell–dendritic cell communication. Delay-induced Hopf bifurcation analysis is performed to determine the critical thresholds of system oscillations. A dual biologic control strategy (TNF-α and IL-17 inhibitors) is shown to regulate disease progression, reinforcing the robustness of biologic-stem cell synergy under temporal perturbations.

- Continuing from the deterministic ODE framework, *Chapter 6* introduces impulsive differential equations to study the discrete-time effect of stem cell transplantation. Periodic impulsive transplantation, demonstrating that timely administered stem-cell therapy can effectively reduce T cell and keratinocyte hyperactivity if applied appropriately, even in the absence of continuous biologics.

- In *Chapter 7*, a model is formulated, integrating T cells, dendritic cells, keratinocytes, and MSCs, considering the effects of five key cytokines that have a major role in the pathogenesis of psoriasis. Quasi-steady-state approximations reduce the complexity of consideration of cytokine dynamics, while detailed stem cell differentiation pathways are modeled. Hopf bifurcation analysis and numerical simulation support the findings of earlier chapters from a cytokine-network perspective by demonstrating how impulsive control via both biologic and stem cell therapy can normalize cytokine imbalance and keratinocyte overgrowth.

- Finally, *Chapter 8* outlines prospective future directions for research and provides a model of our ongoing work.

Chapter 2

Introducing MSC Therapy to Inhibit Th-1 and Th-17 Mediated Cytokines: A Mathematical Study to Regulate Psoriasis

Psoriasis is a chronic autoimmune skin disease marked by immune system dysregulation. The disease is mainly characterized by excessive proliferation and abnormal differentiation of keratinocytes, driven by the hyperactivation of T cell subsets, notably Th_1 and Th_{17}, and infiltration of multiple inflammatory cells. These cells secrete pro-inflammatory cytokines, TNF-α, IFN-γ, IL-17, and IL-22, which collectively promote keratinocyte overgrowth and sustain the inflammatory cycle. On the other hand, mesenchymal stem cells (MSCs), known for their immunosuppressive capabilities, attempt to counteract these effects. However, in psoriatic conditions, local MSCs become dysfunctional, diminishing their regulatory potential. In this *Chapter*[2], we have proposed a mathematical model to explain the dynamics of the disease psoriasis considering the densities of two major subtypes of T cells (Th_1 and Th_{17} cells) and keratinocytes. Incorporating MSCs as a secondary population, we ensure the effect of MSCs. Later we have considered MSC replacement from an external source via an impulsive control approach. All analytical outcomes have been supported by numerical simulations.

2.1 Model Formulation with Suitable Assumptions

Here we have considered a four-dimensional deterministic ODE-based mathematical model, where two subtypes of helper T cells (namely Th_1 and Th_{17}), keratinocytes and matured stem cells as basic cell populations. Figure (2.1) depicts the cytokine network, illustrating the interactions among the considered cell populations that contribute to disease progression.

[2] *Adapted in part from: International Conference on Mathematical Analysis and Application in Modeling, pp. 87–101 (2023), Springer Nature Singapore.*

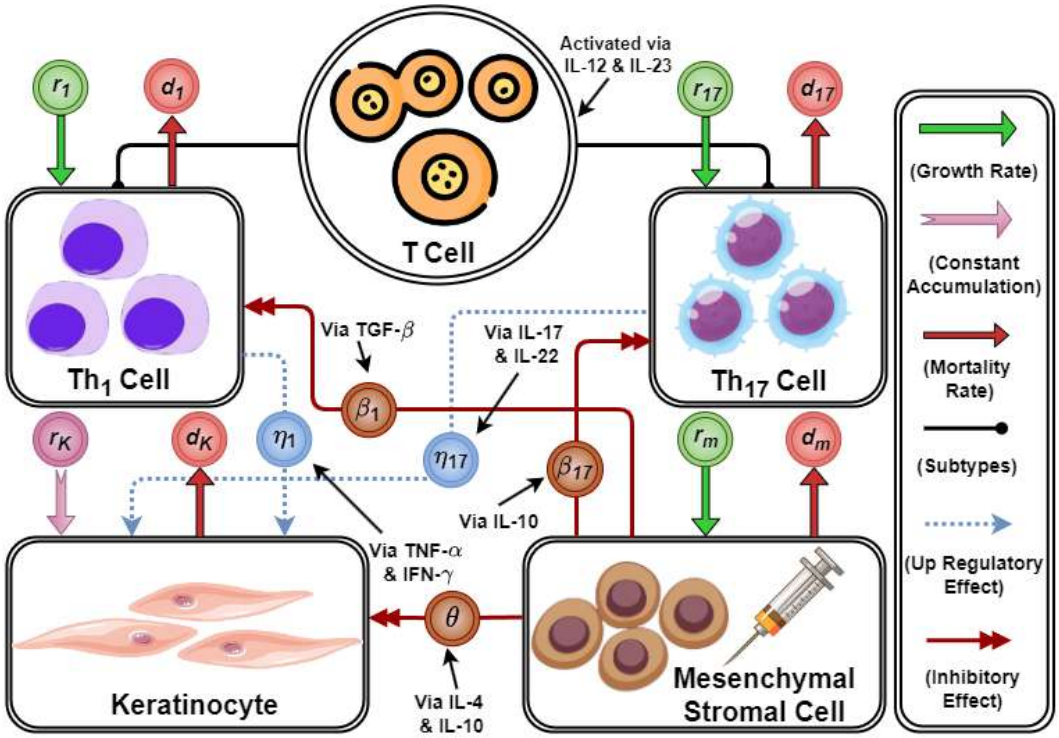

Figure 2.1: Diagrammatic representation of the model's populations relationships.

To formulate the mathematical model, we have considered following hypotheses.

1. $T_1(t)$, $T_{17}(t)$, $K(t)$, and $S_m(t)$ are the concentrations of Th_1 cell, Th_{17} cell, keratinocyte, and MSC respectively at any instant t.

2. Since the concentrations of Th_1, Th_{17}, and S_m cannot increase indefinitely, we employed logistic growth equations. Here, r_1, r_{17}, and r_m denote the intrinsic growth rates, and $T_1^{\max}$, $T_{17}^{\max}$, and $S_m^{\max}$ represent the carrying capacities of Th_1, Th_{17}, and MSC respectively.

3. MSC secrete a variety of tolerogenic anti-inflammatory cytokines which have immunosuppressive properties. MSC inhibits the proliferation of T_1 at the rate of β_1 via TGF-β and T_{17} cells at the rate of β_{17} via the cytokine IL-10.

4. r_K is the constant accumulation of keratinocyte cell population. The up-regulatory effect of Th_1 cells on the growth of keratinocytes occurs at a rate of η_1 through the cytokines TNF-α and IFN-γ. Similarly, Th_{17} cells enhance keratinocyte proliferation at a rate of η_{17} via the cytokines IL-17 and IL-22. Simultaneously, MSCs inhibit this proliferation at the rate of θ via cytokines, namely IL-4 and IL-10.

5. The natural mortality rates of Th_1, Th_{17}, keratinocytes, and MSC are d_1, d_{17}, d_K, and d_m respectively.

Based on the above hypotheses, we have formulated the following mathematical model

$$\begin{aligned}
\frac{dT_1(t)}{dt} &= r_1 T_1(t)\left[1 - \frac{T_1(t)}{T_1^{\max}}\right] - \beta_1 T_1(t) S_m(t) - d_1 T_1(t),\\
\frac{dT_{17}(t)}{dt} &= r_{17} T_{17}(t)\left[1 - \frac{T_{17}(t)}{T_{17}^{\max}}\right] - \beta_{17} T_{17}(t) S_m(t) - d_{17} T_{17}(t),\\
\frac{dK(t)}{dt} &= r_K + \left[\frac{\eta_1 T_1(t) + \eta_{17} T_{17}(t)}{1 + \theta S_m(t)}\right] - d_K K(t),\\
\frac{dS_m(t)}{dt} &= r_m S_m(t)\left[1 - \frac{S_m(t)}{S_m^{\max}}\right] - d_m S_m(t).
\end{aligned} \tag{2.1.1}$$

Since the intrinsic growth rates of each population exceed their corresponding inherent mortality rates ($r_1 > d_1$, $r_{17} > d_{17}$, and $r_m > d_m$), the initial conditions for the feasibility of cell dynamics must satisfy $T_1(0) > 0$, $T_{17}(0) > 0$, $K(0) > 0$, and $S_m(0) > 0$.

Parameter	**Definition**	**Value** (day^{-1})	**Reference**
r_1	Intrinsic growth rate of Th_1 cells	0.15	[52]
r_{17}	Intrinsic growth rate of Th_{17} cells	0.08	[52]
r_m	Intrinsic growth rate of MSCs	0.0033	[41]
r_K	Constant accumulation of Keratinocytes	0.3	[43]
$T_1^{\max}$	Carrying capacity of Th_1 cells	300 mm^{-3}	[52]
$T_{17}^{\max}$	Carrying capacity of Th_{17} cells	300 mm^{-3}	[43]
$S_m^{\max}$	Carrying capacity of MSCs	0.45 mm^{-3}	[41]
β_1	Rate of inhibition of Th_1 via MSC	0.006	chosen
β_{17}	Rate of inhibition of Th_{17} via MSC	0.003	chosen
η_1	Up regulatory effect of Th_1 on Keratinocyte	0.07	[53]
η_{17}	Up regulatory effect of Th_{17} on Keratinocyte	0.06	[53]
θ	Inhibition rate of Keratinocyte proliferation	0.02	chosen
d_1	Natural mortality rate of Th_1	0.03	[52]
d_{17}	Natural mortality rate of Th_{17}	0.03	[43]
d_K	Natural mortality rate of Keratinocytes	0.04	[54]
d_m	Natural mortality rate of MSCs	0.0017	[41]

Table 2.1: Parameters used for numerical simulations. Some values are taken as ranges from peer-reviewed literature, while the remaining parameters are suitably chosen for the model.

2.1.1 Positivity and Boundedness

In this subsection, we have analyzed the positivity and boundedness properties of the solutions of system (2.1.1) by considering the initial conditions to establish that the system is biologically well defined. The following theorem ensure the positivity of the solution of system (2.1.1).

Theorem 2.1.1 *All solutions of the system (2.1.1) along with the initial conditions are positive for all $t > 0$.*

Proof. Let us choose $\rho_1(t) = T_1(t)$, $\rho_2(t) = T_{17}(t)$, $\rho_3(t) = K(t)$, and $\rho_4(t) = S_m(t)$ in order to prove the theorem. Now we rewrite the system (2.1.1) in the following manner:

$$\frac{d\rho(t)}{dt} = \Xi\left(\rho(t)\right), \text{ where } \rho(t) = (\rho_1, \rho_2, \rho_3, \rho_4)^T \text{ and } \Xi = (\Xi_1, \Xi_2, \Xi_3, \Xi_4)^T. \tag{2.1.2}$$

Here Ξ denote the right hand sides of the system (2.1.1), and ^{T} denotes the transpose.

$$\begin{aligned}
\text{We have, } & \Xi_1(0, \rho_2, \rho_3, \rho_4) = 0, \text{ if } \rho_2 \geq 0, \rho_3 \geq 0, \rho_4 \geq 0,\\
& \Xi_2(\rho_1, 0, \rho_3, \rho_4) = 0, \text{ if } \rho_1 \geq 0, \rho_3 \geq 0, \rho_4 \geq 0,\\
& \Xi_3(\rho_1, \rho_2, 0, \rho_4) = r_K + \frac{\eta_1\rho_1 + \eta_2\rho_2}{1 + \theta\rho_4} \geq 0, \text{ if } \rho_1 \geq 0, \rho_2 \geq 0, \rho_4 \geq 0,\\
& \Xi_4(\rho_1, \rho_2, \rho_3, 0) = 0, \text{ if } \rho_1 \geq 0, \rho_2 \geq 0, \rho_3 \geq 0.
\end{aligned}$$

Therefore, the condition $\Xi_i(\rho)|_{\rho_i=0,\ \rho\in\mathbb{R}^4_+} \geq 0$ clearly ensures the positivity of the solutions of the system (2.1.1) using the well-known result of Krasnoselskii and Mark Aleksandrovich [55], which implies that all solutions for the system (2.1.1) starting with the point $\rho_0 = (\rho_1(0), \rho_2(0), \rho_3(0), \rho_3(0))^T \in \mathbb{R}^4_+$, such as $\rho(t) = \rho(t; \rho_0)$, and $\rho(t) \in \mathbb{R}^4_+, \forall t > 0$. It means that the non-negative octant $\mathbb{R}^4_+$ become invariant for the system (2.1.1) and all solutions are positive for all $t > 0$ with respect to the initial conditions.

It is also crucial to show that all the population variables in system (2.1.1) are bounded for all $t > 0$. Which will ensure that the system (2.1.1) is mathematically well defined and epidemiologically meaningful. The following theorem illustrates the invariant region Ω where the solutions of system (2.1.1) are bounded.

Theorem 2.1.2 *All positive solutions of the system (2.1.1) in the region $\Omega \subseteq \mathbb{R}^4_+$ are bounded, where Ω is defined by*

$$\Omega = \left\{\left(T_1, T_{17}, K, S_m\right) \in \mathbb{R}^4_+ : 0 < T_1 \leq \mathcal{M}_1, 0 < T_{17} \leq \mathcal{M}_2, 0 < K \leq \mathcal{M}_3, 0 < S_m \leq \mathcal{M}_4\right\}.$$

Here, $\mathcal{M}_i$ $(i = 1, 2, 3, 4)$ are constants defined by

$$\mathcal{M}_1 = \frac{r_1 T_1^{\max}}{4d_1},\ \mathcal{M}_2 = \frac{r_{17} T_{17}^{\max}}{4d_{17}},\ \mathcal{M}_3 = \frac{r_K + \eta_1\mathcal{M}_1 + \eta_{17}\mathcal{M}_2}{d_K},\ \text{and}\ \mathcal{M}_4 = \frac{r_m S_m^{\max}}{4d_m}.$$

The solutions maintain their biological significance for all $t \in [0, \mathcal{T}]$.

Proof. The maximum value of the quadratic term $r_1 T_1(t)\left[1-\frac{T_1(t)}{T_1^{\max}}\right]$ of the first equation of (2.1.1) is $\frac{r_1 T_1^{\max}}{4}$. Using this fact, from the first equation of system (2.1.1) we have:

$$\frac{dT_1(t)}{dt} \leq \frac{r_1 T_1^{\max}}{4} - d_1 T_1(t) = d_1 \mathcal{M}_1 - d_1 T_1(t).$$

Using the comparison principle [56] we obtain from the above inequality:

$$0 < T_1(t) < \mathcal{M}_1(1-e^{-d_1 t}) + T_1(0)e^{-d_1 t},\ t > 0 \text{ where } T_1(t) \leq \mathcal{M}_1 \text{ if } T_1(0) \leq \mathcal{M}_1.$$

In similar arguments from the second and fourth equations of system (2.1.1) we get:

$$0 < T_{17}(t) < \mathcal{M}_2(1-e^{-d_{17} t}) + T_{17}(0)e^{-d_{17} t},\ t > 0 \text{ where } T_{17}(t) \leq \mathcal{M}_2 \text{ if } T_{17}(0) \leq \mathcal{M}_2.$$

$$0 < S_m(t) < \mathcal{M}_4(1-e^{-d_m t}) + S_m(0)e^{-d_m t},\ t > 0 \text{ where } S_m(t) \leq \mathcal{M}_4 \text{ if } S_m(0) \leq \mathcal{M}_4.$$

Utilizing the facts $T_1(t) \leq \mathcal{M}_1$, $T_{17}(t) \leq \mathcal{M}_2$ and $S_m(t) \leq \mathcal{M}_4$, from the third equation of the system (2.1.1), we obtain:

$$\frac{dK(t)}{dt} < r_K + \eta_1 \mathcal{M}_1 + \eta_{17} \mathcal{M}_2 - d_K K(t) = d_K \mathcal{M}_3 - d_K K(t).$$

By using the same comparison principle, we get:

$$0 < K(t) < \mathcal{M}_3(1-e^{-d_K t}) + K(0)e^{-d_K t},\ t > 0.$$

Note that all solutions $(T_1(t), T_{17}(t), K(t), S_m(t))$ of the system (2.1.1) with positive initial conditions start in Ω and finally reach this set for all $t > 0$. The boundedness is justified because we have proved the positive invariance of the set Ω. This property is provided by the definition of the region Ω and with the following relations:

$$\left.\frac{dT_1(t)}{dt}\right|_{T_1=\mathcal{M}_1} < 0, \qquad \left.\frac{dT_{17}(t)}{dt}\right|_{T_{17}=\mathcal{M}_2} < 0,$$
$$\left.\frac{dS_m(t)}{dt}\right|_{S_m=\mathcal{M}_4} < 0, \qquad \left.\frac{dK(t)}{dt}\right|_{T_1\leq\mathcal{M}_1, T_{17}\leq\mathcal{M}_2, K=\mathcal{M}_3} < 0.$$

This guarantees the boundedness of all solutions of the system (2.1.1) with positive initial conditions.

2.1.2 Feasibility of Equilibrium

Since psoriasis is an auto-immune disease, all of the cell types considered here are non-negative. We put all the equations of the system (2.1.1) to zero and solve for the state variables to determine the endemic equilibrium point $E^*(T_1^*, T_{17}^*, K^*, S_m^*)$, where its co-ordinates are positive. From the fourth equation of the system (2.1.1), we get

$$S_m^* = \frac{(r_m - d_m)S_m^{\max}}{r_m} > 0 \text{ as } r_m > d_m.$$

Utilizing the value of S_m^* and setting the first three equations of the system (2.1.1) to zero, we have determined the values of T_1^*, T_{17}^*, and K^*, which are given by

$$T_1^* = \frac{T_1^{\max}}{r_1}(r_1 - \beta_1 S_m^* - d_1),\ T_{17}^* = \frac{T_{17}^{\max}}{r_{17}}(r_{17} - \beta_{17} S_m^* - d_{17}),\ K^* = \frac{r_K}{d_K} + \frac{\eta_1 T_1^* + \eta_{17} T_{17}^*}{d_K(1+\theta S_m^*)}.$$

Thus, we can uniquely determine the positive endemic equilibrium point E^* if the following conditions are satisfied:

$$r_1 > \beta_1 S_m^* + d_1 \ \text{ and } \ r_{17} > \beta_{17} S_m^* + d_{17}.$$

2.1.3 Stability of the Interior Equilibrium

Here we have analyzed the local stability of the endemic equilibrium point $E^*(T_1^*, T_{17}^*, K^*, S_m^*)$. The variational matrix evaluated at the endemic equilibrium point E^* is given by

$$V(E^*) = \begin{pmatrix} -\frac{r_1 T_1^*}{T_1^{\max}} & 0 & 0 & -\beta_1 T_1^* \\ 0 & -\frac{r_{17} T_{17}^*}{T_{17}^{\max}} & 0 & -\beta_{17} T_{17}^* \\ \frac{\eta_1}{1+\theta S_m^*} & \frac{\eta_{17}}{1+\theta S_m^*} & -d_K & -\frac{\theta(\eta_1 T_1^* + \eta_{17} T_{17}^*)}{(1+\theta S_m^*)^2} \\ 0 & 0 & 0 & -\frac{r_m S_m^*}{S_m^{\max}} \end{pmatrix}.$$

The eigenvalues of the above variational matrix are

$$-\frac{r_1 T_1^*}{T_1^{\max}},\ -\frac{r_{17} T_{17}^*}{T_{17}^{\max}},\ -d_K,\ \text{and}\ -\frac{r_m S_m^*}{S_m^{\max}}.$$

Since all of these eigenvalues are negative, therefore, the endemic equilibrium point $E^*(T_1^*, T_{17}^*, K^*, S_m^*)$ of system (2.1.1) is locally asymptotically stable.

2.2 Pulsed Mesenchymal Stem Cell Replacement Strategy

In the course of stem cell-based therapy, multiple injections of mesenchymal stem cells (MSCs) are typically administered to the affected region of the patient. Due to the limited endogenous production of MSCs in the affected area, we investigate the effects of a pulsed therapeutic approach within the system described in equation (2.2.1). The maximum value of the quadratic term $r_m S_m(t)\big[1 - S_m(t)/S_m^{\max}\big]$ in the fourth equation of system (2.1.1) is $\big[r_m S_m^{\max}/4\big]$. For mathematical simplicity, we use this maximum value instead of the logistic term in the fourth equation of system (2.1.1). The pulsed differential equations describing the dynamics of cell

treatment are as follows:

$$\begin{aligned}
\frac{dT_1(t)}{dt} &= r_1 T_1(t)\Big[1 - \frac{T_1(t)}{T_1^{\max}}\Big] - \beta_1 T_1(t) S_m(t) - d_1 T_1(t),\\
\frac{dT_{17}(t)}{dt} &= r_{17} T_{17}(t)\Big[1 - \frac{T_{17}(t)}{T_{17}^{\max}}\Big] - \beta_{17} T_{17}(t) S_m(t) - d_{17} T_{17}(t),\\
\frac{dK(t)}{dt} &= r_K + \Big[\frac{\eta_1 T_1(t) + \eta_{17} T_{17}(t)}{1 + \theta S_m(t)}\Big] - d_K K(t),\\
\frac{dS_m(t)}{dt} &= \frac{r_m S_m^{\max}}{4} - d_m S_m(t),\\
S_m(n\tau) &= S_m(n\tau)^- + b, \quad \Big[k\tau \le t < (k+1)\tau, \;\; k \in \mathbb{N} \cup \{0\}\Big],
\end{aligned} \tag{2.2.1}$$

where τ is the time interval and the coefficient 'b' represents the average quantity of MSCs infused into the affected region. The term $S_m(k\tau)^-$ denotes the concentration of S_m immediately before the administration of the next MSC dose at $t = k\tau$.

The solution to the fourth equation of the system (2.2.1) can be expressed as follows:

$$S_m(t) = \frac{r_m S_m^{\max}}{4d_m} + Ce^{-d_m t}.$$

C is a constant to be determined using the following initial condition.

When, $0 \le t < \tau$

$$\begin{cases} \frac{dS_m(t)}{dt} = \frac{r_m S_m^{\max}}{4} - d_m S_m(t), \\ S_m(0) = b \end{cases} \implies C = \Big(b - \frac{r_m S_m^{\max}}{4d_m}\Big).$$

Therefore, $S_m(t) = \dfrac{r_m S_m^{\max}}{4d_m} + \Big(b - \dfrac{r_m S_m^{\max}}{4d_m}\Big)e^{-d_m t}$.

Now, $S_m(\tau) = S_m(\tau)^- + b = \dfrac{r_m S_m^{\max}}{4d_m} + b(1 + e^{-d_m\tau}) - \dfrac{r_m S_m^{\max}}{4d_m}e^{-d_m\tau}$.

We analyze the system (2.2.1) for each time interval since the initial condition of the $S_m(t)$ population varies with respect to time.

When, $\tau \le t < 2\tau$

$$\begin{cases} \frac{dS_m(t)}{dt} = \frac{r_m S_m^{\max}}{4} - d_m S_m(t), \\ S_m(\tau) = \frac{r_m S_m^{\max}}{4d_m} + b(1 + e^{-d_m\tau}) - \frac{r_m S_m^{\max}}{4d_m}e^{-d_m\tau}. \end{cases}$$
$$\implies C = \Big[b(1 + e^{-d_m\tau}) - \frac{r_m S_m^{\max}}{4d_m}e^{-d_m\tau}\Big]e^{d_m\tau}.$$

Thus, $S_m(t) = \dfrac{r_m S_m^{\max}}{4d_m} + \Big[b(1 + e^{-d_m\tau}) - \dfrac{r_m S_m^{\max}}{4d_m}e^{-d_m\tau}\Big]e^{-d_m(t-\tau)}$.

So, $S_m(2\tau) = S_m(2\tau)^- + b = \dfrac{r_m S_m^{\max}}{4d_m} + b(1 + e^{-d_m\tau} + e^{-2d_m\tau}) - \dfrac{r_m S_m^{\max}}{4d_m}e^{-2d_m\tau}$.

Continuing this process up to 'k' iterations we get:
When, $k\tau \leq t < (k+1)\tau$

$$\begin{cases} \frac{dS_m(t)}{dt} = \frac{r_m S_m^{\max}}{4} - d_m S_m(t), \\ S_m(k\tau) = \frac{r_m S_m^{\max}}{d_m} + b(1 + e^{-d_m\tau} + e^{-2d_m\tau} + \ldots\ldots + e^{-kd_m\tau}) - \frac{r_m S_m^{\max}}{4d_m} e^{-kd_m\tau}. \end{cases}$$

$$\implies C = \left[b(1 + e^{-d_m\tau} + e^{-2d_m\tau} + \ldots\ldots + e^{-kd_m\tau}) - \frac{r_m S_m^{\max}}{4d_m} e^{-kd_m\tau} \right] e^{d_m\tau}.$$

The concentration of infused MSC after $k-th$ infusion

$$\begin{aligned} S_m(t) &= \frac{r_m S_m^{\max}}{4d_m} + \left[b(1 + e^{-d_m\tau} + e^{-2d_m\tau} + \ldots\ldots + e^{-kd_m\tau}) - \frac{r_m S_m^{\max}}{4d_m} e^{-kd_m\tau} \right] e^{-d_m(t-k\tau)} \\ &= \frac{r_m S_m^{\max}}{4d_m} + \left[b\left(\frac{1 - e^{-(k+1)d_m\tau}}{1 - e^{-d_m\tau}} \right) - \frac{r_m S_m^{\max}}{4d_m} e^{-kd_m\tau} \right] e^{-d_m(t-k\tau)}. \end{aligned} \tag{2.2.2}$$

Observe that the endpoints of each cycle rise monotonically. The events right before and after the end of a positive impulsive periodic orbit involving infused stem cells $S_m(t)$ are described by the following.

$$S_m(k\tau)^- = \frac{r_m S_m^{\max}}{4d_m} + be^{-d_m\tau} \left(\frac{1 - e^{-kd_m\tau}}{1 - e^{-d_m\tau}} \right) - \frac{r_m S_m^{\max}}{4d_m} e^{-kd_m\tau},$$

$$\therefore \lim_{k\to\infty} S_m(k\tau)^- = \frac{r_m S_m^{\max}}{4d_m} + \frac{be^{-d_m\tau}}{1 - e^{-d_m\tau}}.$$

$$S_m(k\tau) = \frac{r_m S_m^{\max}}{4d_m} + b\left(\frac{1 - e^{-(k+1)d_m\tau}}{1 - e^{-d_m\tau}} \right) - \frac{r_m S_m^{\max}}{4d_m} e^{-kd_m\tau},$$

$$\therefore \lim_{k\to\infty} S_m(k\tau) = \frac{r_m S_m^{\max}}{4d_m} + \frac{b}{1 - e^{-d_m\tau}}.$$

Therefore, the concentration of $S_m(t)$ at the ends of a positive impulsive periodic orbit falls within the points of impulse [57].

$$\frac{r_m S_m^{\max}}{4d_m} + \frac{be^{-d_m\tau}}{1 - e^{-d_m\tau}} \leq \tilde{S_m}^* \leq \frac{r_m S_m^{\max}}{4d_m} + \frac{b}{1 - e^{-d_m\tau}}.$$

The advantage of this strategy lies in its ability to produce a substantial amount of anti-inflammatory cytokines, which suppress the cytokine storm and enhance immunity against psoriasis. However, in clinical practice, a limited number of infusions are generally used [22].

2.3 Numerical Simulation

In this section, we have performed several numerical simulations of our proposed system based on our theoretical outcomes. It is essential that the initial values chosen for the

model populations in these simulations adhere to the scientific hypotheses derived from the analytical results of this study. The parameter values employed for the numerical simulations are detailed in Table 2.1.

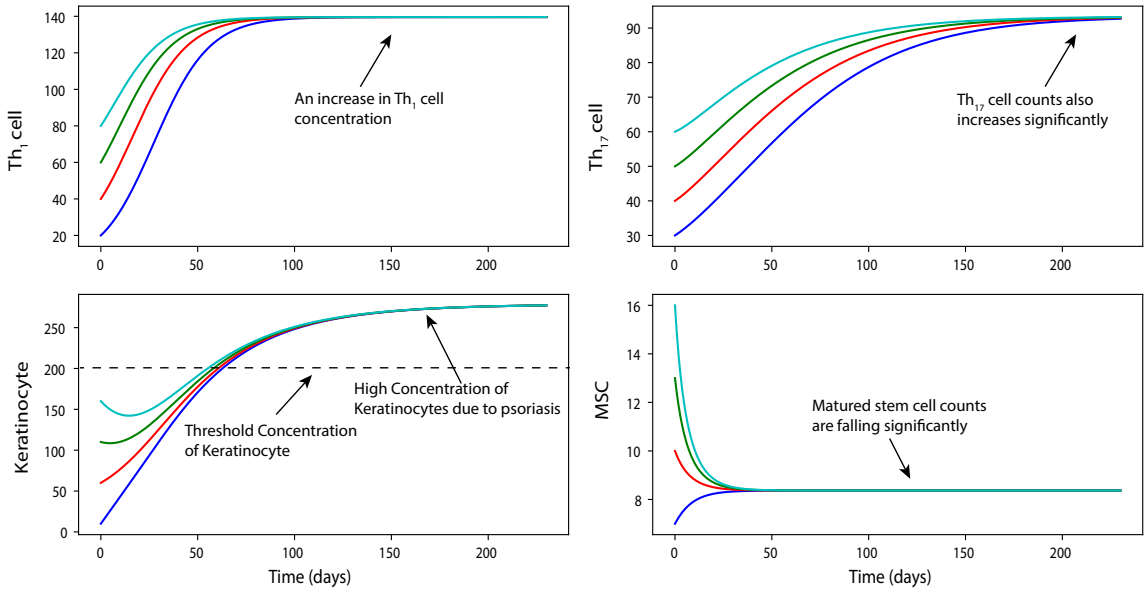

Figure 2.2: Simulation of the system (2.1.1) shows all the system populations are bounded and the trajectories converge to a unique solution with respect to time for different range of initial conditions for (a) Th_1 cells, (b) Th_{17} cells, (c) Keratinocytes, and (d) MSCs. We have used the parameter values given in Table (2.1).

In Figure 2.2, we present the time series solutions of each population for our proposed system (2.1.1) using four different initial conditions. We observe that Th_1 cells, Th_{17} cells, and keratinocyte populations initially exhibit an increasing trend followed by stabilization, with all trajectories converging to a single equilibrium point. In contrast, the population of MSCs declines significantly during disease progression. This figure illustrates the asymptotic stability of the endemic equilibrium point, confirming our analytical findings. The simulation depicts the disease development dynamics in the absence of cell treatment.

In Figure 2.3, we plot two distinct 3D phase portraits of the system (2.1.1), each considering three populations at a time, and identify numerically the endemic equilibrium point E^* for various initial conditions of each sub-population. Figure 2.3(a) illustrates trajectories converging to the equilibrium $E_1^* = (139.6, 93.37, 278.48)$ for Th_1, Th_{17}, and keratinocyte populations. Similarly, Figure 2.3(b) demonstrates convergence to equilibrium $E_2^* = (139.6, 278.48, 8.38)$ for Th_1, keratinocyte, and MSC populations. Since analytical evaluation of the endemic equilibrium is very difficult, we identified it numerically. Consequently, the endemic equilibrium point is $E^*(139.6, 93.37, 278.48, 8.38)$.

The normal concentration of keratinocytes is established at $\hat{K} = 200\ mm^{-3}$ [52]. Concentrations above this threshold indicate a psoriatic state, whereas concentrations below this level are considered indicative of a healthy state. Subsequently, stem cells replacement strat-

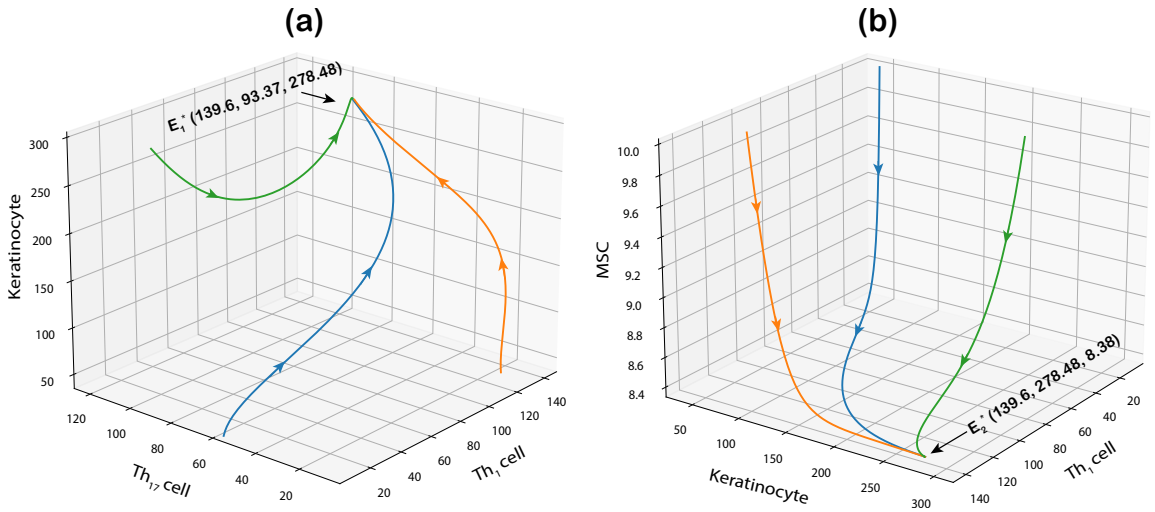

Figure 2.3: In this simulation, we have identified the endemic equilibrium point $E^* = (235.22, 182.94, 687.42, 0.39)$ *of the system (2.1.1) by taking two groups of populations, three at a time for (1)* $E_1^*(T_1^*, T_{17}^*, K^*) = (235.22, 182.94, 687.42)$ *(2)* $E_2^*(T_1^*, K^*, S_m^*) = (235.22, 687.42, 0.39)$.

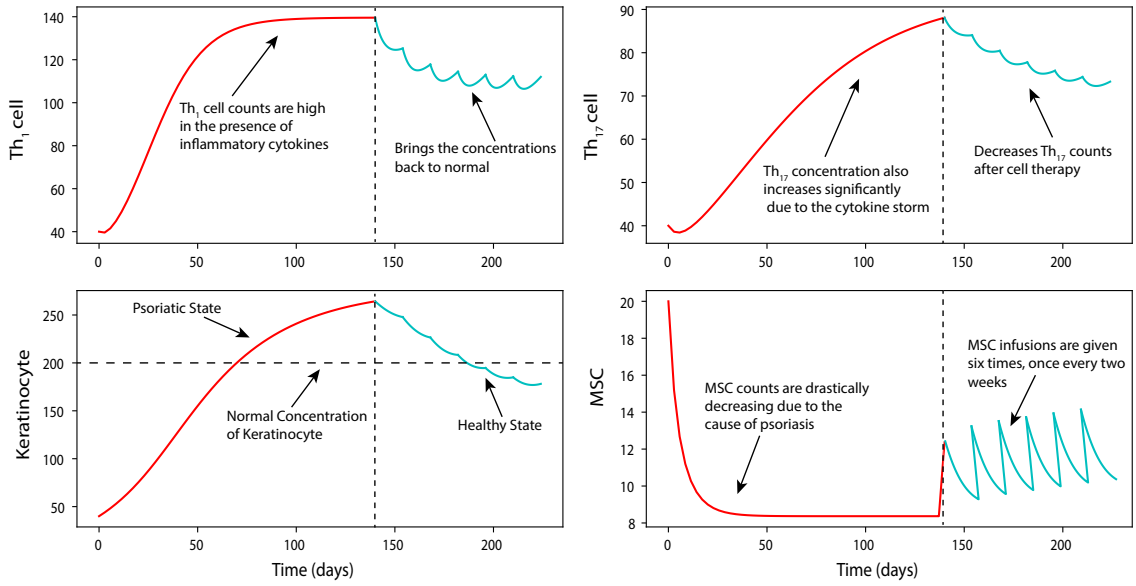

Figure 2.4: The model populations were simulated for 140 days without cell replacement, after which a numerical simulation of the pulsed infusion of MSC (six infusions at 14 day intervals) was performed.

egy is applied in an impulsive manner over conventional biologic medication treatment for severe cases of the disease. In Figure 2.4, we present the numerical simulation for six MSC

infusions at a single dose of 4 cells/mm^3 once every two weeks. This figure shows two distinct colour trajectories for each cell population considered. The red trajectories represent the psoriatic state without any treatment for up to 140 days, while the cyan trajectories depict the dynamics of the pulsed MSC infusions once every 14 days as a course of treatment. Our numerical results indicate that within two months of treatment with MSC, keratinocytes gradually decreased to the desired density levels (i.e. $\leq 200\ mm^{-3}$). Additionally, we observe a significant reduction in the concentrations of Th_1 and Th_{17} cells, and the MSC counts in the affected areas return to normal levels.

2.4 Discussion and Conclusion

In this *Chapter*, we formulated a four-dimensional nonlinear mathematical model to investigate the dynamical changes of psoriasis, incorporating Th_1 and Th_{17} cells, keratinocytes, and MSCs as population densities. The proposed mathematical model apprehends key cellular interactions mediated by cytokine signaling. To ensure biological relevance, we demonstrate the positivity and boundedness of the model system. The model exhibits a unique interior equilibrium point, E^*, and proves its local asymptotical stability.

To explore therapeutic intervention, we implement a pulsed therapeutic control strategy analytically and simulate the administration effect of UC-MSCs after 140 days of disease onset. Based on our numerical findings, within 60 days of interventions, the densities of Th_1 and Th_{17} cells decline significantly, keratinocyte levels fall to the healthy state ($\leq 200\, mm^{-3}$), and local dysregulated MSC concentrations in the affected region increase to normal levels. This indicates a reduction in keratinocyte density, with epidermal homeostasis restored within a few months. Since stem cell therapy is not yet a standard therapeutic approach in clinical practice, rigorous clinical trials are necessary to confirm these findings and address the recurrence associated with the disease. However, for severe psoriasis cases when biologic treatments are ineffective, stem cell therapy offers a promising alternative for achieving complete recovery. Because of factors related to adverse effects and the high expense of stem cell-based treatment, we recommend the impulsive control strategy, allowing clinicians to monitor and evaluate therapeutic responses following each MSC administration. Note that dendritic cells (DCs) are also recognized as key mediators that initiate and sustain the abnormal T cell differentiation through cytokine signaling. Therefore, incorporating the influence of dendritic cells into the model is essential to achieve more biological understanding of the disease. In the subsequent chapter, we incorporate the role of dendritic cells into the mathematical model of psoriasis, along with the effects of healthy MSC transplantation combined with TNF-α inhibition.

Chapter 3

A Mathematical Insight to Control the Disease Psoriasis Using Mesenchymal Stem Cell Transplantation with a Biologic Inhibitor

In this *Chapter*[3], we present a mathematical model to study the progression of psoriasis. The model considers the densities of T cells (without separating subtypes), dendritic cells, keratinocytes, and mesenchymal stem cells (MSCs). To examine possible treatment strategies, we first study the effect of a TNF-α inhibitor by including it as a control input in the system. Using the optimal control framework, we identify the best possible effect of the TNF-α inhibitor and confirm the analytical results through numerical simulations. Since stem cell therapy is usually considered for severe or treatment-resistant cases, we next extend the model to include the effect of impulsive administration of healthy MSCs. This extension gives rise to an impulsive control model that combines continuous biologic therapy with discrete stem cell transplantation. With this modelling approach, we show that combining MSC-based therapy with TNF-α inhibition can significantly improve treatment outcomes. The chapter further provides theoretical analyses of system stability, the role of optimal control, and the impact of impulsive stem cell therapy. All analytical results are supported and validated through detailed numerical simulations.

3.1 Mathematical Model

To describe the progression dynamics of psoriasis, we propose the mathematical model; we divided it into three key populations to illustrate the main epidermal transmission pathway. The densities of helper T cell, dendritic cell, and keratinocyte cell populations are denoted by

[3] *The major portion of this chapter is published in Scientific Reports, Nature, September 2024.*

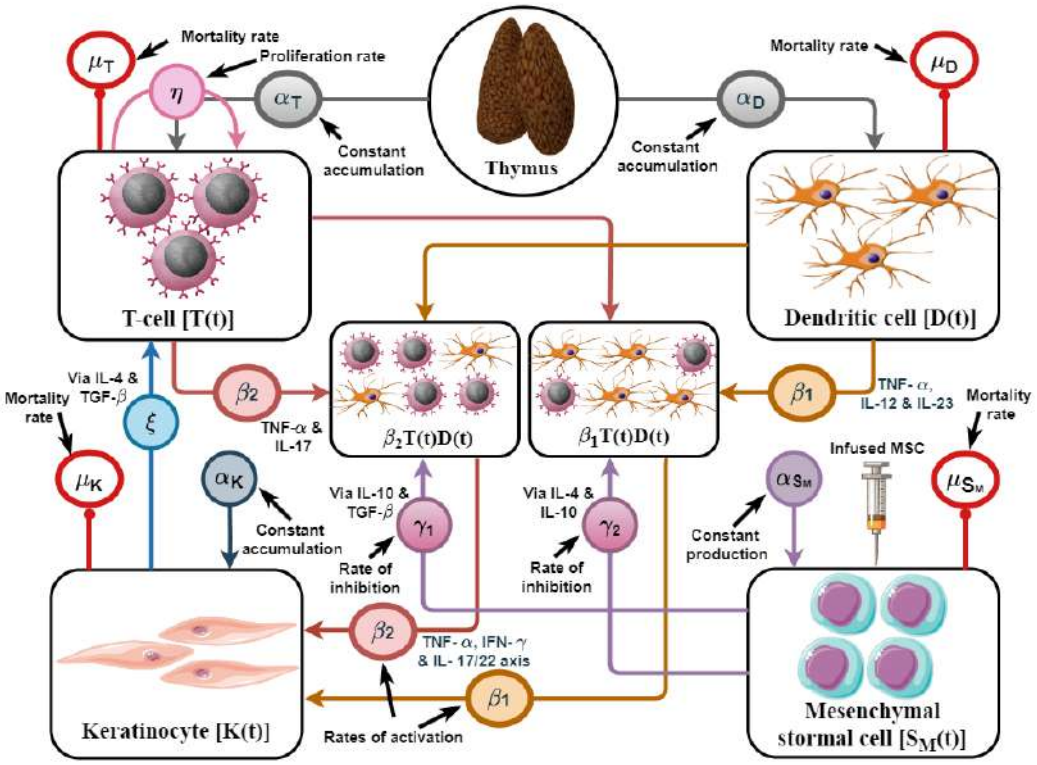

Figure 3.1: Schematic representation of model populations and their interrelationships mediated by cytokine signaling.

T(t), *D(t)*, and *K(t)*, respectively, at any time *'t'*. The following hypotheses are considered when formulating the mathematical model for the disease psoriasis:

1. Here, we have used α_T and α_D as the constant accumulation rates of T cells and dendritic cells, respectively, to construct the growth equations.

2. Psoriasis is a chronic, inflammatory disorder associated with T cells, but the total number of T cells cannot increase endlessly; thus, we take the logistical expansion of T cells. The term $\eta T(1 - \frac{T}{T^{max}})$ serves to highlight the growth of T cells, where η is the proliferation rate and T^{max} is the maximum carrying capacity.

3. In the human immune system, T cells and dendritic cells are two distinct kinds of immune cells with diverse characteristics. Psoriasis begins as a result of the differentiation of Th_1 and Th_{17} cells by activated dermal DC derived cytokines (mainly IL-12 and IL-23) [44]. Here, we have considered β_1 as the rate at which DCs activate T cells (via TNF-α, IL-12, and IL-23) and β_2 as the rate at which T cells activate DCs (through the cytokines TNF-α and IL-17). T cells and DCs engage in mutual interaction (denoted by the terms $\beta_1 TD$ and $\beta_2 TD$) to generate a cytokine storm that eventually infiltrates and contributes to the growth of the keratinocyte population.

4. The hyper-reactivity of T cells is initially inhibited by keratinocytes (via IL-4 and

TGF-β) at a rate of ξ, which is considered in the first population by the term $-\xi TK$. Throughout the typical sequence, the per-capita clearance rates of T cells and DCs are considered to be μ_T and μ_D, respectively.

5. Psoriasis is mainly characterized by the hyper-proliferation and abnormal differentiation of keratinocytes and the infiltration of multiple inflammatory cells. The immune system also plays a crucial role in regulation. However, incorporating all these factors into a mathematical model is complex due to the numerous parameters involved, which complicates computations. For the sake of simplicity, we focus on the significant causes: hyper-proliferation and the infiltration of cells via interaction between immune cells (specifically T cells and DCs) through inflammatory cytokines, which leads to excessive growth in the keratinocyte population. Excessive production of pro-inflammatory cytokines by T cells and dendritic cells (DCs) significantly contributes to the cytokine storm. IFN-γ is a pivotal cytokine in this process, its secretion being stimulated by IL-12. Additionally, the synthesis of IL-17 is promoted by IL-23. Keratinocytes over-proliferate in conjunction with TNF-α and increase IFN-γ and IL-17/22 axis production, which promotes inflammation and maintains hyper-proliferation over the course of the disease [12]. We have taken, α_K as constant accumulation of keratinocyte population and μ_K stands for the keratinocytes inherent mortality rate. The cytokine network in Figure (3.1) illustrates how immune cells interact with one another to promote disease progression.

Combining the above hypotheses, we have formulated the following mathematical model:

$$\begin{aligned}
\frac{dT(t)}{dt} &= \alpha_T + \eta T(t)\big(1 - \frac{T(t)}{T^{max}}\big) - \beta_1 T(t)D(t) - \xi T(t)K(t) - \mu_T T(t) \\
\frac{dD(t)}{dt} &= \alpha_D - \beta_2 T(t)D(t) - \mu_D D(t) \\
\frac{dK(t)}{dt} &= \alpha_K + \beta_1 T(t)D(t) + \beta_2 T(t)D(t) - \mu_K K(t).
\end{aligned} \tag{3.1.1}$$

The ability of MSCs to suppress immune cell function and prevent the entry of infiltrating cells into inflamed areas indicates that this approach could obstruct the migration of T cells [58]. MSCs secrete a substantial amount of tolerogenic anti-inflammatory cytokines, (e.g., TGF-β, IL-4, IL-10) to inhibit the overproduction of T cells and keratinocytes [59]. Moreover, it contributes to increasing the number of immature DCs, resulting in elevated IL-10 expression. Simultaneously, it diminishes the population of mature inflammatory DCs, along with a decrease in the expression of TNF-α and IL-12 [60, 61]. Therefore, transplanting them into the inflamed area of the patient will replace damaged cells and promote the functional recovery of those cells.

In this direction, we have introduced an additional population of matured stem cells (MSCs) to the previously considered cell populations reflected in system (3.1.1) to investigate how this cell therapy inhibits the excessive production of inflammatory cytokines. To express the effect of MSCs on the core populations of our model, we have considered the interactions between T cells and DCs are inhibited by the MSCs at the rates of γ_1 and γ_2, so that the interaction terms are multiplied by $(1+\gamma_1 S_M)^{-1}$ and $(1+\gamma_2 S_M)^{-1}$. MSCs do not affect the

interaction terms explicitly if γ_1 and γ_2 fade away. The coefficient α_{S_M} denotes the constant production or the average of all mature stem cells and μ_{S_M} is the sum of natural mortality and absorption rate in the inflamed region. From the above-mentioned cell biological discussion, the complete mathematical model that includes MSC as a population takes the form:

$$\begin{aligned}
\frac{dT(t)}{dt} &= \alpha_T + \eta T(t)\big(1 - \frac{T(t)}{T^{max}}\big) - \frac{\beta_1 T(t) D(t)}{1 + \gamma_1 S_M(t)} - \xi T(t) K(t) - \mu_T T(t) \\
\frac{dD(t)}{dt} &= \alpha_D - \frac{\beta_2 T(t) D(t)}{1 + \gamma_2 S_M(t)} - \mu_D D(t) \\
\frac{dK(t)}{dt} &= \alpha_K + \frac{\beta_1 T(t) D(t)}{1 + \gamma_1 S_M(t)} + \frac{\beta_2 T(t) D(t)}{1 + \gamma_2 S_M(t)} - \mu_K K(t) \\
\frac{dS_M(t)}{dt} &= \alpha_{S_M} - \mu_{S_M} S_M(t),
\end{aligned} \tag{3.1.2}$$

subject to the initial conditions: $T(0) > 0,\ D(0) > 0,\ K(0) > 0$, and $S_M(0) > 0$.

3.2 Mathematical properties of the Model

3.2.1 Positivity and Boundedness

In this subsection, we have looked at the non-negativity and boundedness properties of the solutions for our formulated mathematical system (3.1.2) to prove that the model is biologically feasible and well-posed. Now we provide the following theorem, which guarantees the non-negativity of the solutions of system (3.1.2).

Theorem 3.2.1 *All solutions of the system (3.1.2) together with the initial conditions are positive for all $t > 0$.*

Proof. To prove this theorem, let us take that $z_1(t) = T(t)$, $z_2(t) = D(t)$, $z_3(t) = K(t)$, and $z_4(t) = S_M(t)$. Rewrite the system (3.1.2) in the following manner.

$$\begin{aligned}
&\frac{dZ(t)}{dt} = \Pi\big(Z(t)\big), \\
&\text{where } Z(t) = \big(z_1(t), z_2(t), z_3(t), z_4(t)\big)^T \text{ and } \Pi = \big(\Pi_1, \Pi_2, \Pi_3, \Pi_4\big)^T.
\end{aligned} \tag{3.2.1}$$

Here ^{T} denotes the transpose and Π denote the right hand sides of the system (3.1.2). It is easy to verify that

$$\Pi_i(Z)|_{z_i=0,\ Z\in\mathbb{R}^4_+} \geq 0. \tag{3.2.2}$$

The condition clearly ensures the non-negativity of the solutions of a system according to the well-known Nagumo finding [62]. It means that all the solutions of the system (3.1.2) starting with a point $Z_0 = (z_1(0), z_2(0), z_3(0), z_3(0))^T \in \mathbb{R}^4_+$, such as $Z(t) = Z(t; Z_0)$, and $Z(t) \in \mathbb{R}^4_+, \forall t > 0$. This implies that the non-negative octant $\mathbb{R}^4_+$ becomes invariant for system (3.1.2).

It is also very essential to show that all the state variables of system (3.1.2) are bounded for all time $t > 0$. This will ensure that the system (3.1.2) is epidemiologically meaningful and mathematically well-posed. The following theorem demonstrates the invariant region Γ where the solutions of system (3.1.2) are bounded.

Theorem 3.2.2 *All non-negative solutions of the system (3.1.2) enter into the region* $\Gamma \subseteq \mathbb{R}^4_+$ *and are ultimately bounded, where* Γ *is defined by* $\Gamma = \left\{(T, D, K, S_M)^T \in \mathbb{R}^4_+ : 0 < T \leq B_1, 0 < D \leq B_2, 0 < K \leq B_3, S_M^{\min} \leq S_M \leq B_4\right\}$, *where* B_i*'s* $(i = 1, 2, 3, 4)$ *are defined by*

$$B_1 = \frac{\alpha_T}{\mu_T} + \frac{\eta T^{\max}}{4\mu_T}, B_2 = \frac{\alpha_D}{\mu_D}, B_3 = \frac{\alpha_K}{\mu_K} + \frac{\beta_1 B_1 B_2}{\mu_K(1 + \gamma_1 S_M^{\min})} + \frac{\beta_2 B_1 B_2}{\mu_K(1 + \gamma_2 S_M^{\min})}, B_4 = \frac{\alpha_{S_M}}{\mu_{S_M}}.$$

Proof. The maximum value of the quadratic term $\eta T(1 - \frac{T}{T^{\max}})$ of the first equation of (3.1.2) is $\frac{\eta T^{\max}}{4}$. Using this fact, from the first equation of system (3.1.2) we have:

$$\frac{dT}{dt} < \alpha_T + \frac{\eta T^{\max}}{4} - \mu_T T = \mu_T B_1 - \mu_T T.$$

Using comparison principle [56], we obtain from the above inequality:

$$0 < T(t) < B_1(1 - e^{-\mu_T t}) + T(0)e^{-\mu_T t} \implies T(t) \leq B_1 \text{ if } T(0) \leq B_1. \tag{3.2.3}$$

In similar manner from the second equation of system (3.1.2) we get:

$$0 < D(t) < B_2(1 - e^{-\mu_D t}) + D(0)e^{-\mu_D t} \implies D(t) \leq B_2 \text{ if } D(0) \leq B_2. \tag{3.2.4}$$

From the fourth equation of system (3.1.2) we obtain:

$$\frac{dS_M}{dt} \leq \alpha_{S_M} - \mu_{S_M} S_M.$$

By solving this inequality for sufficiently large t we have:

$$S_M^{\min} \leq S_M(t) < B_4, \quad t > 0. \tag{3.2.5}$$

Utilizing $T(t) \leq B_1$, $D(t) \leq B_2$ and $S_M(t) \geq S_M^{\min}$, from the third equation we get:

$$\frac{dK}{dt} < \alpha_K + \frac{\beta_1 B_1 B_2}{1 + \gamma_1 S_M^{\min}} + \frac{\beta_2 B_1 B_2}{1 + \gamma_2 S_M^{\min}} - \mu_K K = \mu_K B_3 - \mu_K K.$$

Employing the same comparison principle, we have obtained:

$$0 < K(t) < B_3(1 - e^{-\mu_K t}) + K(0)e^{-\mu_K t} \implies K(t) \leq B_3 \text{ if } K(0) \leq B_3. \tag{3.2.6}$$

Hence, all the solutions $\big(T(t), D(t), K(t), S_M(t)\big)^{\mathrm{T}}$ of system (3.1.2) that start in the region Γ, remain within it. This evidently implies, Γ is invariant set for the system (3.1.2). Furthermore, the set Γ is bounded and therefore all solutions of the system (3.1.2) are eventually bounded. It is noteworthy that in this case, any solution of system (3.1.2) with non-negative

initial conditions eventually enters and remains inside the set Γ. This property is justified by the definition of the set Γ and the subsequent relationships:

$$\left.\frac{dT(t)}{dt}\right|_{\partial\Gamma} < 0, \qquad \left.\frac{dD(t)}{dt}\right|_{\partial\Gamma} < 0, \quad \left.\frac{dK(t)}{dt}\right|_{\partial\Gamma} < 0, \qquad \left.\frac{dS_M(t)}{dt}\right|_{\partial\Gamma} < 0, \tag{3.2.7}$$

which are actually performed at the points of the boundary $\partial\Gamma$ of Γ. Also, note that, these relationships in (3.2.7) hold outside the set Γ, which guarantees the boundedness of all solutions of the system (3.1.2) along with the positive initial conditions.

3.2.2 Feasibility of Positive Equilibrium

To find the interior equilibrium point $E^*(T^*, D^*, K^*, S_M^*)$ we set all the equations of the system (3.1.2) to zero and solve for the state variables when its co-ordinates satisfy the conditions : $T^* > 0$, $D^* > 0$, $K^* > 0$ and $S_M^* > 0$. From the fourth equation of the system (3.1.2), we get:

$$S_M^* = \frac{\alpha_{S_M}}{\mu_{S_M}}.$$

Using the value of S_M^*, we have chosen two constants $\mathcal{P}_1$ and $\mathcal{P}_2$ in order to simplify the computation, which are given by

$$\mathcal{P}_1 = \frac{\beta_1}{1+\gamma_1 S_M^*} \quad \text{and} \quad \mathcal{P}_2 = \frac{\beta_2}{1+\gamma_2 S_M^*}.$$

Following that, we determined the values of D^* and K^* in terms of T^* by using the aforementioned values and setting the second equation of the system (3.1.2) to zero, which are provided by

$$D^* = \frac{\alpha_D}{\mu_D + \mathcal{P}_2 T^*}, \quad K^* = \frac{\alpha_K}{\mu_K} + \frac{\alpha_D(\mathcal{P}_1+\mathcal{P}_2)T^*}{\mu_K(\mu_D+\mathcal{P}_2 T^*)}. \tag{3.2.8}$$

Setting the first equation of the system (3.1.2) to zero and substituting these values of state variables into the equation, we have obtained a cubic equation of T^*.

$$T^{*3} + A_1 T^{*2} + A_2 T^* + A_3 = 0, \tag{3.2.9}$$

$$\begin{aligned}
\text{where } A_1 &= \frac{1}{\eta\mu_K\mathcal{P}_2}\Big[\eta\mu_K\mu_D + \Big\{\big(\xi\alpha_K + \mu_T\mu_K - \eta\mu_K\big)\mathcal{P}_2 + \alpha_D\xi\big(\mathcal{P}_1+\mathcal{P}_2\big)\Big\}T^{\max}\Big],\\
A_2 &= \frac{1}{\eta\mu_K\mathcal{P}_2}\Big[\xi\alpha_K\mu_D - \eta\mu_D\mu_K + \mu_T\mu_D\mu_K + \alpha_D\mu_K\mathcal{P}_1 - \alpha_T\mu_K\mathcal{P}_2\Big]T^{\max},\\
A_3 &= -\frac{\alpha_T\mu_D T^{\max}}{\eta\mathcal{P}_2}.
\end{aligned}$$

Using the parameter values listed in Table (3.1), we have observed that $A_1 > 0$ is positive and $A_2 < 0$ and $A_3 < 0$ are negative. By Descartes' rule of sign the system (3.2.9) has exactly one positive root. By substituting the value of T^* in (3.2.8), we can determine the interior

equilibrium point $E^*(T^*, D^*, K^*, S_M^*)$.

3.2.3 Stability Analysis of Interior equilibrium

The local stability analysis of the interior equilibrium point $E^* = (T^*, D^*, K^*, S_M^*)$ has been examined here. The Jacobian matrix calculated at the interior equilibrium point E^* is provided by

$$J(E^*) = \begin{pmatrix} -(\frac{\alpha_T}{T^*} + \frac{\eta T^*}{T^{\max}}) & -\mathcal{P}_1 T^* & -\xi T^* & \frac{\mathcal{P}_1^2 \gamma_1 T^* D^*}{\beta_1} \\ -\mathcal{P}_2 D^* & -\frac{\alpha_D}{D^*} & 0 & \frac{\mathcal{P}_2^2 \gamma_2 T^* D^*}{\beta_2} \\ (\mathcal{P}_1 + \mathcal{P}_2) D^* & (\mathcal{P}_1 + \mathcal{P}_2) T^* & -\mu_K & -(\frac{\mathcal{P}_1^2 \gamma_1 T^* D^*}{\beta_1} + \frac{\mathcal{P}_2^2 \gamma_2 T^* D^*}{\beta_2}) \\ 0 & 0 & 0 & -\mu_M \end{pmatrix}.$$

The eigenvalues of the above Jacobian matrix determine the stability criterion of the dynamical system at the equilibrium point E^*. The characteristic equation of the matrix J is given by

$$(\lambda + \mu_M)(\lambda^3 + C_1\lambda^2 + C_2\lambda + C_3) = 0, \tag{3.2.10}$$

where the coefficients are

$$\begin{aligned} C_1 =& \Big(\frac{\alpha_T}{T^*} + \frac{\eta T^*}{T^{\max}}\Big) + \frac{\alpha_D}{D^*} + \mu_K, \\ C_2 =& \Big(\frac{\alpha_D}{D^*} + \mu_K\Big)\Big(\frac{\alpha_T}{T^*} + \frac{\eta T^*}{T^{\max}}\Big) + \frac{\alpha_D \mu_K}{D^*} - \mathcal{P}_1\mathcal{P}_2 T^* D^* + \xi\Big(\mathcal{P}_1 + \mathcal{P}_2\Big) T^* D^*, \\ C_3 =& \xi T^*\Big(\mathcal{P}_1 + \mathcal{P}_2\Big)\Big(\alpha_D - \mathcal{P}_2 T^* D^*\Big) + \frac{\alpha_D \mu_K}{D^*}\Big(\frac{\alpha_T}{T^*} + \frac{\eta T^*}{T^{\max}}\Big) - \mu_K \mathcal{P}_1 \mathcal{P}_2 T^* D^*. \end{aligned}$$

Here $C_1 > 0$ and $C_1C_2 - C_3 > 0$, applying the Routh Hurwitz criterion [63], we deduce that all the roots of the equation (3.2.10) is either negative or have negative real parts. We construct the following lemma based on the aforementioned considerations.

Lemma 3.2.1 *The interior equilibrium point $E^*(T^*, D^*, K^*, S_M^*)$ of system (3.1.2) is locally asymptotically stable if the following inequality holds*

$$\max\left\{\left(\frac{\alpha_T}{T^*} + \frac{\eta T^*}{T^{\max}}\right), \left(\frac{\alpha_D}{D^*} - \mathcal{P}_2 T^*\right)\right\} < C_1 < 1.$$

3.3 Optimal Control using TNF-α Inhibitor

The optimal control approach is a powerful mathematical tool for developing and managing treatment policies for various diseases through modeling and system analysis. It is crucial for addressing drug resistance in long-term disease treatment by enabling strategic planning, improving therapies, and evaluating cost-effectiveness. This technique facilitates the creation of precise, individualized treatment regimens by determining time-dependent control functions over specific intervals.

In the context of psoriasis, the interaction rate between T cells and DCs is amplified by the cytokine TNF-α, resulting in the abnormal proliferation of keratinocytes. Effective

control of psoriasis requires the regulation of keratinocyte overgrowth, which is the primary pathological feature of this condition.

In this section, we have examined our formulated mathematical model by introducing one control function, $u(t)$, where $u(t)$ is a permissible control representing the effect of TNF-α inhibitor that can restrict the reaction rates between T cells and dendritic cells. Therefore, the model (3.1.2) equipped with optimum control is governed by the following set of equations for the specified time interval $[t_s, t_f]$.

$$\begin{aligned}
\frac{dT(t)}{dt} &= \alpha_T + \eta T(t)\Big(1 - \frac{T(t)}{T^{max}}\Big) - \frac{\beta_1\big(1-u(t)\big)T(t)D(t)}{1+\gamma_1 S_M(t)} - \xi T(t)K(t) - \mu_T T(t),\\
\frac{dD(t)}{dt} &= \alpha_D - \frac{\beta_2\big(1-u(t)\big)T(t)D(t)}{1+\gamma_2 S_M(t)} - \mu_D D(t),\\
\frac{dK(t)}{dt} &= \alpha_K + \frac{\beta_1\big(1-u(t)\big)T(t)D(t)}{1+\gamma_1 S_M(t)} + \frac{\beta_2\big(1-u(t)\big)T(t)D(t)}{1+\gamma_2 S_M(t)} - \mu_K K(t),\\
\frac{dS_M(t)}{dt} &= \alpha_{S_M} - \mu_{S_M} S_M(t),
\end{aligned} \tag{3.3.1}$$

with the initial conditions given by

$$T(0) = T_0 > 0, D(0) = D_0 > 0, K(0) = K_0 > 0, S_M(0) = S_{M_0} > 0.$$

3.3.1 Description of Objective functional

The problem is in minimizing the objective cost functionally expressed as follows:

$$\mathcal{J}(u(t)) = \int_{t_s}^{t_f} \Big[K(t) + \mathcal{W}u^2(t)\Big]dt, \tag{3.3.2}$$

subject to the optimal control induced system (3.3.1). Since, our aim is to suppress the keratinocytes using TNF-α inhibitor with minimum cost; the control function $u(t)$ represents the effect of the TNF-α inhibitor and $\mathcal{W}$ is the positive weight constant on the benefit of the cost of the TNF-α inhibitor. The control set is defined on the interval $[t_s, t_f]$, where t_s and t_f stand for the treatment's starting and finishing times of control. Let us define the control set of Lebesgue measurable functions as follows:

$$\mathcal{U} = \Big\{u(t) : u(t) \text{ is defined on } [t_s, t_f],\ 0 \le u(t) \le u^{\max} < 1,\ t \in [t_s, t_f]\Big\}.$$

To determine the optimal control function, $u^*(t)$ for the system (3.3.1), we have:

$$\mathcal{J}(u^*(t)) = \min\Big\{\mathcal{J}(u(t)) : u(t) \in \mathcal{U}\Big\}. \tag{3.3.3}$$

We applied Pontryagin's Minimum Principle [64] to derive the necessary conditions for solving the optimal control problem. Within this framework, the system (3.3.1) governed by the optimal control admits non-negative and bounded solutions, provided the bounded and Lebesgue measurable control function with the positive initial conditions.

3.3.2 Optimal control's Characteristics

For characterization of optimal control, we apply Pontryagin's Minimum Principle [64]. In order to do this, let us define the Hamiltonian $\mathcal{H}$ for the control problem (3.3.1) as:

$$\begin{aligned}\mathcal{H} = K(t) + \mathcal{W}u^2(t) + \Theta_1(t)\Bigg[\alpha_T + \eta T(t)\Big(1 - \frac{T(t)}{T^{max}}\Big) - \frac{\beta_1(1-u(t))T(t)D(t)}{1+\gamma_1 S_M(t)} \\ - \xi T(t)K(t) - \mu_T T(t)\Bigg] + \Theta_2(t)\Bigg[\alpha_D - \frac{\beta_2(1-u(t))T(t)D(t)}{1+\gamma_2 S_M(t)} - \mu_D D(t)\Bigg] \\ + \Theta_3(t)\Bigg[\alpha_K + \frac{\beta_1(1-u(t))T(t)D(t)}{1+\gamma_1 S_M(t)} + \frac{\beta_2(1-u(t))T(t)D(t)}{1+\gamma_2 S_M(t)} - \mu_K K(t)\Bigg] \\ + \Theta_4(t)\Bigg[\alpha_{S_M} - \mu_{S_M} S_M(t)\Bigg],\end{aligned} \tag{3.3.4}$$

where $\Theta_i(t)$'s $(i = 1, 2, 3, 4)$ are the adjoint variables to be determined suitably.

The adjoint system with transversality criteria $\Theta_i(t_f) = 0$ for $i = 1, 2, 3, 4$ can be obtained by using Pontryagin's Minimum Principle.

$$\frac{d\Theta_1}{dt} = -\frac{\partial \mathcal{H}}{\partial T}, \ \frac{d\Theta_2}{dt} = -\frac{\partial \mathcal{H}}{\partial D}, \ \frac{d\Theta_3}{dt} = -\frac{\partial \mathcal{H}}{\partial K}, \ \frac{d\Theta_4}{dt} = -\frac{\partial \mathcal{H}}{\partial S_M}.$$

The optimality of the system (3.3.1) consists of the optimal control and corresponding states, thus the adjoint system takes the form:

$$\begin{aligned}\frac{d\Theta_1}{dt} &= -\Theta_1\Bigg[\eta\Big(1 - \frac{2\mathcal{T}}{T^{\max}}\Big) - \frac{\beta_1(1-u^*)\mathcal{D}}{1+\gamma_1\mathcal{S}_\mathcal{M}} - \xi\mathcal{K} - \mu_T\Bigg] + \Theta_2\Bigg[\frac{\beta_2(1-u^*)\mathcal{D}}{1+\gamma_2\mathcal{S}_\mathcal{M}}\Bigg] \\ &\quad - \Theta_3\Bigg[\frac{\beta_1(1-u^*)\mathcal{D}}{1+\gamma_1\mathcal{S}_\mathcal{M}} + \frac{\beta_2(1-u^*)\mathcal{D}}{1+\gamma_2\mathcal{S}_\mathcal{M}}\Bigg], \\ \frac{d\Theta_2}{dt} &= \Theta_1\Bigg[\frac{\beta_1(1-u^*)\mathcal{T}}{1+\gamma_1\mathcal{S}_\mathcal{M}}\Bigg] + \Theta_2\Bigg[\frac{\beta_2(1-u^*)\mathcal{T}}{1+\gamma_2\mathcal{S}_\mathcal{M}} + \mu_D\Bigg] - \Theta_3\Bigg[\frac{\beta_1(1-u^*)\mathcal{T}}{1+\gamma_1\mathcal{S}_\mathcal{M}} + \frac{\beta_2(1-u^*)\mathcal{T}}{1+\gamma_2\mathcal{S}_\mathcal{M}}\Bigg], \\ \frac{d\Theta_3}{dt} &= -1 + \Theta_1\xi\mathcal{T} + \Theta_3\mu_K, \\ \frac{d\Theta_4}{dt} &= -\Theta_1\Bigg[\frac{\gamma_1\beta_1(1-u^*)\mathcal{T}\mathcal{D}}{(1+\gamma_1\mathcal{S}_\mathcal{M})^2}\Bigg] - \Theta_2\Bigg[\frac{\gamma_2\beta_2(1-u^*)\mathcal{T}\mathcal{D}}{(1+\gamma_2\mathcal{S}_\mathcal{M})^2}\Bigg] \\ &\quad + \Theta_3\Bigg[\frac{\gamma_1\beta_1(1-u^*)\mathcal{T}\mathcal{D}}{(1+\gamma_1\mathcal{S}_\mathcal{M})^2} + \frac{\gamma_2\beta_2(1-u^*)\mathcal{T}\mathcal{D}}{(1+\gamma_2\mathcal{S}_\mathcal{M})^2}\Bigg] + \Theta_4\mu_{S_M},\end{aligned} \tag{3.3.5}$$

with transversality conditions $\Theta_i(t_f) = 0$ for all $i = 1, 2, 3, 4$. We now determine the optimal control $u^*(t)$, using the optimality condition provided by

$$\left.\frac{\partial \mathcal{H}}{\partial u}\right|_{u=u^*(t)} = 0. \tag{3.3.6}$$

Differentiating the equation (3.3.4), partially with respect to u and using the condition

(3.3.6) we get:

$$u^*(t) = \frac{1}{2\mathcal{W}}\left[\Theta_3\left(\frac{\beta_1\mathcal{T}\mathcal{D}}{1+\gamma_1\mathcal{S}_\mathcal{M}} + \frac{\beta_2\mathcal{T}\mathcal{D}}{1+\gamma_2\mathcal{S}_\mathcal{M}}\right) - \Theta_1\left(\frac{\beta_1\mathcal{T}\mathcal{D}}{1+\gamma_1\mathcal{S}_\mathcal{M}}\right) - \Theta_2\left(\frac{\beta_2\mathcal{T}\mathcal{D}}{1+\gamma_2\mathcal{S}_\mathcal{M}}\right)\right]$$
$$= \Phi(t) \text{ (say)}.$$

Now, by applying the standard boundedness condition for control and using the properties of the control set $\mathcal{U}$, we assume that the admissible control satisfies

$$0 \leq u(t) \leq u^{\max} < 1.$$

This means that the control function $u(t)$ always takes values within the interval $[0, u^{\max}]$, where $u^{\max}$ is strictly less than one. Hence, we obtain:

$$u^*(t) = \begin{cases} 0, & \text{when} \quad \Phi(t) \leq 0 \\ \Phi(t), & \text{when} \quad 0 \leq \Phi(t) \leq u^{\max} \\ u^{\max}, & \text{when} \quad \Phi(t) \geq u^{\max}. \end{cases} \tag{3.3.7}$$

Based on the analysis for the control-induced model, we derive the following theorem:

Theorem 1 *If the objective cost functional $\mathcal{J}(u)$ attains its minimum value for the optimal control $u^*(t)$ and $(\mathcal{T}, \mathcal{D}, \mathcal{K}, \mathcal{S}_\mathcal{M})$ is the corresponding optimal state for the optimal control problem (3.3.1), then there exist adjoint functions $\Theta_i(t)$ $(i = 1, 2, 3, 4)$ satisfying the transversality conditions $\Theta_i(t_f) = 0$, for $i = 1, 2, 3, 4$. Furthermore, the optimal control solution is given by*

$$u^*(t) = \max\left\{0, \min\{1, \Phi(t)\}\right\}.$$

3.4 Impulsive MSC Replacement on the Control Induced System

MSC is considered as a population in our proposed mathematical model stated in system (3.1.2). We have already used the optimal control strategy mathematically with a biologic TNF-α inhibitor from the initial phase of the treatment of the disease psoriasis by employing the system (3.3.1). In cases where the disease severity is high and the TNF-α inhibitor is not effective in eradicating the disease completely, stem cell replacement therapy will be used in conjunction with the biologic TNF-α inhibitor. A patient with severe psoriasis requires replacement MSC, possibly for complete eradication of the disease, because long-term psoriasis causes a deficit of mature stem cells in the affected part. In stem cell therapies, an intravenous infusion of MSC from the outside of the body is often administered to the patient's affected region to fill this deficiency. Due to this reason, we rely on an impulsive approach [65]. This approach involves administering a certain amount of MSC periodically, at a certain time interval, into the patient's affected region during the course of treatment. The model presented below is almost equivalent to system (3.1.2). The dynamics of cell

therapy can be modelled using impulsive differential equations.

$$\begin{aligned}
\frac{dT(t)}{dt} &= \alpha_T + \eta T(t)\Big(1 - \frac{T(t)}{T^{max}}\Big) - \frac{\beta_1\big(1-u^*\big)T(t)D(t)}{1+\gamma_1 S_M(t)} - \xi T(t)K(t) - \mu_T T(t),\\
\frac{dD(t)}{dt} &= \alpha_D - \frac{\beta_2\big(1-u^*\big)T(t)D(t)}{1+\gamma_2 S_M(t)} - \mu_D D(t),\\
\frac{dK(t)}{dt} &= \alpha_K + \frac{\beta_1\big(1-u^*\big)T(t)D(t)}{1+\gamma_1 S_M(t)} + \frac{\beta_2\big(1-u^*\big)T(t)D(t)}{1+\gamma_2 S_M(t)} - \mu_K K(t),\\
\frac{dS_M(t)}{dt} &= \alpha_{S_M} - \mu_{S_M} S_M(t),\\
S_M(n\tau) &= \delta + S_M(n\tau)^-,
\end{aligned} \tag{3.4.1}$$

where 'δ' represents the average quantity of MSCs administered, and 'τ' denotes the time interval between successive infusions. Each dose, containing a fixed amount δ, is infused into the inflamed region at intervals of τ, for a total of 'n' ($n\tau \le t < (n+1)\tau, \quad n \in \mathbb{N} \cup \{0\}$) impulsive infusions. $S_M(n\tau)^-$ represents the population value just before receiving the next input of MSC, i.e., just before $t = n\tau$.

The production of MSC in the affected region is at an extremely low constant rate. We investigate the effects of pulsed treatment strategy with MSC in this model both mathematically and numerically. However, a restricted number of MSC infusions are feasible for use in clinical trials. These infusions typically involve dosage amounts ranging from (1-6) $\times 10^6/kg$ of body weight. The infusions are administered five to six times, with intervals of 7 to 15 days between each administration throughout the course of treatment [22].

The solution of the last equation of the system (3.4.1) is of the following form.

$$S_M(t) = \frac{\alpha_{S_M}}{\mu_{S_M}} + Ce^{-\mu_{S_M} t},$$

where C is a constant to be determined using the following initial condition.

When $0 \le t < \tau$,

$$\begin{cases} \frac{dS_M}{dt} = \alpha_{S_M} - \mu_{S_M} S_M, \\ S_M(0) = \delta \end{cases} \implies C = \Big(\delta - \frac{\alpha_{S_M}}{\mu_{S_M}}\Big).$$

$$\text{Therefore,} \quad S_M(t) = \frac{\alpha_{S_M}}{\mu_{S_M}} + \Big(\delta - \frac{\alpha_{S_M}}{\mu_{S_M}}\Big)e^{-\mu_{S_M} t}. \tag{3.4.2}$$

$$\text{Now,} \quad S_M(\tau) = S_M(\tau)^- + \delta = \frac{\alpha_{S_M}}{\mu_{S_M}} + \delta(1 + e^{-\mu_{S_M}\tau}) - \frac{\alpha_{S_M}}{\mu_{S_M}} e^{-\mu_{S_M}\tau}.$$

We examine the system at each time interval because the MSC population's initial condition changes over time.

When $\tau \le t < 2\tau$,

$$\begin{cases} \frac{dS_M}{dt} = \alpha_{S_M} - \mu_{S_M} S_M, \\ S_M(\tau) = \frac{\alpha_{S_M}}{\mu_{S_M}} + \delta(1 + e^{-\mu_{S_M}\tau}) - \frac{\alpha_{S_M}}{\mu_{S_M}} e^{-\mu_{S_M}\tau} \end{cases} \implies C = \left[\delta(1+e^{-\mu_{S_M}\tau}) - \frac{\alpha_{S_M}}{\mu_{S_M}} e^{-\mu_{S_M}\tau}\right] e^{\mu_{S_M}\tau}.$$

$$\text{Therefore,} \quad S_M(t) = \frac{\alpha_{S_M}}{\mu_{S_M}} + \left[\delta(1 + e^{-\mu_{S_M}\tau}) - \frac{\alpha_{S_M}}{\mu_{S_M}} e^{-\mu_{S_M}\tau}\right] e^{-\mu_{S_M}(t-\tau)}. \tag{3.4.3}$$

$$\text{Now,} \quad S_M(2\tau) = S_M(2\tau)^- + \delta = \frac{\alpha_{S_M}}{\mu_{S_M}} + \delta(1 + e^{-\mu_{S_M}\tau} + e^{-2\mu_{S_M}\tau}) - \frac{\alpha_{S_M}}{\mu_{S_M}} e^{-2\mu_{S_M}\tau}.$$

Continuing this process up to the nth iteration, we have:

When $n\tau \leq t < (n+1)\tau$,

$$\begin{cases} \frac{dS_M}{dt} = \alpha_{S_M} - \mu_{S_M} S_M, \\ S_M(n\tau) = \frac{\alpha_{S_M}}{\mu_{S_M}} + \delta(1 + e^{-\mu_{S_M}\tau} + e^{-2\mu_{S_M}\tau} + \ldots\ldots + e^{-n\mu_{S_M}\tau}) - \frac{\alpha_{S_M}}{\mu_{S_M}} e^{-n\mu_{S_M}\tau}. \end{cases}$$

$$\implies C = \left[\delta(1 + e^{-\mu_{S_M}\tau} + e^{-2\mu_{S_M}\tau} + \ldots\ldots + e^{-n\mu_{S_M}\tau}) - \frac{\alpha_{S_M}}{\mu_{S_M}} e^{-n\mu_{S_M}\tau}\right] e^{\mu_{S_M}\tau}.$$

Therefore, the concentration of MSC after $n - th$ infusion is given by

$$\begin{aligned} S_M(t) &= \frac{\alpha_{S_M}}{\mu_{S_M}} + \left[\delta(1 + e^{-\mu_{S_M}\tau} + e^{-2\mu_{S_M}\tau} + \ldots\ldots + e^{-n\mu_{S_M}\tau}) - \frac{\alpha_{S_M}}{\mu_{S_M}} e^{-n\mu_{S_M}\tau}\right] e^{-\mu_{S_M}(t-n\tau)} \\ &= \frac{\alpha_{S_M}}{\mu_{S_M}} + \left[\delta\left(\frac{1 - e^{-(n+1)\mu_{S_M}\tau}}{1 - e^{-\mu_{S_M}\tau}}\right) - \frac{\alpha_{S_M}}{\mu_{S_M}} e^{-n\mu_{S_M}\tau}\right] e^{-\mu_{S_M}(t-n\tau)} \\ &\to \frac{\alpha_{S_M}}{\mu_{S_M}} + \left[\frac{\delta e^{-\mu_{S_M}(t-n\tau)}}{1 - e^{-\mu_{S_M}\tau}}\right] \quad \text{as} \quad n \to \infty. \end{aligned} \tag{3.4.4}$$

Our analytical results and numerical findings have demonstrated that pulsed cell therapy can effectively treat severe forms of the disease in combination with a TNF-α inhibitor under optimal control approach. We have also demonstrated how the entire system dynamics will change with this combined control approach numerically.

3.5 Numerical Simulation

In this section, we have performed several types of numerical simulations of our proposed mathematical model of psoriasis described in systems (3.1.2), (3.3.1), and (3.4.1) to validate our analytical results. The initial values have been chosen for the system populations satisfy the biological hypothesis based on the theoretical analyses. The values of the parameters utilized here are depicted in Table 3.1.

In Figure 3.2, we have plotted the time series solution of the proposed system (3.1.2) for various initial conditions of the cell populations. We have observed the rising trend of keratinocyte populations while MSC counts have been sharply declining, and T cell and dendritic cell counts will eventually reach saturation to some extent. This figure demonstrated the stability of the endemic equilibrium point E^*, which justified the analytic outcome of the asymptotic stability of the psoriatic state. This simulation reflects the behaviour of disease progression in the absence of any control or pulsed treatment.

In Figure 3.3, we have plotted two different $3D$ phase portraits of system (3.1.2) by taking three populations at a time for different initial values of model populations. The trajectories

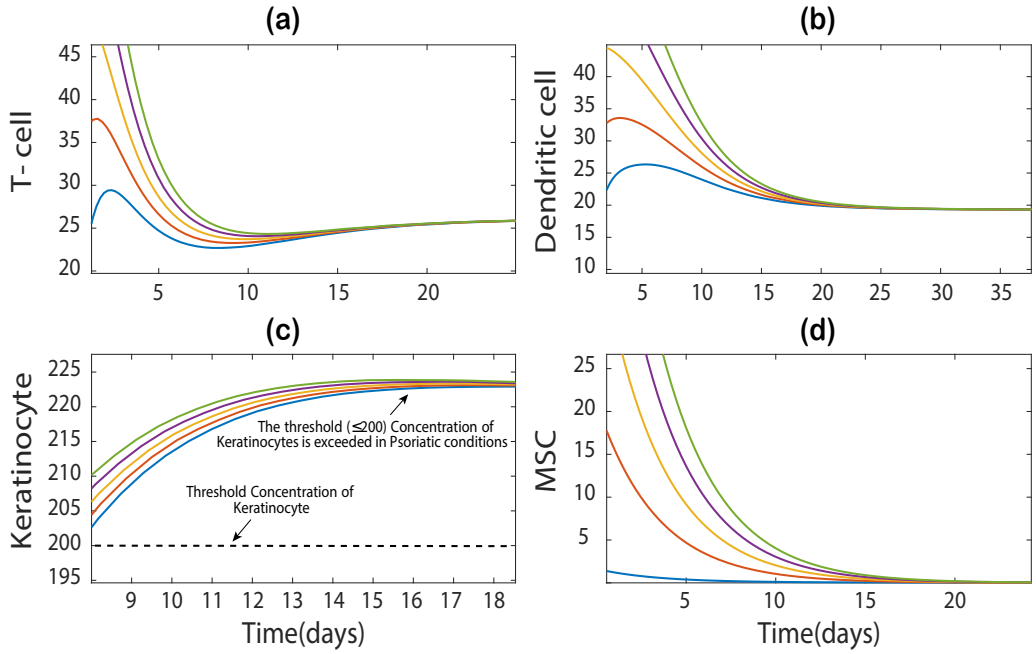

Figure 3.2: Simulation of the system (3.1.2) showing system boundedness and convergence of solutions with various initial conditions to the endemic equilibrium point E^* for (a) T cells (b) Dendritic cells (c) Keratinocytes and (d) Mesenchymal stromal cells using the parameter values given in Table (3.1).

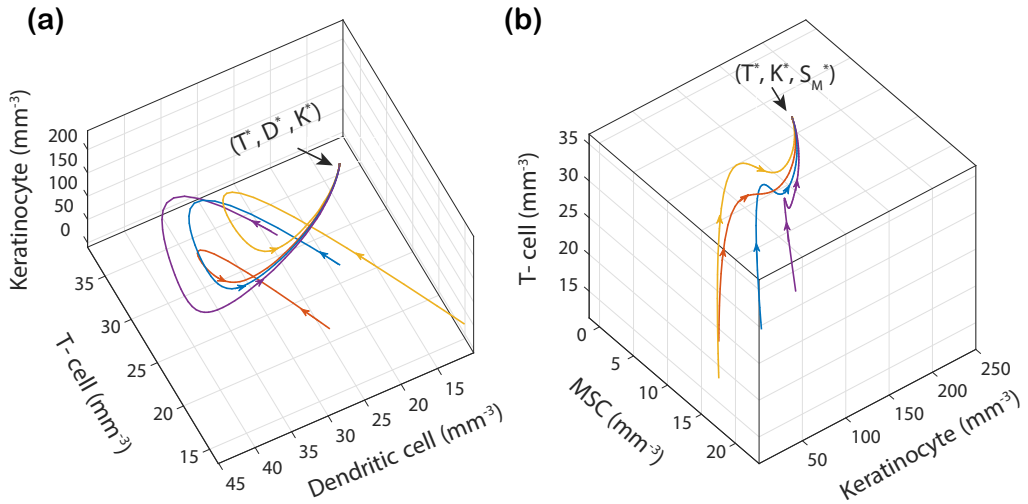

*Figure 3.3: Identifying the endemic equilibrium $E^*(T^*, D^*, K^*, S_M^*)$ of system (3.1.2) by stability analysis of the system employing two groups of cell populations: **(a)** Considering three types of cells (T cell, Dendritic cell and Keratinocyte); **(b)** Considering three sorts of cells (Keratinocyte, Mesenchymal stromal cell and T cell).*

Parameter	Definition	Value	Reference
α_T	Constant accumulation of T cells	25 $\text{mm}^{-3}d^{-1}$	[53]
α_D	Constant accumulation of dendritic-cells	18 $\text{mm}^{-3}d^{-1}$	[40]
α_K	Constant accumulation of keratinocytes	30 $\text{mm}^{-3}d^{-1}$	[53]
β_1	T cell activation rate in response to dendritic cells	0.025 mm^3d^{-1}	[66]
β_2	Dendritic cell activation rate in response to T cells	0.03 mm^3d^{-1}	[66]
γ_1	Inhibition rate of the response of DCs to T cells via MSCs	0.035 mm^3	chosen
γ_2	Inhibition rate of the response of T cells to DCs via MSCs	0.25 mm^3	chosen
η	Proliferation rate of T cells	0.03 d^{-1}	[40, 66]
ξ	Inhibition rate of T cells by keratinocytes	0.003 mm^3d^{-1}	[54]
$T^{\max}$	Maximum carrying capacity of the T cell population	300 mm^{-3}	[52, 43]
μ_T	Mortality rate of T cells	0.06 d^{-1}	[40, 53]
μ_D	Mortality rate of dendritic cells	0.15 d^{-1}	[40, 53]
μ_K	Mortality rate of keratinocytes	0.26 d^{-1}	[40, 43]
α_{S_M}	Constant production of MSCs in the inflamed area	0.0033 $\text{mm}^{-3}d^{-1}$	[41]
μ_{S_M}	Sum of natural mortality and absorption rate of MSCs	0.3 d^{-1}	[53]

Table 3.1: In numerical simulations, the values of the system parameter are employed. We have sourced a few parameter ranges from the literature to help us choose the parameter values. Numerous model parameters were determined from various literature, which allowed for the biological viability of the model behavior.

in Figure 3.3(a) converge to a unique point $E_1^*(26.43, 17.44, 224.29)$ for various initial values of T cells, dendritic cells, and keratinocytes. Similarly, in Figure 3.3(b), keratinocytes, MSCs, and T cells converge to a certain equilibrium state, $E_2^*(26.43, 224.29, 0.34)$. Since it is quite difficult to evaluate the endemic equilibrium analytically, this figure allows us to estimate the endemic equilibrium point $E^*(26.43, 17.44, 224.29, 0.34)$ numerically.

To observe the effect of the optimum control $u^*(t)$ with respect to a TNF-α inhibitor, we have solved the optimal control problem for the mathematical system (3.3.1) numerically by taking the objective functional (3.3.2) and system (3.3.3). In a healthy state, the normal concentration of keratinocytes is considered to be $K^{\sim} = 200\ mm^{-3}$ [52].

In Figure 3.4, we have plotted T cell, dendritic cell and keratinocyte populations with respect to time without optimal control and considered three fixed values ($u = 0.55,\ 0.64,\ 0.7$) of u for the control-induced mathematical model (3.3.1). This figure demonstrates that, although T cell and dendritic cell concentrations rose with the higher values of the control parameter u, the keratinocyte concentrations approached a state that is considerably closer to the healthy state. Even if this option would probably make psoriatic symptoms easier to manage, the disease is not in remission since the concentration of keratinocytes is still

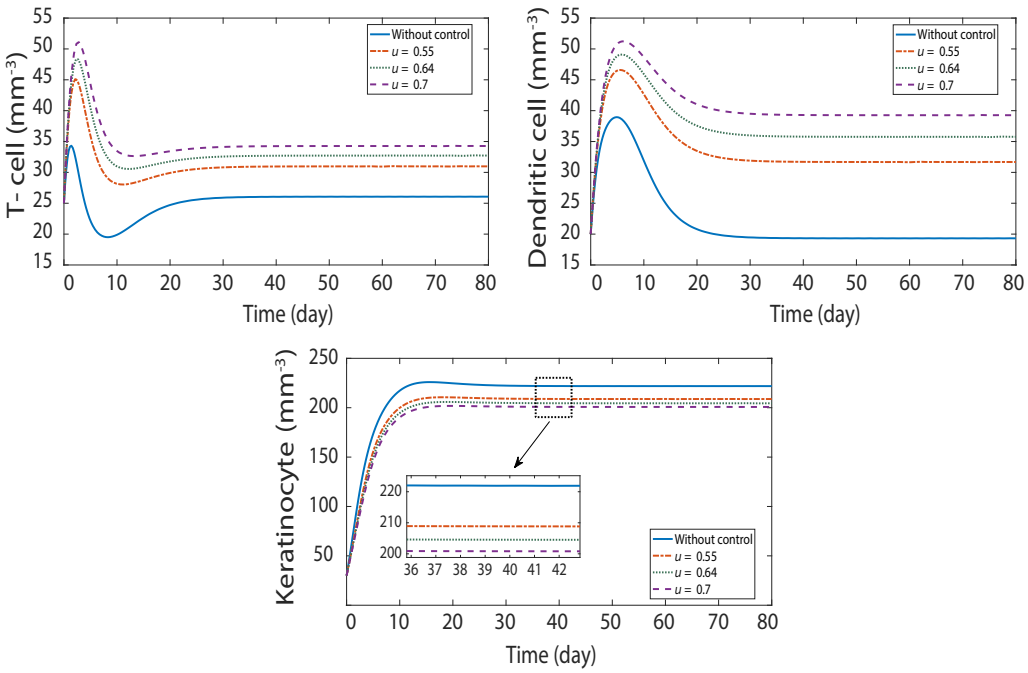

Figure 3.4: Dynamical behavior of T cells, dendritic cells, and keratinocytes in System (3.3.1) for several fixed values of the control variable.

above the threshold value of 200 mm^{-3}. As a result, we need to provide the optimal control strategy for this situation.

In Figure 3.5, we have plotted both the systems of ODEs, without control and with optimal control, where the optimal value of the control function $u(t)$ is $u^{\max} = 0.86$. This allows us to see how treatment with a biologic TNF-α inhibitor reduces keratinocyte density. According to clinical investigations, keratinocyte hyper-proliferation can be effectively reduced by TNF-α inhibitor treatment [67]. However, in the severe form of the disease, this approach will not be enough to reach the keratinocyte density below the threshold $K^{\sim} = 200\ mm^{-3}$.

In Figure 3.6, we have plotted the dynamics of the control function, $u(t)$ described in system (3.3.7), with respect to time using MATLAB. This figure demonstrates that at the initial stage of treatment, it required high doses of a TNF-α inhibitor to control the disease. After that, the dose decreases over time until 74 days. Later, we noticed a significant rise in the control function between 75 and 78 days, depending on the severity of the disease. Then the trajectory gradually decreases, even though the keratinocyte concentration has not reached the desired threshold value of $K^{\sim}$.

In a severe psoriatic scenario, when treatment with a TNF-α inhibitor is unable to yield the desired outcomes, we performed stem cell replacement in combination with TNF-α inhibitor (MSCs derived from the umbilical cord is the best). We have started this approach mathematically and numerically after 80 days of observation of the disease treated with only a biologic TNF-α inhibitor.

In Figure 3.7, we have depicted MSC replacement with six pulsed infusions at a single

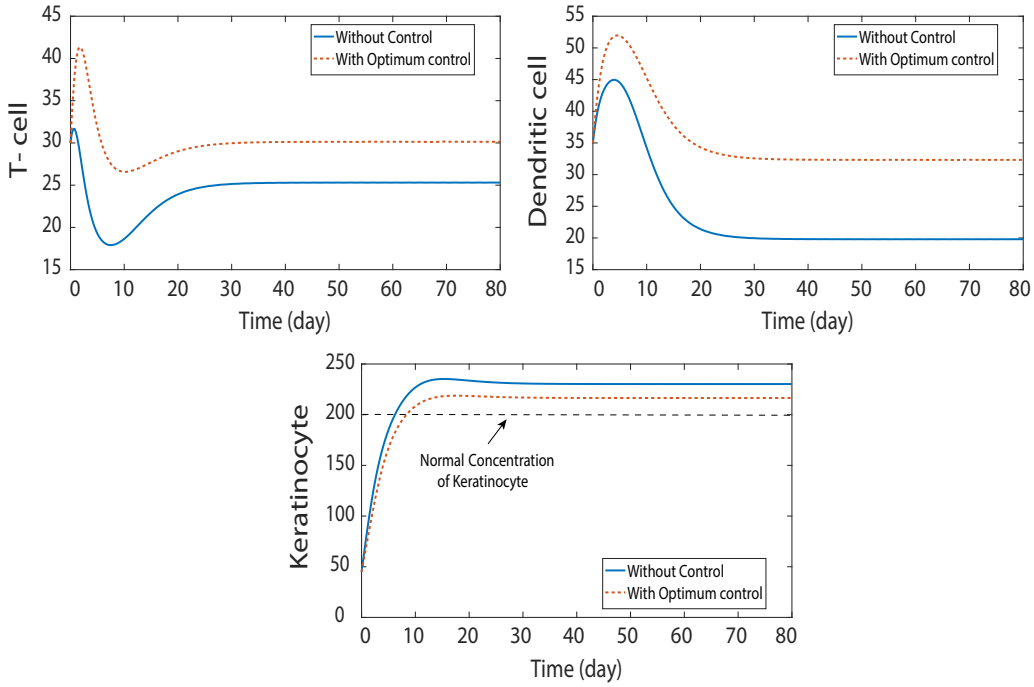

Figure 3.5: Dynamical behavior of all model populations (T cell, Dendritic cell, Keratinocyte and Mesenchymal stem cell) for psoriatic people (blue solid line) and after using optimal control (brown dotted line).

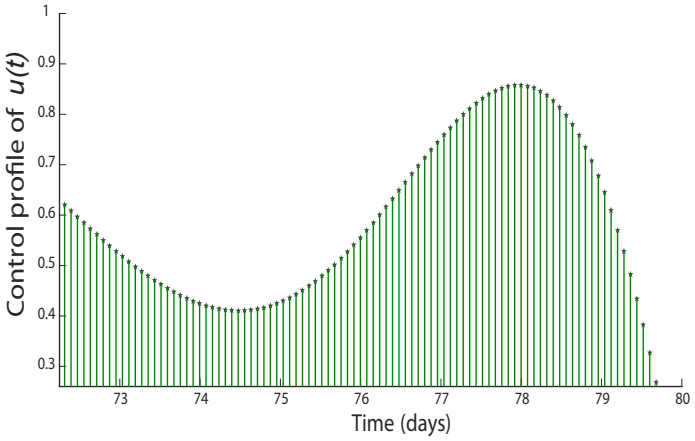

Figure 3.6: Control function $u^*(t)$ with respect to time regulated by TNF-α inhibitor.

dose of 3 cells/mm^3 (i.e., δ=3) once every 10 days simultaneously with optimum control via a TNF-α inhibitor. In this figure, the blue trajectories for the cell populations indicate the uncontrolled psoriatic state. The brown colour trajectories represent the dynamics of the cell densities, with the optimum control strategy alone using a TNF-α inhibitor. Following

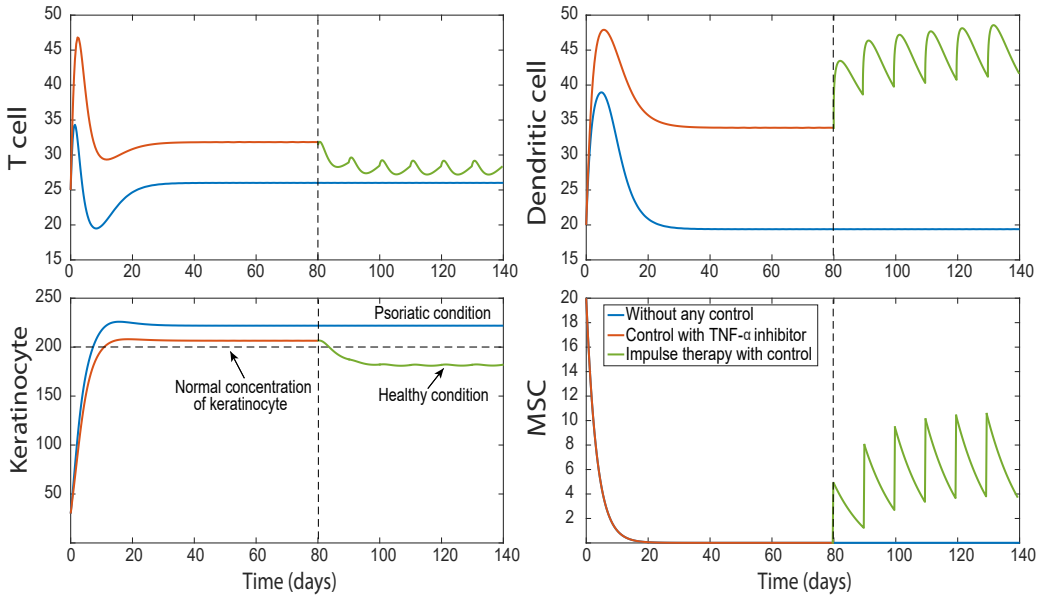

Figure 3.7: Diagrammatic representation of the model populations with optimum control and after 80 days of treatment with TNF-α inhibitor, we perform the numerical simulation of the systemic stem cell therapy simultaneously with the same biologic (i.e., TNF-α inhibitor).

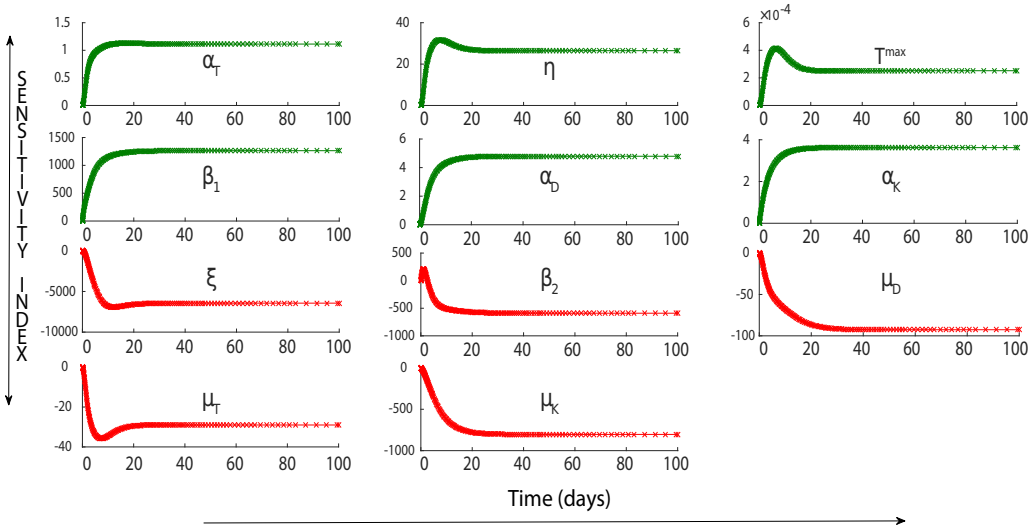

Figure 3.8: The sensitivity indices of the parameters are shown in relation to the excessive growth of the keratinocyte cell population during psoriasis formation. Green trajectories represent parameters with positive sensitivity, while red trajectories represent those with negative sensitivity.

eighty days of treatment with a TNF-α inhibitor, stem cell therapy combined with a TNF-α

inhibitor is started. The dynamics of this combined effect of MSC infusion simultaneously with TNF-α inhibitor are shown by the green colour trajectories, and it is also clearly visible via our numerical simulation that the keratinocytes rapidly decrease to the desired density levels ($\leq 200\ mm^{-3}$) in a short period. Since the differential equation for the MSC population does not depend on the TNF-α inhibitor, the trajectories of MSC with and without TNF-α inhibitor control coincide, leading to a decline in MSC levels in inflamed regions. However, with this combined therapy, T cell and dendritic cell concentrations are raised, and the MSC levels in the inflamed regions return to a normal state. It is important to note that in an impulsive approach, the population must be in an equilibrium state. Consequently, for this approximation, the implementation of treatment strategies will not be impeded.

In Figure 3.8, we have shown the sensitivity index of a few model parameters as a function of time in accordance with Saltelli et al. [68]. We have found that certain parameters are positively and a few are negatively responsive with respect to the excessive growth of the keratinocyte population. The green lines indicate those parameters that are positively sensitive, and the red lines indicate those parameters that are negatively sensitive.

3.6 Discussion and Conclusion

In this *Chapter*, we proposed a model of psoriasis focuses on cell-to-cell interactions among T cells, dendritic cells, keratinocytes, and mesenchymal stem cells (MSCs), which play an important role in regulating immune responses. Although psoriasis involves complex mechanisms such as abnormal cell differentiation and cytokine signaling, our analysis emphasizes keratinocyte hyper-proliferation as the main factor driving disease progression. MSCs are highlighted for their positive role in controlling this hyper-proliferation by producing anti-inflammatory cytokines and restoring immune balance. However, in severe cases, local MSC levels decline, and clinical studies recommend external infusion of healthy MSCs. As shown in Figure 3.7, TNF-α inhibitors alone are often insufficient, which motivates a dual-intervention strategy in our model: combining TNF-α inhibition with periodic MSC transplantation.

We study the dynamical system (3.1.2) under two approaches. First, TNF-α inhibition is analyzed through an optimal control framework in system (3.3.1). Second, the model is extended to include impulsive stem cell therapy, represented by system (3.4.1), which is applied when biologics alone fail. Simulation results show that after 80 days of TNF-α inhibition, the addition of impulsive MSC transplantation leads to a rapid reduction in keratinocyte density within two months, along with normalization of other immune cell levels and restoration of local MSC counts. In conclusion, based on our analytical and numerical results, combined therapy with MSC transplantation and TNF-α inhibition effectively controls keratinocyte hyper-proliferation. This indicates that stem cell therapy could emerge as a promising therapeutic option for severe psoriasis.

Furthermore, we extend this proposed model by developing its fractional-order counterparts to explore the memory effects among immune and skin components across different time scales. To capture the non-local dynamics more effectively, we consider three different fractional operators with varying fractional orders. This approach provides a more accurate description of psoriasis and its control, which have been explored in *Chapter* 4.

Chapter 4

Stem Cell Based Fractional-Order Dynamical Model of Psoriasis: A Mathematical Study

The complex interplay among immune and skin components across different time scales strongly shapes the disease outcome, which can be considered as a memory effect. To capture such non-local characteristics, it is important to incorporate memory effects into mathematical modeling. In this *Chapter*[4], we extend our integer-order psoriasis model (see Chapter 3, equation 3.1.2) to a fractional-order system. By using fractional derivatives, the model provides a more realistic description of autoimmune responses and cytokine-driven progression of psoriasis.

We incorporate three fractional operators: the Caputo, Caputo–Fabrizio, and Atangana–Baleanu–Caputo derivatives, represented by fractional orders λ, ζ, and $\alpha \in (0, 1]$ [27, 28, 29] into the ODE-based system. Since fractional derivatives do not follow standard dimensional rules, a scaling parameter $\mathcal{L}$, called the memory rate parameter (with unit day^{-1}), is introduced for dimensional consistency. Lower fractional orders indicate strong memory effects, whereas values close to one correspond to the classical (memory-free) case. The existence and uniqueness of solutions for the fractional model corresponding to the Atangana–Baleanu operator in the Caputo sense are examined using the Banach contraction principle, and stability is analyzed under the generalized Ulam–Hyers criteria. To study control strategies, we also formulate a fractional optimal control framework considering general fractional order involving two biologic inhibitors targeting TNF-α and IL-23. Three different control strategies are tested numerically with respect to each considered operator, and the conditions for optimality are derived through a generalized fractional optimal control problem (FOCP). The FOCP is solved using the Forward–Backward Sweep Method (FBSM), and the results highlight the distinct non-local dynamics generated by different fractional operators. The aim of this chapter is to compare the behavior of fractional and classical models and to analyze how different operators and fractional orders influence the system dynamics and

[4] *The major portion of this chapter is published in the Jambura Journal of Biomathematics (JJBM), September 2025.*

outcomes of the control effectiveness.

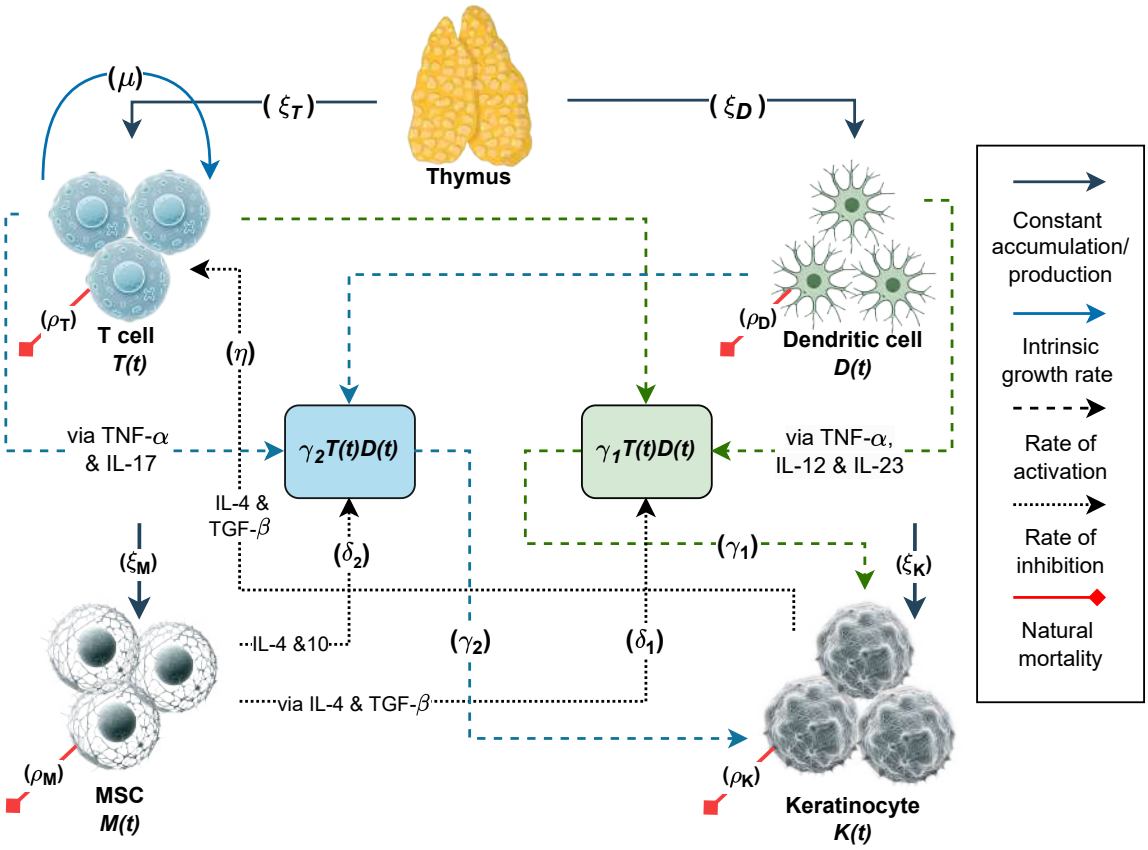

Figure 4.1: Schematic representation of the model within a cytokine network.

4.1 Fractional-Order Modelling Approach

Fractional-order derivatives, owing to their ability to capture memory effects, often yield more accurate and realistic results than traditional integer-order models. Based on the work provided in the *Chapter* 3, we extend the classical integer-order model (3.1.2) of psoriasis by incorporating three widely used fractional-order operators: the Caputo, Caputo–Fabrizio, and Atangana–Baleanu derivatives in the Caputo sense. In our model, $T(t)$, $D(t)$, $K(t)$, and $M(t)$ denote the concentrations of T cells, dendritic cells, keratinocytes, and mesenchymal stem cells (MSCs), respectively, at time t. The interactions among immune cells, keratinocytes, and MSCs, mediated by cytokines and contributing to disease progression, are illustrated in Figure 4.1. Accordingly, the proposed models corresponding to the aforementioned operators are formulated as follows:

4.1.1 The model with Caputo sense

$$\begin{aligned}
\mathcal{L}^{1-\lambda\ C}D_t^{\lambda}[T(t)] &= \xi_T + \mu T(t)\left[1-\frac{T(t)}{T^{max}}\right] - \frac{\gamma_1 T(t)D(t)}{1+\delta_1 M(t)} - \eta T(t)K(t) - \rho_T T(t),\\
\mathcal{L}^{1-\lambda\ C}D_t^{\lambda}[D(t)] &= \xi_D - \frac{\gamma_2 T(t)D(t)}{1+\delta_2 M(t)} - \rho_D D(t),\\
\mathcal{L}^{1-\lambda\ C}D_t^{\lambda}[K(t)] &= \xi_K + \frac{\gamma_1 T(t)D(t)}{1+\delta_1 M(t)} + \frac{\gamma_2 T(t)D(t)}{1+\delta_2 M(t)} - \rho_K K(t),\\
\mathcal{L}^{1-\lambda\ C}D_t^{\lambda}[M(t)] &= \xi_M - \rho_M M(t),
\end{aligned} \tag{4.1.1}$$

where $\lambda \in (0,1]$ is the fractional order for all the model population taken in the Caputo sense and 't' is time in days.

4.1.2 The model with Caputo-Fabrizio sense

$$\begin{aligned}
\mathcal{L}^{1-\zeta\ CF}D_t^{\zeta}[T(t)] &= \xi_T + \mu T(t)\left[1-\frac{T(t)}{T^{max}}\right] - \frac{\gamma_1 T(t)D(t)}{1+\delta_1 M(t)} - \eta T(t)K(t) - \rho_T T(t),\\
\mathcal{L}^{1-\zeta\ CF}D_t^{\zeta}[D(t)] &= \xi_D - \frac{\gamma_2 T(t)D(t)}{1+\delta_2 M(t)} - \rho_D D(t),\\
\mathcal{L}^{1-\zeta\ CF}D_t^{\zeta}[K(t)] &= \xi_K + \frac{\gamma_1 T(t)D(t)}{1+\delta_1 M(t)} + \frac{\gamma_2 T(t)D(t)}{1+\delta_2 M(t)} - \rho_K K(t),\\
\mathcal{L}^{1-\zeta\ CF}D_t^{\zeta}[M(t)] &= \xi_M - \rho_M M(t),
\end{aligned} \tag{4.1.2}$$

where $\zeta \in (0,1]$ is the fractional order for all the model population taken in the Caputo-Fabrizio sense and 't' is time in days.

4.1.3 The model with Atangana-Baleanu-Caputo sense

$$\begin{aligned}
\mathcal{L}^{1-\alpha\ ABC}D_t^{\alpha}[T(t)] &= \xi_T + \mu T(t)\left[1-\frac{T(t)}{T^{max}}\right] - \frac{\gamma_1 T(t)D(t)}{1+\delta_1 M(t)} - \eta T(t)K(t) - \rho_T T(t),\\
\mathcal{L}^{1-\alpha\ ABC}D_t^{\alpha}[D(t)] &= \xi_D - \frac{\gamma_2 T(t)D(t)}{1+\delta_2 M(t)} - \rho_D D(t),\\
\mathcal{L}^{1-\alpha\ ABC}D_t^{\alpha}[K(t)] &= \xi_K + \frac{\gamma_1 T(t)D(t)}{1+\delta_1 M(t)} + \frac{\gamma_2 T(t)D(t)}{1+\delta_2 M(t)} - \rho_K K(t),\\
\mathcal{L}^{1-\alpha\ ABC}D_t^{\alpha}[M(t)] &= \xi_M - \rho_M M(t),
\end{aligned} \tag{4.1.3}$$

where $\alpha \in (0,1]$ is the fractional order for all the model population taken in the Atangana-Baleanu-Caputo sense and 't' is time in days.

The initial conditions are given by

$$T(0) = T_0 > 0,\ D(0) = D_0 > 0,\ K(0) = K_0 > 0,\ M(0) = M_0 > 0. \tag{4.1.4}$$

In the fractional-order models (4.1.1)–(4.1.3), the terms ξ_T, ξ_D, ξ_K, and ξ_M represent the constant accumulation rates of T cells, dendritic cells, keratinocytes, and mesenchymal stem cells (MSCs), respectively. Since T cells cannot increase endlessly, the logistical expression $\mu T(t)(1-\frac{T(t)}{T^{max}})$ highlights the growth of T cells, where μ is the proliferation rate and T^{max} is the maximum carrying capacity. The interaction term $\frac{\gamma_1 T(t)D(t)}{1+\delta_1 M(t)}$ represents a saturated incidence function, where $\gamma_1 D(t)$ quantifies the interaction strength with T cells, and the denominator describes inhibition by MSCs. As $D(t)$ increases, the interaction saturates, while an increase in $M(t)$ suppresses this interaction. Although MSCs do not directly inhibit T cell–dendritic cell interactions under normal conditions, during autoimmune responses they modulate these interactions via cytokine-mediated regulatory mechanisms. When $\delta_1 \to 0$, the term reduces to a classical bilinear incidence. This Holling type-II functional form more realistically captures immune saturation effects and prevents unbounded growth in interaction terms. A similar mechanism is modeled by the term $\frac{\gamma_2 T(t)D(t)}{1+\delta_2 M(t)}$. Both terms ultimately contribute to keratinocyte population growth, while $M(t)$ suppresses the T cell–dendritic cell interaction loop and limits infiltration by producing anti-inflammatory cytokines. δ_1 and δ_2 denote the respective scaling coefficients of inhibition. In early stages of disease progression, keratinocytes also suppress T cell over-activation via anti-inflammatory cytokines, modeled by the term $\eta T(t)K(t)$. The per-capita mortality rates for T cells, dendritic cells, keratinocytes, and MSCs are denoted by ρ_T, ρ_D, ρ_K, and ρ_M, respectively. The model parameters are also summarized in Table 4.1.

4.1.4 Resolving the Dimensional Inconsistency Issues of Fractional-Order Systems

Fractional-order epidemiological models, in their standard form, often exhibit dimensional inconsistency and undermines both the mathematical integrity and biological relevance of the model. For example, the Caputo fractional derivative of order λ has the dimension $(\text{time})^{-\lambda}$, whereas the right-hand side of system (4.1.1) carries $(\text{time})^{-1}$. A detailed mathematical discussion of this imbalance can be found in [70, 71]. To resolve this, we introduce a scaling factor $\mathcal{L}$, called the *memory rate parameter*, with units (day^{-1}). Multiplying the left-hand side of each equation by $\mathcal{L}^{1-\lambda}$ yields

$$(\text{day}^{-1})^{1-\lambda} \cdot \text{day}^{-\lambda} = \text{day}^{-1},$$

thereby ensuring dimensional balance in system (4.1.1). The same correction is applied to systems (4.1.2) and (4.1.3), which involve the Caputo–Fabrizio and Atangana–Baleanu derivatives of orders ζ and $\alpha \in (0,1]$, respectively. This adjustment is essential for maintaining dimensional consistency in all fractional-order model formulations and the inclusion of $\mathcal{L}$ is mathematically justified and biologically essential, including those with non-singular kernels such as exponential (Caputo–Fabrizio) and Mittag–Leffler (Atangana–Baleanu) types [72]. For instance, the Caputo–Fabrizio derivative has the effective dimension

$$[\,{}^{CF}D_t^{\alpha} f(t)\,] \sim \frac{[f(t)]}{T^{\alpha}}, \quad 0 < \alpha < 1.$$

Parameter	Definition of parameter	Value (unit)
ξ_T	Constant accumulation rate of T cells in the proximity region	25 $\text{mm}^{-3}d^{-1}$
ξ_D	Constant accumulation rate of dendritic cells in the proximity region	15 $\text{mm}^{-3}d^{-1}$
ξ_K	Constant accumulation rate of keratinocytes in the inflamed area	30 $\text{mm}^{-3}d^{-1}$
ξ_M	Constant accumulation rate of MSCs near the inflamed region	0.5 $\text{mm}^{-3}d^{-1}$
μ	Intrinsic growth rate T cell population	0.03 d^{-1}
$T^{\max}$	Maximum carrying capacity of T cell population	300 mm^{-3}
γ_1	Activation rate of T cells through DC mediated cytokines	0.03 mm^3d^{-1}
γ_2	Rate of activation of DCs via T cell mediated cytokines	0.03 mm^3d^{-1}
δ_1	Inhibition scaling coefficient of MSCs on DC activation	0.035 mm^3
δ_2	Inhibition scaling coefficient of MSCs on T cell activation	0.25 mm^3
η	Initial inhibition rate of T cell hyper-activity by keratinocytes	0.003 mm^3d^{-1}
ρ_T	Natural mortality rate of T cells	0.06 d^{-1}
ρ_D	Natural mortality rate of DCs	0.16 d^{-1}
ρ_K	Inherent mortality rate of keratinocytes	0.25 d^{-1}
ρ_M	Natural mortality rate of MSCs	0.3 d^{-1}

Table 4.1: This table presents the model parameters, their definitions, and the assigned values used in the numerical simulations. Some parameter values are sourced from various literature [52, 53, 69] and some are estimated, which allowed for the biological viability of the proposed systems.

Proof: The Laplace transform of the Caputo–Fabrizio derivative is given by

$$\mathcal{L}\left\{{}^{CF}D_t^{\alpha} f(t)\right\}(s) = M(\alpha)\frac{s}{s+\lambda}\tilde{f}(s),$$

where $M(\alpha)$ is a normalization constant with $M(0) = M(1) = 1$, and $\lambda = \frac{\alpha}{1-\alpha}$. Since $s \sim 1/T$ and $\tilde{f}(s) \sim [f] \cdot T$, one infers that

$$\frac{s}{s+\lambda} \sim (1/T)^{\alpha},$$

which confirms the scaling of dimension $[f(t)]/T^{\alpha}$.

Alternative Proof: The Caputo–Fabrizio exponential kernel for $\alpha \in (0,1)$ is

$$e^{-\frac{\alpha t}{1-\alpha}} = \frac{1}{(e^t)^{\frac{\alpha}{1-\alpha}}} \approx \frac{1}{(1+t+\frac{t^2}{2!}+\frac{t^3}{3!}+\cdots)^{\alpha}} \leq \frac{1}{(1+t)^{\alpha}} \leq \frac{1}{t^{\alpha}}.$$

Since $t \sim T$, this again implies

$$[\,{}^{CF}D_t^{\alpha} f(t)\,] \sim \frac{[f(t)]}{T^{\alpha}}.$$

Thus, the Caputo–Fabrizio derivative effectively modifies the time scaling to behave as a derivative of order α.

Similarly, the Atangana–Baleanu fractional derivative in the Caputo sense has dimension

$$[\,{}^{ABC}D_t^{\alpha} f(t)\,] \sim \frac{[f(t)]}{T^{\alpha}}, \quad 0 < \alpha < 1.$$

Proof: Consider $f(t) = t^{\gamma}$, with $[f(t)] = T^{\gamma}$. Then the Atangana–Baleanu–Caputo derivative is

$${}^{ABC}D_t^{\alpha} t^{\gamma} = \frac{B(\alpha)\Gamma(\gamma+1)}{(1-\alpha)\Gamma(\gamma+1-\alpha)} t^{\gamma-\alpha},$$

which implies

$$[\,{}^{ABC}D_t^{\alpha} t^{\gamma}\,] = T^{\gamma-\alpha} = \frac{[f(t)]}{T^{\alpha}}.$$

Hence, the Atangana–Baleanu derivative reduces the time exponent by α, confirming its effective scaling.

4.2 Positivity and Boundedness

Let us denote $\mathbb{R}^4_+ = \{z(t) \in \mathbb{R}^4 : z(t) > 0\}$ and define the state vector as $z(t) = (T(t), D(t), K(t), M(t))^T$, where ^{T} indicates the transpose. Our objective is to investigate the positivity and to establish the existence of a positively invariant region in which the solutions of the fractional-order model (4.1.3), formulated using the Atangana–Baleanu–Caputo (ABC) fractional derivative.

Now, we state the following theorem, which guarantees the positivity of the solutions of the system (4.1.3).

Theorem 4.2.1 *If the initial condition satisfies $(T_0, D_0, K_0, M_0)^T \in Int(\mathbb{R}^4_+)$, then all the solutions of the fractional-order model (4.1.3) remain positive for all $t > 0$.*

Proof. Consider the first equation of the fractional-order system (4.1.3). Evaluating it at $T = 0$ and $z(t) \in \mathbb{R}^4_+$, we obtain:

$$\begin{aligned} &\mathcal{L}^{1-\alpha}\,{}^{ABC}\mathcal{D}_t^{\alpha}[T(t)]\big|_{T=0,\, z(t)\in\mathbb{R}^4_+} = \xi_T, \\ &\Rightarrow {}^{ABC}\mathcal{D}_t^{\alpha}[T(t)]\big|_{T=0,\, z(t)\in\mathbb{R}^4_+} = \mathcal{L}^{\alpha-1}\xi_T > 0. \end{aligned} \tag{4.2.1}$$

In similar manner from the remaining equations of the system (4.1.3) one can easily verify

$$ {}^{ABC}\mathcal{D}_t^{\alpha}[D(t)]\big|_{D=0,\, z(t)\in\mathbb{R}^4_+} > 0, \quad {}^{ABC}\mathcal{D}_t^{\alpha}[K(t)]\big|_{K=0,\, z(t)\in\mathbb{R}^4_+} > 0, \quad {}^{ABC}\mathcal{D}_t^{\alpha}[M(t)]\big|_{M=0,\, z(t)\in\mathbb{R}^4_+} > 0. \tag{4.2.2} $$

These inequalities confirm that the fractional derivatives of each model variable are strictly positive at the boundary, ensuring that the trajectories point inward at the boundary of the positive octant. Therefore, by the Nagumo condition [62], the solution remains in $\mathbb{R}^4_+$ for all $t > 0$, completing the proof.

It is also essential to show that the solutions of the fractional-order system (4.1.3) remain bounded for all time $t > 0$. The following theorem establishes the invariant region Π, where the solutions of system (4.1.3) are biologically feasible and mathematically well-posed.

Suppose $\Pi = \{z(t) \in \mathbb{R}^4 : 0 < T(t) + D(t) + K(t) + M(t) \leq \frac{\kappa}{\rho}\}$. The following theorem confirms that Π is positively invariant for the system (4.1.3).

Theorem 4.2.2 *The closed set* Π *is positively invariant with respect to the fractional-order system* (4.1.3).

Proof. Let us define the total population as $Y(t) = T(t) + D(t) + K(t) + M(t)$. By adding the equations of the system (4.1.3), we obtain the following inequality involving the Atangana–Baleanu–Caputo (ABC) fractional derivative:

$$ \begin{aligned} \mathcal{L}^{1-\alpha}\, {}^{ABC}\mathcal{D}_t^{\alpha}[Y(t)] &\leq (\xi_T + \xi_D + \xi_K + \xi_M) + \frac{\mu T^{\max}}{4} - \rho Y(t) \\ &= \kappa - \rho Y(t), \end{aligned} \tag{4.2.3} $$

where $\kappa = \xi_T + \xi_D + \xi_K + \xi_M + \frac{\mu T^{\max}}{4}$, and $\rho = \min\{\rho_T, \rho_D, \rho_K, \rho_M\}$. The term $\frac{\mu T^{\max}}{4}$ represents the maximum value of the logistic growth term $\mu T(t)(1 - \frac{T(t)}{T^{\max}})$.

Applying the Laplace transform and using the known identity for the Mittag-Leffler function, the solution $Y(t)$ satisfies:

$$ Y(t) \leq Y(0)\, \mathbf{E}_{\alpha}(-\rho \mathcal{L}^{\alpha-1} t^{\alpha}) + \int_0^t \kappa \mathcal{L}^{\alpha-1} \sigma^{\alpha-1}\, \mathbf{E}_{\alpha,\alpha}(-\rho \mathcal{L}^{\alpha-1} \sigma^{\alpha})\, d\sigma. \tag{4.2.4} $$

Expanding the Mittag-Leffler function in series and simplifying the integral expression gives:

$$ Y(t) \leq Y(0)\, \mathbf{E}_{\alpha}(-\rho \mathcal{L}^{\alpha-1} t^{\alpha}) + \frac{\kappa}{\rho}\left(1 - \mathbf{E}_{\alpha}(-\rho \mathcal{L}^{\alpha-1} t^{\alpha})\right). \tag{4.2.5} $$

Clearly, if $Y(0) \leq \frac{\kappa}{\rho}$, then for all $t > 0$,

$$ 0 < Y(t) \leq \frac{\kappa}{\rho} \quad \Rightarrow \quad 0 < T(t) + D(t) + K(t) + M(t) \leq \frac{\kappa}{\rho}. \tag{4.2.6} $$

Therefore, it follows that the closed set Π remains positively invariant within the framework of the fractional-order system (4.1.3).

4.3 Existence and Uniqueness

In this section, we analyze the existence and uniqueness of solutions to the fractional-order model by employing the Banach contraction mapping principle, corresponding to the Atangana-Baleanu fractional derivative defined in the Caputo sense. To analyze the existence of solutions, we now state the following lemma and fixed-point theorem.

Lemma 4.3.1 *[29] Let $\alpha \in [0,1]$. If the Atangana-Baleanu-Caputo derivative satisfies*

$$^{ABC}\mathcal{D}_0^{\alpha}\mathcal{H}(t) = \mathcal{J}(t,\mathcal{H}(t)), \quad t \in (0,T), \quad \mathcal{H}(0) = \mathcal{H}_0,$$

then the function $\mathcal{H}(t)$ is given by

$$\mathcal{H}(t) = \mathcal{H}_0 + \frac{1-\alpha}{\mathbf{B}(\alpha)} f(t) + \frac{\alpha}{\Gamma(\alpha)\mathbf{B}(\alpha)} \int_0^t f(s)(t-s)^{\alpha-1} ds.$$

Theorem 4.3.1 *[73] Let $\mathbb{X}$ be a convex subset of a Banach space $\mathcal{Z}$ and suppose operators $\mathcal{X}_1, \mathcal{X}_2 : \mathbb{X} \to \mathbb{X}$ satisfy:*

1. *$\mathcal{X}_1 h + \mathcal{X}_2 h \in \mathbb{X}$ for all $h \in \mathbb{X}$,*
2. *$\mathcal{X}_1$ is a contraction,*
3. *$\mathcal{X}_2$ is compact and continuous.*

Then the operator equation $\mathcal{X}_1 h + \mathcal{X}_2 h = h$ has at least one solution in $\mathbb{X}$.

4.3.1 Existence of Solutions

We considered our formulated mathematical model (4.1.3) and rewritten in the following form:

$$\begin{aligned}
\mathcal{J}_1(t,T,D,K,M) &= \xi_T + \mu T(t)\left[1 - \frac{T(t)}{T^{max}}\right] - \frac{\gamma_1 T(t) D(t)}{1+\delta_1 M(t)} - \eta T(t) K(t) - \rho_T T(t), \\
\mathcal{J}_2(t,T,D,K,M) &= \xi_D - \frac{\gamma_2 T(t) D(t)}{1+\delta_2 M(t)} - \rho_D D(t), \\
\mathcal{J}_3(t,T,D,K,M) &= \xi_K + \frac{\gamma_1 T(t) D(t)}{1+\delta_1 M(t)} + \frac{\gamma_2 T(t) D(t)}{1+\delta_2 M(t)} - \rho_K K(t), \\
\mathcal{J}_4(t,T,D,K,M) &= \xi_M - \rho_M M(t).
\end{aligned} \tag{4.3.1}$$

Using the equation (4.3.1), the proposed system (4.1.3) can be written in the following form:

$$\begin{cases} \mathcal{L}^{1-\alpha}\ {}^{ABC}D_0^{\alpha}\mathcal{H}(t) = \mathcal{J}(t,\mathcal{H}(t)), \quad t \in [0,T],\ 0 < \alpha \leq 1 \\ \mathcal{H}(0) = \mathcal{H}_0 > 0. \end{cases} \tag{4.3.2}$$

Applying the Lemma 4.3.1 on the problem (4.3.2), we obtained

$$\mathcal{H}(t) = \mathcal{H}_0(t) + \mathcal{L}^{\alpha-1}[\mathcal{J}(t,\mathcal{H}(t)) - \mathcal{J}_0(t)]\frac{1-\alpha}{\mathbf{B}(\alpha)} + \frac{\alpha\mathcal{L}^{\alpha-1}}{\mathbf{B}(\alpha)\Gamma(\alpha)} \int_0^t (t-s)^{\alpha-1}\mathcal{J}(s,\mathcal{H}(s))ds, \tag{4.3.3}$$

where

$$\mathcal{H}(t)=\begin{cases}T(t)\\D(t)\\K(t)\\M(t)\end{cases},\mathcal{H}_0(t)=\begin{cases}T(0)\\D(0)\\K(0)\\M(0)\end{cases},\mathcal{J}(t,\mathcal{H}(t))=\begin{cases}\mathcal{J}_1(t,\mathcal{H}(t))\\\mathcal{J}_2(t,\mathcal{H}(t))\\\mathcal{J}_3(t,\mathcal{H}(t))\\\mathcal{J}_4(t,\mathcal{H}(t))\end{cases},\mathcal{J}_0(t)=\begin{cases}\mathcal{J}_1(0)\\\mathcal{J}_2(0)\\\mathcal{J}_3(0)\\\mathcal{J}_4(0)\end{cases}. \tag{4.3.4}$$

Now, we prove that all kernels $\mathcal{J}_1$, $\mathcal{J}_2$, $\mathcal{J}_3$ and $\mathcal{J}_4$ satisfy the Lipschitz condition. Since all the populations of our system are bounded therefore there exist some positive constants for which we can write all the populations in the form: $u_1 \le T \le U_1$, $u_2 \le D \le U_2$, $u_3 \le K \le U_3$ and $u_4 \le M \le U_4$.

First, we prove that the kernel $\mathcal{J}_1$ satisfies the Lipschitz condition. Let $T(t)$ and $T_1(t)$ are two functions, then utilize the norm function properties, we have

$$\begin{aligned}&\big\|\mathcal{J}_1(t,T(t))-\mathcal{J}_1(t,T_1(t))\big\|\\=&\Big\|\Big(\mu T(t)\Big[1-\frac{T(t)}{T^{max}}\Big]-\frac{\gamma_1 T(t)D(t)}{1+\delta_1 M(t)}-\eta T(t)K(t)-\rho_T T(t)\Big)-\\&\Big(\mu T_1(t)\Big[1-\frac{T_1(t)}{T^{max}}\Big]-\frac{\gamma_1 T_1(t)D(t)}{1+\delta_1 M(t)}-\eta T_1(t)K(t)-\rho_T T_1(t)\Big)\Big\|\\\le&\Big(\mu+\frac{2\mu U_1}{T^{max}}+\frac{\gamma_1 U_2}{1+\delta_1 u_4}+\eta U_3+\rho_T\Big)\|T(t)-T_1(t)\|\\=&\mathcal{V}_1\|T(t)-T_1(t)\|,\quad \text{where } \mathcal{V}_1=\Big(\mu+\frac{2\mu U_1}{T^{max}}+\frac{\gamma_1 U_2}{1+\delta_1 u_4}+\eta U_3+\rho_T\Big).\end{aligned} \tag{4.3.5}$$

Similarly, we can prove that the other kernels also satisfy the Lipschitz condition and therefore there exist $\mathcal{V}_2$, $\mathcal{V}_3$, $\mathcal{V}_4$ such that

$$\begin{aligned}\big\|\mathcal{J}_2(t,D(t))-\mathcal{J}_2(t,D_1(t))\big\|&\le\mathcal{V}_2\|D(t)-D_1(t)\|,\\\big\|\mathcal{J}_3(t,K(t))-\mathcal{J}_3(t,K_1(t))\big\|&\le\mathcal{V}_3\|K(t)-K_1(t)\|,\\\big\|\mathcal{J}_4(t,M(t))-\mathcal{J}_4(t,M_1(t))\big\|&\le\mathcal{V}_4\|M(t)-M_1(t)\|,\end{aligned}$$

where

$$\mathcal{V}_2=\frac{\gamma_1 U_1}{1+\delta_2 u_4}+\rho_D,\ \mathcal{V}_3=\rho_K \text{ and } \mathcal{V}_4=\rho_M.$$

The Lipschitz condition of all kernels in terms of equation (4.3.2) is written in the following lemma:

Lemma 4.3.2 *There exists a constant $\mathcal{V}_k > 0$, such that for all $\mathcal{H}_1, \mathcal{H}_2$, the following inequality holds:*

$$\|\mathcal{J}(t,\mathcal{H}_1(t))-\mathcal{J}(t,\mathcal{H}_2(t))\|\le\mathcal{V}_k\|\mathcal{H}_1-\mathcal{H}_2\|.$$

Let $\mathbb{X}=C([0,T];\mathbb{R})$ be the Banach space of all continuous functions from [0, T] to $\mathbb{R}$ defined by

$$\|\mathcal{H}(t)\|=\max_{t\in[0,T]}|\mathcal{H}(t)|,$$

where $|\mathcal{H}(t)| = |T(t)| + |D(t)| + |K(t)| + |M(t)|$ and $T, D, K, M \in C([0,T])$.

From the equation (4.3.3), we consider two operator $\mathcal{X}_1$ and $\mathcal{X}_2$ as

$$\begin{aligned}\mathcal{X}_1(\mathcal{H}) &= \mathcal{H}_0(t) + \mathcal{L}^{\alpha-1}[\mathcal{J}(t,\mathcal{H}(t)) - \mathcal{J}_0(t)]\frac{1-\alpha}{\mathbf{B}(\alpha)},\\ \mathcal{X}_2(\mathcal{H}) &= \frac{\alpha\mathcal{L}^{\alpha-1}}{\mathbf{B}(\alpha)\Gamma(\alpha)}\int_0^t (t-s)^{\alpha-1}\mathcal{J}(s,\mathcal{H}(s))ds.\end{aligned} \tag{4.3.6}$$

Now, we will prove that the operator $\mathcal{X}_1(\mathcal{H})$ is a contraction, and the operator $\mathcal{X}_2(\mathcal{H})$ is compact and continuous. Before proceeding with the proof, we make the following assumption:

(L_1) There exist constants κ_1 and κ_2 such that $|\mathcal{J}(t,\mathcal{H}(t)| \leq \kappa_1\mathcal{H}(t) + \kappa_2$, where $\mathcal{H}(t) \leq m$. (4.3.7)

First, we prove that $\mathcal{X}_1(\mathcal{H})$ is a contraction using the Banach contraction principle. Let $\mathcal{H}_1 \in \mathbb{X}$ and $\mathcal{H}_2 \in \mathbb{X}$. By applying the lemma (4.3.2) to the operator $\mathcal{X}_1$, as defined in the equation (4.3.6), we have:

$$\begin{aligned}\|\mathcal{X}_1(\mathcal{H}_1) - \mathcal{X}_1(\mathcal{H}_2)\| &= \mathcal{L}^{\alpha-1}\frac{1-\alpha}{\mathbf{B}(\alpha)} \times \max_{t\in(0,T)} |\mathcal{J}(t,\mathcal{H}_1(t) - \mathcal{J}(t,\mathcal{H}_2(t))|\\ &\leq \mathcal{L}^{\alpha-1}\frac{(1-\alpha)\mathcal{V}_k}{\mathbf{B}(\alpha)}\|\mathcal{H}_1 - \mathcal{H}_2\|.\end{aligned}$$

This implies that the operator $\mathcal{X}_1(\mathcal{H})$ is a contraction. Next, we prove that the other operator, $\mathcal{X}_2(\mathcal{H})$, is compact.

$$\begin{aligned}|\mathcal{X}_2(\mathcal{H})| &= \max_{t\in(0,T)} \frac{\alpha\mathcal{L}^{\alpha-1}}{\mathbf{B}(\alpha)\Gamma(\alpha)} \times \left\| \int_0^t (t-s)^{\alpha-1}\mathcal{J}(s,\mathcal{H}(s))ds \right\|\\ &\leq \frac{\alpha\mathcal{L}^{\alpha-1}}{\mathbf{B}(\alpha)\Gamma(\alpha)}\int_0^T (t-s)^{\alpha-1}\Big|\mathcal{J}(s,\mathcal{H}(s))\Big|ds\\ &\leq \frac{T^\alpha\mathcal{L}^{\alpha-1}}{\mathbf{B}(\alpha)\Gamma(\alpha)}[\kappa_1 m + \kappa_2].\end{aligned}$$

Therefore, the operator $\mathcal{X}_2(\mathcal{H})$ is bounded. Next, we need to prove that the operator is continuous. To do so, let us assume that $t_1, t_2 \in [0,T]$, where $t_2 > t_1$.

$$\begin{aligned}&|\mathcal{X}_2(\mathcal{H}(t_2)) - \mathcal{X}_2(\mathcal{H}(t_1))|\\ &= \frac{\alpha\mathcal{L}^{\alpha-1}}{\mathbf{B}(\alpha)\Gamma(\alpha)}\left| \int_0^{t_2} (t_2-s)^{\alpha-1}\mathcal{J}(s,\mathcal{H}(s))ds - \int_0^{t_1} (t_1-s)^{\alpha-1}\mathcal{J}(s,\mathcal{H}(s))ds \right|\\ &\leq \mathcal{L}^{\alpha-1}\frac{[\kappa_1 m + \kappa_2]}{\mathbf{B}(\alpha)\Gamma(\alpha)}\left[t_2^\alpha - t_1^\alpha\right].\end{aligned}$$

This implies that $|\mathcal{X}_2(\mathcal{H}(t_2)) - \mathcal{X}_2(\mathcal{H}(t_1))| \to 0$ as $t_2 \to t_1$, and hence the operator $\mathcal{X}_2(\mathcal{H})$ is compact. Since $\mathcal{X}_1(\mathcal{H})$ is a contraction and $\mathcal{X}_2(\mathcal{H})$ is compact, it follows from Theorem 4.3.1 that equation (4.3.3) admits at least one solution.

4.3.2 Uniqueness of Solutions

Theorem 4.3.2 *The integral problem (4.3.2), together with Lemma 4.3.2, admits a unique solution if the following condition is satisfied:*

$$\mathcal{L}^{\alpha-1}\left[\frac{(1-\alpha)\mathcal{V}_k}{\mathbf{B}(\alpha)}+\frac{T^{\alpha}\mathcal{V}_k}{\mathbf{B}(\alpha)\Gamma(\alpha)}\right]<1. \tag{4.3.8}$$

Consequently, the solution of the fractional system (4.1.3) is also unique under the condition (4.3.8).

Proof. Let $\Psi:\mathbb{X}\to\mathbb{X}$ be the operator defined by

$$\Psi(\mathcal{H}(t))=\mathcal{H}_0(t)+\mathcal{L}^{\alpha-1}\left[\mathcal{J}(t,\mathcal{H}(t))-\mathcal{J}_0(t)\right]\frac{1-\alpha}{\mathbf{B}(\alpha)}+\frac{\alpha\mathcal{L}^{\alpha-1}}{\mathbf{B}(\alpha)\Gamma(\alpha)}\int_0^t(t-s)^{\alpha-1}\mathcal{J}(s,\mathcal{H}(s))\,ds.$$

Now, consider two functions $\mathcal{H}_1,\mathcal{H}_2\in\mathbb{X}$. Then

$$\begin{aligned}\left\|\Psi(\mathcal{H}_1(t))-\Psi(\mathcal{H}_2(t))\right\| &\le \mathcal{L}^{\alpha-1}\cdot\frac{1-\alpha}{\mathbf{B}(\alpha)}\cdot\max_{t\in[0,T]}\left|\mathcal{J}(t,\mathcal{H}_1(t))-\mathcal{J}(t,\mathcal{H}_2(t))\right|\\ &\quad+\frac{\alpha\mathcal{L}^{\alpha-1}}{\mathbf{B}(\alpha)\Gamma(\alpha)}\cdot\max_{t\in[0,T]}\left|\int_0^t(t-s)^{\alpha-1}\left[\mathcal{J}(s,\mathcal{H}_1(s))-\mathcal{J}(s,\mathcal{H}_2(s))\right]ds\right|\\ &\le \mathcal{L}^{\alpha-1}\left[\frac{(1-\alpha)\mathcal{V}_k}{\mathbf{B}(\alpha)}+\frac{T^{\alpha}\mathcal{V}_k}{\mathbf{B}(\alpha)\Gamma(\alpha)}\right]\cdot\left\|\mathcal{H}_1-\mathcal{H}_2\right\|\\ &= \Lambda\cdot\left\|\mathcal{H}_1-\mathcal{H}_2\right\|.\end{aligned}$$

Therefore, by the Banach contraction principle, Ψ is a contraction mapping if $\Lambda<1$. Hence, by the fixed-point theorem, the fractional system (4.1.3) admits a unique solution under the condition $\Lambda<1$.

Remark 4.3.1 *When $\Lambda\ge1$, the operator $\Psi:\mathbb{X}\to\mathbb{X}$ is no longer a contraction mapping, i.e., the distance property $d(\Psi(x),\Psi(y))<d(x,y)$ is lost. If Λ=1, the distance property of the operator is preserved or reduced, but not strictly reduced, which means the uniqueness of a fixed point is not guaranteed, and solutions may be non-unique or not necessarily approachable by standard iterations. Whenever $\Lambda>1$, the operator increases distances between two points, implying that the iterative sequence would diverge. Therefore, for $\Lambda\ge1$, the model is invalid for biological interpretation.*

Biological Interpretation: The existence and uniqueness of solutions in a fractional model ensure that the biological system exhibits a consistent and predictable response during treatment. Existence guarantees that a meaningful outcome occurs under given conditions, while uniqueness confirms the reproducibility of this response. The fractional aspect captures memory effects in biological processes, reflecting the influence of past therapeutic interventions. This enhances the model's reliability in representing the dynamics of the immune response.

4.4 Stability Analysis

In this section, we present the stability analysis for our fractional system (4.1.3) in the context of Ulam-Hyers stability and generalized Ulam-Hyers stability. The concept of Ulam-Hyers stability, introduced by Ulam in [74], provides a framework for analyzing the robustness of solutions to perturbations in functional equations. Before presenting the proof of the system's stability, we introduce some definitions that will be utilized in the subsequent stability analysis. Let $\epsilon > 0$ and $h : [0, T] \to [0, \infty]$ be a continuous function. We consider the following inequalities.

$$|\mathcal{L}^{1-\alpha}\ {}^{ABC}D^{\alpha}_{0+}\mathcal{H}(t) - \mathcal{J}(t, \mathcal{H}(t))| \leq \epsilon, \quad t \in [0, T], \quad \text{and} \tag{4.4.1}$$

$$|\mathcal{L}^{1-\alpha}\ {}^{ABC}D^{\alpha}_{0+}\mathcal{H}(t) - \mathcal{J}(t, \mathcal{H}(t))| \leq \epsilon h(t), \quad t \in [0, T]. \tag{4.4.2}$$

Definition 4.4.1 *The solutions of the proposed mathematical model (4.1.3) are said to be Ulam-Hyers stable if, for every $\epsilon > 0$ and for a function $\bar{\mathcal{H}} \in \mathbb{X}$ satisfying the inequality (4.4.1), there exists a solution $\mathcal{H}(t)$ of system (4.1.3) such that*

$$|\bar{\mathcal{H}}(t) - \mathcal{H}(t)| < \mathcal{N}_k \epsilon, \quad t \in [0, T], \tag{4.4.3}$$

where $\mathcal{N}_k$ is a positive constant.

Definition 4.4.2 *The solutions of the system (4.1.3) are said to be generalized Ulam–Hyers stable if there exists a continuous function $\Phi_k : \mathbb{R}_+ \to \mathbb{R}_+$ with $\Phi_k(0) = 0$, such that for arbitrary $\epsilon > 0$ and for each $\bar{\mathcal{H}} \in \mathbb{X}$ satisfying the inequality (4.4.2), there exists a solution $\mathcal{H} \in \mathbb{X}$ of the system (4.1.3) such that*

$$|\bar{\mathcal{H}}(t) - \mathcal{H}(t)| < \Phi_k \epsilon, \quad t \in [0, T]. \tag{4.4.4}$$

Remark 4.4.1 *We aim to analyze the stability of the proposed system (4.1.3). A function $\mathcal{H} \in \mathbb{X}$ satisfies the inequality (4.4.1) if and only if there exists a perturbation function $g \in \mathbb{X}$ such that the following conditions hold:*

(i) $|g(t)| \leq \epsilon, \quad t \in [0, T],$

(ii) $\mathcal{L}^{1-\alpha}\ {}^{ABC}D^{\alpha}_{0+}\mathcal{H}(t) = \mathcal{J}(t, \mathcal{H}(t)) + g(t), \quad t \in [0, T].$

Theorem 4.4.1 *Let $\mathcal{H} \in \mathbb{X}$ satisfy the inequality (4.4.1) and the properties described in Remark 4.4.1. Then $\mathcal{H}$ satisfies the following inequality:*

$$\left|\mathcal{H}(t) - \left(\mathcal{H}_0 + \frac{\mathcal{L}^{\alpha-1}(1-\alpha)}{\mathbf{B}(\alpha)}\Big[\mathcal{J}(t, \mathcal{H}(t)) - \mathcal{J}_0(t)\Big] + \frac{\mathcal{L}^{\alpha-1}\alpha}{\mathbf{B}(\alpha)\Gamma(\alpha)}\int_0^t \mathcal{J}(s, \mathcal{H}(s))(t-s)^{\alpha-1}ds\right)\right| \leq \Omega\epsilon,$$

$$\text{where } \Omega = \frac{\mathcal{L}^{\alpha-1}\left(\Gamma(\alpha)(1-\alpha) + T^{\alpha}\right)}{\mathbf{B}(\alpha)\Gamma(\alpha)}.$$

Proof. Considering the second part of the Remark 4.4.1 and applying the theorem in [75], we obtained

$$\mathcal{H}(t) = \mathcal{H}_0 + \frac{\mathcal{L}^{\alpha-1}(1-\alpha)}{\mathbf{B}(\alpha)}\Big[\mathcal{J}(t,\mathcal{H}(t)) - \mathcal{J}_0(t)\Big] + \frac{\mathcal{L}^{\alpha-1}\alpha}{\mathbf{B}(\alpha)\Gamma(\alpha)}\int_0^t \mathcal{J}(s,\mathcal{H}(s))(t-s)^{\alpha-1}ds + \frac{\mathcal{L}^{\alpha-1}(1-\alpha)}{\mathbf{B}(\alpha)}g(t) + \frac{\mathcal{L}^{\alpha-1}\alpha}{\mathbf{B}(\alpha)\Gamma(\alpha)}\int_0^t g(s)(t-s)^{\alpha-1}ds.$$

Using the first part of Remark 4.4.1 along with our assumption, we get

$$\begin{aligned}
&\left|\mathcal{H}(t) - \left(\mathcal{H}_0 + \frac{\mathcal{L}^{\alpha-1}(1-\alpha)}{\mathbf{B}(\alpha)}\Big[\mathcal{J}(t,\mathcal{H}(t)) - \mathcal{J}_0(t)\Big] + \frac{\mathcal{L}^{\alpha-1}\alpha}{\mathbf{B}(\alpha)\Gamma(\alpha)}\int_0^t \mathcal{J}(s,\mathcal{H}(s))(t-s)^{\alpha-1}ds\right)\right| \\
&\leq \frac{\mathcal{L}^{\alpha-1}(1-\alpha)}{\mathbf{B}(\alpha)}|g(t)| + \frac{\mathcal{L}^{\alpha-1}\alpha}{\mathbf{B}(\alpha)\Gamma(\alpha)}\int_0^t (t-s)^{\alpha-1}|g(s)|ds \\
&\leq \frac{\mathcal{L}^{\alpha-1}(1-\alpha)}{\mathbf{B}(\alpha)}\epsilon + \frac{\mathcal{L}^{\alpha-1}T^\alpha}{\mathbf{B}(\alpha)\Gamma(\alpha)}\epsilon = \Omega\epsilon.
\end{aligned}$$

Theorem 4.4.2 *Suppose that $\mathcal{J} : [0,T]\times\mathbb{R}^4 \to \mathbb{R}$ is continuous for every $\mathcal{H}\in\mathbb{X}$ and our two assumption (L_1) are satisfied with condition $1-\Lambda > 0$. Then our proposed fractional system (4.1.3) is Ulam-Hyers stable and also generalized Ulam-Hyers stable. Where*

$$\Lambda = \mathcal{L}^{\alpha-1}\left[\frac{(1-\alpha)\mathcal{V}_k}{\mathbf{B}(\alpha)} + \frac{T^\alpha\mathcal{V}_k}{\mathbf{B}(\alpha)\Gamma(\alpha)}\right].$$

Proof. Suppose that $\mathcal{H}\in\mathbb{X}$ be the solution satisfies the inequality (4.4.1) and $\mathcal{H}_1\in\mathbb{X}$ be the unique solution of the system (4.1.3). Then

$$\begin{aligned}
&\Big|\mathcal{H}(t) - \mathcal{H}_1(t)\Big| \\
=&\left|\mathcal{H}(t) - \left(\mathcal{H}_0 + \frac{\mathcal{L}^{\alpha-1}(1-\alpha)}{\mathbf{B}(\alpha)}\Big[\mathcal{J}(t,\mathcal{H}_1(t)) - \mathcal{J}_0(t)\Big] + \frac{\mathcal{L}^{\alpha-1}\alpha}{\mathbf{B}(\alpha)\Gamma(\alpha)}\int_0^t \mathcal{J}(s,\mathcal{H}_1(s))(t-s)^{\alpha-1}ds\right)\right| \\
\leq&\left|\mathcal{H}(t) - \left(\mathcal{H}_0 + \frac{\mathcal{L}^{\alpha-1}(1-\alpha)}{\mathbf{B}(\alpha)}\Big[\mathcal{J}(t,\mathcal{H}(t)) - \mathcal{J}_0(t)\Big] + \frac{\mathcal{L}^{\alpha-1}\alpha}{\mathbf{B}(\alpha)\Gamma(\alpha)}\int_0^t \mathcal{J}(s,\mathcal{H}(s))(t-s)^{\alpha-1}ds\right)\right| \\
+&\left|\left(\mathcal{H}_0 + \frac{\mathcal{L}^{\alpha-1}(1-\alpha)}{\mathbf{B}(\alpha)}\Big[\mathcal{J}(t,\mathcal{H}(t)) - \mathcal{J}_0(t)\Big] + \frac{\mathcal{L}^{\alpha-1}\alpha}{\mathbf{B}(\alpha)\Gamma(\alpha)}\int_0^t \mathcal{J}(s,\mathcal{H}(s))(t-s)^{\alpha-1}ds\right)\right. \\
-&\left.\left(\mathcal{H}_0 + \frac{\mathcal{L}^{\alpha-1}(1-\alpha)}{\mathbf{B}(\alpha)}\Big[\mathcal{J}(t,\mathcal{H}_1(t)) - \mathcal{J}_0(t)\Big] + \frac{\mathcal{L}^{\alpha-1}\alpha}{\mathbf{B}(\alpha)\Gamma(\alpha)}\int_0^t \mathcal{J}(s,\mathcal{H}_1(s))(t-s)^{\alpha-1}ds\right)\right| \\
\leq&\ \Omega\epsilon + \frac{\mathcal{L}^{\alpha-1}(1-\alpha)}{\mathbf{B}(\alpha)}\mathcal{V}_k|\mathcal{H}(t) - \mathcal{H}_1(t)| + \mathcal{L}^{\alpha-1}\frac{T^\alpha\mathcal{V}_k}{\mathbf{B}(\alpha)\Gamma(\alpha)}|\mathcal{H}(t) - \mathcal{H}_1(t)| \\
=&\ \Omega\epsilon + \Lambda|\mathcal{H}(t) - \mathcal{H}_1(t)|.
\end{aligned}$$

Hence,

$$|\mathcal{H}(t) - \mathcal{H}_1(t)| \leq \mathcal{N}_k\epsilon, \quad \text{where } \mathcal{N}_k = \frac{\Omega}{1-\Lambda}.$$

Here we consider $\Phi_k(\epsilon) = \mathcal{N}_k\epsilon$ such that $\Phi_k(0) = 0$. So we conclude the the system (4.1.3) is Ulam-Hyers stable as well as generalized Ulam-Hyers stable.

Biological Significance: The generalized Ulam-Hyers stability signifies that under small perturbations or uncertainties characteristic in biological processes, such as minor fluctuations in stem cell proliferation rates or therapeutic interventions, the system's trajectory, representing the progression or degradation of psoriasis, remains close to its ideal and equilibrium state. This mathematical robustness suggests that the disease dynamics are not excessively sensitive to minor biological noise, and that therapeutic strategies aiming to shift the system to a stable equilibrium are likely to be effective and maintainable in a real-world, dynamic biological environment.

4.5 Fractional Order control problem

In the case of psoriasis, the interaction rates between T cells and dendritic cells are highly stimulated by the effects of the cytokines TNF-α and IL-23, which result in the abnormal differentiation of T cells and hyper-proliferation of keratinocytes. To control the effects of these cytokines, we have considered our model by introducing two control functions, namely, $u_1(t)$ and $u_2(t)$ $(j = 1, 2)$ which are permissible controls representing the effect of biologics TNF-α inhibitors and IL-23 blockers respectively in order to restrict the interaction rates γ_1 and γ_2, respectively. Therefore, equations (4.1.1)–(4.1.3) equipped with optimum controls is given by the following system of equations specified in the time interval $[0, t_f]$.

$$\begin{aligned}
\mathcal{L}^{(1-a)F}D_t^a[T(t)] &= \xi_T + \mu T(t)\left[1 - \frac{T(t)}{T^{max}}\right] - \frac{\gamma_1\big[1-u_1(t)\big]T(t)D(t)}{1+\delta_1 M(t)} - \eta T(t)K(t) - \rho_T T(t),\\
\mathcal{L}^{(1-a)F}D_t^a[D(t)] &= \xi_D - \frac{\gamma_2\big[1-u_2(t)\big]T(t)D(t)}{1+\delta_2 M(t)} - \rho_D D(t),\\
\mathcal{L}^{(1-a)F}D_t^a[K(t)] &= \xi_K + \frac{\gamma_1\big[1-u_1(t)\big]T(t)D(t)}{1+\delta_1 M(t)} + \frac{\gamma_2\big[1-u_2(t)\big]T(t)D(t)}{1+\delta_2 M(t)} - \rho_K K(t),\\
\mathcal{L}^{(1-a)F}D_t^a[M(t)] &= \xi_M - \rho_M M(t),
\end{aligned} \tag{4.5.1}$$

subject to the initial conditions:

$$T(0) = T_0 > 0,\ D(0) = D_0 > 0,\ K(0) = K_0 > 0,\ M(0) = M_0 > 0.$$

Note that we do not specify a particular fractional operator at this stage, as our objective is to simulate the fractional-order control system using all three considered fractional operators for comparative analysis.

In the following subsection we explain the solution of the above mentioned control induced system with respect to three different fractional operators with different kernels. For this we have written the three fractional system in a vector notation in general form as:

$$\mathcal{L}^{(1-a)F}D_t^a\big(X_i(t)\big) = \psi\big(X_i(t), u_j(t)\big)\ \ \big[i = 1, 2, 3, 4 \text{ and } j = 1, 2\big]. \tag{4.5.2}$$

Where 'F' symbolized the three different fractional operators and 'a' is the order of the corresponding method. $\psi\big(X_i(t), u_j\big)$ denotes the right hand side of each fractional order control system.

4.5.1 The description of Objective functional :

Here, we construct an objective cost functional in order to minimizing the effect of two key inflammatory cytokines, TNF-α and IL-23, which are associated to the interactions between T cells and dendritic cells simultaneously, reducing the related cost of these biologic treatments. For this, we use two control measures: (i) a TNF-α inhibitor and (ii) an IL-23 blocker those inhibit the effects of the cytokine TNF-α and IL-23. Thus, our considered cost functional takes the form:

$$\text{Minimize } \; Z(u_1, u_2) = {}_0I^a_{t_f}\big[K^2(t) + \mathcal{P}_1 u_1^2(t) + \mathcal{P}_2 u_2^2(t)\big], \tag{4.5.3}$$

subject to the optimal control-induced system (4.5.1) along with the specified initial conditions. Here, ${}_0I^a_{t_f}$ denotes the fractional integral operator. The terms $\mathcal{P}_1$ and $\mathcal{P}_2$ represent the positive weight constants associated with the control functions $u_1(t)$ and $u_2(t)$, respectively, and the units of $\mathcal{P}_1$ and $\mathcal{P}_2$ are the same as $K^2(t)$. We used a quadratic cost functional to measure cost in the control problem, since it fits the nonlinearity and it also prevents the bang-bang or singular optimal control cases [76]. The control set is defined over the time interval $[0, t_f]$, where t_f denotes the total duration of control implementation. The admissible set of Lebesgue measurable controls is given by:

$$U = \big\{\big(u_1(t), u_2(t)\big) : \; 0 < u_j(t) < 1, \; (j = 1, 2), \; t \in [0, t_f]\big\}.$$

The aim of the optimum control problem is to determine the optimal control functions for the system (4.5.1), represented by $u_j^*(t)$ where $j = 1, 2$.

$$Z\big[u_1^*(t), u_2^*(t)\big] = \min\big\{Z(u_1(t), u_2(t)) : u_j(t) \in U, (j = 1, 2)\big\}. \tag{4.5.4}$$

Applying the fractional optimality conditions based on Pontryagin's Minimum principle [64] we state and prove the following theorem and determine the conditions for solving this optimum control problem for the control induced system (4.5.1).

Before presenting the proof of the following theorem, we first state the lemma given by

Lemma 4.5.1 *[77] Assume that $z : [0, t_f] \to \mathbb{R}$ and $0 < \alpha \leq 1$. Then, the following identity holds:*

$$ {}^F_t D^\alpha_{t_f} z(t) = {}^F_0 D^\alpha_t z(t_f - t),$$

where ${}^F D^\alpha$ denotes the fractional derivative in Caputo sense.

Theorem 4.5.1 *Suppose $\mathcal{T}, \mathcal{D}, \mathcal{K}, \mathcal{M}$ be the optimal state solutions for the fractional order model (4.5.1) associated with the optimal controls u_1^*, u_2^* which minimizes the cost functional (4.5.3) over admissible control set $\mathcal{U}$. then there exist adjoint variables θ_i $(i = 1, 2, 3, 4)$*

satisfying

$$\begin{aligned}
\mathcal{L}^{(1-a)F}D_t^a[\theta_1(t')] &= -\theta_1\Big[\mu\Big(1-\frac{2T}{T^{\max}}\Big)-\frac{\gamma_1(1-u_1)D}{1+\delta_1 M}-\eta K-\rho_T\Big]+\theta_2\Big[\frac{\gamma_2(1-u_2)D}{1+\delta_2 M}\Big]\\
&\quad-\theta_3\Big[\frac{\gamma_1(1-u_1)D}{1+\delta_1 M}+\frac{\gamma_2(1-u_2)D}{1+\delta_2 M}\Big],\\
\mathcal{L}^{(1-a)F}D_t^a[\theta_2(t')] &= \theta_1\Big[\frac{\gamma_1(1-u_1)T}{1+\delta_1 M}\Big]+\theta_2\Big[\frac{\gamma_2(1-u_2)T}{1+\delta_2 M}+\rho_D\Big]-\theta_3\Big[\frac{\gamma_1(1-u_1)T}{1+\delta_1 M}+\frac{\gamma_2(1-u_2)T}{1+\delta_2 M}\Big],\\
\mathcal{L}^{(1-a)F}D_t^a[\theta_3(t')] &= -2K+\theta_1\big[\eta T\big]+\theta_3\big[\rho_K\big],\\
\mathcal{L}^{(1-a)F}D_t^a[\theta_4(t')] &= -\theta_1\Big[\frac{\delta_1\gamma_1(1-u_1)TD}{(1+\delta_1 M)^2}\Big]-\theta_2\Big[\frac{\delta_2\gamma_2(1-u_2)TD}{(1+\delta_2 M)^2}\Big]\\
&\quad+\theta_3\Big[\frac{\delta_1\gamma_1(1-u_1)TD}{(1+\delta_1 M)^2}+\frac{\delta_2\gamma_2(1-u_2)T\mathcal{D}}{(1+\delta_2 M)^2}\Big]+\theta_4\Big[\rho_M\Big],
\end{aligned}\tag{4.5.5}$$

where $t'=t_f-t$ *with the transversality conditions*

$$\theta_1(t_f)=\theta_2(t_f)=\theta_3(t_f)=\theta_4(t_f)=0.\tag{4.5.6}$$

Furthermore, optimal solutions (u_1^*,u_2^*) *that minimizes the fractional optimal control in* U*, are given by:*

$$u_i^*(t)=\max\left[0,\min\left\{1,\frac{(\theta_3-\theta_i)(\gamma_i\mathcal{T}\mathcal{D})}{2\mathcal{P}_i(1+\delta_i\mathcal{M})}\right\}\right],\quad (i=1,2).\tag{4.5.7}$$

Proof. To characterize the optimal control, we apply Pontryagin's Minimum Principle, we define the Hamiltonian function $H(T,D,K,M,\theta_i,u_j,t)$ as following:

$$\begin{aligned}
H &= K^2+\mathcal{P}_1u_1^2+\mathcal{P}_2u_2^2\\
&\quad+\theta_1\mathcal{L}^{(a-1)}\Big[\xi_T+\mu T\Big(1-\frac{T}{T^{max}}\Big)-\frac{\gamma_1\big(1-u_1\big)TD}{1+\delta_1 M}-\eta TK-\rho_T T\Big]\\
&\quad+\theta_2\mathcal{L}^{(a-1)}\Big[\xi_D-\frac{\gamma_2\big(1-u_2\big)TD}{1+\delta_2 M}-\rho_D D\Big]\\
&\quad+\theta_3\mathcal{L}^{(a-1)}\Big[\xi_K+\frac{\gamma_1\big(1-u_1\big)TD}{1+\delta_1 M}+\frac{\gamma_2\big(1-u_2\big)TD}{1+\delta_2 M}-\rho_K K\Big]\\
&\quad+\theta_4\mathcal{L}^{(a-1)}\Big[\xi_M-\rho_M M\Big],
\end{aligned}\tag{4.5.8}$$

where $\theta_i(t)$'s $(i=1,2,3,4)$ are the adjoint variables obtained by using right fractional derivative of the equation (4.5.8) over $[0,t_f]$ with respect to optimal state variables $\mathcal{T},\mathcal{D},\mathcal{K},\mathcal{M}$ that satisfy:

$$\mathcal{L}^{(1-a)F}_t D^a_{t_f}[\theta_1(t)]=-\frac{\partial H(T,D,K,M,\theta_i,u_j^*,t)}{\partial T}=-\theta_1\Big[\mu\Big(1-\frac{2T}{T^{\max}}\Big)-\frac{\gamma_1(1-u_1)D}{1+\delta_1 M}-\eta K-\rho_T\Big]$$

$$
\begin{aligned}
&+\theta_2\Big[\frac{\gamma_2(1-u_2)D}{1+\delta_2 M}\Big]-\theta_3\Big[\frac{\gamma_1(1-u_1)D}{1+\delta_1 M}+\frac{\gamma_2(1-u_2)D}{1+\delta_2 M}\Big],\\
\mathcal{L}^{(1-a)}_{t}{}^{F}D^{a}_{t_f}[\theta_2(t)] &= -\frac{\partial H(T,D,K,M,\theta_i,u_j^*,t)}{\partial D}=\theta_1\Big[\frac{\gamma_1(1-u_1)T}{1+\delta_1 M}\Big]+\theta_2\Big[\frac{\gamma_2(1-u_2)T}{1+\delta_2 M}+\rho_D\Big]\\
&-\theta_3\Big[\frac{\gamma_1(1-u_1)T}{1+\delta_1 M}+\frac{\gamma_2(1-u_2)T}{1+\delta_2 M}\Big],\\
\mathcal{L}^{(1-a)}_{t}{}^{F}D^{a}_{t_f}[\theta_3(t)] &= -\frac{\partial H(T,D,K,M,\theta_i,u_j^*,t)}{\partial K}=-2K+\theta_1\big[\eta T\big]+\theta_3\big[\rho_K\big],\\
\mathcal{L}^{(1-a)}_{t}{}^{F}D^{a}_{t_f}[\theta_4(t)] &= -\frac{\partial H(T,D,K,M,\theta_i,u_j^*,t)}{\partial M}=-\theta_1\Big[\frac{\delta_1\gamma_1(1-u_1)TD}{(1+\delta_1 M)^2}\Big]-\theta_2\Big[\frac{\delta_2\gamma_2(1-u_2)TD}{(1+\delta_2 M)^2}\Big]\\
&+\theta_3\Big[\frac{\delta_1\gamma_1(1-u_1)TD}{(1+\delta_1 M)^2}+\frac{\delta_2\gamma_2(1-u_2)TD}{(1+\delta_2 M)^2}\Big]+\theta_4\Big[\rho_M\Big].
\end{aligned}
\tag{4.5.9}
$$

According to Lemma 4.5.1, the adjoint system can be equivalently expressed using the left-sided fractional derivative as follows:

$$
\begin{aligned}
\mathcal{L}^{(1-a)}_{0}{}^{F}D^{a}_{t}[\theta_1(t')] &= -\theta_1(t')\Big[\mu\Big(1-\frac{2T(t')}{T^{\max}}\Big)-\frac{\gamma_1(1-u_1(t'))D(t')}{1+\delta_1 M(t')}-\eta K-\rho_T\Big]\\
&+\theta_2(t')\Big[\frac{\gamma_2(1-u_2(t'))D(t')}{1+\delta_2 M(t')}\Big]\\
&-\theta_3(t')\Big[\frac{\gamma_1(1-u_1(t'))D(t')}{1+\delta_1 M(t')}+\frac{\gamma_2(1-u_2(t'))D(t')}{1+\delta_2 M(t')}\Big],\\
\mathcal{L}^{(1-a)}_{0}{}^{F}D^{a}_{t}[\theta_2(t')] &= \theta_1(t')\Big[\frac{\gamma_1(1-u_1(t'))T(t')}{1+\delta_1 M(t')}\Big]+\theta_2(t')\Big[\frac{\gamma_2(1-u_2(t'))T(t')}{1+\delta_2 M(t')}+\rho_D\Big]\\
&-\theta_3(t')\Big[\frac{\gamma_1(1-u_1(t'))T(t')}{1+\delta_1 M(t')}+\frac{\gamma_2(1-u_2(t'))T(t')}{1+\delta_2 M(t')}\Big],\\
\mathcal{L}^{(1-a)}_{0}{}^{F}D^{a}_{t}[\theta_3(t')] &= -2K(t')+\theta_1(t')\big[\eta T\big]+\theta_3(t')\big[\rho_K\big],\\
\mathcal{L}^{(1-a)}_{0}{}^{F}D^{a}_{t}[\theta_4(t')] &= -\theta_1(t')\Big[\frac{\delta_1\gamma_1(1-u_1(t'))T(t')D(t')}{(1+\delta_1 M(t'))^2}\Big]-\theta_2(t')\Big[\frac{\delta_2\gamma_2(1-u_2(t'))T(t')D(t')}{(1+\delta_2 M(t'))^2}\Big]\\
&+\theta_3(t')\Big[\frac{\delta_1\gamma_1(1-u_1(t'))T(t')D(t')}{(1+\delta_1 M(t'))^2}+\frac{\delta_2\gamma_2(1-u_2(t'))T(t')D(t')}{(1+\delta_2 M(t'))^2}\Big]\\
&+\theta_4(t')\Big[\rho_M\Big],\quad \text{where } t'=t_f-t.
\end{aligned}
\tag{4.5.10}
$$

Here ${}^{F}D^{a}$ denotes the arbitrary fractional differential operator. Since, it is very vast to incorporate considered differential operators into this control problem, we solve and compare with different kernels by numerical simulations. In order to determine the optimal controls $u_1^*(t)$ and $u_2^*(t)$ using the first order necessary condition for optimality provided by

$$
\frac{\partial H}{\partial u_1}\Big|_{(\mathcal{T},\mathcal{D},\mathcal{K},\mathcal{M},\theta_i,u_j^*,t)}=0=\frac{\partial H}{\partial u_2}\Big|_{(\mathcal{T},\mathcal{D},\mathcal{K},\mathcal{M},\theta_i,u_j^*,t)}.
\tag{4.5.11}
$$

Thus, utilizing the above-mentioned equation (4.5.11), we have

$$u_1^*(t) = \frac{(\theta_3 - \theta_1)(\gamma_1 \mathcal{TD})}{2\mathcal{P}_1(1+\delta_1\mathcal{M})} \text{ and } u_2^*(t) = \frac{(\theta_3 - \theta_2)(\gamma_2 \mathcal{TD})}{2\mathcal{P}_2(1+\delta_2\mathcal{M})}. \tag{4.5.12}$$

To ensure that the control functions u_1^* and u_2^* represent optimal solutions, the second-order sufficient conditions for a minima must be satisfied. For the present problem, we obtain:

$$\left.\frac{\partial^2 H}{\partial u_i^2}\right|_{u_i=u_i^*} = 2\mathcal{P}_i > 0, \quad \text{for } i = 1, 2, \tag{4.5.13}$$

which confirms that u_i^* minimizes the Hamiltonian and satisfies the second-order condition under Pontryagin's Minimum Principle.

The conventional control's boundedness criterion and the characteristics of the control set U, we have the compact form of control profiles i.e., the equation (4.5.7).

4.5.2 FBSM-Based Numerical Schemes for Different Fractional Operators

Let us take the state variables of the control system $X_1(t) = T(t), X_2(t) = D(t), X_3(t) = K(t)$, and $X_4(t) = M(t)$. We have also considered the functions $f_i (i = 1, 2, 3, 4)$ as:

$$\begin{aligned}
f_1(t) &= \mathcal{L}^{(a-1)}\left[\xi_T + \mu T(t)\left[1 - \frac{T(t)}{T^{max}}\right] - \frac{\gamma_1\big[1-u_1(t)\big]T(t)D(t)}{1+\delta_1 M(t)} - \eta T(t)K(t) - \rho_T T(t)\right],\\
f_2(t) &= \mathcal{L}^{(a-1)}\left[\xi_D - \frac{\gamma_2\big[1-u_2(t)\big]T(t)D(t)}{1+\delta_2 M(t)} - \rho_D D(t)\right],\\
f_3(t) &= \mathcal{L}^{(a-1)}\left[\xi_K + \frac{\gamma_1\big[1-u_1(t)\big]T(t)D(t)}{1+\delta_1 M(t)} + \frac{\gamma_2\big[1-u_2(t)\big]T(t)D(t)}{1+\delta_2 M(t)} - \rho_K K(t)\right],\\
f_4(t) &= \mathcal{L}^{(a-1)}\left[\xi_M - \rho_M M(t)\right].
\end{aligned} \tag{4.5.14}$$

Combining the above system and rewrite it shortly we can have:

$$f_i^{(j)} \equiv f_i\big(X_1(j), X_2(j), X_3(j), X_4(j), u_1(j), u_2(j)\big) \quad (i = 1, 2, 3, 4).$$

The superscript $^{(j)}$ represent the value of each functions at $j-th$ time point.

In similar manner corresponding to the adjoint variables $\theta_i (i = 1, 2, 3, 4)$ let us construct the functions $g_i (i = 1, 2, 3, 4)$ as following:

$$\begin{aligned}
g_1(t) = \mathcal{L}^{(a-1)}\Bigg[&- \theta_1\Big[\mu\Big(1 - \frac{2T}{T^{\max}}\Big) - \frac{\gamma_1(1-u_1)D}{1+\delta_1 M} - \eta K - \rho_T\Big] + \theta_2\Big[\frac{\gamma_2(1-u_2)D}{1+\delta_2 M}\Big]\\
&- \theta_3\Big[\frac{\gamma_1(1-u_1)D}{1+\delta_1 M} + \frac{\gamma_2(1-u_2)D}{1+\delta_2 M}\Big]\Bigg],
\end{aligned}$$

$$
\begin{aligned}
g_2(t) &= \mathcal{L}^{(a-1)}\Big[\theta_1\Big[\frac{\gamma_1(1-u_1)T}{1+\delta_1 M}\Big] + \theta_2\Big[\frac{\gamma_2(1-u_2)T}{1+\delta_2 M} + \rho_D\Big] - \theta_3\Big[\frac{\gamma_1(1-u_1)T}{1+\delta_1 M} + \frac{\gamma_2(1-u_2)T}{1+\delta_2 M}\Big]\Big],\\
g_3(t) &= \mathcal{L}^{(a-1)}\Big[-2K + \theta_1\big[\eta T\big] + \theta_3\big[\rho_K\big]\Big],\\
g_4(t) &= \mathcal{L}^{(a-1)}\Big[-\theta_1\Big[\frac{\delta_1\gamma_1(1-u_1)TD}{(1+\delta_1 M)^2}\Big] - \theta_2\Big[\frac{\delta_2\gamma_2(1-u_2)TD}{(1+\delta_2 M)^2}\Big]\\
&\qquad + \theta_3\Big[\frac{\delta_1\gamma_1(1-u_1)TD}{(1+\delta_1 M)^2} + \frac{\delta_2\gamma_2(1-u_2)TD}{(1+\delta_2 M)^2}\Big] + \theta_4\Big[\rho_M\Big]\Big].
\end{aligned}
\tag{4.5.15}
$$

Combining the above system and rewrite it shortly we can have:

$$
g_i^{(j)} \equiv g_i\big(X_1(j), X_2(j), X_3(j), X_4(j), \theta_1(j), \theta_2(j), \theta_3(j), \theta_4(j), u_1(j), u_2(j)\big) \;\; (i = 1, 2, 3, 4).
$$

The superscript $^{(j)}$ represent the value of each functions at $j-th$ time point.

In the beginning, we explain a numerical approach using the Forward-Backward Sweep Method (FBSM) by the following steps:

Step 1. (Initialization)

1. a: Order of the fractional derivative.
2. Dividing the time interval $[0, t_f]$ into the n number of time steps, where $h = \frac{t_f}{n}(t_k = kh,\ k = 0, 1, \cdots, n)$ is the step size.
3. Initial condition for each state variable $X_i (i = 1, 2, 3, 4)$ and the terminal condition for each adjoint variable $\theta_i(n)(i = 1, 2, 3, 4)$ together with the consideration of the control parameters $u_1(0)$ and $u_2(0)$.

Step 2. (Forward Sweep for State Variables with Control)

$$
X_i(t) = \text{Forward update}\big(X_i, f_i, u_i\big) \;\; \big[t = 1, 2, \cdots n-1\big].
$$

Step 3. (Backward Sweep for Adjoint Variables)

$$
\theta_i(n-t) = \text{Backward update}\big(X_i, \theta_i, g_i, u_i\big) \;\; \big[t = 1, 2, \cdots n-1\big].
$$

Step 4. (Update the Control Parameters)

Updating both u_i $(i = 1, 2)$ by using a convex combination of the previous controls and the values given by the equation (4.5.7) by:

$$
u_i^{New}(t) = \pi\Big[\max\Big\{0, \min\Big(1, \frac{(\theta_3 - \theta_i)(\gamma_i TD)}{2\mathcal{P}_i(1+\delta_i M)}\Big)\Big\}\Big] + (1-\pi)u_i^{Old}(t). \tag{4.5.16}
$$

Step 5. (Check Convergence)

If two successive iteration provides sufficiently close values of the control parameters, then the iteration stops, otherwise repeat Step 2 to Step 5.

The Forward-Backward update rules for the control problem, formulated using the Caputo operators [(i)-(ii)], the Caputo-Fabrizio operators [(iii)-(iv)], and the Atangana-Baleanu operators [(v)-(vi)] in the Caputo sense, are presented as follows:

(i) Forward Caputo Numerical Scheme

$$\begin{aligned} X_i(1) &= X_i(0) + \frac{h^\lambda}{\Gamma(\lambda+2)}\Big[(t+1)^\lambda(t+2+\lambda) - t^\lambda(t+2+2\lambda)\Big] f_i^{(0)}, \\ X_i(t+1) &= X_i(0) + \frac{h^\lambda}{\Gamma(\lambda+2)} \sum_{j=1}^{t} \Big[{}^C\Xi_1 f_i^{(j)} - {}^C\Xi_2 f_i^{(j-1)}\Big], \\ &\big(i = 1,2,3,4 \text{ and } t = 1,2,\cdots,n-1\big). \end{aligned} \tag{4.5.17}$$

(ii) Backward Caputo Numerical Scheme

$$\begin{aligned} \theta_i(n-1) &= \frac{h^\lambda}{\Gamma(\lambda+1)}\Big[(t+1)^\lambda(t+2+\lambda) - t^\lambda(t+2+2\lambda)\Big], \\ \theta_i(n-t) &= \frac{h^\lambda}{\Gamma(\lambda+1)} \sum_{j=1}^{t-1} \Big[{}^C\Xi_1 g_i^{(n-j)} - {}^C\Xi_2 g_i^{(n-j+1)}\Big], \\ &\big(i = 1,2,3,4 \text{ and } t = 2,3,\cdots,n\big). \end{aligned} \tag{4.5.18}$$

Here we have taken the Caputo fractional order $a = \lambda$ and the coefficients ${}^C\Xi_i (i = 1,2)$ are given by:

$$\begin{aligned} {}^C\Xi_1 &= (t-j+1)^\lambda(t-j+2+\lambda) - (t-j)^\lambda(t-j+2+2\lambda), \\ {}^C\Xi_2 &= (t-j+1)^{(\lambda+1)}(t-j+2+\lambda) - (t-j)^\lambda(t-j+1+\lambda). \end{aligned}$$

(iii) Forward Caputo-Fabrizio Numerical Scheme

$$\begin{aligned} X_i(1) &= X_i(0) + \Big[\frac{1}{2}(2-\zeta)(1-\zeta) + \frac{3h}{4}\zeta(2-\zeta)\Big] f_i^{(0)}, \\ X_i(t+1) &= X_i(t) + \Big[{}^{CF}\Xi_1 f_i^{(t)} - {}^{CF}\Xi_2 f_i^{(t-1)}\Big], \\ &\big(i = 1,2,3,4 \text{ and } t = 1,2,\cdots,n-1\big). \end{aligned} \tag{4.5.19}$$

(iv) Backward Caputo-Fabrizio Numerical Scheme

$$\begin{aligned} \theta_i(n-1) &= \Big[\frac{1}{2}(2-\zeta)(1-\zeta) + \frac{3h}{4}\zeta(2-\zeta)\Big] g_i^{(n)}, \\ \theta_i(n-t) &= \theta_i(n-t+1) + \Big[{}^{CF}\Xi_1 g_i^{(n-t+1)} - {}^{CF}\Xi_2 g_i^{(n-t+2)}\Big], \\ &\big(i = 1,2,3,4 \text{ and } t = 1,2,\cdots,n-1\big). \end{aligned} \tag{4.5.20}$$

We have taken the Caputo-Fabrizio fractional order $a = \zeta$ and the coefficients ${}^{CF}\Xi_i (i = 1,2)$ are given by:

$${}^{CF}\Xi_1 = \frac{1}{2}(2-\zeta)(1-\zeta) + \frac{3h}{4}\zeta(2-\zeta), \qquad {}^{CF}\Xi_2 = \frac{1}{2}(2-\zeta)(1-\zeta) + \frac{h}{4}\zeta(2-\zeta).$$

(v) Forward Atangana-Baleanu Numerical Scheme

$$
\begin{aligned}
X_i(1) &= X_i(0) + {}^{ABC}\Xi_1 f_i^{(0)} + {}^{ABC}\Xi_2\Big[(t+1)^{\alpha}(t+2+\alpha) - t^{\alpha}(t+2+2\alpha)\Big] f_i^{(0)},\\
X_i(t+1) &= X_i(0) + {}^{ABC}\Xi_1 f_i^{(t)} + {}^{ABC}\Xi_2 \sum_{j=1}^{t}\Big[{}^{C}\Xi_1^{(\alpha)} f_i^{(j)} - {}^{C}\Xi_2^{(\alpha)} f_i^{(j-1)}\Big],\\
&\big(i = 1,2,3,4 \text{ and } t = 1,2,\cdots,n-1\big).
\end{aligned}
\tag{4.5.21}
$$

(vi) Backward Atangana-Baleanu Numerical Scheme

$$
\begin{aligned}
\theta_i(n-1) &= {}^{ABC}\Xi_1 g_i^{(n)} + {}^{ABC}\Xi_2\Big[(t+1)^{\alpha}(t+2+\alpha) - t^{\alpha}(t+2+2\alpha)\Big] g_i^{(n)},\\
\theta_i(n-t) &= {}^{ABC}\Xi_1 g_i^{(n-t+1)} + {}^{ABC}\Xi_2 \sum_{j=1}^{t-1}\Big[{}^{C}\Xi_1^{(\alpha)} g_i^{(n-j)} - {}^{C}\Xi_2^{(\alpha)} g_i^{(n-j+1)}\Big],\\
&\big(i = 1,2,3,4 \text{ and } t = 2,\cdots,n\big).
\end{aligned}
\tag{4.5.22}
$$

Here, $a = \alpha$ is taken as the Atangana-Baleanu-Caputo fractional order and the coefficients are given by:

$$
\begin{aligned}
{}^{ABC}\Xi_1 &= \frac{(1-\alpha)\Gamma(\alpha)}{(1-\alpha)\Gamma(\alpha)+\alpha}, \quad {}^{ABC}\Xi_2 = \frac{h^{\alpha}}{(\alpha+1)(1-\alpha)\Gamma(\alpha)+\alpha},\\
{}^{C}\Xi_1^{(\alpha)} &= (t-j+1)^{\alpha}(t-j+2+\alpha) - (t-j)^{\alpha}(t-j+2+2\alpha),\\
{}^{C}\Xi_2^{(\alpha)} &= (t-j+1)^{(\alpha+1)}(t-j+2+\alpha) - (t-j)^{\alpha}(t-j+1+\alpha).
\end{aligned}
$$

4.6 Numerical Simulation

In this section, we present the results of numerical simulations designed to analyze the formulated model in accordance with analytical predictions. These simulations are carefully structured to ensure consistency with fundamental mathematical principles derived from prior analytical investigations. The initial values for the model variables are selected to adhere to these foundational criteria, ensuring that the system behaves in a manner consistent with expected theoretical outcomes. To conduct these simulations, we utilized Python. The initial population values used in the simulations are set as follows: $T_0 = 30$, $D_0 = 25$, $K_0 = 20$, and $M_0 = 15$. The corresponding parameter values employed throughout the numerical experiments are listed in Table 4.1, providing a clear reference for the simulation setup. By employing different fractional-order derivatives, we examined how varying memory effects influence the stability and dynamics of the cell populations within the system.

The first set of simulations, depicted in Figure 4.2, showcases the temporal evolution of T cells, dendritic cells, keratinocytes, and mesenchymal stem cells within system (4.1.1), using the Caputo kernel function. These simulations were conducted for different values of the fractional-order parameter λ, specifically $\lambda = 0.6$, 0.7, 0.8, and 0.9. The results reveal a distinct pattern: as the value of λ decreases, the stabilization of the cell populations occurs more gradually, indicating that lower values of λ introduce a stronger memory effect.

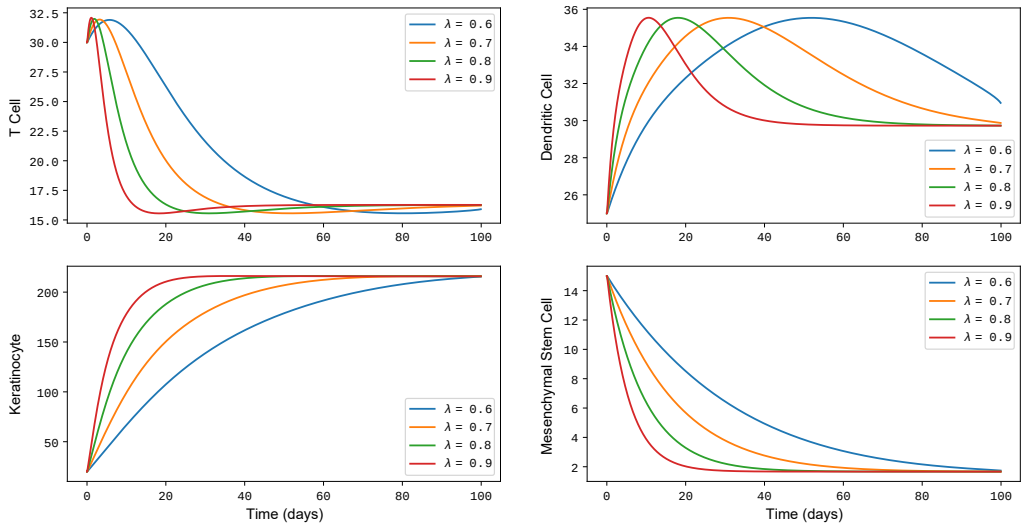

Figure 4.2: Population density of T cells, dendritic cells, keratinocytes, and MSCs with respect to time for different values of the fractional order λ (= 0.6, 0.7, 0.8, 0.9) in the Caputo sense. For this simulation, we considered the system (4.1.1) by taking the memory rate parameter value $\mathcal{L}$=0.7 day^{-1}.

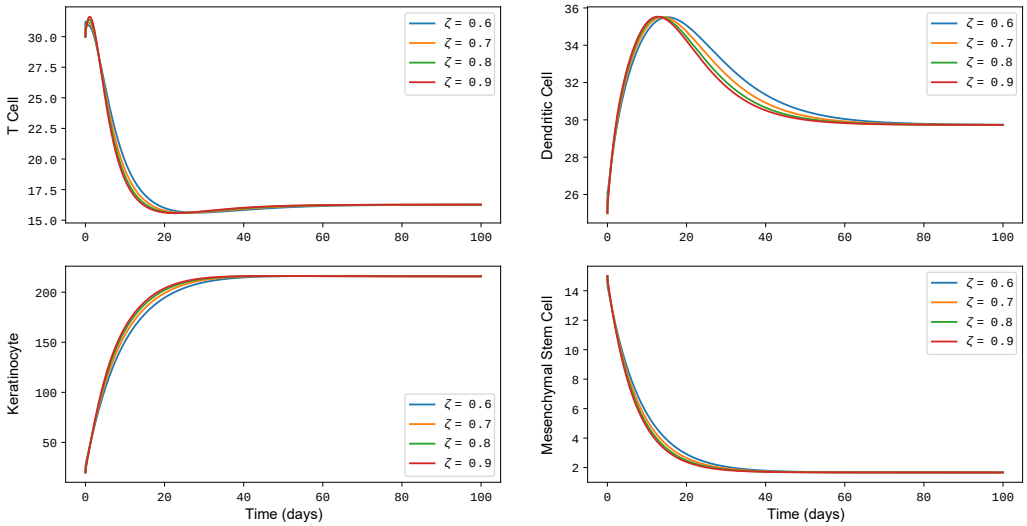

Figure 4.3: Population density of T cells, dendritic cells, keratinocytes, and MSCs with respect to time for different values of the fractional order ζ (= 0.6, 0.7, 0.8, 0.9) in the Caputo-Fabrizio sense. For this simulation, we take the memory rate parameter value $\mathcal{L}$=0.7 day^{-1} by considering the system (4.1.2).

This suggests that the system retains past states for longer durations when λ is smaller, leading to delayed convergence to equilibrium. In contrast, higher values of λ result in

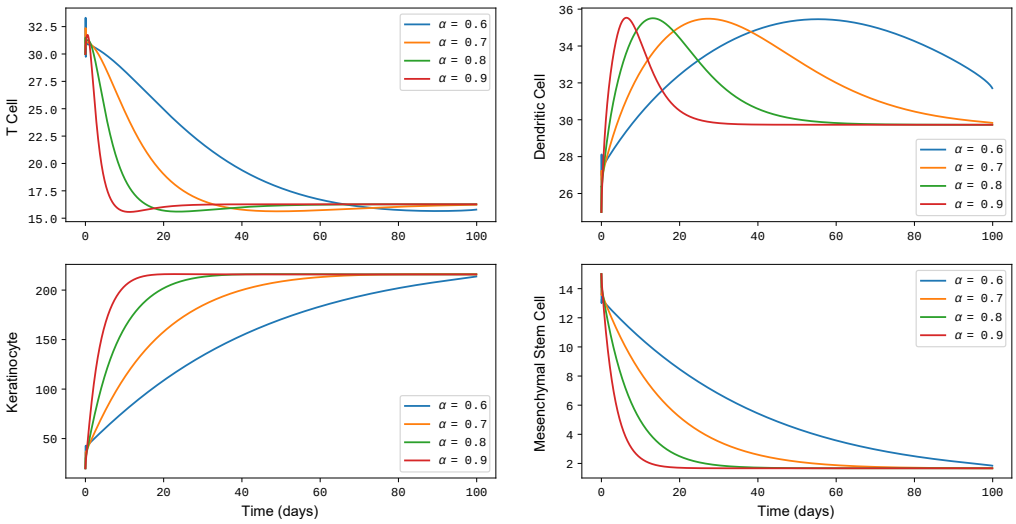

Figure 4.4: Population density of T cells, dendritic cells, keratinocytes, and MSCs with respect to time for different values of the fractional order α (= 0.6, 0.7, 0.8, 0.9) in the Atangana-Baleanu-Caputo sense. For this simulation, we considered the system (4.1.3) considering the memory rate parameter value $\mathcal{L}$=0.7 day^{-1}.

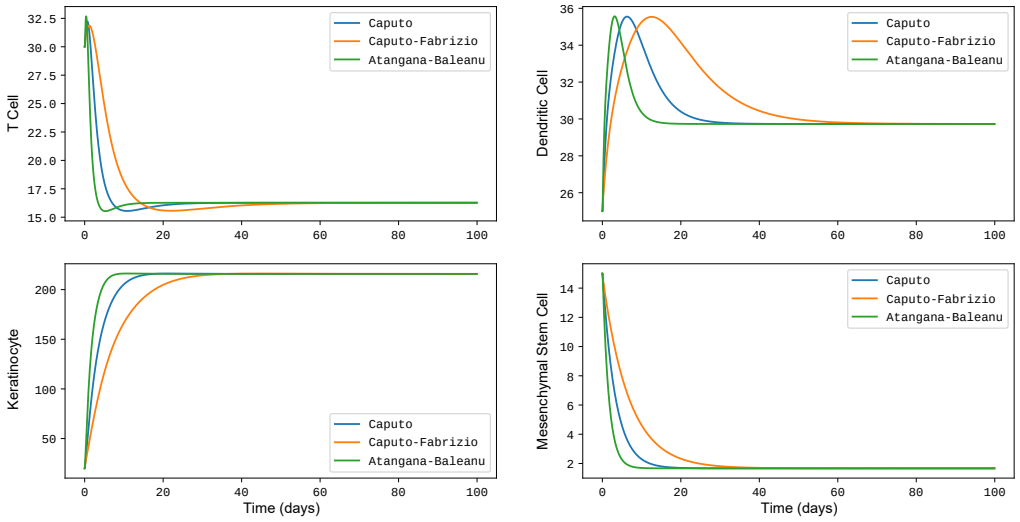

Figure 4.5: Time evolution of the population densities of T cells, dendritic cells, keratinocytes, and mesenchymal stem cells shown in a single plot for the systems (4.1.1), (4.1.2), and (4.1.3). The simulations are performed by fixing the memory rate parameter value of $\mathcal{L}$=0.7 day^{-1}, with all fractional-order parameters set to $\lambda = \zeta = \alpha = 0.9$. The dynamics are evaluated using three distinct fractional differential operators: Caputo, Caputo-Fabrizio, and Atangana–Baleanu in the Caputo sense, each with their respective kernel functions.

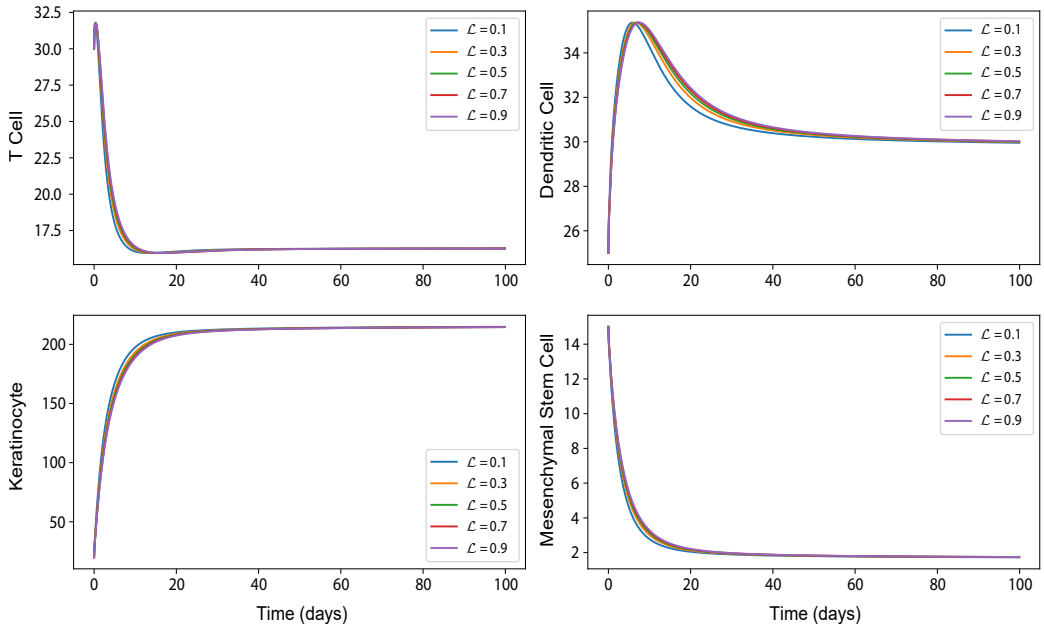

Figure 4.6: Temporal evolution of system population dynamics under varying memory rate parameter $\mathcal{L}$ within the Caputo fractional operator framework. The fractional order parameter is fixed at $\lambda = 0.9$, with $\mathcal{L}$ values set to 0.1, 0.3, 0.5, 0.7, and 0.9 day^{-1}. The figure shows that the trajectories remain nearly similar despite variations in the memory rate parameter.

faster stabilization, signifying that the system is less influenced by its history. This behavior highlights the significant role that fractional-order derivatives play in modeling biological processes with memory-dependent dynamics.

The second set of simulations, illustrated in Figure 4.3, investigates the behavior of the model under system (4.1.2) using the Caputo-Fabrizio kernel function. Here, we varied the fractional-order parameter ζ across values $\zeta = 0.6$, 0.7, 0.8, and 0.9 to assess how different fractional orders impact system stability. Unlike the Caputo kernel function, which showed a pronounced effect of ζ on stabilization rates, the Caputo-Fabrizio formulation exhibits a more uniform response across different values of ζ. This implies that the influence of fractional-order variation is less significant in this case, leading to a more consistent stabilization pattern regardless of the specific ζ value used. This observation underscores a fundamental difference between the two kernel functions: while the Caputo kernel function results in gradual stabilization for lower orders, the Caputo-Fabrizio approach produces less sensitivity to fractional-order changes, suggesting that it represents memory effects in a different manner.

The final set of simulations, represented in Figure 4.4, examines system (4.1.3) while varying the fractional-order parameter α ($\alpha = 0.6$, 0.7, 0.8, and 0.9), again using the Caputo kernel function. The results demonstrate a trend similar to that observed in Figure 4.2: as the value of α decreases, the system takes longer to reach a stable state. This reinforces the finding that lower fractional orders amplify memory effects, delaying stabilization across

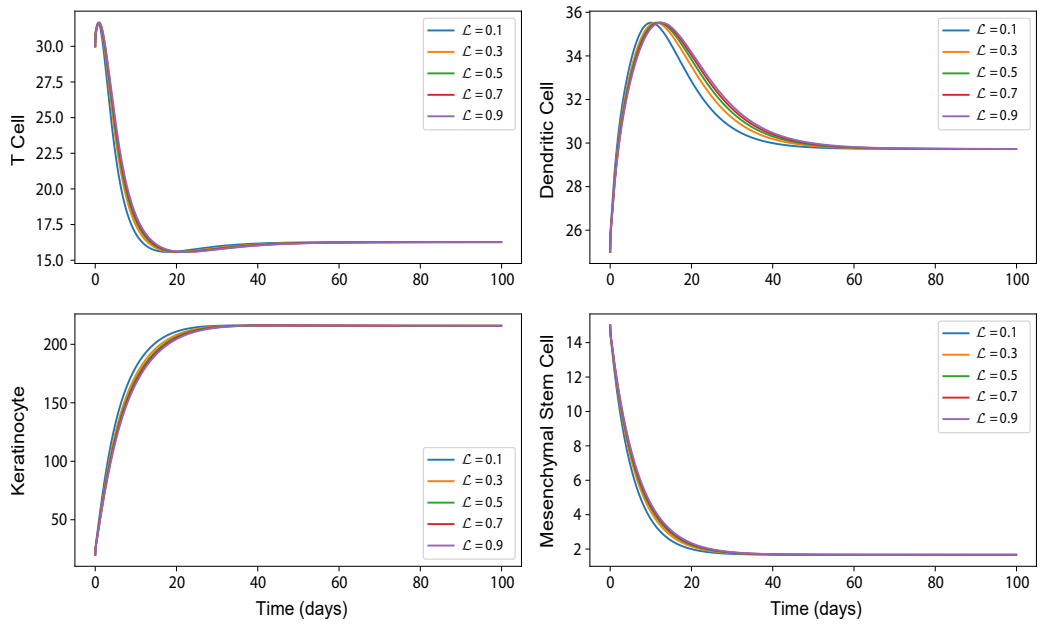

Figure 4.7: All system population dynamics with respect to time by varying the memory rate parameter $\mathcal{L}$ values considering the Caputo-Fabrizio fractional operator structure. The fractional order parameter is fixed at $\zeta = 0.9$, with $\mathcal{L}$ values set to 0.1, 0.3, 0.5, 0.7, and 0.9 day^{-1}. The figure indicates that the trajectories exhibit minimal variation despite changes in the memory rate parameter.

multiple configurations of the model. Taken together, these simulations emphasize the profound impact of fractional-order parameters on biological system behavior. The comparison between the Caputo and Caputo-Fabrizio kernel functions highlights the importance of selecting an appropriate mathematical framework when modeling dynamic systems influenced by historical dependencies. Ultimately, these insights contribute to a deeper understanding of fractional-order modeling in biological processes, offering a powerful approach for capturing the complex, memory-driven dynamics of cellular populations.

In Figure 4.5, we analyze the temporal evolution of the model's population densities—T cells, dendritic cells, keratinocytes, and mesenchymal stem cells—by employing three distinct numerical schemes based on the Caputo, Caputo-Fabrizio, and Atangana-Baleanu-Caputo operators. The fractional-order parameters were fixed at $\lambda = \zeta = \alpha = 0.9$ to provide a uniform basis for comparison. The results reveal a clear distinction in how each operator influences the system's stabilization behavior. Among the three approaches, the Caputo-Fabrizio operator exhibits the most rapid convergence to the stability orbit, indicating a weaker memory effect and faster adaptation of population densities to equilibrium. The Atangana-Baleanu-Caputo operator follows, displaying a moderate speed of convergence to stabilization behavior, while the Caputo operator demonstrates the slowest approach to stability, reflecting its stronger historical dependency. This finding underscores the fundamental differences in how these fractional operators encode memory effects in biological systems. The Atangana-Baleanu-Caputo

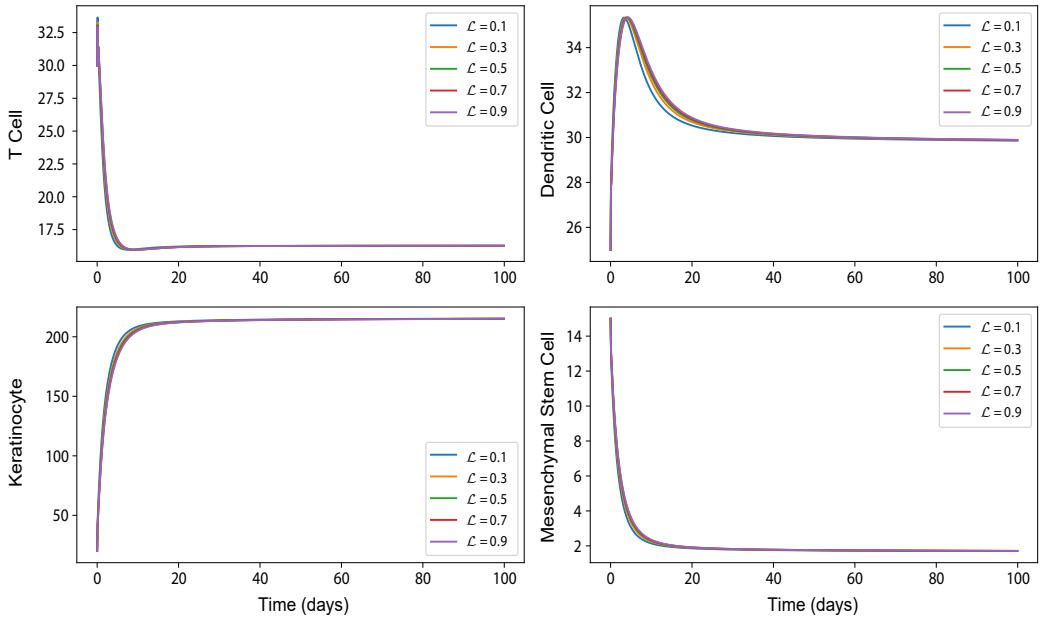

Figure 4.8: Using the Atangana-Baleanu-Caputo fractional scheme, all system population densities with respect to time are plotted by varying the memory rate parameter $\mathcal{L}$ values of 0.1, 0.3, 0.5, 0.7, and 0.9 day^{-1} while fixing the value of the fractional order parameter α at 0.9. Although the memory rate parameter changes, the figure shows that the trajectories show negligible variation.

scheme, by allowing for a more balanced and responsive adaptation, could be particularly useful in applications where rapid recovery and stabilization of biological populations are crucial.

In Figures 4.6, 4.7, and 4.8, we extend our analysis by investigating the influence of the memory rate parameter ($\mathcal{L}$) on system dynamics while utilizing three different fractional operators: Caputo, Caputo-Fabrizio, and Atangana-Baleanu-Caputo. The fractional-order parameter was consistently set at 0.9, while $\mathcal{L}$ was varied across 0.1, 0.3, 0.5, 0.7, and 0.9 day^{-1}. The objective was to determine whether the rate at which past states influence present behavior significantly alters population trajectories. Interestingly, the results across all three figures demonstrate minimal variation in system trajectories despite changes in $\mathcal{L}$, suggesting that within this specific modeling framework, the system exhibits low sensitivity to variations in the memory rate parameter. This indicates that while the choice of fractional operator plays a crucial role in defining system behavior, adjustments to $\mathcal{L}$ do not significantly impact the model's predictive power in this context. These insights are valuable in biological modeling, as they suggest that certain fractional-order parameters may have a dominant effect on system behavior, while others, such as the memory rate parameter $\mathcal{L}$, may have a more limited role.

We now analyze the impact of control strategies on the fractionalized model (4.5.1) under different fractional operators, applying distinct formulations across the three considered frac-

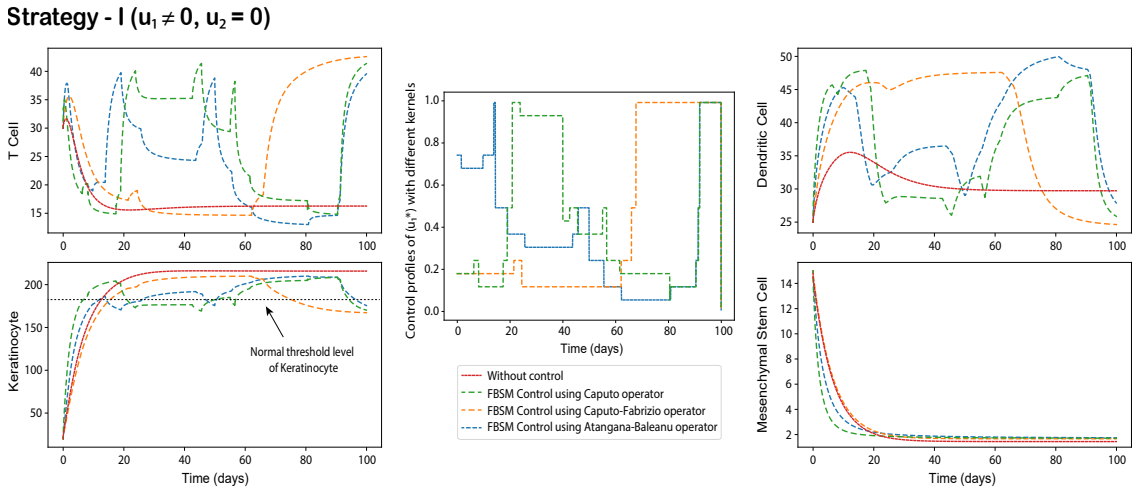

Figure 4.9: Control-induced system along with the control profile of the optimal control functions, considering $u_1 \neq 0, u_2 = 0$, over time using three different fractional operator kernels: Caputo, Caputo-Fabrizio, and Atangana-Baleanu. The uncontrolled system populations are represented by red solid trajectories, while the fractional-order controlled systems are illustrated using different colored dotted trajectories corresponding to the respective kernels. The control functions highlight how each kernel's distinct memory effect influences the density and timing of optimal treatment interventions required to regulate the immune response.

tional approaches. This step aims to enhance our understanding of how various mathematical interpretations of fractional dynamics can be utilized to design effective control interventions relevant to real-world scenarios. For the numerical implementation of optimal control strategies via the Forward-Backward Sweep Method (FBSM), all fractional orders are fixed as $\lambda = \zeta = \alpha = 0.9$, and the memory rate parameter is set to $\mathcal{L} = 0.7$ day^{-1}. The weight constants in the objective functional are chosen as $\mathcal{P}_1 = \mathcal{P}_2 = 0.5$, and all other parameter values used in the simulations are taken from Table 4.1.

Strategy-I $(u_1 \neq 0, u_2 = 0)$

In this control strategy, we investigate the effects of administering a TNF-α inhibitor by setting $u_1 \neq 0$, while excluding the use of an IL-23 blocker by fixing $u_2 = 0$. Figure 4.9, provides a comparative analysis between the uncontrolled system (depicted by red trajectories) and the controlled system, which is simulated using three different fractional operators: Caputo, Caputo-Fabrizio, and Atangana-Baleanu-Caputo—through FBSM. The controlled system is represented using three distinct colored dotted trajectories, corresponding to each fractional operator, allowing for a direct comparison of their effects on population dynamics. Additionally, the control profile of u_1 is illustrated to capture its evolution under the influence of the three kernel functions. The numerical results in Figure 4.9, reveal that TNF-α inhibition leads to a gradual, but not substantial, decline in keratinocyte density, indicating partial sup-

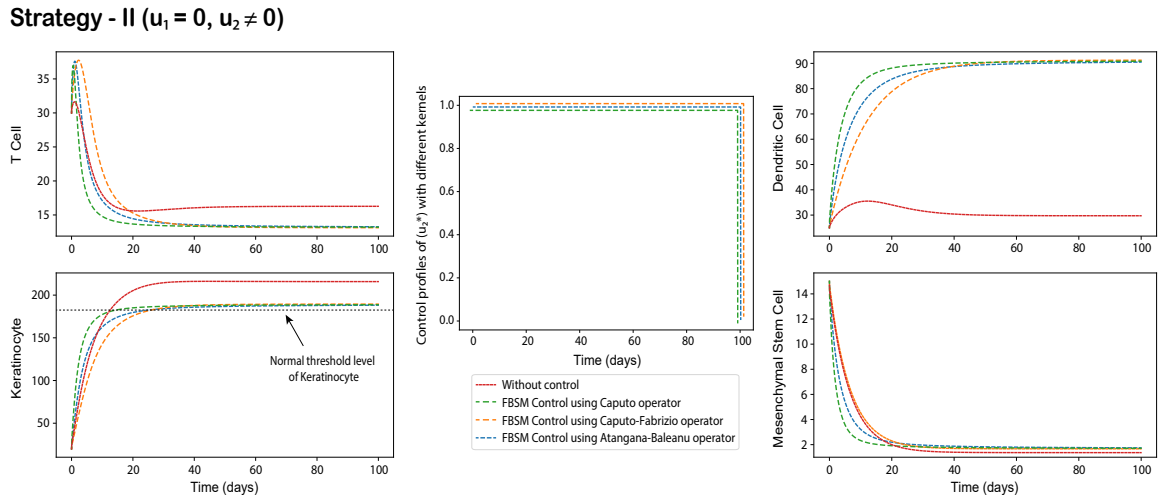

Figure 4.10: Comparison of the uncontrolled and controlled system dynamics under the influence of the optimal control function $u_2 \neq 0$ while $u_1 = 0$, utilizing three fractional operator kernels: Caputo, Caputo-Fabrizio, and Atangana-Baleanu. Red solid trajectories represent the uncontrolled system populations, whereas the controlled system is depicted through distinct colored dotted trajectories corresponding to each fractional operator. The control profiles illustrate the impact of different kernel memory effects on the timing and intensity of optimal treatment interventions for immune response regulation.

pression of the inflammatory response. T cell density increases significantly, while dendritic cell density decreases. These outcomes suggest that while TNF-α inhibition can diminish certain pro-inflammatory pathways, it does not fully eliminate immune activation, resulting in a partial disruption of cytokine-mediated interactions but not complete normalization of keratinocyte proliferation. The different responses observed across the three fractional operators highlight the importance of memory effects, as each approach captures unique aspects of immune regulation and inflammation dynamics.

Strategy-II $(u_1 = 0, u_2 \neq 0)$

In this control strategy, we focus on the effects of an IL-23 blocker by setting $u_2 \neq 0$, while excluding the use of a TNF-α inhibitor by fixing $u_1 = 0$. Again in Figure 4.10, we compare controlled and uncontrolled dynamics across the same three fractional operators (distinguished by different colored trajectories). The control profile of u_2 is illustrated. Simulations show a slight reduction in keratinocyte density, though levels remain above healthy thresholds, indicating that IL-23 blockade alone is insufficient to achieve complete disease remission. Additionally, T-cell density declines modestly, whereas dendritic cell density increases, pointing to limited regulation of the immune response. Biologically, these results imply that IL-23 inhibition alone cannot fully disrupt the inflammatory cytokine network, allowing immune infiltration to persist and thus preventing restoration of tissue homeosta-

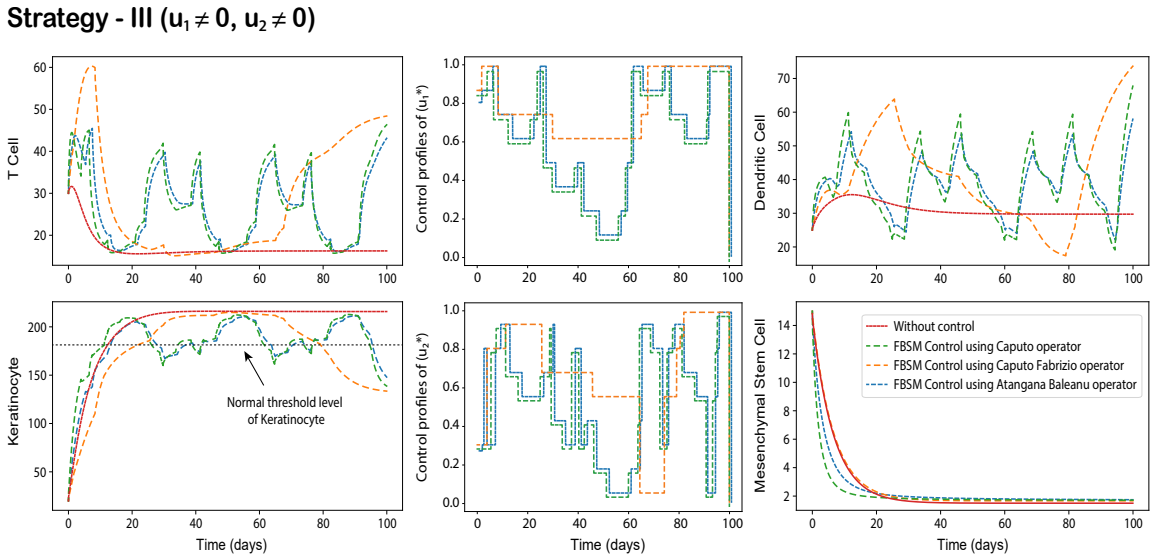

Figure 4.11: Visualization of the system dynamics under both control functions ($u_1 \neq 0, u_2 \neq 0$) compared to the uncontrolled case, using three fractional operator kernels: Caputo, Caputo-Fabrizio, and Atangana-Baleanu. The red solid trajectories indicate the uncontrolled system populations, while the controlled system is represented by colored dotted trajectories corresponding to each fractional operator. The control profiles demonstrate how the distinct memory effects of each kernel influence the optimal timing and magnitude of treatment interventions for immune response regulation.

sis. Note that, across all three fractional operators, similar population trends are observed, suggesting that under the control of IL-23 inhibition, the memory effects inherent to each operator do not significantly alter the qualitative behavior of the system. This emphasizes the potential need for a combined therapeutic approach.

Strategy-III ($u_1 \neq 0, u_2 \neq 0$)

In this control strategy, we conduct numerical simulations on fractionalized systems represented by equations (4.1.1), (4.1.2), and (4.1.3), governed by three distinct fractional-order differential operators: Caputo, Caputo-Fabrizio, and Atangana-Baleanu-Caputo, to evaluate the behavior of the model under simultaneous application of both control measures: the TNF-α inhibitor ($u_1 \neq 0$) and IL-23 blocker ($u_2 \neq 0$) (see Figure 4.11). The red trajectories depict the uncontrolled system, while the controlled responses are illustrated by three differently colored dotted trajectories corresponding to each fractional operator, allowing a comparative assessment of the system's dynamics. The evolution of the control profiles u_1 and u_2 are also presented, reflecting how each fractional kernel influences treatment intensity over time. Results indicate that the combined control strategy successfully reduces keratinocyte density to a healthy state, effectively curing inflammation-induced proliferation. The densities of T cells and dendritic cells increase significantly. Biologically, this implies that cytokine-driven inflammatory interactions are suppressed, slowing immune infiltration, a key contributor to

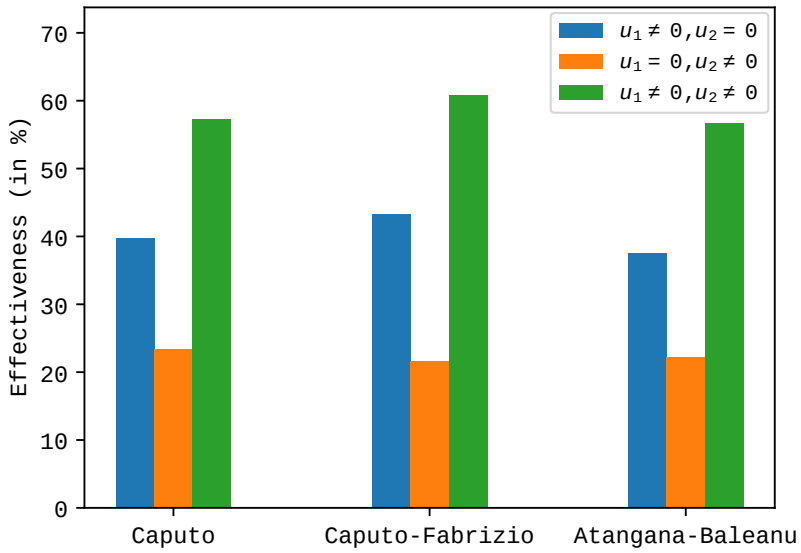

Figure 4.12: Effectiveness analysis of control strategies I (blue), II (orange), and III (green), expressed in percentage, for the three considered fractional operators with fixed fractional parameters $\lambda = \zeta = \alpha = 0.9$. Strategy I shows that the moderate effectiveness with all considered operators, among them Caputo–Fabrizio, yields the highest effectiveness. Strategy II demonstrates weaker effectiveness, and the control using all fractional operators provides almost similar outcomes. Among them, the Caputo operator provides the highest effectiveness. Strategy III, the combined strategy, provides the strongest overall results, with the Caputo–Fabrizio operator again achieving the highest effectiveness among all operators.

psoriasis progression. Notably, the Caputo and Atangana-Baleanu-Caputo operators exhibit similar trends across all cell populations, indicating comparable memory effects, whereas the Caputo-Fabrizio operator produces distinct control profiles and immune dynamics due to its faster memory decay. These differences underscore that for a fixed fractional-order parameter value, optimal control strategies depend on the chosen operator: Caputo demands sustained interventions due to strong memory retention, suitable for chronic cases; Caputo-Fabrizio allows short-term interventions, making it ideal for acute flares but less effective for long-term control; and Atangana-Baleanu-Caputo offers a balanced memory effect, supporting a hybrid approach with intensive early therapy followed by maintenance dosing. These findings emphasize the importance of fractional-order modelling in tailoring control strategies, as varying memory effects directly influence the design and efficacy of therapeutic interventions.

Figure 4.12 presents the effectiveness analysis (in %) of three control strategies using bar plots, with fixed fractional parameters $\lambda = \zeta = \alpha = 0.9$. From a biological perspective, Strategy I (e.g., targeting a single pathway) shows moderate effectiveness, with the Caputo–Fabrizio operator yielding the best outcome. Strategy II (targeting an alternative pathway) shows weaker responses with comparable results across all operators, where the Caputo operator performs slightly better. Strategy III, representing a combined therapeutic

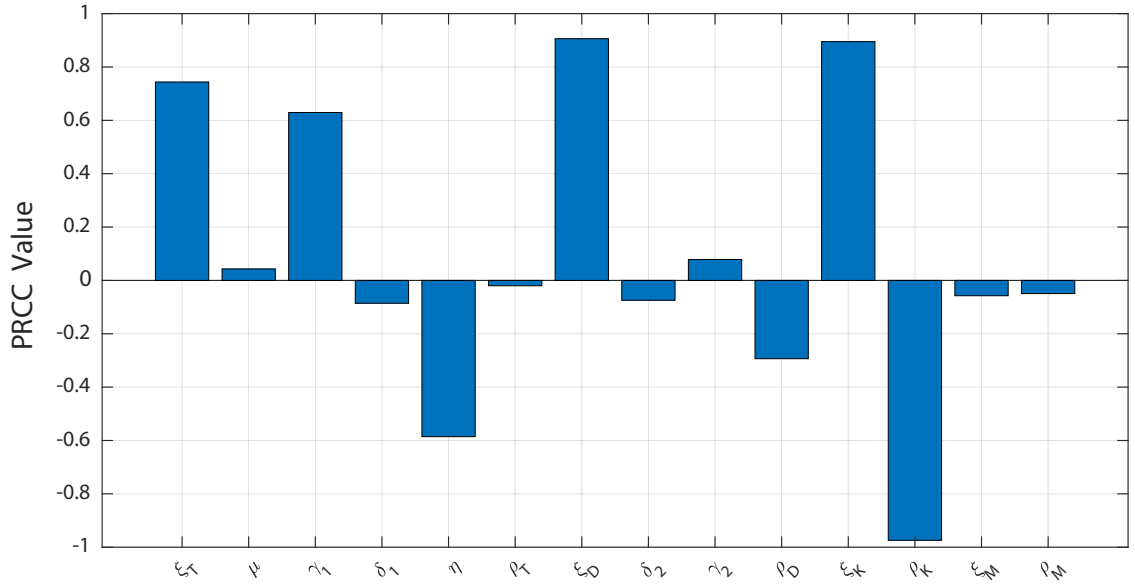

Figure 4.13: Partial Rank Correlation Coefficient (PRCC) bar plots of system parameters with respect to the keratinocyte population, based on a sample size of 1000. PRCC values are computed at day 100, with all p-values reported up to four decimal places. The horizontal axis represents the model parameters, while the vertical axis indicates their corresponding PRCC values.

approach (e.g., TNF-α and IL-23 inhibition), demonstrates the highest effectiveness, particularly under the Caputo–Fabrizio operator. These results suggest that combination therapy provides superior control over psoriatic inflammation.

Additionally, Figure 4.13 presents a global sensitivity analysis of key model parameters affecting the keratinocyte population, using Latin Hypercube Sampling (LHS) combined with the Partial Rank Correlation Coefficients (PRCC) method. For each parameter, the PRCC and corresponding p-value are computed; a p-value < 0.05 indicates statistical significance. The bar plot reveals that parameters ξ_T, μ, γ_1, ξ_D, γ_2, and ξ_K positively influence disease progression, whereas δ_1, η, ρ_T, δ_2, ρ_D, ρ_K, ξ_M, and ρ_M exert negative effects. Keratinocyte levels are used as a marker for disease prediction, and the sensitivity analysis helps identify key parameters that could serve as potential targets for therapeutic intervention in psoriasis.

4.7 Discussion and Conclusion

ODEs are widely used to describe biological systems, as they model instantaneous processes that respond immediately to changes in time. FDEs on the other hand, introduce a memory effect by allowing historical states to influence current behavior through fractional-order parameters. The main advantage of these fractional operators lies in their non-local nature, which provides greater flexibility and adaptability compared to classical ODE-based ap-

proaches. In this chapter, we applied FDEs to a cell-biological model of psoriasis and analyzed the system under three operators: Caputo, Caputo-Fabrizio, and Atangana-Baleanu-Caputo. The results show that decreasing the fractional parameters λ (Caputo) and α (Atangana-Baleanu-Caputo) slows the stabilization of equilibrium, indicating a stronger memory effect. In contrast, the Caputo-Fabrizio operator produces similar stabilization patterns across values of ζ, suggesting a different way of representing memory. Overall, this framework shows how keratinocyte and mesenchymal stem cell populations gradually approach equilibrium when memory effects are considered.

To further examine therapeutic outcomes, we incorporated fractionalized optimal control theory using Caputo, Caputo-Fabrizio, and Atangana-Baleanu-Caputo formulations. Two biologic drugs, TNF-α inhibitors and IL-23 blockers, were tested under three treatment strategies using the Forward-Backward Sweep Method (FBSM). Among the three strategies described in *Chapter* 4, Strategy III, which combines both drugs, was found to be the most effective. Simulations confirm that this approach restores keratinocyte density to healthy levels while suppressing inflammatory cytokine production and immune cell activity. Effectiveness analysis further highlights the Caputo-Fabrizio operator as yielding the best therapeutic outcome.

The interactions between T cells and dendritic cells through cytokine-mediated feedback loops are not immediate; they involve delays due to signal processing, cell communication, and cytokine activity. Such immune-related delays may play a key role in the unstable or oscillatory behavior observed during psoriasis flare-ups. In the following *Chapter* 5, we investigate these delay effects in the system and apply an optimal control strategy using two biologics that inhibit TNF-α and IL-17 in a cost-effective manner.

Chapter 5

A Mathematical Study for Psoriasis Transmission with Immune-Mediated Time Delays and Optimal Control Strategies

In psoriasis, dendritic cells activate T cells, which in turn release excessive pro-inflammatory cytokines, leading to abnormal keratinocyte growth in the epidermis. At the same time, anti-inflammatory cytokines attempt to restore balance. In reality, these immune processes are not immediate; they involve time gaps due to signal processing, cell communication, and cytokine feedback. Such immune-related delays may play a key role in triggering the unstable or oscillatory behavior observed during psoriasis flare-ups. In this *Chapter*[5], we study and analyze our mathematical model of psoriasis that explicitly incorporates two intracellular immune-mediated time delays to demonstrate their biological significance in the progression of the disease.

The model captures the interactions among T cells, dendritic cells, keratinocytes, and local mesenchymal stem cells. It features two cytokine-mediated feedback loops between T cells and dendritic cells, while stem cells attempt to regulate the immune response through anti-inflammatory signaling. A key challenge lies in identifying the critical time delays that modulate these interactions. To address this, we introduce two different delays into distinct interaction terms of the model. We test the hypothesis that these delays can critically influence the onset and persistence of psoriatic pathology. Using stability analysis of the interior equilibrium, we determine parameter relations, their ranges, and delay thresholds that give rise to Hopf bifurcations, thereby linking delays to disease progression and deriving conditions for instability. Our analysis demonstrates that both immune-mediated delays strongly influence system stability, with threshold values of τ_1^* and τ_2^* inducing oscillations through Hopf bifurcations.

We further apply optimal control to the delayed system using two biologic drugs: a TNF-α inhibitor and an IL-17 inhibitor. Numerical simulations support the theoretical analysis

[5] *A major portion of this chapter has been communicated to a peer-reviewed international journal.*

and show that these drugs effectively reduce keratinocyte density. The results suggest that incorporating time delays in the model provides deeper insight into psoriasis dynamics and aids in planning improved therapeutic strategies. All theoretical findings are supported by simulations, and a comparison with recent clinical data is also presented in this chapter.

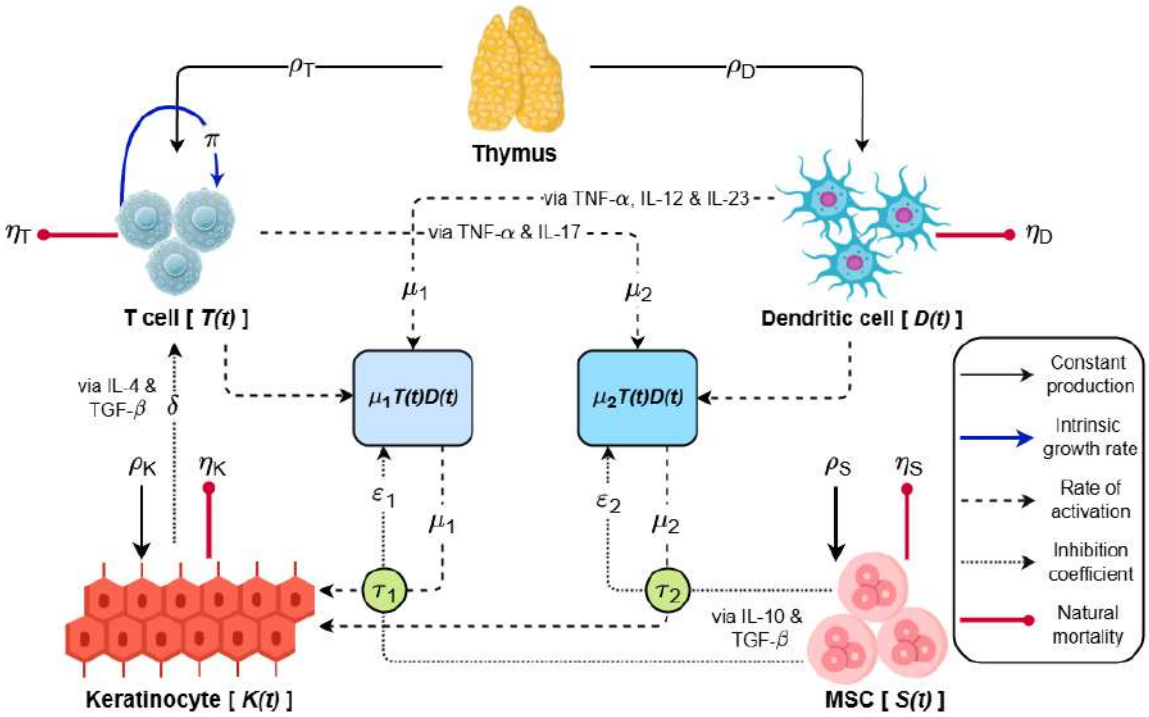

Figure 5.1: Schematic representation of model populations and their interrelationships mediated by cytokine signaling.

5.1 The Model Introducing Immune Delays

In this section, we present a mathematical model for psoriasis in the presence of immune-mediated delays. In our earlier work, Kushary et al. [69] formulated a four-dimensional deterministic model based on ordinary differential equations (ODEs). The model incorporates the key cellular populations involved in psoriasis, namely T cells, dendritic cells, keratinocytes, and mesenchymal stem cells, formulated under suitable biological assumptions.

The interactions between T cells and dendritic cells, mediated by pro-inflammatory cytokines, are not instantaneous. Anti-inflammatory cytokines attempt to counterbalance these signals, which leads to a lag in immune activation and inflammatory cell infiltration. To capture this effect, we introduce two distinct intracellular immune response delays into the previous model. These delays represent the time gap in the interaction between T cells and dendritic cells, and their subsequent influence on keratinocyte proliferation.

Based on these considerations, the delayed mathematical model is formulated as follows:

$$\begin{aligned}
\frac{dT(t)}{dt} &= \rho_T + \pi T(t)\left(1 - \frac{T(t)}{T^{max}}\right) - \frac{\mu_1 T(t-\tau_1)D(t-\tau_1)}{1+\epsilon_1 S(t-\tau_1)} - \delta T(t)K(t) - \eta_T T(t),\\
\frac{dD(t)}{dt} &= \rho_D - \frac{\mu_2 T(t-\tau_2)D(t-\tau_2)}{1+\epsilon_2 S(t-\tau_2)} - \eta_D D(t),\\
\frac{dK(t)}{dt} &= \rho_K + \frac{\mu_1 T(t-\tau_1)D(t-\tau_1)}{1+\epsilon_1 S(t-\tau_1)} + \frac{\mu_2 T(t-\tau_2)D(t-\tau_2)}{1+\epsilon_2 S(t-\tau_2)} - \eta_K K(t),\\
\frac{dS(t)}{dt} &= \rho_S - \eta_S S(t),
\end{aligned} \tag{5.1.1}$$

subject to the initial conditions:

$$T(\theta) > 0,\ D(\theta) > 0,\ K(\theta) > 0,\ S(\theta) > 0, \text{where } \theta \in [-\tau, 0], \tau = \max\{\tau_1, \tau_2\}.$$

Here, $T(t)$, $D(t)$, $K(t)$, and $S(t)$ denote the population densities of T cells, dendritic cells, keratinocytes, and mesenchymal stem cells (MSCs), respectively, at time t. The interaction network among these cell populations is shown in the schematic diagram (Figure 5.1), and the model parameters are described in detail in Table 5.1. The parameter τ represents the time delay, measured in days.

Let $C = C([-\tau, 0], \mathbb{R}^4_+)$ be the Banach space of all continuous functions $\varphi : [-\tau, 0] \to \mathbb{R}^4_+$, equipped with the usual supremum norm defined by

$$||\varphi|| = \sup_{-\tau<\theta<0} \{|\varphi_1(\theta)|, |\varphi_2(\theta)|, |\varphi_3(\theta)|, |\varphi_4(\theta)|\},$$

where $\varphi = (\varphi_1, \varphi_2, \varphi_3, \varphi_4)$ and $T(\theta) = \varphi_1(\theta)$, $D(\theta) = \varphi_2(\theta)$, $K(\theta) = \varphi_3(\theta)$, $S(\theta) = \varphi_4(\theta)$ with $\theta \in [-\tau, 0]$. To make the model feasible from the biological point of view, initial functions are assumed to be $\varphi_i(\theta) \geq 0$ for $\theta \in [-\tau, 0]$ and $\varphi_i(0) > 0$ for $i = 1, 2, 3, 4$. Using the fundamental theory of functional differential equations [23], we can guarantee the uniqueness of the solutions of the system (5.1.1) with the initial conditions mentioned above.

5.2 Properties of the Delayed Model

5.2.1 Positivity and Boundedness

Positivity and boundedness in a mathematical model are essential to establish well-posedness. It provides a reliable basis for the prediction of the system and gives meaningful insight into the outcome of the model. In this subsection, we analyze the positivity and boundedness of the delay-induced system (5.1.1) through the following theorem.

Theorem 5.2.1 *Consider the system of equations (5.1.1) with initial history* $X(\theta) = \big(\varphi_1(\theta), \varphi_2(\theta), \varphi_3(\theta), \varphi_4(\theta)\big) \in C\big([-\tau, 0], \mathbb{R}^4_+\big)$ *such that* $\varphi_i(0) > 0$ *for* $i = 1, 2, 3, 4$. *Then-*

1. *Every solution remains positive for all* $t \geq 0$, *i.e.,* $X(t) \in \mathbb{R}^4_+$. *Hence,* $\mathbb{R}^4_+$ *is a positively invariant region for (5.1.1).*

2. *Every positive solution is bounded and ultimately enters the domain of attraction* $\Delta \subseteq \mathbb{R}^4_+$, *where* $\Delta = \big\{(T,D,K,S) \in \mathbb{R}^4_+ : \ 0 < T+D+K \le \frac{4\rho+\pi T^{\max}}{4\eta}, \ \ 0 < S \le \frac{\rho_S}{\eta_S}\big\}$, *with* $\rho = \rho_T + \rho_D + \rho_K$ *and* $\eta = \min\{\eta_T, \eta_D, \eta_K\}$.

Proof. Let $X(t) = \big(T(t), D(t), K(t), S(t)\big)^\top$ and

$$F(X) = \begin{pmatrix} \rho_T + \pi T(t)\big(1 - \frac{T(t)}{T^{\max}}\big) - \frac{\mu_1 T(t-\tau_1)D(t-\tau_1)}{1+\epsilon_1 S(t-\tau_1)} - \delta T(t)K(t) - \eta_T T(t) \\ \rho_D - \frac{\mu_2 T(t-\tau_2)D(t-\tau_2)}{1+\epsilon_2 S(t-\tau_2)} - \eta_D D(t) \\ \rho_K + \frac{\mu_1 T(t-\tau_1)D(t-\tau_1)}{1+\epsilon_1 S(t-\tau_1)} + \frac{\mu_2 T(t-\tau_2)D(t-\tau_2)}{1+\epsilon_2 S(t-\tau_2)} - \eta_K K(t) \\ \rho_S - \eta_S S(t) \end{pmatrix}.$$

Then system (5.1.1) can be written as

$$\frac{dX}{dt} = F(X), \qquad X(\theta) \in C\big([-\tau, 0], \mathbb{R}^4_+\big). \tag{5.2.1}$$

1. Let $x_1 = T$, $x_2 = D$, $x_3 = K$, $x_4 = S$. From the form of F it follows that

$$F_i(X)\big|_{x_i=0,\ X\in\mathbb{R}^4_+} \ \ge \ 0, \qquad i = 1,2,3,4.$$

By Lemma 2 of Yang et al. [78] and Theorem 1.1 of Bodnar et al. [79], any solution $X(t)$ of (5.2.1) with $X(\theta) \in C([-\tau,0],\mathbb{R}^4_+)$ satisfies $X(t) \in \mathbb{R}^4_+$ for all $t \ge 0$. Therefore, $\mathbb{R}^4_+$ is a positively invariant region for (5.1.1).

2. Adding the first three equations of (5.1.1) gives

$$\frac{d}{dt}(T+D+K) = \rho + \pi T\Big(1 - \frac{T}{T^{\max}}\Big) - \eta_T T - \eta_D D - \eta_K K \ \le \ \rho + \pi T\Big(1 - \frac{T}{T^{\max}}\Big) - \eta(T+D+K),$$

where $\rho = \rho_T + \rho_D + \rho_K$ and $\eta = \min\{\eta_T, \eta_D, \eta_K\}$.

The quadratic term satisfies $\pi T\left(1 - \frac{T}{T^{\max}}\right) \le \frac{\pi T^{\max}}{4}$. Hence,

$$\frac{d}{dt}(T+D+K) \ \le \ \Big(\rho + \frac{\pi T^{\max}}{4}\Big) - \eta\,(T+D+K).$$

By the comparison principle [56], for $t > 0$,

$$T(t) + D(t) + K(t) \ \le \ \frac{4\rho + \pi T^{\max}}{4\eta}\big(1 - e^{-\eta t}\big) + \big(T(0) + D(0) + K(0)\big)e^{-\eta t},$$

so for large t,

$$T(t) + D(t) + K(t) \ \le \ \frac{4\rho + \pi T^{\max}}{4\eta}.$$

For the fourth equation we have the explicit solution

$$S(t) = \frac{\rho_S}{\eta_S}\big(1 - e^{-\eta_S t}\big) + S(0)e^{-\eta_S t} \implies S(t) \to \frac{\rho_S}{\eta_S} \quad \text{as } t \to \infty.$$

Therefore, every positive solution ultimately enters and remains in

$$\Delta = \Big\{(T, D, K, S) \in \mathbb{R}^4_+ : \ 0 < T + D + K \leq \tfrac{4\rho+\pi T^{\max}}{4\eta}, \ \ 0 < S \leq \tfrac{\rho_S}{\eta_S}\Big\},$$

which satisfies $\Delta \subseteq \mathbb{R}^4_+$.

5.2.2 Feasibility of Positive Equilibrium

To determine the interior equilibrium point $E^*(T^*, D^*, K^*, S^*)$ of the delay-induced system, we set all the equations of the system (5.1.1) to zero and solve for the state variables under the conditions $T^* > 0$, $D^* > 0$, $K^* > 0$, and $S^* > 0$. From the fourth equation of the system (5.1.1), we get $S^* = \rho_S/\eta_S$. Using the value of S^*, we introduce two constants, ξ_1 and ξ_2, to simplify the computations. These constants are defined as follows:

$$\xi_1 = \frac{\mu_1}{1 + \epsilon_1 S^*} \quad \text{and} \quad \xi_2 = \frac{\mu_2}{1 + \epsilon_2 S^*}. \tag{5.2.2}$$

Subsequently, we determined the values of D^* and K^* in terms of T^* using the aforementioned constants and by setting the second equation of the system (5.1.1) to zero. These values are given by

$$D^* = \frac{\rho_D}{\eta_D + \xi_2 T^*} \ \text{ and } \ K^* = \frac{\rho_K}{\eta_K} + \frac{\rho_D(\xi_1 + \xi_2)T^*}{\eta_K(\eta_D + \xi_2 T^*)}. \tag{5.2.3}$$

By setting the first equation of the system (5.1.1) to zero and substituting the obtained values of the state variables into this equation, we derive a cubic equation in terms of T^*.

$$T^{*3} + P_1 T^{*2} + P_2 T^* + P_3 = 0, \tag{5.2.4}$$

$$\begin{aligned}
\text{where} \ \ P_1 &= \frac{1}{\pi\eta_K\xi_2}\Big[\pi\eta_K\eta_D + \big\{\big(\delta\rho_K + \eta_T\eta_K - \pi\eta_K\big)\xi_2 + \rho_D\delta\big(\xi_1 + \xi_2\big)\big\}T^{\max}\Big], \\
P_2 &= \frac{1}{\pi\eta_K\xi_2}\Big[\delta\rho_K\eta_D - \pi\eta_D\eta_K + \eta_T\eta_D\eta_K + \rho_D\eta_K\xi_1 - \rho_T\eta_K\xi_2\Big]T^{\max}, \\
P_3 &= -\frac{\rho_T\eta_D T^{\max}}{\pi\xi_2}.
\end{aligned}$$

Using the parameter values listed in Table 5.1, we observe that $P_1 > 0$ is positive, while $P_2 < 0$ and $P_3 < 0$. According to Descartes' rule of signs [80], the system (5.2.4) has exactly one positive root. By substituting the value of T^* into (5.2.3), we can determine the interior equilibrium point $E^*(T^*, D^*, K^*, S^*)$.

5.2.3 Stability and Hopf-bifurcation Analysis

The non-delayed system admits a unique positive interior equilibrium point, since the extinction of any population is biologically unrealistic. Without loss of generality, we denote this equilibrium as $E^*(T^*, D^*, K^*, S^*)$. The exact values of the state variables at E^* were

determined earlier in our previous work by Kushary et al. [69].

In this subsection, we study the local stability of the delay-induced system (5.1.1) in a neighborhood of the interior equilibrium point E^*.

Let $\hat{T}(t) = T(t) - T^*, \hat{D}(t) = D(t) - D^*, \hat{K}(t) = K(t) - K^*$, and $\hat{S}(t) = S(t) - S^*$ represent the perturbed variables near the equilibrium point E^*. Linearizing the delay-induced system (5.1.1) about E^*, we derive the following system:

$$\frac{dY(t)}{dt} = J(0)Y(t) + J(\tau_1)Y(t-\tau_1) + J(\tau_2)Y(t-\tau_2), \tag{5.2.5}$$

where $Y(t) = \left[\hat{T}(t), \hat{D}(t), \hat{K}(t), \hat{S}(t)\right]^T$ and $J(0), J(\tau_1)$, and $J(\tau_2)$ represent the 4×4 Jacobian matrices of the system evaluated at E^* for the current state, the delayed state with delay τ_1, and the delayed state with delay τ_2, respectively. Their explicit forms are:

$$J(0) = \begin{pmatrix} -\left(\frac{\rho_T}{T^*} + \frac{\pi T^*}{Tmax}\right) & 0 & -\delta T^* & 0 \\ 0 & -\eta_D & 0 & 0 \\ 0 & 0 & -\eta_K & 0 \\ 0 & 0 & 0 & -\eta_S \end{pmatrix}, \quad J(\tau_1) = \begin{pmatrix} -\mu_1 D^* & -\mu_1 T^* & 0 & \frac{\xi_1^2 \epsilon_1 T^* D^*}{\mu_1} \\ 0 & 0 & 0 & 0 \\ \mu_1 D^* & \mu_1 T^* & 0 & -\frac{\xi_1^2 \epsilon_1 T^* D^*}{\mu_1} \\ 0 & 0 & 0 & 0 \end{pmatrix},$$

$$\text{and} \quad J(\tau_2) = \begin{pmatrix} 0 & 0 & 0 & 0 \\ -\mu_2 D^* & -\mu_2 T^* & 0 & \frac{\xi_2^2 \epsilon_2 T^* D^*}{\mu_2} \\ \mu_2 D^* & \mu_2 T^* & 0 & -\frac{\xi_2^2 \epsilon_2 T^* D^*}{\mu_2} \\ 0 & 0 & 0 & 0 \end{pmatrix}. \tag{5.2.6}$$

Now, the characteristic equation of the system (5.1.1) is given by

$$\begin{aligned} &\left|\lambda I - J(0) - e^{-\lambda\tau_1} J(\tau_1) - e^{-\lambda\tau_2} J(\tau_2)\right| = 0, \\ \therefore\ &(\lambda + \eta_S)\left[(\lambda^3 + A_1\lambda^2 + A_2\lambda + A_3) + e^{-\lambda\tau_1}(B_1\lambda^2 + B_2\lambda + B_3)\right. \\ &\left. + e^{-\lambda\tau_2}(C_1\lambda^2 + C_2\lambda + C_3)\right] = 0, \end{aligned} \tag{5.2.7}$$

where the coefficients are

$$\begin{aligned} &A_1 = \frac{\rho_T}{T^*} - \xi_1 D^* + \frac{\pi T^*}{T^{max}} + \eta_D + \eta_K,\ A_2 = \left(\frac{\rho_T}{T^*} - \xi_1 D^* + \frac{\pi T^*}{T^{max}}\right)(\eta_D + \eta_K) + \eta_D\eta_K, \\ &A_3 = \left(\frac{\rho_T}{T^*} - \xi_1 D^* + \frac{\pi T^*}{T^{max}}\right)(\eta_D + \eta_K)\eta_D\eta_K,\ B_1 = \xi_1 D^*, \\ &B_2 = \delta\xi_1 T^* D^* + \xi_1 D^*(\eta_D + \eta_K),\ B_3 = \eta_D \xi_1 D^*\left(\delta T^* + \eta_K\right),\ C_1 = \xi_2 T^*, \\ &C_2 = \delta\xi_2 T^* D^* - \xi_2 T^*\left(-\frac{\rho_T}{T^*} + \xi_1 D^* - \frac{\pi T^*}{T^{max}} - \eta_K\right), \\ &C_3 = \delta\eta_D\xi_2 T^* D^* + \eta_K \xi_2 T^*\left(\frac{\rho_T}{T^*} - \xi_1 D^* + \frac{\pi T^*}{T^{max}}\right). \end{aligned}$$

The interior steady state E^* is said to be locally asymptotically stable (LAS) if all roots λ of the characteristic equation (5.2.7) are negative or possess negative real parts. The following

cases will now be analyzed in detail.

Case - I $(\tau_1 = \tau_2 = 0)$

In this case, the characteristic equation (5.2.7) simplifies to the following form:

$$(\lambda + \eta_S)[\lambda^3 + \bar{A}_1\lambda^2 + \bar{A}_2\lambda + \bar{A}_3] = 0, \tag{5.2.8}$$

where $\bar{A}_1 = A_1 + B_1 + C_1, \bar{A}_2 = A_2 + B_2 + C_2$, and $\bar{A}_3 = A_3 + B_3 + C_3$.

One of the eigenvalues is $\lambda = -\eta_S < 0$. Thus, the interior equilibrium E^* is LAS in the absence of delays if following conditions are satisfied:

$$\bar{A}_1 > 0,\ \bar{A}_3 > 0 \text{ and } \bar{A}_1\bar{A}_2 - \bar{A}_3 > 0.$$

Case - II $(\tau_1 > 0$ **and** $\tau_2 = 0)$

For this case, the characteristic equation (5.2.7) takes the form:

$$\begin{gathered}(\lambda + \eta_S)[(\lambda^3 + M_1\lambda^2 + M_2\lambda + M_3) + e^{-\lambda\tau_1}(B_1\lambda^2 + B_2\lambda + B_3)] = 0,\\ \text{where } M_1 = A_1 + C_1, M_2 = A_2 + C_2, \text{ and } M_3 = A_3 + C_3.\end{gathered} \tag{5.2.9}$$

The root $\lambda = -\eta_S$ is negative. Thus, we are only interested in analyzing the following equation:

$$(\lambda^3 + M_1\lambda^2 + M_2\lambda + M_3) + e^{-\lambda\tau_1}(B_1\lambda^2 + B_2\lambda + B_3) = 0. \tag{5.2.10}$$

Since, the characteristic equation (5.2.10) is transcendental in λ, the stability of the system (5.1.1) cannot be analyzed using the classical Routh-Hurwitz criteria [63]. The equation (5.2.10) admits purely imaginary solutions as a necessary condition for a stability change at the interior equilibrium E^*. Let $\lambda = i\omega(\tau_1)$ be a root of equation (5.2.10). Substituting $\lambda = i\omega$ into equation (5.2.10) and separating the real and imaginary components, we obtain:

$$\begin{aligned}M_1\omega^2 - M_3 &= (B_3 - B_1\omega^2)\cos\omega\tau_1 + B_2\omega\sin\omega\tau_1,\\ M_2\omega - \omega^2 &= (B_3 - B_1\omega^2)\sin\omega\tau_1 + B_2\omega\cos\omega\tau_1.\end{aligned} \tag{5.2.11}$$

Squaring and adding the above two equations and substituting $\omega^2 = \sigma$, we get the following equation:

$$\begin{gathered}\Psi(\sigma) \equiv \sigma^3 + R_1\sigma^2 + R_2\sigma + R_3 = 0,\\ \text{where } R_1 = M_1^2 - 2M_2 - B_1^2, R_2 = M_2^2 - 2M_1M_3 + 2B_1B_3 - B_2^2, \text{ and } R_3 = M_3^2 - B_3^2.\end{gathered} \tag{5.2.12}$$

The equation (5.2.10) does not admit purely imaginary roots if the equation (5.2.12) satisfies the Routh-Hurwitz's criteria [63]. The results are summarized in the following proposition:

Proposition 1. The interior equilibrium E^* is LAS for all $\tau_1 > 0$ if the following conditions are hold:

$$R_1 > 0,\ R_3 > 0, \text{ and } R_1R_2 - R_3 > 0.$$

If $R_3 < 0$, the equation (5.2.12) has at least one positive root. Let $\sigma = \omega^2$ denote the smallest positive root. In this case, the characteristic equation (5.2.10) will have purely imaginary roots, says $(\pm i\omega)$. We now determine the critical value of τ_1, denoted as τ_1^* that corresponds to the point at which the stability of the interior equilibrium E^* changes. The critical value τ_1^* is determined from the system of equations (5.2.11) to analyze the conditions under which the system transitions from stability to instability as τ_1 increases, as follows:

$$\tau_1^n = \frac{1}{\omega}\cos^{-1}\left[\frac{(B_2 - M_1B_1)\omega^4 + (M_1B_3 + M_3B_1 - M_2B_2)\omega^2 - M_3B_3}{B_1^2\omega^4 + B_2 + B_3^2}\right] + \frac{2n\pi}{\omega}, \quad \forall n \in \mathbb{N} \cup \{0\}. \tag{5.2.13}$$

Let us assume that for $\omega_1 = \omega(\tau_1)$, $\tau_1^* = \min_{n\geq 0}\{\tau_1^n\}$. Based on this assumption and summarizing the above discussions, we have derived the following theorem.

Theorem 5.2.2 *If $R_3 < 0$, according to Butler lemma [81] the interior equilibrium E^* is LAS when $\tau_1 < \tau_1^*$ and becomes unstable when $\tau_1 > \tau_1^*$, where*

$$\tau_1^* = \frac{1}{\omega_1}\arccos\left[\frac{(B_2 - M_1B_1)\omega_1^4 + (M_1B_3 + M_3B_1 - M_2B_2)\omega_1^2 - M_3B_3}{B_1^2\omega_1^4 + B_2 + B_3^2}\right]. \tag{5.2.14}$$

Furthermore, when $\tau_1 = \tau_1^*$, a Hopf bifurcation [82] occurs, meaning that a family of periodic solutions of the system (5.1.1) bifurcates as τ_1 crosses the critical value τ_1^*. This bifurcation is ensured by the transversality condition:

$$3\omega_1^4 + 2R_1\omega_1^2 + R_2 > 0. \tag{5.2.15}$$

Proof. Now, considering λ as a function of τ_1, i.e., $\lambda = \lambda(\tau_1)$, and differentiating equation (5.2.10) with respect to τ_1, we derive the following expression:

$$\left(\frac{d\lambda(\tau_1)}{d\tau_1}\right)^{-1} = -\frac{3\lambda^2 + 2A_1\lambda + M_1}{\lambda(\lambda^3 + A_1\lambda^2 + M_1\lambda + M_2)} + \frac{B_1}{\lambda(B_1\lambda + B_2)} - \frac{\tau_1}{\lambda}. \tag{5.2.16}$$

From this above equation, we get:

$$\begin{aligned}\therefore \ \text{sign}\left[Re\left(\frac{d\lambda(\tau_1)}{d\tau_1}\right)\right]_{\tau_1=\tau_1^*} &= \text{sign}\left[Re\left(\frac{d\lambda(\tau_1)}{d\tau_1}\right)^{-1}\right]_{\tau=\tau_1^*,\,\omega=\omega_1} \\ &= \text{sign}\left[3\omega_1^4 + (2M_1^2 - 4M_2 - 2B_1^2)\omega_1^2 + (M_2^2 - 2M_1M_3 + 2B_1B_3 - B_2^2)\right] \\ &= \text{sign}\left[3\omega_1^4 + 2R_1\omega_1^2 + R_2\right].\end{aligned}$$

Hence, we conclude that the delayed system (5.1.1) undergoes a Hopf bifurcation at the critical value $\tau_1 = \tau_1^*$ if the transversality condition $\left[Re(\frac{d\lambda}{d\tau_1})\right]_{\tau_1=\tau_1^*} > 0$, i.e., when $3\omega_1^4 + 2R_1\omega_1^2 + R_2 > 0$ is satisfied.

Case - III $(\tau_1 = 0$ **and** $\tau_2 > 0)$

In this case, the characteristic equation (5.2.7) reduces to:

$$\begin{aligned}&(\lambda+\eta_S)\left[(\lambda^3+N_1\lambda^2+N_2\lambda+N_3)+e^{-\lambda\tau_2}(C_1\lambda^2+C_2\lambda+C_3)\right]=0,\\ &\text{where}\ \ N_1=A_1+B_1, N_2=A_2+B_2,\ \text{and}\ N_3=A_3+B_3.\end{aligned} \tag{5.2.17}$$

Following a similar approach as for the system described in (5.2.9), it can be shown that a critical value $\tau_2=\tau_2^*$ exists for the positive interior equilibrium point E^*, at which the stability transitions for the delayed system (5.1.1). Without repeating the detailed analytical calculations presented in Case - II, we provide the general expression that characterizes the transition from stability to instability as the value of τ_2 increases.

$$\tau_2^n=\frac{1}{\omega}\cos^{-1}\left[\frac{(C_2-N_1C_1)\omega^4+(N_1C_3+N_3C_1-C_2N_2)\omega^2-C_3N_3}{C_1^2\omega^4+C_2+C_3^2}\right]+\frac{2n\pi}{\omega},\ \ \forall n\in\mathbb{N}\cup\{0\}. \tag{5.2.18}$$

Assuming that for $\omega_2=\omega(\tau_2)$, the sequence $\{\tau_2^n\}$ represents the critical values of τ_2, where $n\geq 0$. The minimum value in this sequence, $\tau_2^*=\min_{n\geq 0}\{\tau_2^n\}$, is identified as the critical point. The results are summarized in the following theorem without proving it.

Theorem 5.2.3 *The interior equilibrium E^* is LAS if $\tau_2<\tau_2^*$ and becomes unstable if $\tau_2>\tau_2^*$, where*

$$\tau_2^*=\frac{1}{\omega_2}\arccos\left[\frac{(C_2-N_1C_1)\omega_2^4+(N_1C_3+N_3C_1-C_2N_2)\omega_2^2-C_3N_3}{C_1^2\omega_2^4+C_2+C_3^2}\right]. \tag{5.2.19}$$

Moreover, the delayed system (5.1.1) undergoes a Hopf bifurcation at $\tau_2=\tau_2^*$ when transversality condition $3\omega_2^4+2R_1\omega_2^2+R_2>0$ hold where $R_1=M_1^2-2M_2-C_1^2$ and $R_2=M_2^2-2M_1M_3+2C_1C_3-C_2^2$.

Case - IV ($\tau_1>0$ **and** $\tau_2>0$)
The analysis of this case is extensive and complex, making it challenging to derive precise information regarding the nature of the eigenvalues and the conditions under which stability switches occur. Instead of performing detailed analytical calculations, we have numerically demonstrated the emergence of Hopf-bifurcating periodic solutions for the system (5.1.1) and provided the necessary biological interpretations. The result, stated without proof, is presented in the following theorem.

Theorem 5.2.4 *The non-delayed system is asymptotically stable under the given conditions. However, there exists a critical threshold τ^* beyond which the stability of the system undergoes a change. Specifically*

1. *The steady state E^* remains LAS when $\tau_1+\tau_2<\tau^*$.*
2. *The steady state E^* becomes unstable when $\tau_1+\tau_2>\tau^*$.*
3. *A Hopf bifurcation occurs at $\tau_1+\tau_2=\tau^*$, provided the transversality condition $\left[Re(\frac{d\lambda}{d\tau})\right]_{\tau=\tau^*}>0$ is satisfied.*

5.3 Optimal Control Strategy on Delayed system

The incorporation of optimal control strategies with delays has become important in studying biological systems where cellular communication is not instantaneous. In psoriasis, cyclic interactions between T cells and dendritic cells are central to disease progression and are further amplified by pro-inflammatory cytokines such as TNF-α and IL-17. This amplification promotes abnormal keratinocyte proliferation, leading to epidermal thickening and plaque formation. Intracellular delays are very significant, as cytokine secretion and downstream responses do not occur immediately. When these time lags are reduced, feedback between T cells and dendritic cells intensifies, accelerating the inflammatory cycle and keratinocyte infiltration. To address this, we design an optimal control framework with two biologic cytokine inhibitors, represented by control functions $v_1(t)$ and $v_2(t)$, incorporated into the delay-induced system (5.1.1). These functions denote the effects of time-dependent biologic agents that block TNF-α and IL-17, thereby weakening the interacting feedback loop and restoring a more balanced immune response in psoriasis.

1. $v_1(t)$: Represents the effect of a TNF-α inhibitor, which can modulate the reaction rates between T cells and dendritic cells.

2. $v_2(t)$: Represents the inhibition of the IL-17 axis, targeting its associated pathways.

Thus, the delayed system (5.1.1), augmented with optimal control functions, is described by the following set of equations over the specified time interval $[0, t_f]$.

$$\begin{aligned}
\frac{dT(t)}{dt} &= \rho_T + \pi T(t)\Big(1 - \frac{T(t)}{T^{\max}}\Big) - \frac{\mu_1\big\{1 - v_1(t)\big\}T(t-\tau_1)D(t-\tau_1)}{1 + \epsilon_1 S(t-\tau_1)} - \delta T(t)K(t) - \eta_T T(t),\\
\frac{dD(t)}{dt} &= \rho_D - \frac{\mu_2\big\{1 - v_2(t)\big\}T(t-\tau_2)D(t-\tau_2)}{1 + \epsilon_2 S(t-\tau_2)} - \eta_D D(t),\\
\frac{dK(t)}{dt} &= \rho_K + \frac{\mu_1\big\{1 - v_1(t)\big\}T(t-\tau_1)D(t-\tau_1)}{1 + \epsilon_1 S(t-\tau_1)} + \frac{\mu_2\big\{1 - v_2(t)\big\}T(t-\tau_2)D(t-\tau_2)}{1 + \epsilon_2 S(t-\tau_2)} - \eta_K K(t),\\
\frac{dS(t)}{dt} &= \rho_S - \eta_S S(t),
\end{aligned} \tag{5.3.1}$$

with $T_0(t) > 0,\ D_0(t) > 0,\ K_0(t) > 0$ and $S_0(t) > 0,\ \ \forall t \in [-\tau, 0]$.

5.3.1 Description of the Objective Functional

Our primary objective is to minimize the cost associated with each biologic treatment to reduce the overall treatment expense of psoriasis. To achieve this, we define an objective cost functional for the minimization problem, expressed as follows

$$J(v_1(t), v_2(t)) = \int_0^{t_f} \Big[K(t) + L_1 v_1^2(t) + L_2 v_2^2(t)\Big] dt, \tag{5.3.2}$$

subject to the control system (5.3.1). The parameters L_1 and L_2 represent positive weight constants on the benefit of the cost of the TNF-α and IL-17 inhibitors, respectively. Our aim

is to determine the optimal control $v^*(.) = (v_1(.), v_2(.))$ that satisfies the following:

$$J(v^*) = \min\Big\{J(v) : v(t) \in U_1 \times U_2\Big\}. \tag{5.3.3}$$

The Lebesgue measurable control set is defined on the interval $[0, t_f]$, where t_f represents the terminal time of control.

$$U_1 \times U_2 = \big\{v(t) = (v_1, v_2) : 0 \leq v_i(t) \leq v_i^{\max} < 1, \forall t \in [0, t_f],\ i = 1, 2\big\}. \tag{5.3.4}$$

Pontryagin's Minimum Principle with delays has been applied to establish the necessary conditions for solving this optimal control problem [83]. The optimal control-induced system (5.3.1) has been shown to admit non-negative, bounded solutions for a bounded Lebesgue-measurable control function and the non-negative initial conditions.

5.3.2 Optimal Control's Characteristics

To characterize the optimal control, Pontryagin's Minimum Principle reduces the problem (5.3.1)–(5.3.4) to a problem of minimizing the Hamiltonian H, defined as

$$\begin{aligned}
H =& K(t) + L_1 v_1^2(t) + L_2 v_2^2(t) \\
&+ \Gamma_1(t)\left[\rho_T + \pi T(t)\Big(1 - \frac{T(t)}{T^{\max}}\Big) - \frac{\mu_1\big\{1 - v_1(t)\big\}T(t-\tau_1)D(t-\tau_1)}{1 + \epsilon_1 S(t-\tau_1)} - \delta T(t)K(t) - \eta_T T(t)\right] \\
&+ \Gamma_2(t)\left[\rho_D - \frac{\mu_2\big\{1 - v_2(t)\big\}T(t-\tau_2)D(t-\tau_2)}{1 + \epsilon_2 S(t-\tau_2)} - \eta_D D(t)\right] \\
&+ \Gamma_3(t)\left[\rho_K + \frac{\mu_1\big\{1 - v_1(t)\big\}T(t-\tau_1)D(t-\tau_1)}{1 + \epsilon_1 S(t-\tau_1)} + \frac{\mu_2\big\{1 - v_2(t)\big\}T(t-\tau_2)D(t-\tau_2)}{1 + \epsilon_2 S(t-\tau_2)} - \eta_K K(t)\right] \\
&+ \Gamma_4(t)\left[\rho_S - \eta_S S(t)\right],
\end{aligned} \tag{5.3.5}$$

where, $\Gamma_i(t)$'s $(i = 1, 2, 3, 4)$ are the adjoint variables to be determined suitably. The adjoint system with transversality criteria $\Gamma_i(t_f) = 0$ for $i = 1, 2, 3, 4$ can be obtained by using Pontryagin's Minimum Principle [83] as:

$$\begin{aligned}
\frac{d\Gamma_1(t)}{dt} &= -\frac{\partial H}{\partial T}(t) - \sum_{i=1}^{2} \chi[0, t_f - \tau_i](t)\frac{\partial H}{\partial T}(t + \tau_i), \\
\frac{d\Gamma_2(t)}{dt} &= -\frac{\partial H}{\partial D}(t) - \sum_{i=1}^{2} \chi[0, t_f - \tau_i](t)\frac{\partial H}{\partial D}(t + \tau_i), \\
\frac{d\Gamma_3(t)}{dt} &= -\frac{\partial H}{\partial K}(t), \\
\frac{d\Gamma_4(t)}{dt} &= -\frac{\partial H}{\partial S}(t) - \sum_{i=1}^{2} \chi[0, t_f - \tau_i](t)\frac{\partial H}{\partial S}(t + \tau_i).
\end{aligned}$$

The optimality of the considered system consists of the optimal states and the corresponding adjoint system takes the form

$$\begin{aligned}
\frac{d\Gamma_1(t)}{dt} =& -\Gamma_1(t)\left[\pi\Big(1-\frac{2T^*(t)}{T^{\max}}\Big)-\delta K^*(t)-\eta_T\right]\\
&+\chi[0,t_f-\tau_1](t)\Big(\Gamma_1-\Gamma_3\Big)(t+\tau_1)\left[\frac{\mu_1\{1-v_1^*(t)\}D^*(t)}{1+\epsilon_1 S^*(t)}\right]\\
&+\chi[0,t_f-\tau_2](t)\Big(\Gamma_2-\Gamma_3\Big)(t+\tau_2)\left[\frac{\mu_2\{1-v_2^*(t)\}D^*(t)}{1+\epsilon_2 S^*(t)}\right],\\
\frac{d\Gamma_2(t)}{dt} =&\eta_D\Gamma_2(t)+\chi[0,t_f-\tau_1](t)\Big(\Gamma_1-\Gamma_3\Big)(t+\tau_1)\left[\frac{\mu_1\{1-v_1^*(t)\}T^*(t)}{1+\epsilon_1 S^*(t)}\right]\\
&+\chi[0,t_f-\tau_2](t)\Big(\Gamma_2-\Gamma_3\Big)(t+\tau_2)\left[\frac{\mu_2\{1-v_2^*(t)\}T^*(t)}{1+\epsilon_2 S^*(t)}\right],\\
\frac{d\Gamma_3(t)}{dt} =& -1+\delta T^*\Gamma_1(t)+\eta_K\Gamma_3(t),\\
\frac{d\Gamma_4(t)}{dt} =&\eta_S\Gamma_4(t)-\chi[0,t_f-\tau_1](t)\Big(\Gamma_1-\Gamma_3\Big)(t+\tau_1)\left[\frac{\epsilon_1\mu_1\{1-v_1^*(t)\}T^*(t)D^*(t)}{\{1+\epsilon_1 S^*(t)\}^2}\right],\\
&-\chi[0,t_f-\tau_2](t)\Big(\Gamma_2-\Gamma_3\Big)(t+\tau_2)\left[\frac{\epsilon_2\mu_2\{1-v_2^*(t)\}T^*(t)D^*(t)}{\{1+\epsilon_2 S^*(t)\}^2}\right].
\end{aligned} \tag{5.3.6}$$

We determine optimal controls $v_i^*(t)$ $(i=1,2)$, using the optimality condition given by

$$\left.\frac{\partial H}{\partial v_1}\right|_{v_1=v_1^*(t)}=0 \qquad \text{and} \qquad \left.\frac{\partial H}{\partial v_2}\right|_{v_2=v_2^*(t)}=0. \tag{5.3.7}$$

Taking partial differentiation of the equation (5.3.5) with respect to v_1 and v_2 separately and applying the condition (5.3.7), we obtain

$$\begin{aligned}
v_1^*(t)&=\frac{1}{2L_1}\Big(\Gamma_3-\Gamma_1\Big)(t)\left[\frac{\mu_1 T^*(t-\tau_1)D^*(t-\tau_1)}{1+\epsilon_1 S^*(t-\tau_1)}\right]=\Pi_1(t)\ \ \text{(say)},\\
v_2^*(t)&=\frac{1}{2L_2}\Big(\Gamma_3-\Gamma_2\Big)(t)\left[\frac{\mu_2 T^*(t-\tau_2)D^*(t-\tau_2)}{1+\epsilon_1 S^*(t-\tau_2)}\right]=\Pi_2(t)\ \ \text{(say)}.
\end{aligned}$$

Now, using the conventional control's boundedness criteria and following the characteristics of the control set $U_1\times U_2$ that the admissible control takes the values such that $0\le v_i(t)\le v_i^{\max}<1$ $(i=1,2)$, we can have

$$v_1^*(t)=\begin{cases}0, & \text{when } \Pi_1(t)\le 0\\ \Pi_1(t), & \text{when } 0\le\Pi_1(t)\le v_1^{\max}\\ v_1^{\max}, & \text{when } \Pi_1(t)\ge v_1^{\max}\end{cases} \quad \text{and } v_2^*(t)=\begin{cases}0, & \text{when } \Pi_2(t)\le 0\\ \Pi_2(t), & \text{when } 0\le\Pi_2(t)\le v_2^{\max}\\ v_2^{\max}, & \text{when } \Pi_2(t)\ge v_2^{\max}\end{cases}. \tag{5.3.8}$$

From this result, we can derive the following theorem.

Theorem 5.3.1 *If the objective cost functional $J\big(v_1(t), v_2(t)\big)$ attains its minimum value for optimal controls $v_1^*(t)$ and $v_2^*(t)$, moreover (T^*, D^*, K^*, S^*) be the corresponding optimal state for the optimal control problem (5.3.1), then there exist adjoint functions $\Gamma_i(t)$ satisfying the transversality conditions $\Gamma_i(t_f) = 0$, for $i = 1, 2, 3, 4$. Furthermore, the optimal control solutions are given by*

$$v_j^*(t) = \max\left\{0,\ \min\left\{1,\ \frac{1}{2L_j}\Big(\Gamma_3 - \Gamma_j\Big)(t)\left[\frac{\mu_j T^*(t-\tau_j)D^*(t-\tau_j)}{1+\epsilon_j S^*(t-\tau_j)}\right]\right\}\right\}, \quad \text{for } j = 1, 2. \tag{5.3.9}$$

5.4 Numerical Simulations

In this section, we perform several numerical simulations to validate our analytical results for both the delayed system (5.1.1) and the optimal control system on the delay-induced model (5.3.1). The initial values for the model populations are chosen to satisfy the biological assumptions underlying this study. To demonstrate the behavior of the model, numerical simulations have been performed using the parameter values provided in Table 5.1.

5.4.1 Simulations of the Stability of Equilibrium

The initial values of all model populations for the simulation are chosen as follows:

$$\big(T(\theta), D(\theta), K(\theta), S(\theta)\big) = (10, 25, 140, 25), \quad \theta \in [-\tau, 0], \quad \text{where } \tau = \max\{\tau_1, \tau_2\}. \tag{5.4.1}$$

Initially, when both delay parameters are set to $\tau_1 = \tau_2 = 0$, representing the non-delayed system, the model populations, namely, T cells $[T(t)]$, dendritic cells $[D(t)]$, keratinocytes $[K(t)]$, and mesenchymal stem cells $[S(t)]$, exhibit asymptotically stable behavior. However, introducing time delays τ_1 and τ_2 (see Figure 5.2), all system populations, except mesenchymal stem cells $[S(t)]$, show oscillatory dynamics. For this simulation, the intracellular delay parameters are set to $\tau_1 = \tau_2 = 1.2$, while the remaining parameter values are taken from Table 5.1.

Since introducing non-zero delays into the system (5.1.1) does not alter the asymptotic behavior of the MSC population, our focus shifts to the dynamics of the other state populations. In Figure (5.3), we illustrate the behavior of the first three cell types: T cells, dendritic cells, and keratinocytes, for both non-delayed system ($\tau_1 = \tau_2 = 0$), represented by blue trajectories and the delayed system ($\tau_1 = 1.2, \tau_2 = 1$), represented by orange trajectories. Without delays, all system populations are asymptotically stable and converge to the endemic steady state. The introduction of non-zero delays exhibits stable periodic oscillations in the populations of these cell types. Moreover, the resulting limit cycles are depicted in a 3-D plot with respect to these populations, providing a comprehensive visualization of the periodic behavior. The simulation demonstrates the significant effect of intracellular delays on the autoimmune response for psoriasis transmission for the considered model system.

Parameter	Definition	Value (Unit)
ρ_T	Constant accumulation rate of T cells	25 $\text{mm}^{-3}d^{-1}$
ρ_D	Constant accumulation rate of dendritic cells	25 $\text{mm}^{-3}d^{-1}$
ρ_K	Constant accumulation rate of keratinocytes	5 $\text{mm}^{-3}d^{-1}$
ρ_S	Constant production of all mature stem cells	0.5 $\text{mm}^{-3}d^{-1}$
π	Logistic growth rate T cells	0.003 d^{-1}
$T^{\max}$	Maximum carrying capacity of T cells	300 mm^{-3}
μ_1	Rate of activation of T cells via dendritic cells	0.03 mm^3d^{-1}
μ_2	Rate of activation of dendritic cells via T cells	0.03 mm^3d^{-1}
ϵ_1	Inhibition scaling coefficient of MSCs on DC activation	0.05 mm^3
ϵ_2	Inhibition scaling coefficient of MSCs on T cell activation	0.05 mm^3
δ	Rate of inhibition of T cells hyper-activity via keratinocyte	0.003 mm^3d^{-1}
η_T	Natural mortality rate of T cells	0.1 d^{-1}
η_D	Natural mortality rate of dendritic cells	0.16 d^{-1}
η_K	Natural mortality rate of Keratinocyte	0.25 d^{-1}
η_S	Natural mortality rate of mature stem cells	0.3 d^{-1}

Table 5.1: Parameter values used in the numerical simulations for the entire model system. Several parameter ranges were obtained from previous studies [40, 84, 69]. Due to the lack of sufficient primary data related to immune-mediated delay factors, some parameter values were chosen to ensure the biological plausibility of the model behavior.

5.4.2 Simulations with Different Time Delays

In this subsection, we examine numerically the influence of time delays on first three model populations of the system (5.1.1) and perform some simulations in order to depicted the delay induced Hopf bifurcating positions by considering each delay parameters separately at a time.

If the time delay parameter τ_2 is fixed to zero ($\tau_2 = 0$), and τ_1 =0.8 and $\tau_1 = 1$ respectively, we observe in Figure 5.4(a) that the oscillation increases as τ_1 increases and periodic oscillation is seen at $\tau_1 = 1$ day. For $\tau_1 = 0.8$, the cell densities initially oscillate but eventually achieve local asymptotic stability, confirming our analytical finding stated in **Case-II** in the subsection 5.2.3. The trajectories for $\tau_1 = 0.8$ and $\tau_1 = 1$ are illustrated using two distinct color codes. In this scenario, the stability of the endemic equilibrium E^* depends on the value of the time delay τ_1, where τ_2 is fixed to zero. Larger values of τ_1 lead to regular oscillatory solutions, indicating that an increased time delay between the interactions of T cells with dendritic cells and keratinocytes results in sustained oscillations. Stability switch occurs through Hopf bifurcation which are depicted in the Figure 5.4(b) where we present the delay-induced Hopf-bifurcation, focusing on T cells, dendritic cells, and keratinocyte cells populations only. In this analysis, τ_1 serves as the bifurcation parameter. The parameter

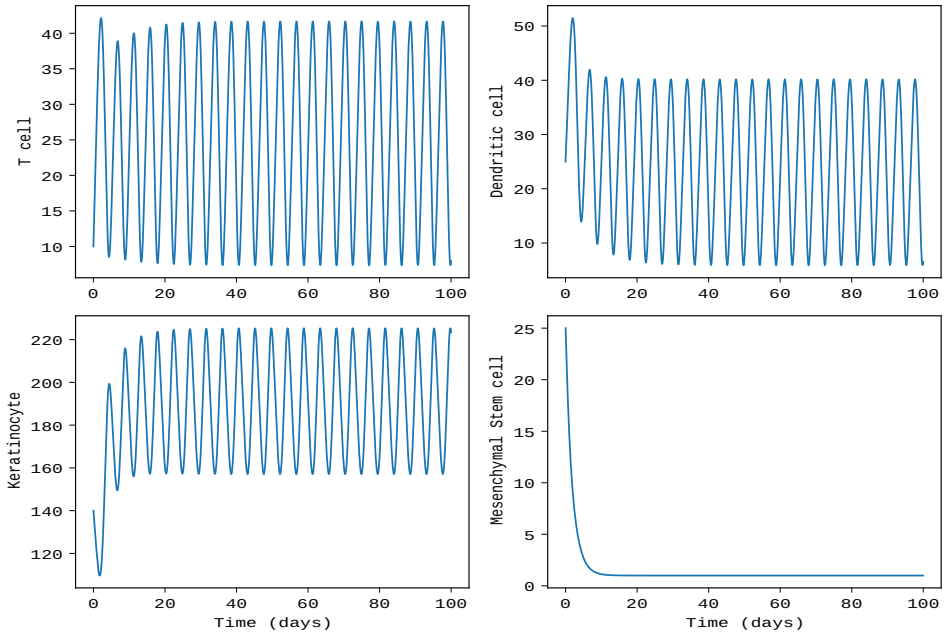

Figure 5.2: The dynamics of the model populations, namely T cells, dendritic cells, keratinocytes, and mesenchymal stem cells, for the delayed system with $\tau_1 = \tau_2 = 1.2$.

τ_1 is varied within the range of 0.7 to 1. The figure illustrates that, for $\tau_2 = 0$, there exists a critical value τ_1^* at which the endemic equilibrium point E^* transitions from stability to instability. This observation highlights the critical role of the delay parameter τ_1 in determining the stability of the system (5.1.1). Biologically, this implies that an increase in the time lag within the interaction term of the T cell growth equation—mediated by dendritic cell mediated cytokines infiltrating and accelerates fluctuations in the model cell concentrations, excluding the MSC population. These fluctuations manifest as oscillatory dynamics and this behavior arises from the inflammatory response in the upper epidermal layer caused by the over-expression of keratinocytes, which, in turn, amplifies the progression and dissemination of the disease.

In Figure 5.5(a), the time delay $\tau_1 = 0$ is fixed, and the trajectories are plotted for three distinct values of τ_2, color coded as follows: red for $\tau_2 = 0.85$, and blue for $\tau_2 = 1.2$. It is evident that as the value of τ_2 increases, the oscillations in the system populations become more pronounced initially but gradually diminish over time, indicating stabilization of the system. This demonstrates that larger values of τ_2 contribute to enhanced system stability. In Sub-figure 5.5(b), we present the bifurcation diagram by varying the bifurcation parameter τ_2 from 0.8 to 1.2 while keeping $\tau_1 = 0$. The diagram reveals the occurrence of a Hopf bifurcation at a critical value $\tau_2 = \tau_2^*$. For $\tau_2 < \tau_2^*$, all system populations except the mesenchymal stem cell (MSC) exhibit stable behavior, whereas for $\tau_2 > \tau_2^*$, the stability is lost. This indicates that increasing the time delay in the interaction term of the dendritic cell growth equation (stimulated by T cell-derived cytokines) infiltrating the keratinocyte population induces more oscillatory behavior in the system, excluding the MSC population. This observation highlights the significant impact of the bifurcation parameter τ_2 on system

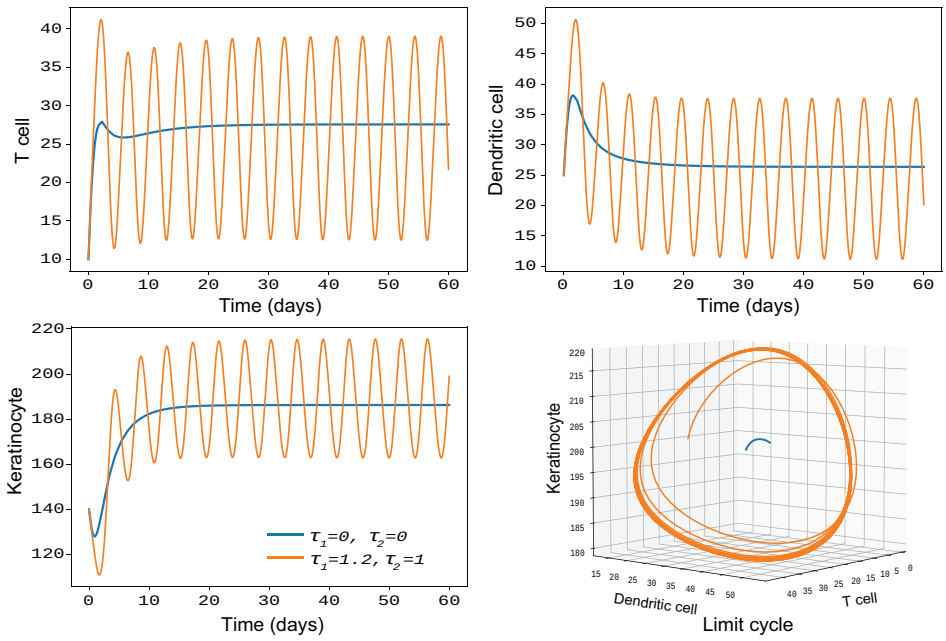

Figure 5.3: This figure illustrates the populations of three cell types T cells, dendritic cells, and keratinocytes, for both the non-delayed system ($\tau_1 = \tau_2 = 0$, shown with blue trajectories) and the delayed system ($\tau_1 = 1.2, \tau_2 = 1$, shown with orange trajectories). The introduction of non-zero delays results in periodic solutions, with the corresponding limit cycles depicted in a 3D plot.

stability from a biological point of view.

In Figure 5.6, the stability region of the endemic equilibrium point is depicted in the $\tau_1 - \tau_2$ plane. The color gradient represents the maximum real part of the eigenvalue, denoted as $Re(\lambda_{\max})$, where λ corresponds to the eigenvalue of the Jacobian matrix at the interior equilibrium point of the delayed system (5.1.1). The equilibrium point is unstable in the region where $Re(\lambda_{\max}) > 0$. It is observed that the critical values of τ_1 and τ_2, denoted as τ_1^* and τ_2^*, increase in the figures. Consequently, the area of the stability region for the endemic equilibrium expands with increasing values of τ_1 and τ_2. The values of all other parameters used in the analysis are provided in Table 5.1.

5.4.3 Simulations of Optimal Control for the Delayed Model

In this subsection, we numerically solve the optimal control problem for the delayed system (5.3.1) and present the results obtained through simulation. The parameter values used for the simulations are taken from Table 5.1, while the initial values are specified in equation (5.4.1). The weight constants in the objective functional are set as $L_1 = L_2 = 0.5$.

The optimal system (5.3.1) represents a two-point boundary value problem (BVP) with boundary conditions provided at two time points, $t = 0$ and $t = t_f$. For the numerical simulations, we utilized the bvp4c solver in MATLAB, which is specifically designed for

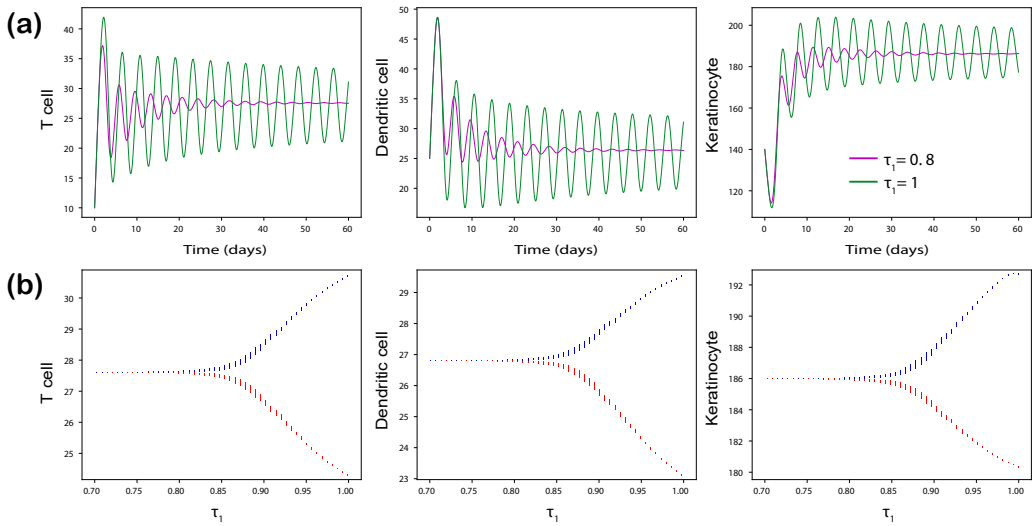

Figure 5.4: In sub-figure (a), the populations of T cells, dendritic cells, and keratinocytes are shown for the delay parameter $\tau_2 = 0$, with trajectories plotted for two distinct values of τ_1 (0.8 and 1), each represented by a different color code. Sub-figure (b) depicts the Hopf bifurcation with respect to the delay parameter τ_1 while keeping $\tau_2 = 0$.

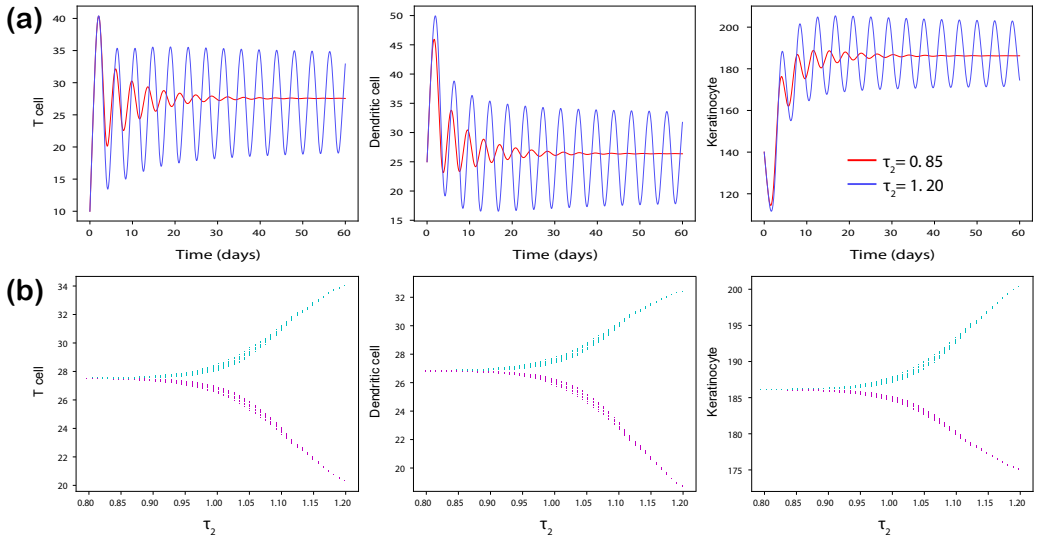

Figure 5.5: In Sub-figure (a), the populations of T cells, dendritic cells, and keratinocytes are shown with a fixed delay of $\tau_1 = 0$. The trajectories are plotted for two distinct values of τ_2 (0.85 and 1.2), each represented by a different color. Sub-figure (b) illustrates the Hopf bifurcation with respect to the delay parameter τ_2, while the other delay parameter, τ_1, is fixed at 0.

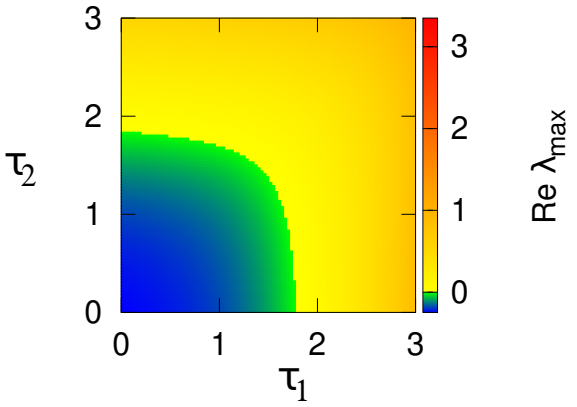

Figure 5.6: The stability region of the endemic equilibrium point is shown in the $\tau_1 - \tau_2$ plane. The color coding denotes the $max[Re(\lambda)]$, where λ is the eigenvalues corresponding to the delayed system.

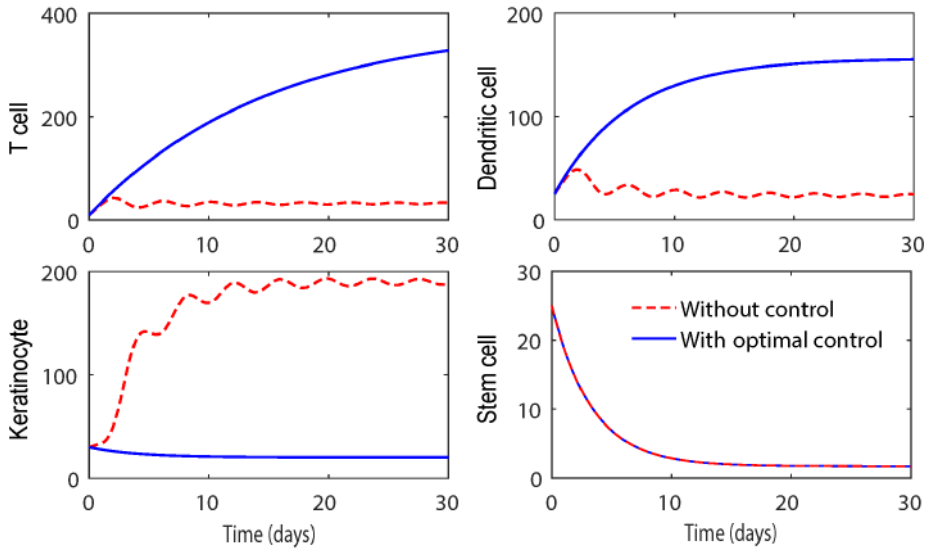

Figure 5.7: Numerical solution of the optimal control problem with $\tau_1 = \tau_2 = 1.1$ and remaining parameter values taken from Table 5.1. The red dotted trajectories represent the disease dynamics without optimal control, while the blue trajectories depict the population behavior under the influence of optimal control.

solving nonlinear two-point BVPs. For a detailed understanding of this numerical method, readers may refer to the work by Torres et al. [85].

To solve the system, we define the state variables $T(t), D(t), K(t), S(t)$, the adjoint variables $\Gamma_1(t), \Gamma_2(t), \Gamma_3(t)$, $\Gamma_4(t)$, and the control functions $v_j(t)$ $(j = 1, 2)$. A combination of forward-backward difference approximations is employed to solve the control-induced system

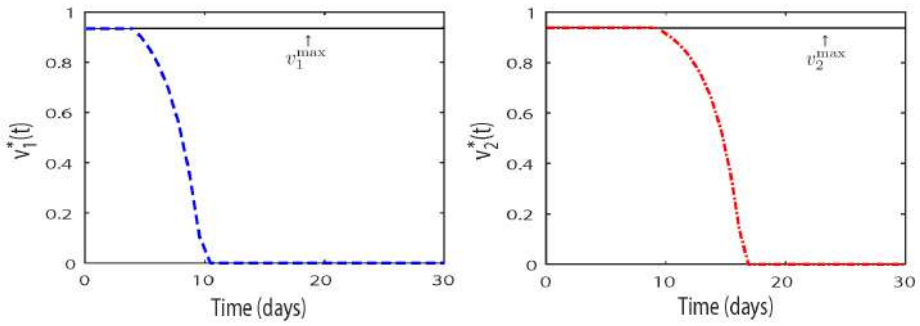

Figure 5.8: Numerical approximation of Pontryagin's extremals and the corresponding optimal control profiles $v_1^*(t)$ and $v_2^*(t)$.

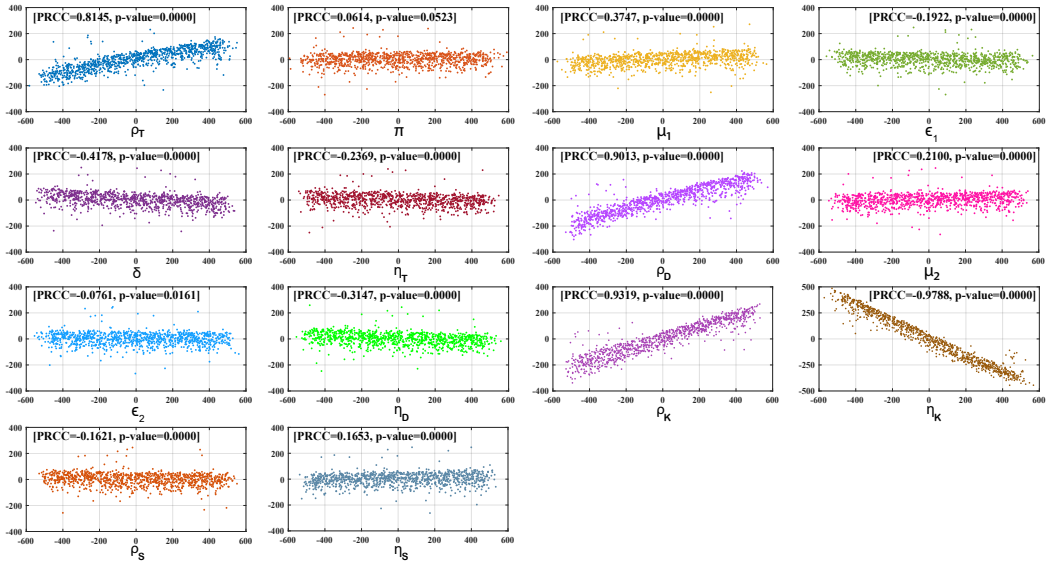

Figure 5.9: PRCC scatter plots of all system parameters against keratinocyte population ($N = 1000$). PRCC values are computed at day 100, with p values up to four decimal places. The x-axis shows residuals from regressing the rank-transformed parameter on all others, and the y-axis shows residuals from regressing keratinocyte values on all parameters except the one analyzed.

along with the adjoint system. The solutions are then plotted, with all state variables shown over time in Figure 5.7. The red dotted trajectories represent the system population concentrations without control, while the blue trajectories correspond to the population behavior under optimal control.

To determine the optimal control profiles, we apply the transversality conditions and enforce the boundedness of controls within the interval $[0, 1]$ as per Pontryagin's principle. The control functions $v_1^*(t)$ and $v_2^*(t)$ for the delayed system (5.3.1) are computed and plotted over 30 days, as shown in Figure 5.8. From the results, we observe a similar pattern for both

control profiles, though notable differences exist. The control v_1^* (represented by trajectories with blue dots), associated with the TNF-α inhibitor drug, modulates the system within a short span of approximately 10 days. In contrast, the control v_2^* (indicated by red dotted trajectories), corresponding to the IL-17 inhibitor, requires about 18 days to regulate the system effectively. This indicates that the combination of these biologic inhibitors optimally controls the delayed model system, mitigating the auto-immune response and keratinocyte over-expression. The inflammatory cytokine loop, regulated predominantly by T cell and dendritic cell mediated interactions, is thus brought under control, achieving an optimal therapeutic outcome.

In addition to these, Figure 5.9 presents the global sensitivity analysis of all parameters in our system using Latin Hypercube Sampling (LHS) with the Partial Rank Correlation Coefficients (PRCC) method, focusing on the keratinocyte population. We evaluate the PRCC and p-value for each parameter, where the p-value indicates the level of uncertainty associated with each parameter's PRCC value. p-value < 0.05 for each parameter signifies the statistical significance of the corresponding PRCC value. This scatter plot shows that the parameters ρ_T, μ_1, ρ_D, and ρ_K have a positive influence on disease progression, while the parameters δ, η_T, η_D, and η_K have a negative influence. In this study, we consider the keratinocyte level as a marker for disease prediction. The overall sensitivity analysis helps in identifying the precise point of treatment for psoriatic disease.

5.5 Discussion and Conclusion

Psoriasis involve complicated immune interactions, where time delays play an important role in the start and growth of symptoms. These delays come from immune activation, cytokine release, and cell recruitment, which do not happen immediately. In this *Chapter*, we introduced two intracellular delays, τ_1 and τ_2, in the mathematical model to capture these immune processes. The analysis showed that both delays have a strong effect on the stability of the system. When the delays cross certain threshold values, the system loses stability and starts oscillating. This reflects the prolonged immune response in psoriasis and explains how delays may lead to flare-ups. Thus, the model gives a realistic picture of how timing in immune interactions shapes disease progression.

Further applying optimal control strategies via the effects of two biologic inhibitors targeting TNF-α and IL-17 pathways in the delay-induced system (5.3.1). The results show that these controls reduce oscillations and help to stabilize the immune response with respect to different response times. The TNF-α inhibitor acts faster (about 10 days), while the IL-17 inhibitor takes longer (18–20 days) to achieve control.

In the following chapter, we present a psoriasis model that includes different stages of stem cell maturation. The study investigates the therapeutic potential of local stem cell replacement in comparison with biologic cytokine inhibitors, with both strategies analyzed under impulsive control frameworks.

Chapter 6

Stem Cell vs. Biologic Therapy in a Psoriasis Model: A Comparative Mathematical Study through Impulsive Control Framework

In this *Chapter*[2], we formulate a mathematical model based on ODEs to understand how psoriasis develops and how it can be controlled. The model includes three main cells: helper T cells, dendritic cells, and keratinocytes, along with two more cell types: local embryonic stem cells (SCs) and mesenchymal stem cells (MSCs). Stem cells can grow and become MSCs after several stages, and MSCs can directly control immune cells and keratinocytes by releasing anti-inflammatory cytokines like IL-4 and IL-10. These MSCs also help in repairing damaged tissues and balancing the abnormal stem cells in psoriatic skin. We checked the mathematical properties of our model, such as positivity, boundedness, and stability. First, we tested the effect of the drug Infliximab, an FDA-approved TNF-α inhibitor, but it did not give good results in severe cases. Further, we studied stem cell transplantation, and our results showed that the disease could be removed within two months of treatment. The impulsive cell replacement strategy induced a periodic behavior in the system, and we studied its stability using Floquet theory. Numerical results supported our analysis, and overall we found that stem cell transplantation may be more effective than common biological drugs for treating severe psoriasis.

6.1 The Model with Stem Cells

We divide our mathematical model into three main cell populations to describe the epidermal transmission channel. Here, $T(t)$, $D(t)$, and $K(t)$ represent the population densities of helper T cells, dendritic cells, and keratinocytes. The development of psoriasis is driven by cytokines

[2] *A substantial portion of this chapter has been submitted for publication in a peer-reviewed international journal.*

released from these cells. The constant input rates of T cells and dendritic cells are denoted by C_T and C_D, which define their growth in the psoriatic state [86]. Dendritic cells stimulate T cells at a rate γ, influenced by cytokines IL-10 and IL-12 [87]. Keratinocytes are activated by T cells through TNF-α and IL-17/22 at rate δ_1, and by dendritic cells mainly through IL-15 and IL-23 at rate δ_2 [88, 54]. Keratinocytes also proliferate continuously at rate C_K as they migrate from the dermis to the epidermis [69]. The natural death rates of T cells, dendritic cells, and keratinocytes are given by λ_T, λ_D, and λ_K, respectively. Figure 6.1 illustrates these mutual interactions among immune cells via the cytokine network that drives disease progression. Based on these assumptions, we propose the following mathematical model.

$$\begin{aligned}
\frac{dT(t)}{dt} &= C_T - \gamma T(t)D(t) - \delta_1 T(t)K(t) - \lambda_T T(t),\\
\frac{dD(t)}{dt} &= C_D - \delta_2 D(t)K(t) - \lambda_D D(t),\\
\frac{dK(t)}{dt} &= C_K + \big[\delta_1 T(t)K(t) + \delta_2 D(t)K(t)\big] - \lambda_K K(t).
\end{aligned} \tag{6.1.1}$$

To show the dynamics of stem cells, we have developed a mathematical model based on ordinary differential equations. Here, $S(t)$ and $S_M(t)$ represent the densities of embryonic stem cells and mesenchymal stem cells. The growth equations are given by

$$\begin{aligned}
\frac{dS(t)}{dt} &= \rho_0 + \big[\zeta(p_S - p_D) - \lambda_S\big]S(t)\\
\frac{dS_M(t)}{dt} &= \big[\zeta A(2p_D + p_A)\big]S(t) - \lambda_M S_M(t).
\end{aligned} \tag{6.1.2}$$

Here, ρ_0 denotes the constant production rate of stem cells. The division probabilities are defined as: p_S for symmetric self-renewal (two stem cells), p_D for symmetric differentiation (two committed cells), and p_A for asymmetric division (one stem cell and one committed cell) [89], with $p_S + p_D + p_A = 1$. The parameter A represents the maturity amplification factor, and ζ is the differentiation rate. The natural death rates of stem cells (SCs) and mesenchymal stem cells (MSCs) are λ_S and λ_M, respectively [90]. MSCs help maintain immune balance by suppressing T-cell hyperactivity at rate ξ [91], and by controlling keratinocyte overproduction at rate η through tolerogenic cytokines such as IL-4 and IL-10 [61]. Based on these assumptions, the stem-cell-induced model is formulated as:

$$\begin{aligned}
\frac{dS(t)}{dt} &= \rho_0 + \big[\zeta(p_S - p_D) - \lambda_S\big]S(t),\\
\frac{dS_M(t)}{dt} &= \big[\zeta A(2p_D + p_A)\big]S(t) - \lambda_M S_M(t),\\
\frac{dT(t)}{dt} &= C_T - \gamma T(t)D(t) - \delta_1 T(t)K(t) - \xi T S_M(t) - \lambda_T T(t),\\
\frac{dD(t)}{dt} &= C_D - \delta_2 D(t)K(t) - \lambda_D D(t),\\
\frac{dK(t)}{dt} &= C_K + \frac{\delta_1 T(t)K(t) + \delta_2 D(t)K(t)}{1 + \eta S_M(t)} - \lambda_K K(t),
\end{aligned} \tag{6.1.3}$$

subject to the initial conditions $S(0) > 0$, $S_M(0) > 0$, $T(0) > 0$, $D(0) > 0$ and $K(0) > 0$.

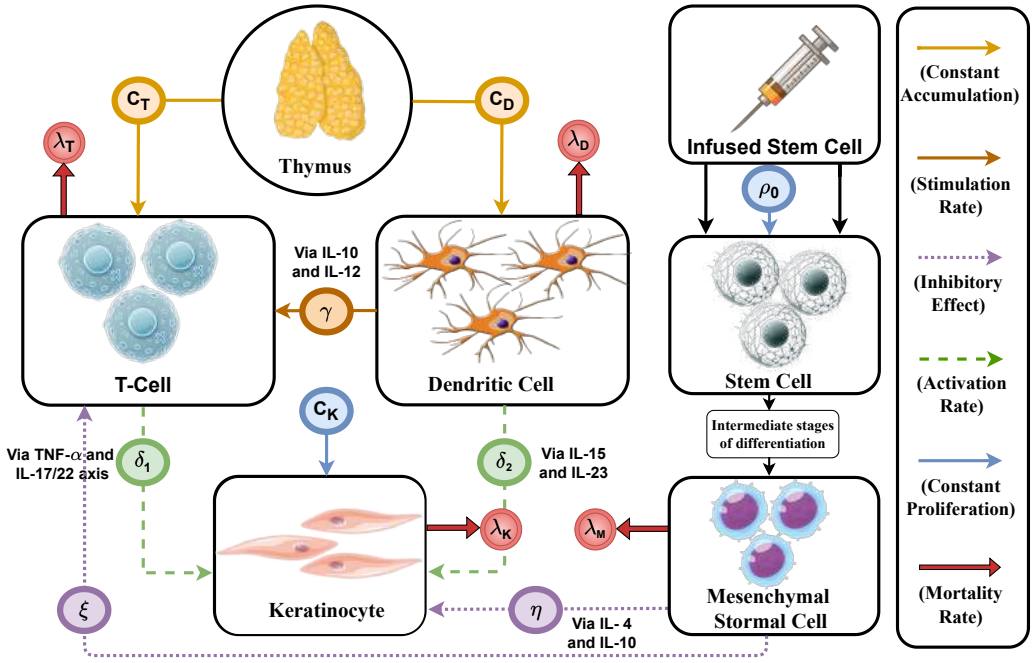

Figure 6.1: Schematic diagram of cell–cell interactions through cytokine signaling, with shaded arrows indicating effects driving psoriasis dynamics.

6.2 Stem-Cell Maturation

Stem-cell-based therapies have the capacity to promote the differentiation of stem cells into mature types of cells in order to repair damaged cells or tissues [22]. Healthy stem-cell transplantation is needed for the treatment of psoriasis in severe cases, which ultimately differentiated to MSCs (the n-th stage is regarded as the mature stage; i.e., $S_n(t) = S_M(t)$) and inhibits the overproduction of T cells and keratinocytes. $S_i(t)$ signifies the population density of stem cells at the i-th stage of differentiation ($i = 1, 2, \cdots, n-1$) and $S_n(t)$ denotes the density of mature SCs at the n-th stage.

We assume that cytokines are secreted by specific cells at a maximum rate of α, and this secretion is reduced by a negative feedback mechanism. This forms a self-limiting process with rate μ [92]. The delivery of these signals is also controlled by mechanisms that respond to the quantity of mature cells. This means that when mature cells are present, the production of signaling factors decreases at a rate β. The differential equation that describes how signalling molecules change over time is as follows:

$$\frac{dX}{dt} = \alpha - \mu X - \beta S_n X.$$

Substituting $Y(t) = \mu X(t)/\alpha$ and $Z = \beta/\mu$, the above equation changes to

$$\frac{dY}{dt} = \mu\Big[1 - Y - ZS_nY\Big].$$

The amount of cytokines quickly stabilizes because they are secreted at a much faster rate than cell proliferation and differentiation. The signal intensity using the quasi-steady-state approximation is given by $Y(t) = 1/\big(1 + ZS_n(t)\big)$. The following scheme represents the stem cell lineage:

$$\begin{aligned}
\frac{dS_1}{dt} &= \rho_0 + f_1\big[Y, S_1\big] \\
\frac{dS_2}{dt} &= f_2\big[Y, S_2\big] + g_1\big[Y, S_1\big] \\
&\vdots \\
\frac{dS_n}{dt} &= f_n\big[Y, S_n\big] + g_{n-1}\big[Y, S_{n-1}\big].
\end{aligned} \tag{6.2.1}$$

The functions $f_i[Y(t), S_i(t)]$ and $g_i[Y(t), S_i(t)]$, respectively, denote a change in $S_i(t)$ resulting from activities taking place at the i-th and $(i-1)$-th stages of maturation [93]. $f_i[Y(t), S_i(t)]$ is positive if the number of cells produced by self-renewal and proliferation is greater than the number of cells produced by differentiation or cell death. Otherwise $f_i[Y(t), S_i(t)]$ is negative. The term $f_n[Y(t), S_n(t)]$ is negative since mature cells cannot multiply because they are unable to go through mitosis; this term instead indicates cell death. To complete the chain, we suppose that the regulatory signal relies on the quantity of mature cells or that $Y(t) = Y(S_n(t))$ is negative. The following presumptions form the basis of the definitions of f and g:

1. $f_i(Y, 0) = 0$ for all Y.
2. $g_i(Y, S_i) \geq 0$, with equality when $S_i = 0$ for all Y.
3. If $S_i > 0$, then $f_i(Y, S_i)$ is strictly monotone increasing in Y.
4. For each $i < n$ and for all $S_i > 0$, there exists a signal concentration $Y_i^* > 0$ such that $f_i(Y_i^*, S_i) = 0$.
5. $\frac{\partial f_i(Y,S_i)}{\partial S_i} > 0$ at $S_i = 0$ if $Y > Y_i^*$ and $\frac{\partial f_i(Y,S_i)}{\partial S_i} < 0$ at $S_i = 0$ if $Y < Y_i^*$.
6. Cell densities are balanced in healthy tissue.

The type-i sub-population proliferate at a rate l_i, the self-renewal percentage is denoted by b_i, and the death rate is denoted by λ_i. Then, $l_iS_i(t)$ gives the flow to mitosis at time 't'. The percentage b_i of daughter cells remains undifferentiated. The amount of cells (i.e., the influx) that enter the i-th population after cell division is given by $2b_il_iS_i(t)$, while the flux to the next cell compartment is given by $2\big(1 - b_i\big)l_iS_i(t)$. The flux to death is provided by

$\lambda_n S_i(t)$. Thus we have,

$$\begin{aligned} f_i(t) &= \big(2b_i - 1\big) l_i S_i(t) - \lambda_i S_i(t), \quad \big(i = 1, 2, \cdots, n-1\big) \\ g_i(t) &= 2\big(1 - b_{i-1}\big) l_{i-1} S_{i-1}(t), \quad \big(i = 2, 3, \cdots, n-1\big) \\ f_n(t) &= -\lambda_n S_n(t). \end{aligned} \tag{6.2.2}$$

Here, we assume that the concentration of mature stem cells determines the feedback signal and is given by $Y \equiv Y(S_n(t)) = 1/\big(1 + ZS_n(t)\big)$, where Z is a positive constant. The expression confirms the empirical hypothesis that the signal amount reaches its maximum value of 1 in the absence of mature stem cells and decreases asymptotically to zero in the presence of mature stem cells. It is theoretically impossible to evaluate this expression without mature cells because essential processes rely on the presence of mature cells. Therefore, the proliferation rates are stable throughout time and the signal feedback $Y(S_n(t))$ regulates the self-renewal fractions; i.e., $b_i(t) \equiv b_i\big[Y(S_n(t))\big] = b_i^{max} Y(S_n(t))$, where b_i^{max} is the maximal fraction of self-renewal. For the sake of simplicity, it is also anticipated that the mortality rate will stay constant over time throughout all stages of differentiation. As a result, we arrive at the following equations:

$$\begin{aligned} \frac{dS_1(t)}{dt} &= \rho_0 + \big[2b_1^{max} Y - 1\big] l_1 S_1(t) - \lambda_1 S_1(t), \\ &\vdots \\ \frac{dS_i(t)}{dt} &= \big[2b_i^{max} Y - 1\big] l_i S_i(t) + 2\big[1 - a_{i-1}^{max} Y\big] l_{i-1} S_{i-1}(t) - \lambda_i S_i(t), \\ &\vdots \\ \frac{dS_n(t)}{dt} &= 2\big[1 - b_{n-1}^{max} Y\big] l_{n-1} S_{n-1}(t) - \lambda_n S_n(t), \end{aligned} \tag{6.2.3}$$

where $Y(t) = 1/\big[1 + ZS_n(t)\big]$. To establish the model parameters and initial conditions, we utilize the following assumptions:

(1) $t \in [0, \infty)$.
(2) $S_i(0) \geq 0$, for $i = 1, \cdots, n$.
(3) $\lambda_i \geq 0$, for $i = 1, \cdots, (n-1)$, and $\lambda_n > 0$.
(4) $l_i > 0$ for $i = 1, \cdots, (n-1)$.
(5) $b_i^{\max} \in [0, 1)$, for $i = 1, \cdots, n-1$.
(6) $Z > 0$.

6.3 Full-Scale Model with Stem-Cell Maturation

Each organ of the body produces new cells to replace old ones and maintain tissue balance. In this psoriasis model, we consider different stages of the stem cell lineage as described in system (6.2.3). Immature and mature cells are treated as separate populations to distinguish stem cells from their immediate offspring. With $(n+3)$ state variables and $(n+3)$ ODEs, the model explains stem cell maturation and the interaction of mature cells with immune cells in the psoriatic epidermis [94]. For simplicity, we assume that mature cells stop dividing after the third stage $(n = 3)$ [90]. To introduce stem cells from an external source, we use a small

positive constant Z so that the feedback term $\left[1/\left(1+ZS_M(t)\right)\right]$ stays in $(0,1)$ and remains close to 1. Hence, $b_i^{\max}Y\ \left[=b_i^{\max}/(1+ZS_M(t))\right]$ is replaced by b_i for $i=1,\ldots,n-1$. Based on this, the stem-cell-induced mathematical model is structured as follows:

$$\begin{aligned}
&\frac{dS_1(t)}{dt}=\rho_0-\sigma_1S_1(t),\quad \frac{dS_2(t)}{dt}=\rho_1S_1(t)-\sigma_2S_2(t),\quad \frac{dS_M(t)}{dt}=\rho_2S_2(t)-\lambda_MS_M(t),\\
&\frac{dT(t)}{dt}=C_T-\gamma T(t)D(t)-\delta_1T(t)K(t)-\xi T(t)S_M(t)-\lambda_TT(t),\\
&\frac{dD(t)}{dt}=C_D-\delta_2D(t)K(t)-\lambda_DD(t),\\
&\frac{dK(t)}{dt}=C_K+\frac{\delta_1T(t)K(t)+\delta_2D(t)K(t)}{1+\eta S_M(t)}-\lambda_KK(t),
\end{aligned}\tag{6.3.1}$$

with $\sigma_i=\lambda_i-(2b_i-1)l_i, \rho_i=2(1-b_i)l_i\ (i=1,2)$, subject to the initial conditions $S_1(0)>0,\ S_2(0)>0,\ S_M(0)>0,\ T(0)>0,\ D(0)>0$ and $K(0)>0$.

6.4 Properties of the Full-Scale Model

In this section, we study the positivity and boundedness of the full-scale model populations, the existence criterion of the endemic equilibrium point and its global stability analysis for system (6.3.1). It is necessary for the model to be well-posed and biologically realistic.

6.4.1 Positivity of the Invariant Region and Boundedness of the Model

We discussed the positivity of the solutions and boundedness properties of our proposed system (6.3.1), to ensure that the model is well-posed and epidemiologically feasible. Now, we prove the following theorem, which guarantees the positivity of the solutions of system.

Theorem 6.4.1 *All solutions of the system (6.3.1) with positive initial conditions remain positive for all $t>0$.*

Proof. Let us choose $x_1(t)=S_1(t), x_2(t)=S_2(t), x_3(t)=S_M(t), x_4(t)=T(t), x_5(t)=D(t)$, and $x_6(t)=K(t)$. Rewriting the system (6.3.1) in the following manner

$$\frac{dx(t)}{dt}=\Gamma\left[x(t)\right],\tag{6.4.1}$$

where $x(t)=\left[x_1(t),x_2(t),x_3(t),x_4(t),x_5(t),x_6(t)\right]^T$ and $\Gamma=\left[\Gamma_1,\Gamma_2,\Gamma_3,\Gamma_4,\Gamma_5,\Gamma_6\right]^T$. Here ^{T} denotes the transpose and Γ denote the right-hand side of system (6.3.1). Thus we have

$$\Gamma_i(x)|_{x_i=0,x\in\mathbb{R}^6_+}\geq 0,\quad \forall i=1,\ldots,6.$$

Using the result of Nagumo, this condition ensures the positivity of the solutions of our system (6.3.1) [62]. Hence all solutions of the system starting from $x(0)=$

$\big[x_1(0), x_2(0), x_3(0), x_4(0), x_5(0), x_6(0)\big]^T$ belong to $\mathbb{R}^6_+$, such as $x(t) = x\big[t; x(0)\big]$, and $x(t) \in \mathbb{R}^6_+, \forall t > 0$. This implies that the non-negative octant $\mathbb{R}^6_+$ becomes invariant for the system (6.3.1).

It is also important to show that all the model variables of system (6.3.1) are bounded for all time $t > 0$. This will ensure that the system is biologically meaningful and mathematically well-posed. Before showing the boundedness of the solution of the system, we cite the following lemma [35].

Lemma 6.4.1 *Suppose P is a variable satisfying $\frac{dP(t)}{dt} < R - Q(\varphi)P(t)$, where R is a constant and $Q(\varphi)$ is independent of P and t. Then if $P(0) < R/Q(\varphi)$, it follows that $P(t) < R/Q(\varphi)$ for all t.*

The following theorem demonstrates the invariant region Π where the solutions of system (6.3.1) are bounded.

Theorem 6.4.2 *All non-negative solutions of the system (6.3.1) enter into the region $\Pi \subseteq \mathbb{R}^6_+$ and are ultimately bounded, where Π is defined by $\Pi = \big\{(S_1, S_2, S_M, T, D, K)^T \in \mathbb{R}^6_+ : 0 < S_1(t) \leq G_1, 0 < S_2(t) \leq G_2, 0 < S_M(t) \leq G_3, 0 < T(t) \leq G_4,\ 0 < D(t) \leq G_5,\ 0 < K(t) \leq G_6\big\}$. The G_i's $(i = 1, 2, 3, 4, 5, 6)$ are defined by*

$$G_1 = \frac{\rho_0}{\sigma_1}, G_2 = \frac{\rho_0\rho_1}{\sigma_1\sigma_2}, G_3 = \frac{\rho_0\rho_1\rho_2}{\sigma_1\sigma_2\lambda_M}, G_4 = \frac{C_T}{\lambda_T},$$
$$G_5 = \frac{C_D}{\lambda_D}, G_6 = \frac{C_K(1 + \eta S_M^{\min})}{\lambda_K(1 + \eta S_M^{\min}) - (\delta_1 G_4 + \delta_2 G_5)}.$$

The solutions of system (6.3.1) maintain their biological significance for all $t \in [0, \mathcal{T}]$.

Proof. From the first equation of the system (6.3.1) we have:

$$\frac{dS_1}{dt} = \rho_0 - \sigma_1 S_1.$$

Using Lemma 6.4.1, we obtain:

$$\lim_{t\to\infty} \sup \big[S_1(t)\big] \leq \frac{\rho_0}{\sigma_1}.$$

From the second equation of the system (6.3.1), we have:

$$\frac{dS_2}{dt} = \rho_1 S_1 - \sigma_2 S_2 \leq \frac{\rho_0\rho_1}{\sigma_1} - \sigma_2 S_2.$$

The comparison principle [56] and Lemma 6.4.1 ensure the following inequality:

$$0 < S_2(t) \leq G_2(1 - e^{-\sigma_2 t}) + S_2(0)e^{-\sigma_2 t},\ t > 0, \text{ where } S_2(t) \leq G_2 \text{ if } S_2(0) \leq G_2.$$

In similar manner, from the third, fourth and fifth equations of system (6.3.1), we get:

$0 < S_M(t) \leq G_3(1 - e^{-\lambda_M t}) + S_M(0)e^{-\lambda_M t},\ t > 0$ where $S_M(t) \leq G_3$ if $S_M(0) \leq G_3$.
$0 < T(t) \leq G_4(1 - e^{-\lambda_T t}) + T(0)e^{-\lambda_T t},\ t > 0$ where $T(t) \leq G_4$ if $T(0) \leq G_4$.
$0 < D(t) \leq G_5(1 - e^{-\lambda_D t}) + D(0)e^{-\lambda_D t},\ t > 0$ where $D(t) \leq G_5$ if $D(0) \leq G_5$.

Using the bounds for T-cell and DC concentrations, from the last equation we have:

$$\frac{dK}{dt} < C_K + \frac{\delta_1 G_4 + \delta_2 G_5}{1 + \eta S_M^{\min}} K - \lambda_K K = C_K - \Big(\lambda_K - \frac{\delta_1 G_4 + \delta_2 G_5}{1 + \eta S_M^{\min}}\Big) K.$$

Utilizing the comparison principle and Lemma 6.4.1, we obtain:

$$0 < K(t) < G_6 \left[1 - \exp\left\{-\Big(\lambda_K - \frac{\delta_1 G_4 + \delta_2 G_5}{1 + \eta S_M^{\min}}\Big)t\right\}\right] + K(0)\exp\left\{-\Big(\lambda_K - \frac{\delta_1 G_4 + \delta_2 G_5}{1 + \eta S_M^{\min}}\Big)t\right\},$$

where $t > 0$, and $K(t) \leq G_6$ if $K(0) \leq G_6$.

Therefore, all solutions $\big(S_1(t), S_2(t), S_M(t), T(t), D(t), K(t)\big)^{\mathrm{T}}$ that begin in the region Π remain there for all $t > 0$. Hence Π is an invariant set for system (6.3.1). Moreover, all solutions of the system are bounded, since the set Π is bounded.

Note that, any solution of system (6.3.1) with positive initial conditions ultimately enters and remains inside the set Π. The following relationships and the definition of the set Π justify this characteristic.

$$\left.\frac{dS_1}{dt}\right|_{\partial\Pi} < 0, \quad \left.\frac{dS_2}{dt}\right|_{\partial\Pi} < 0, \quad \left.\frac{dS_M}{dt}\right|_{\partial\Pi} < 0, \quad \left.\frac{dT}{dt}\right|_{\partial\Pi} < 0, \quad \left.\frac{dD}{dt}\right|_{\partial\Pi} < 0, \quad \left.\frac{dK}{dt}\right|_{\partial\Pi} < 0, \quad (6.4.2)$$

which are carried out at the points of the boundary $\partial\Pi$ of Π. Note that these relationships in (6.4.2) also hold outside the set Π, which guarantees the boundedness of all solutions $\big(S_1(t), S_2(t), S_M(t), T(t), D(t), K(t)\big)^{\mathrm{T}}$ of system (6.3.1) along with the positive initial conditions.

6.4.2 Existence of the Endemic Equilibrium Point

An endemic equilibrium point E^* exists when its co-ordinates satisfy the conditions:

$$S_1^* > 0, \quad S_2^* > 0, \quad S_M^* > 0, \quad T^* > 0, \quad D^* > 0, \quad \text{and} \quad K^* > 0.$$

When the disease is being treated by using stem-cell replacement, we obtain the endemic endemic equilibrium point by setting the equations of the system (6.3.1) to zero and then solve for the state variables.

$$S_1^* = \frac{\rho_0}{\sigma_1}, \quad S_2^* = \frac{\rho_1 S_1^*}{\sigma_2} = \frac{\rho_0\rho_1}{\sigma_1\sigma_2}, \quad S_M^* = \frac{\rho_2 S_2^*}{\lambda_M} = \frac{\rho_0\rho_1\rho_2}{\sigma_1\sigma_2\lambda_M}. \quad (6.4.3)$$

Now, we set the fifth equation of system (6.3.1) to zero and find the value of K in terms

of D. We set the fourth equation to zero and put $S_M^* = m$, we get two state variables T and K in terms of D as follows:

$$\begin{aligned} T &= C_T\delta_2 D\big[\gamma\delta_2 D^2 + \xi m\delta_2 D + \delta_1(C_D - \lambda_D D) + \lambda_T\delta_2 D\big]^{-1} \\ K &= \delta_2^{-1}D^{-1}\big(C_D - \lambda_D D\big). \end{aligned} \tag{6.4.4}$$

Using the values expressed in system (6.4.4), we obtain a fourth-order polynomial of D from the sixth equation of the system (6.3.1) and put it into the standard form:

$$F(D) = D^4 + A_0D^3 + A_1D^2 + A_2D + A_3. \tag{6.4.5}$$

The coefficients are given by

$$\begin{aligned} A_0 &= \frac{1}{\gamma\delta_2 h_2\lambda_D}\Big[\delta_2 h_2\lambda_T\lambda_D + \delta_2 h_2\xi m\lambda_D - \gamma\delta_2 h_2 C_D - \gamma\delta_2\lambda_D\lambda_K - \delta_1 h_2\lambda_D^2 - \gamma\delta_2^2 C_K\Big], \\ A_1 &= \frac{1}{\gamma\delta_2 h_2\lambda_D}\Big[\gamma\delta_2 C_D\lambda_K + 2\delta_1 h_2 C_D\lambda_D + \delta_2 h_1 C_T\lambda_D + \delta_1\delta_2 C_K\lambda_D + \delta_1\lambda_D^2\lambda_K - \delta_2 h_2\xi m C_D \\ &\qquad - \delta_2 h_2 C_D\lambda_T - \delta_2\xi m\lambda_D\lambda_K - \delta_2\lambda_T\lambda_D\lambda_K - \delta_2^2 C_K\lambda_T - \delta_2^2\xi m C_K\Big], \\ A_2 &= \frac{1}{\gamma\delta_2 h_2\lambda_D}\Big[\delta_2\xi m C_D\lambda_K + \delta_2 C_D\lambda_T\lambda_K - 2\delta_1 C_D\lambda_D\lambda_K - \delta_2 h_1 C_T C_D - \delta_1\delta_2 C_D C_K - \delta_1 h_2 C_D^2\Big], \\ A_3 &= \frac{\delta_1 C_D^2\lambda_K}{\gamma\delta_2 h_2\lambda_D}, \end{aligned}$$

where $m = \frac{\rho_0\rho_1\rho_2}{\sigma_1\sigma_2\lambda_M}$ and $h_i = \frac{\delta_i}{(1+\eta m)}$, $i = 1, 2$.

The polynomial (6.4.5) has at least one positive real root D^* if the following conditions are satisfied simultaneously.

$$\begin{aligned} &A_0 < 0,\ A_1 > 0,\ A_2 < 0,\ A_3 > 0,\ 3A_0^2 \geq 8A_1, \\ &A_0^3 - 4A_0A_1 + 8A_2 = 0,\ 3A_0^4 - 16A_0^2A_1 + 16A_1^2 + 16A_0A_2 - 64A_3 = 0. \end{aligned}$$

Using the value of D^*, we can determine the values of T^* and K^* with the help of the system (6.4.4). From these considerations, we construct the following Lemma.

Lemma 6.4.2 *For the positive value of D^*, if $C_D > \lambda_D D^*$, then the endemic equilibrium E^* exists.*

6.4.3 Global Stability of the Interior Equilibrium

In this subsection, we perform the global stability analysis of the endemic equilibrium point E^* for the system (6.3.1). To accomplish this, we define the Lyapunov function

$$\begin{aligned} \mathcal{L} = \frac{1}{2}(S_1 - S_1^*)^2 + \frac{1}{2}(S_2 - S_2^*)^2 + \frac{1}{2}(S_M - S_M^*)^2 + \frac{1}{2}(T - T^*)^2 \\ + \frac{1}{2}(D - D^*)^2 + \frac{1}{2}(K - K^*)^2. \end{aligned}$$

$$\therefore \frac{d\mathcal{L}}{dt} = (S_1 - S_1^*)\frac{dS_1}{dt} + (S_2 - S_2^*)\frac{dS_2}{dt} + (S_M - S_M^*)\frac{dS_M}{dt} + (T - T^*)\frac{dT}{dt} + (D - D^*)\frac{dD}{dt} + (K - K^*)\frac{dK}{dt}.$$

$$\leq (\bar{S}_2 - S_2^*)\big[\rho_1(\bar{S}_1 - S_1^*) + \rho_2(\bar{S}_M - S_M^*)\big] + \bar{K}(\bar{K} - K^*)\big[(\delta_1\bar{T} + \delta_2\bar{D})/(1 + \eta S_M^{\min}) - (\delta_1 T^* + \delta_2 D^*)/(1 + \eta S_M^*)\big] + T^*\big[\gamma(\bar{T}D^* + T^*\bar{D}) + \delta_1(\bar{T}K^* + T^*\bar{K}) + \xi(\bar{T}S_M^* + T^*\bar{S}_M)\big] + \delta_2 D^*(\bar{D}K^* + D^*\bar{K}) - T^*\big[\gamma(T^{\min}D^{\min} + T^*D^*) + \delta_1(T^{\min}K^{\min} + T^*K^*) + \xi(T^{\min}S_M^{\min} + T^*S_M^*)\big] - \delta_2 D^*(D^{\min}K^{\min} + D^*K^*).$$

For the sake of simplicity, write

$$W_1 = \bar{S}_1 - S_1^*,\ W_2 = \bar{S}_2 - S_2^*,\ W_3 = \bar{S}_M - S_M^*,\ W_4 = \bar{K} - K^*$$
$$\Omega_1 = \bar{T}D^* + T^*\bar{D},\ \Omega_2 = \bar{T}K^* + T^*\bar{K},\ \Omega_3 = \bar{T}S_M^* + T^*\bar{S}_M,\ \Omega_4 = \bar{T}D^* + T^*\bar{D}$$
$$\Theta_1 = T^{\min}D^{\min} + T^*D^*,\ \Theta_2 = T^{\min}K^{\min} + T^*K^*,\ \Theta_3 = T^{\min}S_M^{\min} + T^*S_M^*,$$
$$\Theta_4 = D^{\min}K^{\min} + D^*K^*\ \Delta = (\delta_1\bar{T} + \delta_2\bar{D})(1 + \eta S_M^{\min})^{-1} - (\delta_1 T^* + \delta_2 D^*)(1 + \eta S_M^*)^{-1}.$$

Therefore, we get

$$\frac{d\mathcal{L}}{dt} \leq \big(R_E - 1\big)\Big[T^*(\gamma\Theta_1 + \delta_1\Theta_2 + \xi\Theta_3) + \delta_2 D^*\Theta_4\Big],$$

$$\text{where } R_E = \frac{W_2(\rho_1 W_1 + \rho_2 W_3) + K^{\max}W_4\Delta + T^*(\gamma\Omega_1 + \delta_1\Omega_2 + \xi\Omega_3) + \delta_2 D^*\Omega_4}{T^*(\gamma\Theta_1 + \delta_1\Theta_2 + \xi\Theta_3) + \delta_2 D^*\Theta_4}.$$

From the aforementioned notions, we create the following lemma.

Lemma 6.4.3 *If $R_E < 1$, then the endemic equilibrium point E^* is globally asymptotically stable.*

6.5 The Model with a Biological Drug

In this section, we analyzed the drug-induced system using an impulsive approach to understand the effects of a biological TNF-α inhibitor, Infliximab, used during the initial phase of treatment.

$$\frac{dS_1(t)}{dt} = \rho_0 - \sigma_1 S_1(t), \quad \frac{dS_2(t)}{dt} = \rho_1 S_1(t) - \sigma_2 S_2(t), \quad \frac{dS_M(t)}{dt} = \rho_2 S_2(t) - \lambda_M S_M(t),$$
$$\frac{dT(t)}{dt} = C_T - \gamma T(t)D(t) - \delta_1\Big(\frac{I_{50}}{I_{50} + I(t)}\Big)T(t)K(t) - \xi T S_M(t) - \lambda_T T(t),$$
$$\frac{dD(t)}{dt} = C_D - \delta_2\Big(\frac{I_{50}}{I_{50} + I(t)}\Big)D(t)K(t) - \lambda_D D(t),$$
$$\frac{dK(t)}{dt} = C_K + \frac{1}{1 + \eta S_M(t)}\left[\delta_1\Big(\frac{I_{50}}{I_{50} + I(t)}\Big)T(t)K(t) + \delta_2\Big(\frac{I_{50}}{I_{50} + I(t)}\Big)D(t)K(t)\right] - \lambda_K K(t). \tag{6.5.1}$$

The Hill function, given by $I_{50}/\big(I_{50}+I(t)\big)$, quantifies the extent to which Infliximab inhibits the activation rates of keratinocytes by T cells and dendritic cells. Parameters δ_1 and δ_2 decrease in response to the action of the drug, reflecting its suppressive effects [95]. Here, I_{50} represents the concentration of Infliximab required to reduce keratinocyte hyperproliferation by 50%. The temporal dynamics of Infliximab concentration, $I(t)$ governed by the following equation:

$$\begin{aligned} &\frac{dI(t)}{dt} = -rI(t) \ \text{ when } \ t \neq t_k \\ &I(t_k^+) = I(t_k^-) + I_c \ \text{ when } \ t = t_k \ \text{ for } \ k = 1, 2, \cdots, n. \end{aligned} \tag{6.5.2}$$

Here, r represents the drug clearance rate. $I(t_k^-)$ and $I(t_k^+)$ denote the concentration of Infliximab just before and after the intake of the k-th dose. I_c is the dosage of Infliximab administered at each impulse time $t = t_k$, for $k = 1, 2, \cdots, n$.

Using impulsive differential equations to assess drug adherence disturbs the internal steady state, leading to periodic solutions in the model that exhibit discontinuities. Clearly, systems (6.5.1) and (6.5.2) indicate that only the drug exhibits direct discontinuities, while the solutions remain continuous. In the absence of the drug (i.e., $I(t) = 0$), the system reduces to (6.3.1). We assume that the drug is administered at fixed time intervals. Let $\vartheta = t_{k+1} - t_k$ represent the period of Infliximab, and, for t satisfying $t_k < t < t_{k+1}$, we have

$$I(t) = I(t_k^+)e^{-r(t-t_k)} \, .$$

The recursion relation at the moment of impulse is given by

$$I(t_k^+) = I(t_k^-) + I_c \, .$$

From this equation, combined with the recursion relation, we obtained

$$I(t_k^+) = I_c\left(\frac{1-e^{-kr\vartheta}}{1-e^{-r\vartheta}}\right) \to \frac{I_c}{1-e^{-r\vartheta}} \ \text{ as } \ k \to \infty.$$

Therefore, we derived the left and right ends of the impulsive periodic orbit as given by

$$\begin{aligned} &I(t_{k+1}^-) = \frac{I_c e^{-r\vartheta}}{1-e^{-r\vartheta}} \quad \text{as} \quad k \to \infty \quad \text{and} \\ &I(t_{k+1}^+) = I(t_{k+1}^-) + I_c = \frac{I_c e^{-r\vartheta}}{1-e^{-r\vartheta}} + I_c = \frac{I_c}{1-e^{-r\vartheta}} \quad \text{as} \quad k \to \infty. \end{aligned}$$

Let I^* be the impulsive periodic orbit of Infliximab, which satisfies,

$$\frac{I_c e^{-r\vartheta}}{1-e^{-r\vartheta}} \leq I^* \leq \frac{I_c}{1-e^{-r\vartheta}}. \tag{6.5.3}$$

In this section, we do not go through the detailed calculations regarding the stability of the periodic orbit. Instead, we illustrate numerically the effects of impulsive drug therapy on system populations.

6.6 Impulsive Stem Cell Transplantation and the Stability of its Period

Stem cells are essential because they can regenerate themselves. In severe cases where drug treatments fail to achieve a complete cure, stem-cell transplantation can offer a solution. In severe psoriasis, where the skin condition is chronic and local stem cells are deficient, stem-cell replacement might be necessary. To fill this deficiency, healthy stem cells are infused intravenously or directly into the patient's affected area. These stem cells have the ability to differentiate and develop into mature stem cells, which aid in the restoration of the immune system's normal function. During the process of maturation, these stem cells produce lots of anti-inflammatory cytokines that reduce inflammation and repair the lesions caused by psoriasis. Clinicians assess therapeutic effects after each administration, with the number of infusions determined by the severity of the disease and the factors of each patient [91]. These repeated infusions introduce time-dependent discontinuities in the system that can be analytically modeled using an impulsive approach.

6.6.1 Dynamics of the Impulsive Model

In impulse stem cell transplantation, we administer a specific amount of healthy stem cells periodically, at a fixed time interval during the treatment course. This approach requires the population to be in an equilibrium state, ensuring that treatment strategies can be effectively implemented without disruption. The system with impulse differential equations for cell treatment is described as:

$$\begin{aligned}
\frac{dS_1(t)}{dt} &= \rho_0 - \sigma_1 S_1(t),\ t \neq n\tau \quad \text{and} \quad S_1(n\tau) = S_1(n\tau)^- + b,\ t = n\tau \\
\frac{dS_2(t)}{dt} &= \rho_1 S_1(t) - \sigma_2 S_2(t), \\
\frac{dS_M(t)}{dt} &= \rho_2 S_2(t) - \lambda_M S_M(t), \\
\frac{dT(t)}{dt} &= C_T - \gamma T(t) D(t) - \delta_1 T(t) K(t) - \xi T(t) S_M(t) - \lambda_T T(t), \\
\frac{dD(t)}{dt} &= C_D - \delta_2 D(t) K(t) - \lambda_D D(t), \\
\frac{dK(t)}{dt} &= C_K + \frac{\delta_1 T(t) K(t) + \delta_2 D(t) K(t)}{1 + \eta S_M(t)} - \lambda_K K(t),
\end{aligned} \tag{6.6.1}$$

where $n\tau \leq t < (n+1)\tau$, $n \in \mathbb{N} \cup \{0\}$ and $\sigma_i = \lambda_i - (2b_i - 1)l_i,\ \rho_i = 2(1 - b_i)l_i\ (i = 1, 2)$. $S_1(n\tau)^-$ is the population value just before $(t = n\tau)$ receiving the next dose of impulse. Using the data from Table 6.1, one can observe that σ_1, σ_2, ρ_1 and ρ_2 are all positive parameters. The populations are governed by the initial condition:

$$S_1(0) > 0,\ S_2(0) > 0,\ S_M(0) > 0,\ T(0) > 0,\ D(0) > 0, \text{ and } K(0) > 0.$$

We examine the above-mentioned model to comprehend the consequences of administering

healthy stem cells from outside. Here, 'b' is the average of all healthy SC infused with n infusions, once per τ-time interval. However, in actual practice, a limited number of infusions are employed where clinicians administer a single dose ranging from $(1-3)\times 10^6/kg$, repeated 2 to 5 times and spaced 7 to 15 days apart, as documented in Cheng et al. [22].

The solution of the first equation of the system (6.6.1) is of the following form

$$S_1(t) = \frac{\rho_0}{\sigma_1} + Ce^{-\sigma_1 t},$$

where C is a constant to be determined using the following initial condition.

For $0 \le t < \tau$, $S_1(0) = b \implies C = \left(b - \frac{\rho_0}{\sigma_1}\right)$. Thus

$$S_1(t) = \frac{\rho_0}{\sigma_1} + \left(b - \frac{\rho_0}{\sigma_1}\right)e^{-\sigma_1 t} \implies S_1(\tau) = S_1(\tau)^- + b = \frac{\rho_0}{\sigma_1} + b(1 + e^{-\sigma_1\tau}) - \frac{\rho_0}{\sigma_1}e^{-\sigma_1\tau}.$$

We analyze system (6.6.1) for each time interval since the initial condition of the stem cell $[S_1(t)]$ population varies with respect to time.

For $\tau \le t < 2\tau$,

$$S_1(\tau) = \frac{\rho_0}{\sigma_1} + b(1 + e^{-\sigma_1\tau}) - \frac{\rho_0}{\sigma_1}e^{-\sigma_1\tau} \implies C = \left[b(1 + e^{-\sigma_1\tau}) - \frac{\rho_0}{\sigma_1}e^{-\sigma_1\tau}\right]e^{\sigma_1\tau}.$$

Thus we have

$$\begin{aligned} S_1(t) &= \frac{\rho_0}{\sigma_1} + \left[b(1 + e^{-\sigma_1\tau}) - \frac{\rho_0}{\sigma_1}e^{-\sigma_1\tau}\right]e^{-\sigma_1(t-\tau)} \\ S_1(2\tau) &= S_1(2\tau)^- + b = \frac{\rho_0}{\sigma_1} + b(1 + e^{-\sigma_1\tau} + e^{-2\sigma_1\tau}) - \frac{\rho_0}{\sigma_1}e^{-2\sigma_1\tau}. \end{aligned}$$

Continuing this process up to n iterations, we get, for $n\tau \le t < (n+1)\tau$,

$$\begin{aligned} S_1(n\tau) &= \frac{\rho_0}{\sigma_1} + b(1 + e^{-\sigma_1\tau} + e^{-2\sigma_1\tau} + \ldots\ldots + e^{-n\sigma_1\tau}) - \frac{\rho_0}{\sigma_1}e^{-n\sigma_1\tau} \\ \implies C &= \left[b(1 + e^{-\sigma_1\tau} + e^{-2\sigma_1\tau} + \ldots\ldots + e^{-n\sigma_1\tau}) - \frac{\rho_0}{\sigma_1}e^{-n\sigma_1\tau}\right]e^{\sigma_1\tau}. \end{aligned}$$

The concentration of infused stem cell $[S_1(t)]$ after n-th infusion is

$$\begin{aligned} S_1(t) &= \frac{\rho_0}{\sigma_1} + \left[b(1 + e^{-\sigma_1\tau} + e^{-2\sigma_1\tau} + \ldots\ldots + e^{-n\sigma_1\tau}) - \frac{\rho_0}{\sigma_1}e^{-n\sigma_1\tau}\right]e^{-\sigma_1(t-n\tau)} \\ &= \frac{\rho_0}{\sigma_1} + \left[b\left(\frac{1 - e^{-(n+1)\sigma_1\tau}}{1 - e^{-\sigma_1\tau}}\right) - \frac{\rho_0}{\sigma_1}e^{-n\sigma_1\tau}\right]e^{-\sigma_1(t-n\tau)}. \end{aligned} \tag{6.6.2}$$

Observe that the endpoints of each cycle rise monotonically. The events immediately before and after the end of a positive impulsive periodic orbit involving infused stem cells are

described by the following:

$$S_1(n\tau)^- = \frac{\rho_0}{\sigma_1} + be^{-\sigma_1\tau}\left(\frac{1-e^{-n\sigma_1\tau}}{1-e^{-\sigma_1\tau}}\right) - \frac{\rho_0}{\sigma_1}e^{-n\sigma_1\tau} \implies \lim_{n\to\infty} S_1(n\tau)^- = \frac{\rho_0}{\sigma_1} + \frac{be^{-\sigma_1\tau}}{1-e^{-\sigma_1\tau}}.$$
$$S_1(n\tau)^+ = \frac{\rho_0}{\sigma_1} + b\left(\frac{1-e^{-(n+1)\sigma_1\tau}}{1-e^{-\sigma_1\tau}}\right) - \frac{\rho_0}{\sigma_1}e^{-n\sigma_1\tau} \implies \lim_{n\to\infty} S_1(n\tau)^+ = \frac{\rho_0}{\sigma_1} + \frac{b}{1-e^{-\sigma_1\tau}}.$$

The concentration of $S_1(t)$ at the ends of a positive impulsive periodic orbit therefore fall within the points of impulse [57].

$$\frac{\rho_0}{\sigma_1} + \frac{be^{-\sigma_1\tau}}{1-e^{-\sigma_1\tau}} \leq \tilde{S_1}^* \leq \frac{\rho_0}{\sigma_1} + \frac{b}{1-e^{-\sigma_1\tau}}.$$

6.6.2 Stability of the Equilibrium-Like Periodic Orbit

The impulsive effect of the population $S_1(t)$ will influence the other populations of system (6.6.1) as well, leading to the appearance of periodic orbits in those populations. The periodic orbit is of the form $\bar{E}^*\left[\tilde{S_1}^*, \tilde{S_2}^*, \tilde{S_M}^*, \tilde{T}^*, \tilde{D}^*, \tilde{K}^*\right]$. The values of $\tilde{S_2}^*, \tilde{S_M}^*, \tilde{T}^*, \tilde{D}^*$ and $\tilde{K}^*$ are easily determined, replacing S_1^* by $\tilde{S_1}^*$ and using the existence conditions of the endemic equilibrium point. Due to the impulse-driven periodicity of $S_1(t)$, the trajectories can be either steady or exhibit a vibration. To figure out the asymptotic expansion of the solutions and examine how they behave, we aim to apply Floquet's theory utilizing a one-dimensional perturbation to the system populations.

$$\begin{aligned}
S_1(t) &= \mathcal{S}_1^0 + \varepsilon\mathcal{S}_1^1(t) + \varepsilon^2\mathcal{S}_1^2(t) + \cdots & S_2(t) &= \mathcal{S}_2^0 + \varepsilon\mathcal{S}_2^1(t) + \varepsilon^2\mathcal{S}_2^2(t) + \cdots \\
S_M(t) &= \mathcal{S}_M^0 + \varepsilon\mathcal{S}_M^1(t) + \varepsilon^2\mathcal{S}_M^2(t) + \cdots & T(t) &= \mathcal{T}^0 + \varepsilon\mathcal{T}^1(t) + \varepsilon^2\mathcal{T}^2(t) + \cdots \\
D(t) &= \mathcal{D}^0 + \varepsilon\mathcal{D}^1(t) + \varepsilon^2\mathcal{D}^2(t) + \cdots & K(t) &= \mathcal{K}^0 + \varepsilon\mathcal{K}^1(t) + \varepsilon^2\mathcal{K}^2(t) + \cdots
\end{aligned}$$

Here $\varepsilon \ll 1$ and $\mathcal{S}_1^0 = \tilde{S_1}^*, \mathcal{S}_2^0 = \tilde{S_2}^*, \mathcal{S}_M^0 = \tilde{S_M}^*, \mathcal{T}^0 = \tilde{T}^*, \mathcal{D}^0 = \tilde{D}^*, \mathcal{K}^0 = \tilde{K}^*$. Substituting these into system (6.6.1) and taking only the first-order terms of ε, we have another system as follows

$$\begin{aligned}
\frac{d\mathcal{S}_1^1}{dt} &= -\sigma_1\mathcal{S}_1^1, & \frac{d\mathcal{S}_2^1}{dt} &= \rho_1\mathcal{S}_1^1 - \sigma_2\mathcal{S}_2^1, \\
\frac{d\mathcal{S}_M^1}{dt} &= \rho_2\mathcal{S}_2^1 - \lambda_M\mathcal{S}_M^1, & \frac{d\mathcal{T}^1}{dt} &= -\gamma\tilde{T}^*\mathcal{D}^1 - \delta_1\tilde{T}^*\mathcal{K}^1 - \xi\tilde{T}^*\mathcal{S}_M^1 - P_0\mathcal{T}^1, \\
\frac{d\mathcal{D}^1}{dt} &= -\delta_2\tilde{D}^*\mathcal{K}^1 - P_1\mathcal{D}^1, & \frac{d\mathcal{K}^1}{dt} &= P_2\mathcal{S}_M^1 + P_3\mathcal{T}^1 + P_4\mathcal{D}^1 + P_5\mathcal{K}^1,
\end{aligned} \tag{6.6.3}$$

where
$$\begin{aligned}
P_0 &= \gamma\tilde{D}^* + \delta_1\tilde{K}^* + \xi\tilde{S_M}^* + \lambda_T, & P_1 &= \delta_2\tilde{K}^* + \lambda_D, \\
P_2 &= \eta\left(C_K - \lambda_K\tilde{S_M}^*\right)/\left(1+\eta\tilde{S_M}^*\right), & P_3 &= \delta_1\tilde{K}^*/\left(1+\eta\tilde{S_M}^*\right), \\
P_4 &= \delta_2\tilde{K}^*/\left(1+\eta\tilde{S_M}^*\right), & P_5 &= \left(\delta_1\tilde{T}^* + \delta_2\tilde{D}^*\right)/\left(1+\eta\tilde{S_M}^*\right) - \lambda_K.
\end{aligned}$$

We rewrite system (6.6.3) in matrix form

$$\frac{d}{dt}\begin{pmatrix}\mathcal{S}_1^1\\ \mathcal{S}_2^1\\ \mathcal{S}_M^1\\ \mathcal{T}^1\\ \mathcal{D}^1\\ \mathcal{K}^1\end{pmatrix}=\begin{pmatrix}-\sigma_1 & 0 & 0 & 0 & 0 & 0\\ \rho_1 & -\sigma_2 & 0 & 0 & 0 & 0\\ 0 & \rho_2 & -\lambda_M & 0 & 0 & 0\\ 0 & 0 & -\xi\tilde{T}^* & -P_0 & -\gamma\tilde{T}^* & -\delta_1\tilde{T}^*\\ 0 & 0 & 0 & 0 & -P_1 & -\delta_2\tilde{D}^*\\ 0 & 0 & P_2 & P_3 & P_4 & P_5\end{pmatrix}\begin{pmatrix}\mathcal{S}_1^1\\ \mathcal{S}_2^1\\ \mathcal{S}_M^1\\ \mathcal{T}^1\\ \mathcal{D}^1\\ \mathcal{K}^1\end{pmatrix}. \tag{6.6.4}$$

The coefficient matrix is decomposed into the following block matrices

$$\mathcal{A}_1=\begin{pmatrix}-\sigma_1 & 0 & 0\\ \rho_1 & -\sigma_2 & 0\\ 0 & \rho_2 & -\lambda_M\end{pmatrix},\qquad \mathcal{A}_2=\begin{pmatrix}0 & 0 & -\xi\tilde{T}^*\\ 0 & 0 & 0\\ 0 & 0 & P_2\end{pmatrix},$$
$$\mathcal{A}_3=\begin{pmatrix}-P_0 & -\gamma\tilde{T}^* & -\delta_1\tilde{T}^*\\ 0 & -P_1 & -\delta_2\tilde{D}^*\\ P_3 & P_4 & P_5\end{pmatrix},\qquad \mathcal{O}=\begin{pmatrix}0 & 0 & 0\\ 0 & 0 & 0\\ 0 & 0 & 0\end{pmatrix}.$$

The eigenvalues of $\mathcal{A}_1$ are $-\sigma_1$, $-\sigma_2$ and $-\lambda_M$. We cannot easily determine the eigenvalues of $\mathcal{A}_3$. With three distinct real eigenvalues ς_1, ς_2 and ς_3 (if they exist), it satisfies the following equation:

$$(\varsigma_i+P_0)\Big\{(\varsigma_i+P_1)(P_5-\varsigma_i)-P_4\delta_2\tilde{D}^*\Big\}+P_3\Big\{\gamma\delta_2T^*\tilde{D}^*-\delta_1\tilde{T}^*(\varsigma_i+P_1)\Big\}=0,\ \forall i=1,2,3.$$

We now compute the eigenvectors corresponding to all eigenvalues of the coefficient matrix $\mathcal{A}$. For the eigenvalue $-\sigma_1$, the eigenvectors are in the form $[1\ V_{21}\ V_{31}\ V_{41}\ V_{51}\ V_{61}]^T$. The eigenvectors corresponding to the eigenvalues $-\sigma_2$ and $-\lambda_M$ are given by $[0\ 1\ V_{32}\ V_{42}\ V_{52}\ V_{62}]^T$ and $[0\ 0\ 1\ V_{43}\ V_{53}\ V_{63}]^T$, respectively. Furthermore, the eigenvectors corresponding to the eigenvalues ς_1, ς_2 and ς_3 are of the form of $[0\ 0\ 0\ 1\ V_{54}\ V_{64}]^T$, $[0\ 0\ 0\ 1\ V_{55}\ V_{65}]^T$ and $[0\ 0\ 0\ 1\ V_{56}\ V_{66}]^T$, respectively. Due to the vastness of V_{ij}'s values, we will not mention them here. The solutions of system (6.6.3) are given by:

$$\begin{aligned}
\mathcal{S}_1^1(t)&=c_1e^{-\sigma_1t}+c_2V_{12}e^{-\sigma_2t}+c_3V_{13}e^{-\lambda_Mt}+c_4V_{14}e^{\varsigma_1t}+c_5V_{15}e^{\varsigma_2t}+c_6V_{16}e^{\varsigma_3t},\\
\mathcal{S}_2^1(t)&=c_2e^{-\sigma_2t}+c_3V_{23}e^{-\lambda_Mt}+c_4V_{24}e^{\varsigma_1t}+c_5V_{25}e^{\varsigma_2t}+c_6V_{26}e^{\varsigma_3t},\\
\mathcal{S}_M^1(t)&=c_3e^{-\lambda_Mt}+c_4V_{34}e^{\varsigma_1t}+c_5V_{35}e^{\varsigma_2t}+c_6V_{36}e^{\varsigma_3t},\\
\mathcal{T}^1(t)&=c_4e^{\varsigma_1t}+c_5V_{45}e^{\varsigma_2t}+c_6V_{46}e^{\varsigma_3t},\\
\mathcal{D}^1(t)&=c_4e^{\varsigma_1t}+c_5V_{55}e^{\varsigma_2t}+c_6V_{56}e^{\varsigma_3t},\\
\mathcal{K}^1(t)&=c_4e^{\varsigma_1t}+c_5V_{65}e^{\varsigma_2t}+c_6V_{66}e^{\varsigma_3t}.
\end{aligned} \tag{6.6.5}$$

where the c_i's $(i=1,2,\ldots,6)$ are arbitrary constants.

The stability of the derived solutions (6.6.5) will be examined using the Floquet's theory [96]. The fundamental matrix is constructed by imposing the identity matrix of order six (I_6) as an initial condition. Solving system (6.6.3) and using the first column of (I_6) as the initial condition, the first column of the fundamental matrix can be derived. Again,

solving system (6.6.3) with the second column of I_6 as the initial condition, we derive the second column of the fundamental matrix. Proceeding in this manner, we have been able to determine the columns of the fundamental matrix. Further, we determined the monodromy matrix by utilizing the period $t = \tau$, given by

$$\mathcal{R}(\tau, I_6) = \begin{pmatrix} e^{-\sigma_1\tau} & 0 & 0 & 0 & 0 & 0 \\ \mathcal{M}_{21} & e^{-\sigma_2\tau} & 0 & 0 & 0 & 0 \\ \mathcal{M}_{31} & \mathcal{M}_{32} & e^{-\lambda_M\tau} & 0 & 0 & 0 \\ \mathcal{M}_{41} & \mathcal{M}_{42} & \mathcal{M}_{43} & \mathcal{M}_{44} & \mathcal{M}_{45} & \mathcal{M}_{46} \\ \mathcal{M}_{51} & \mathcal{M}_{52} & \mathcal{M}_{53} & \mathcal{M}_{54} & \mathcal{M}_{55} & \mathcal{M}_{56} \\ \mathcal{M}_{61} & \mathcal{M}_{62} & \mathcal{M}_{63} & \mathcal{M}_{64} & \mathcal{M}_{65} & \mathcal{M}_{66} \end{pmatrix}.$$

The values of $\mathcal{M}_{ij}$'s are described follows. However, we spare the details of s_{ij}'s values due to their complexity.

$$\begin{aligned}
\mathcal{M}_{21} &= V_{21}\big(e^{-\sigma_1\tau} - e^{-\sigma_2\tau}\big),\\
\mathcal{M}_{31} &= V_{31}e^{-\sigma_1\tau} - V_{21}V_{32}e^{-\sigma_2\tau} + s_{13}e^{-\lambda_M\tau},\\
\mathcal{M}_{32} &= V_{32}\big(e^{-\sigma_2\tau} - e^{-\lambda_M\tau}\big),\\
\mathcal{M}_{41} &= V_{41}e^{-\sigma_1\tau} - V_{21}V_{42}e^{-\sigma_2\tau} + s_{13}V_{43}e^{-\lambda_M\tau} + s_{14}e^{\varsigma_1\tau} + s_{15}e^{\varsigma_2\tau} + s_{16}e^{\varsigma_3\tau},\\
\mathcal{M}_{42} &= V_{42}e^{-\sigma_2\tau} - V_{32}V_{43}e^{-\lambda_M\tau} + s_{24}e^{\varsigma_1\tau} + s_{25}e^{\varsigma_2\tau} + s_{26}e^{\varsigma_3\tau},\\
\mathcal{M}_{43} &= V_{43}e^{-\lambda_M\tau} + s_{34}e^{\varsigma_1\tau} + s_{35}e^{\varsigma_2\tau} + s_{36}e^{\varsigma_3\tau},\\
\mathcal{M}_{44} &= s_{44}e^{\varsigma_1\tau} + s_{45}e^{\varsigma_2\tau} + s_{46}e^{\varsigma_3\tau},\\
\mathcal{M}_{45} &= s_{54}e^{\varsigma_1\tau} + s_{55}e^{\varsigma_2\tau} + s_{56}e^{\varsigma_3\tau},\\
\mathcal{M}_{46} &= s_{64}e^{\varsigma_1\tau} + s_{65}e^{\varsigma_2\tau} + s_{66}e^{\varsigma_3\tau},\\
\mathcal{M}_{51} &= V_{51}e^{-\sigma_1\tau} - V_{21}V_{52}e^{-\sigma_2\tau} + s_{13}V_{53}e^{-\lambda_M\tau} + s_{14}V_{54}e^{\varsigma_1\tau} + s_{15}V_{55}e^{\varsigma_2\tau} + s_{16}V_{56}e^{\varsigma_3\tau},\\
\mathcal{M}_{52} &= V_{52}e^{-\sigma_2\tau} - V_{32}V_{53}e^{-\lambda_M\tau} + s_{24}V_{54}e^{\varsigma_1\tau} + s_{25}V_{55}e^{\varsigma_2\tau} + s_{26}V_{56}e^{\varsigma_3\tau},\\
\mathcal{M}_{53} &= V_{53}e^{-\lambda_M\tau} + s_{34}V_{54}e^{\varsigma_1\tau} + s_{35}V_{55}e^{\varsigma_2\tau} + s_{36}V_{56}e^{\varsigma_3\tau},\\
\mathcal{M}_{54} &= s_{44}V_{54}e^{\varsigma_1\tau} + s_{45}V_{55}e^{\varsigma_2\tau} + s_{46}V_{56}e^{\varsigma_3\tau},\\
\mathcal{M}_{55} &= s_{54}V_{54}e^{\varsigma_1\tau} + s_{55}V_{55}e^{\varsigma_2\tau} + s_{56}V_{56}e^{\varsigma_3\tau},\\
\mathcal{M}_{56} &= s_{64}V_{54}e^{\varsigma_1\tau} + s_{65}V_{55}e^{\varsigma_2\tau} + s_{66}V_{56}e^{\varsigma_3\tau},\\
\mathcal{M}_{61} &= V_{61}e^{-\sigma_1\tau} - V_{21}V_{62}e^{-\sigma_2\tau} + s_{13}V_{63}e^{-\lambda_M\tau} + s_{14}V_{64}e^{\varsigma_1\tau} + s_{15}V_{65}e^{\varsigma_2\tau} + s_{16}V_{66}e^{\varsigma_3\tau},\\
\mathcal{M}_{62} &= V_{62}e^{-\sigma_2\tau} - V_{32}V_{63}e^{-\lambda_M\tau} + s_{24}V_{64}e^{\varsigma_1\tau} + s_{25}V_{65}e^{\varsigma_2\tau} + s_{26}V_{66}e^{\varsigma_3\tau},\\
\mathcal{M}_{63} &= V_{63}e^{-\lambda_M\tau} + s_{34}V_{64}e^{\varsigma_1\tau} + s_{35}V_{65}e^{\varsigma_2\tau} + s_{36}V_{66}e^{\varsigma_3\tau},\\
\mathcal{M}_{64} &= s_{44}V_{64}e^{\varsigma_1\tau} + s_{45}V_{65}e^{\varsigma_2\tau} + s_{46}V_{66}e^{\varsigma_3\tau},\\
\mathcal{M}_{65} &= s_{54}V_{64}e^{\varsigma_1\tau} + s_{55}V_{65}e^{\varsigma_2\tau} + s_{56}V_{66}e^{\varsigma_3\tau},\\
\mathcal{M}_{66} &= s_{64}V_{64}e^{\varsigma_1\tau} + s_{65}V_{65}e^{\varsigma_2\tau} + s_{66}V_{66}e^{\varsigma_3\tau}.
\end{aligned}$$

According to Floquet's theory, a periodic orbit is stable if all the eigenvalues of the monodromy matrix have absolute values less than one. To calculate the Floquet multipliers, we need to find the eigenvalues of the matrix $\mathcal{R}(\tau, I_6)$. These eigenvalues are the same as

those of two block matrices, $\mathcal{R}_1$ and $\mathcal{R}_2$. They can be obtained directly by dividing the matrix $\mathcal{R}(\tau, I_6)$ into the following block matrices:

$$\mathcal{R}_1 = \begin{pmatrix} e^{-\sigma_1\tau} & 0 & 0 \\ \mathcal{M}_{21} & e^{-\sigma_2\tau} & 0 \\ \mathcal{M}_{31} & \mathcal{M}_{32} & e^{-\lambda_M\tau} \end{pmatrix} \quad \text{and} \quad \mathcal{R}_2 = \begin{pmatrix} \mathcal{M}_{44} & \mathcal{M}_{45} & \mathcal{M}_{46} \\ \mathcal{M}_{54} & \mathcal{M}_{55} & \mathcal{M}_{56} \\ \mathcal{M}_{64} & \mathcal{M}_{65} & \mathcal{M}_{66} \end{pmatrix}.$$

The eigenvalues of the matrix $\mathcal{R}_1$ are $e^{-\sigma_1\tau}$, $e^{-\sigma_2\tau}$ and $e^{-\lambda_M\tau}$ such that $\mid e^{-\sigma_1\tau} \mid < 1$, $\mid e^{-\sigma_2\tau} \mid < 1$ and $\mid e^{-\lambda_M\tau} \mid < 1$. Therefore the stability of the periodic orbit of system (6.6.1) depends on the eigenvalues of the matrix $\mathcal{R}_2$. According to Lutkepohl[97], the following theorem ensures the stability of the periodic orbit.

Theorem 6.6.1 *The periodic orbit $\bar{E}^*$ of system (6.6.1) is stable if $det(I_3 - z\mathcal{R}_2) \neq 0$ for $|z| \leq 1$.*

Significance of the Periodic Behavior
Floquet theory is employed to predict the long-term periodic behavior of the system by analyzing the stability of equilibrium-like periodic orbits, denoted as $\bar{E}^*\left[\tilde{S_1}^*, \tilde{S_2}^*, \tilde{S_M}^*, \tilde{T}^*, \tilde{D}^*, \tilde{K}^*\right]$. By evaluating the Floquet multipliers of the monodromy matrix, this approach determines whether $\bar{E}^*$ remains stable, thereby indicating the effectiveness of stem cell therapy in controlling psoriasis. Conversely, if $\bar{E}^*$ is found to be unstable, this suggests that adjustments to the dosage amount and dosing interval of stem cell replacement therapy are necessary to achieve therapeutic control over psoriasis.

6.7 Numerical Simulations

In this section, we performed numerical simulations for our formulated model based on our analytical results. The initial values we have chosen for the model variables satisfy the basic criteria of the analytical approaches during the investigation. For these numerical simulations, we have utilized the parameter values shown in Table 6.1.

In Figure 6.2, we plotted system (6.3.1) with respect to time, which shows the behaviour of each cell population during the progression of the disease. This figure clearly demonstrates that the concentrations of SCs, differentiated SCs and MSCs largely decrease over time. However, the concentration of T cells, dendritic cells and keratinocytes is significantly high.

In Figure 6.3, we plotted the phase portraits of system (6.3.1) by taking a set of initial conditions. This figure depicts that the trajectories of all model variables ($S_1(t)$, $S_2(t)$, $S_M(t)$, $T(t)$, $D(t)$ and $K(t)$) are bounded and ultimately converge. This figure validated our analytical computation of the global stability of the endemic equilibrium point E^*.

In Figure 6.4, we simulated two different 3D phase portraits of system (6.3.1) variables using three distinct initial conditions and taking three populations at a time. Here we have determined the endemic equilibrium point E^*(1.28, 1.04, 0.74, 86.5, 53.5, 223.8) numerically by considering two groups: in Figure 6.4(a), we identified the equilibrium $E_1^*(S_1^*, S_2^*, S_M^*)$=(1.28, 1.04, 0.74), and in Figure 6.4(b), we identified the equilibrium $E_2^*(T^*, D^*, K^*)$=(86.5, 53.5, 223.8). In both of these figures, the trajectories from different initial conditions converge to a unique point.

Parameter	Definition	Value (day^{-1})	Reference
ρ_0	Constant production of stem cells	0.1	[41]
b_1	Self renewal percentage of S_1 cells	0.55	[98]
b_2	Self renewal percentage of S_2 cells	0.35	[90]
l_1	Proliferation rate of S_1 cells	0.47	[93]
l_2	Proliferation rate of S_2 cells	0.60	[90]
λ_1	Death rate of S_1 cells	0.125	[99]
λ_2	Death rate of S_2 cells	0.343	[93]
λ_M	Death rate of matured stem cells S_M	1.1	[100]
C_T	Constant accumulation of T cells	15 mm^{-3}	[66]
C_D	Constant accumulation of Dendritic cells	20 mm^{-3}	[52]
C_K	Continuous self-proliferation of keratinocyte	30 mm^{-3}	[53]
γ	Stimulation of T cells via DCs	0.001	[66]
δ_1	Activation rate of keratinocytes via T cells	0.0002	[54]
δ_2	Activation rate of keratinocytes via DCs	0.001	sample
ξ	Inhibition rate of T cell hyperactivity through MSCs	0.007	sample
η	Inhibition rate of KCs overproduction through MSCs	0.1	sample
λ_T	Natural mortality of T cells	0.07	[53]
λ_D	Natural mortality of DCs	0.15	[66]
λ_K	Natural mortality of keratinocytes	0.2	[54]
r	The clearance rate of Infliximab	0.25	[53]

Table 6.1: The values of the system parameters used in numerical simulations.

In Figure 6.5, we provide a comprehensive illustration of three distinct phases.

1. In first phase, the red trajectories represent untreated system populations, with significantly low concentrations of stem cells, their differentiated progenies and MSCs in the affected region, with considerably high levels of T cells and keratinocytes. We set a threshold concentration of $\tilde{K}(= 200\ \text{mm}^{-3})$, where values below this threshold indicate a healthy state, and values above indicate a psoriatic state.

2. The second phase begins after 80 days, as indicated by the cyan trajectories. In this phase, we have shown numerically the effect of treatment with Infliximab, given in eight weekly doses of 5 mg/kg. This treatment slightly reduces keratinocyte levels but increases T cell concentrations, suggesting incomplete recovery and the possibility of disease to re-occur, as the functional stem-cell count in the affected area remains low, similar to the psoriatic state. Note that we have employed $I_{50} = 0.01$ for numerical simulations.

3. After 140 days, we introduce an impulsive stem-cell-replacement strategy, shown by

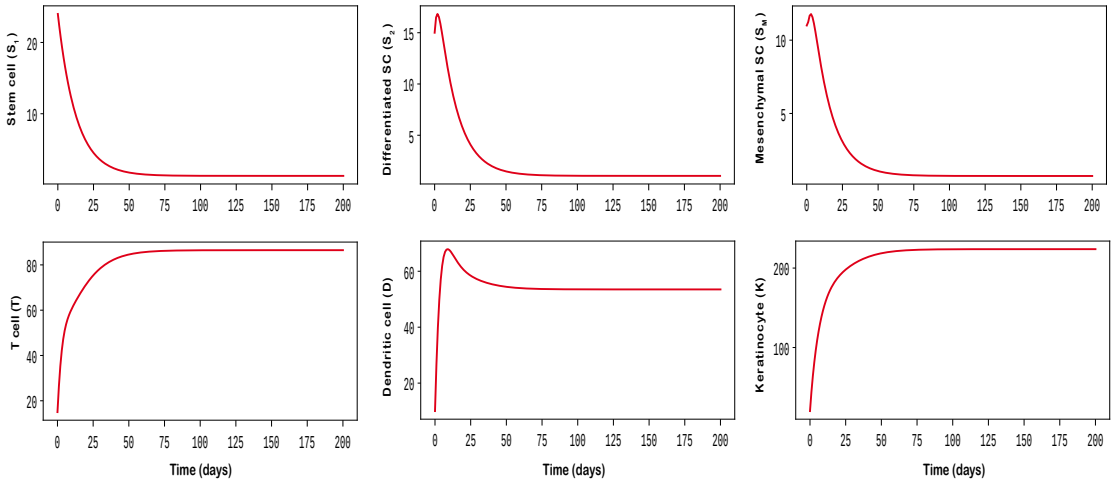

Figure 6.2: The time plot of system (6.3.1) demonstrates the qualitative behaviour of all cell populations during the progression of the disease. Parameter values are given in Table 6.1.

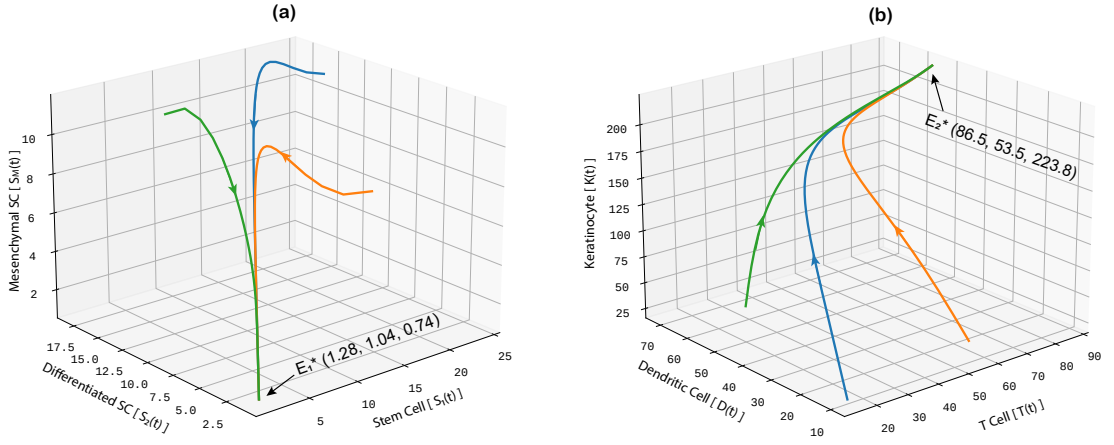

Figure 6.3: 3D plots of three populations showing the endemic equilibrium $E^*(S_1^*, S_2^*, S_M^*, T^*, D^*, K^*) = (1.28, 1.04, 0.74, 86.5, 53.5, 223.8)$*, grouped as (a) stem cells, differentiated stem cells, and mesenchymal stem cells* $E_1^* = (1.28, 1.04, 0.74)$*, and (b) T cells, dendritic cells, and keratinocytes* $E_2^* = (86.5, 53.5, 223.8)$*, using three different initial conditions.*

the soft green coloured trajectories in the third phase. This involves administering a fixed amount of 6 cells/mm^3 of healthy stem cells from an external source, with six infusions given at 10-day intervals. Numerical simulations of this strategy show

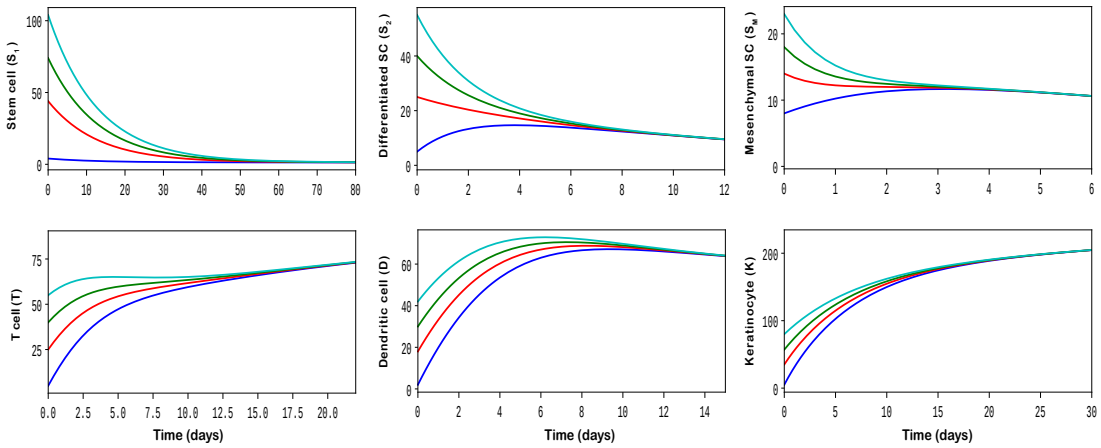

Figure 6.4: Each population of the untreated system is plotted with respect to time by taking Table 6.1 parameter values for four distinct initial conditions. This simulation shows that each population of the system (6.3.1) is bounded and converges to a fixed point.

promising results, with a significant decrease in T-cell counts and keratinocyte density returning to a healthy state within two months of the treatment phase.

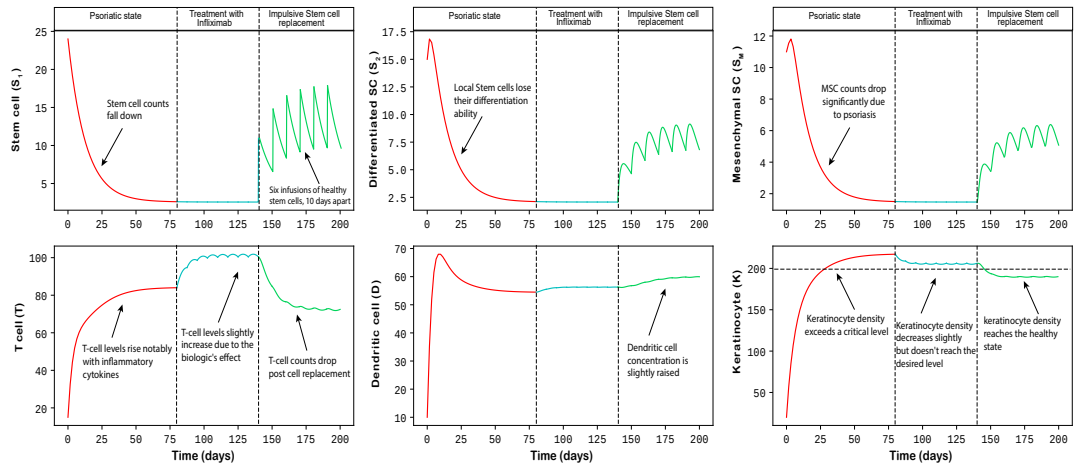

Figure 6.5: This figure shows three different phases. The red trajectories represent the populations of untreated systems in a psoriatic state. The cyan trajectories show the effects of treatment with Infliximab, given 8 infusions of 5 mg/kg weekly. The green trajectories depict the effects of stem cell transplantation, with six impulsive infusions given at 10-day intervals.

In Figure 6.6, we compare the effects of two treatments: Infliximab and healthy stem-cell transplantation, administered impulsively.

1. Figure 6.6(a) shows how different doses of Infliximab affect the keratinocyte population for our formulated system. The red trajectory shows the density of keratinocytes without treatment. The cyan, dark green and blue lines depict the effects of impulses using different doses ($I_c = 0.005, 0.01, 0.05$) of Infliximab, with 14 infusions administered weekly. The treatment with this drug causes a slight decrease in keratinocyte density, but it does not bring the levels below the healthy threshold level $\tilde{K}$.

2. Figure 6.6(b) illustrates the effects of impulsive healthy stem-cell transplantation on keratinocyte regulation. Prior to treatment, stem cell counts were low, while keratinocyte concentrations remained elevated at approximately 230 mm^{-3} (depicted by the red trajectories). After 80 days, a cell-replacement strategy was implemented, administering stem cell doses of 2, 4, 6, and 8 cells/mm^3, as indicated by the yellow, soft green, violet, and magenta trajectories respectively. These doses were delivered six times at intervals of 10 days. The results indicate that increasing the number of healthy stem cells led to a gradual reduction in keratinocyte density. A dosage of 6 cells/mm^3 effectively restored keratinocyte levels to a physiologically normal range (below $\tilde{K}$). However, at higher infusion doses, particularly 8 cells/mm^3, the system exhibited oscillatory behavior, suggesting a destabilizing effect of excessive stem cell administration. This finding underscores the importance of optimizing both dosage and frequency to achieve therapeutic efficacy. Biologically, these results highlight the delicate balance required in stem cell therapy for psoriasis.

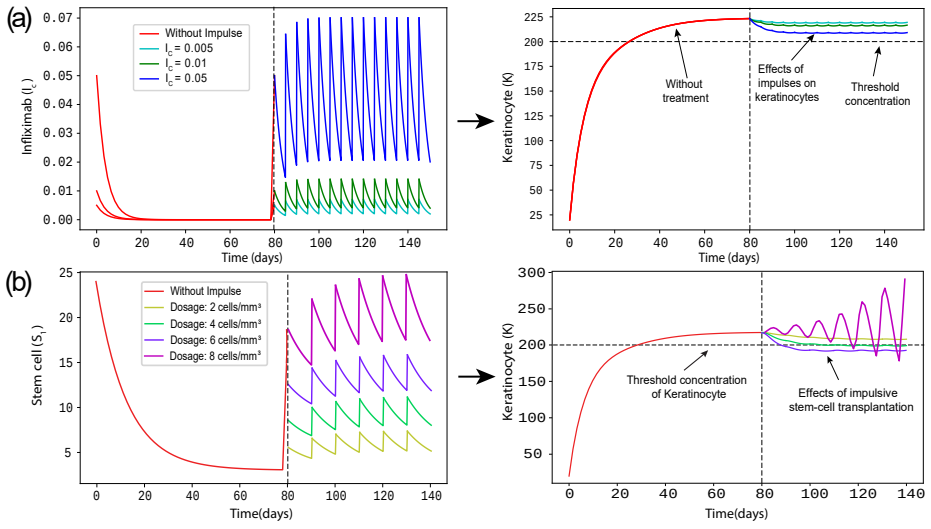

Figure 6.6: This figure compares impulsive treatments with Infliximab and stem-cell transplantation. Sub-figure (a) shows keratinocyte dynamics under varying Infliximab doses. In sub-figure (b), red lines denote untreated populations up to day 80, after which coloured trajectories illustrate stem-cell replacement with different doses.

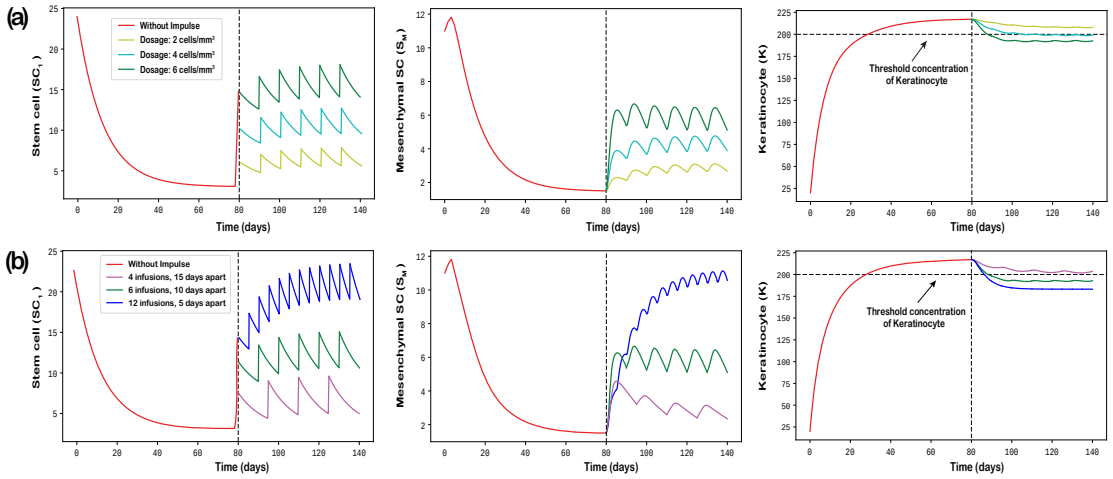

Figure 6.7: The effects of impulses for three populations: stem cells ($S_1(t)$), mesenchymal stem cells ($S_M(t)$) and keratinocytes ($K(t)$). In sub-figure (a), we vary the amounts with fixed repetitions and time intervals. In sub-figure (b), we vary the number of infusions and the intervals with a fixed amount of healthy stem cells.

Further, focusing solely on impulsive stem-cell-replacement strategies and simulating the effects for three system populations: stem cells ($S_1(t)$), mesenchymal stem cells ($S_M(t)$) and keratinocytes ($K(t)$). In both sub-figures, the impulsive effects are shown after 80 days. Before that, the red trajectories indicate the population densities in a psoriatic state without any treatment.

1. In Figure 6.7(a), we simulated the effect of different amounts of stem cells given at fixed intervals and repetitions (six doses, each 10 days apart). The yellow, cyan and dark green trajectories represent these different doses. We observe that as the dose amounts increase, the high keratinocyte density gradually decreases and reaches a healthy level (i.e., below the threshold concentration $\tilde{K}$).

2. In Figure 6.7(b), we perform the numerical simulation by varying the number of infusions and the intervals between two consecutive infusions, while keeping the dose amount and total treatment span fixed (6 cells/mm^3 for each infusion). These impulsive effects are shown by the magenta, dark green and blue trajectories. We observe that increasing the number of infusions with shorter intervals helps keratinocyte levels quickly reach the desired density.

Figure 6.8 presents a global sensitivity analysis of all system parameters using Latin Hypercube Sampling (LHS) in conjunction with the Partial Rank Correlation Coefficients (PRCC) method, with a focus on the keratinocyte population. PRCC values and corresponding p-values are evaluated for key parameters, where the p-value quantifies the level of uncertainty associated with the PRCC estimate. A p-value < 0.05 indicates statistical significance, confirming the parameter's impact on disease dynamics. The scatter plot reveals

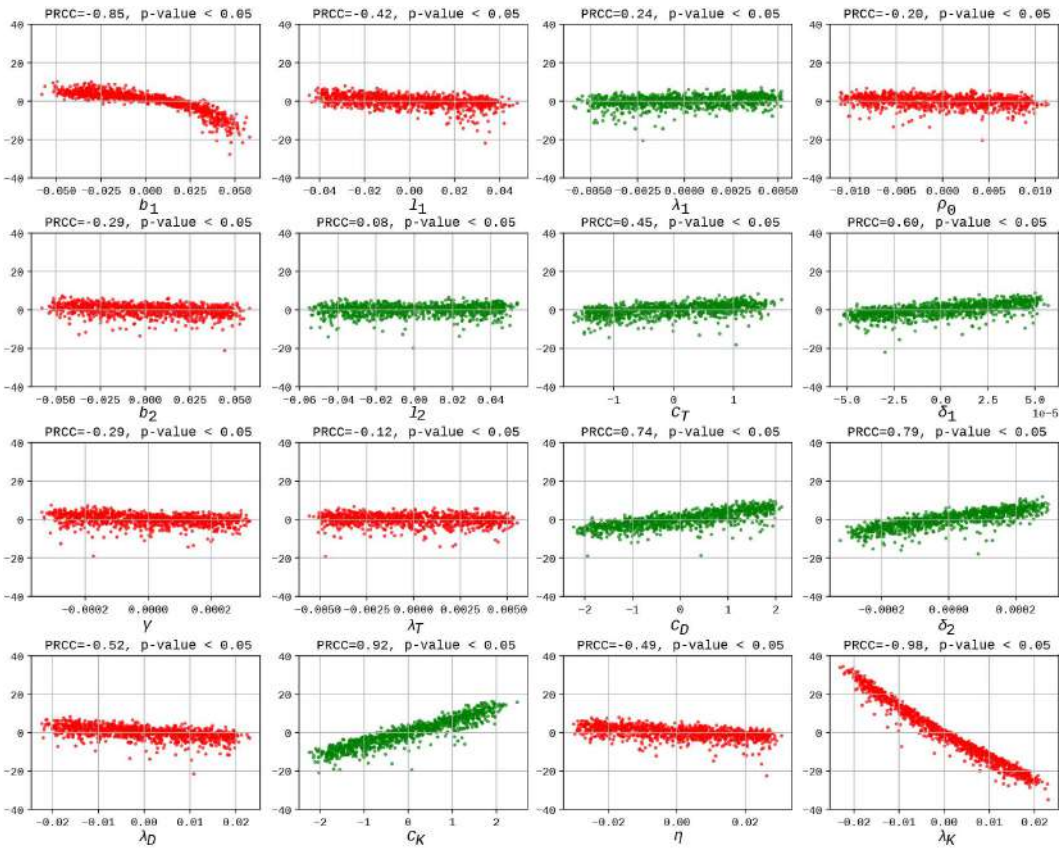

Figure 6.8: Scatter plots showing the relationship between key parameters and the keratinocyte population for $N = 1000$ samples. PRCC values are computed at 100 days with p-values reported to four decimals. The axes show residuals from regressions of rank-transformed parameters and keratinocyte population, highlighting the sensitivity of keratinocyte dynamics to parameter variations.

that parameters $\lambda_1, l_2, C_T, \delta_1, C_D, \delta_2, C_K$ positively influence disease progression, while parameters $b_1, l_1, \rho_0, b_2, \gamma, \lambda_T, \lambda_D, \eta, \lambda_K$ exhibit a negative influence. In this study, we consider keratinocyte levels as a marker for disease progression. The comprehensive sensitivity analysis provides critical insights into identifying optimal intervention points for psoriatic disease management, aiding in the refinement of therapeutic strategies.

6.8 Discussion and Conclusion

In this *Chapter*, we formulate an ODE-based model that includes immune cells (T cells and dendritic cells), keratinocytes, and two types of stem cells (embryonic stem cells and mesenchymal stem cells). We described how stem cells mature into MSCs and how MSCs can control overactive T cells and reduce the proliferative growth of keratinocytes. Using impulsive differential equations, we applied Floquet theory to show that stem-cell transplantation

can create stable periodic solutions. We also did numerical simulations to compare the effects of stem-cell therapy and the biologic Infliximab (a TNF-α inhibitor). The results showed that increasing the drug dose can reduce keratinocyte levels but cannot fully bring the system to a healthy state in severe psoriasis. On the other hand, stem-cell therapy was more effective, and we found that giving 6 cells/mm^3 in six infusions at 10-day intervals can control keratinocyte growth and bring the system to a healthy state. From this we suggest that in severe cases, stem-cell transplantation may be used at the start of treatment instead of drugs. Both the mathematical analysis and the simulations support that stem-cell transplantation could be a future alternative for treating severe psoriasis.

In the next chapter, we study the effects of five key cytokines, both pro-inflammatory and anti-inflammatory, which play a major role in the progression and suppression of psoriasis. We also examine how these cytokines influence and interact with activated immune cells and skin cell compartments.

Chapter 7

Impulsive Stem Cell Transplantation to Modulate Psoriasis: Insights of Complex Cytokine Network

In this *Chapter*[7], we present a mathematical model to understand the complex interactions that occur in psoriasis. To capture these underlying processes, we have developed a dynamical system that incorporates the major cellular and molecular components known to drive the disease. The model includes epidermal stem-cell differentiation, activated T cells, activated dendritic cells, keratinocytes, and five important cytokines: tumor necrosis factor (TNF), transforming growth factor-beta (TGF-β), interleukin-23 (IL-23), interleukin-17 (IL-17), and interleukin-10 (IL-10). These components form a tightly connected network of signals, where cytokines regulate both immune cells and skin cells, while in turn the activated cells release cytokines that influence the network. Thus, the model is designed to represent two-way interactions between immune cells, skin cells, and cytokines.

To make the analysis easier, a quasi-steady-state approximation has been used for cytokine variables, which reduces the overall complexity of the system while retaining the key biological features. We first prove that the system is well-posed and has a bounded region, ensuring that the populations and cytokine levels remain biologically meaningful. The stability of the equilibrium point is then studied to understand under what conditions the skin returns to a healthy state or shifts towards a psoriatic state. In addition, a detailed sensitivity analysis is carried out to identify the most influential parameters in the system. This analysis highlights the biological factors that play a dominant role in controlling the abnormal growth of keratinocytes, that is the hallmark of psoriasis. Further, we perform a Hopf bifurcation analysis with respect to two crucial parameters: the rate of TNF-driven keratinocyte up-regulation (ζ_3) and the rate of IL-10 production by stem cells (p_7).

The model is also used to test potential therapeutic interventions through numerical

[7] *A substantial portion of this chapter has been submitted for publication in a peer-reviewed international journal.*

simulations. Two treatment strategies are considered: inhibition of TNF using impulsive drug administration and infusion of stem cells to restore balance in the skin environment. The simulations show that while TNF inhibition can temporarily reduce keratinocyte growth and inflammation, its effect is only short-term. Stem cell infusion, however, has the potential to stabilize periodic orbits and achieve long-term control over both immune activation and keratinocyte dynamics. Based on the study within this chapter, we explored that the cytokine balance plays a central role in the system, which behaves in a stable or unstable manner.

7.1 The Model

7.1.1 Model Incorporating Stem Cells and Cytokines

Initially, we formulated a mathematical model representing the underlying dynamics of psoriasis, incorporating two distinct stem cell compartments. Specifically, $S_E(t)$, $S_M(t)$, $T_A(t)$, $D_A(t)$, and $K_C(t)$ denote, respectively, the densities of epidermal stem cells, mature stem cells, activated T cells, activated dendritic cells, and keratinocytes at time t.

Since stem cells are self-renewing with no external source of replenishment [41], the growth equation of the epidermal stem cell population $S_E(t)$ in the basal epidermal layer is modeled using a logistic growth term to limit the population size through a maximal carrying capacity. This ensures that the system approaches a well-defined steady state. The governing equation is given by

$$\frac{dS_E(t)}{dt} = \left[\alpha_S \left(1 - \frac{S_E(t)}{S_E^{\max}}\right) + \gamma\left(\pi_S - \pi_D\right) - \mu_E\right] S_E(t), \tag{7.1.1}$$

where α_S is the intrinsic proliferation rate, $S_E^{\max}$ represents the maximum growth capacity of the epidermal stem cell population, and π_S and π_D denote the probabilities of symmetric self-renewal (division into two identical cells of the same phenotypes) and symmetric differentiation (division into two cells of distinct phenotypes), respectively. The parameter γ denotes a scaling factor for net stem cell division, and μ_E represents the apoptosis rate of $S_E(t)$.

The growth equation of mature stem cells, $S_M(t)$ in the dermis is given by

$$\frac{dS_M(t)}{dt} = \Big[\gamma A(2\pi_D + \pi_A)\Big] S_E(t) - \mu_M S_M(t), \tag{7.1.2}$$

where π_A is the probability corresponding to the asymmetric cell division (here stem cell can be differentiated into one cell of the same phenotype and another cell with different characteristics) [89]. Thus, $\pi_S + \pi_D + \pi_A = 1$. These three possible stem cell differentiation patterns are shown diagrammatically in the schema (Figure 7.1). Here, A denotes the amplification factor, representing the enhancement in mature stem cell production due to pro-inflammatory stimulation. In the context of psoriasis, inflammatory cytokines can upregulate mature stem cell proliferation and differentiation signals, effectively increasing the yield of $S_M(t)$ from symmetric and asymmetric divisions of stem cells. $A > 1$ implies amplification beyond baseline proliferation rates, whereas $A = 1$ would correspond to no additional inflammatory stimulation. μ_M is the apoptosis rate of $S_M(t)$.

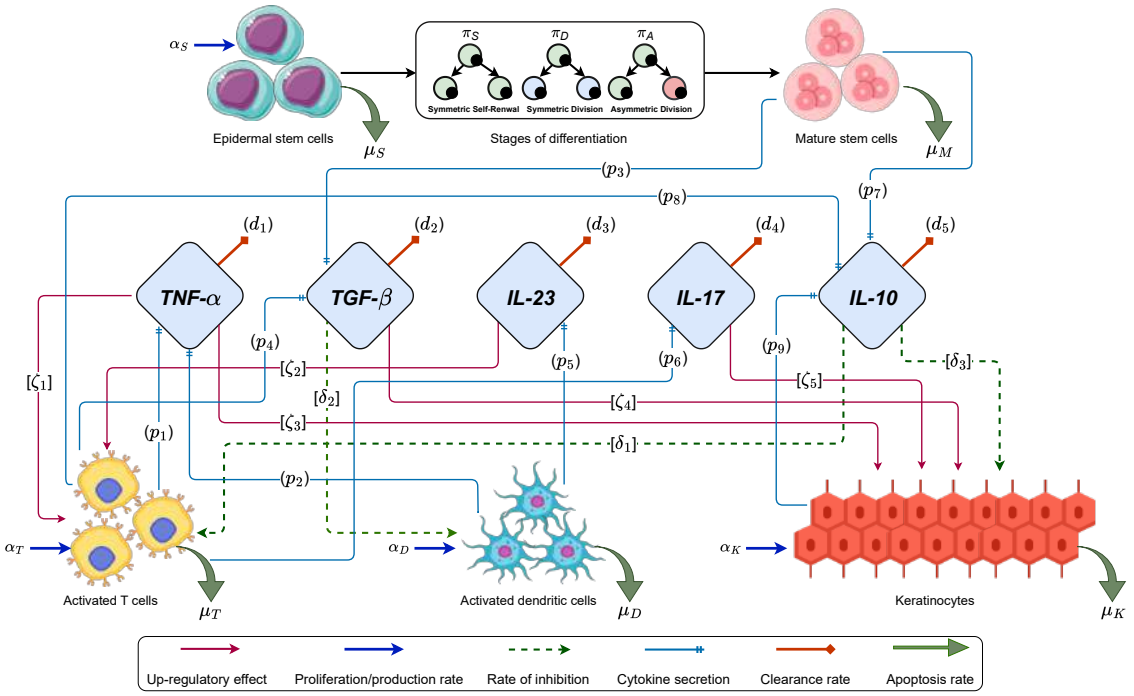

Figure 7.1: A schematic diagram of the interactions between model populations through cytokine signaling pathways.

It is important to note that the differentiation of undifferentiated epidermal stem cells into mature stem cells typically occurs through multiple intermediate stages, which are not explicitly considered in the present formulation. In the subsequent subsection 7.1.2, we introduce an additional population representing intermediate differentiated stem cells in order to more explicitly capture the differentiation process. For modeling purposes, we assume that $S_E(t)$ do not directly regulate keratinocytes or immune cells, whereas $S_M(t)$ interact with immune cells and keratinocytes through cytokine-mediated pathways or as direct contact. That is, $S_M(t)$ and $K_C(t)$ are well-mixed within the dermal–epidermal microenvironment.

To model the growth equations of activated T cells and dendritic cells to characterize psoriasis dynamics within the cytokine environment, we employed logistic growth expressions to impose an upper limit on proliferation rates, since neither cell population can grow indefinitely. The parameters α_T and α_D denote the proliferation rates of activated T cells and dendritic cells, respectively, while $T_A^{\max}$ and $D_A^{\max}$ represent their corresponding carrying capacities. The governing equations are given by

$$\frac{dT_A(t)}{dt} = \alpha_T T_A(t)\Big(1 - \frac{T_A(t)}{T_A^{\max}}\Big) + \Big[\zeta_1 T_\alpha(t) + \zeta_2 I_{23}(t)\Big] - \delta_1 I_{10}(t) T_A(t) - \mu_T T_A(t), \quad (7.1.3)$$

$$\frac{dD_A(t)}{dt} = \alpha_D D_A(t)\Big(1 - \frac{D_A(t)}{D_A^{\max}}\Big) - \delta_2 T_\beta(t) D_A(t) - \mu_D D_A(t), \quad (7.1.4)$$

where ζ_1 and ζ_2 are the activation rates of activated T cells in response to the pro-

inflammatory cytokines TNF and IL-23, respectively, mediated via activated dendritic cells [101]. The parameter δ_1 represents the suppression rate of activated T cells due to the anti-inflammatory cytokine IL-10 [91], while δ_2 denotes the suppression rate of activated dendritic cells due to TGF-β [87]. μ_T and μ_D correspond to the apoptosis rates of activated T cells and dendritic cells, respectively.

The temporal dynamics of the keratinocyte population is described by

$$\frac{dK_C(t)}{dt} = \alpha_K + \left[\frac{\zeta_3 T_\alpha(t) + \zeta_4 T_\beta(t) + \zeta_5 I_{17}(t)}{1 + \omega S_M(t)}\right] - \delta_3 I_{10}(t) K_C(t) - \mu_K K_C(t), \tag{7.1.5}$$

where α_K denotes the baseline production rate of keratinocytes arising from normal homeostatic regulation. Hyper-proliferation of keratinocytes is driven by the inflammatory cytokines TNF, TGF-β, and IL-17, with ζ_3, ζ_4, and ζ_5 representing the corresponding activation rates [101]. Mature stem cells act to inhibit both the release of these inflammatory cytokines and the associated keratinocyte hyper-proliferation through negative feedback mechanisms [102]. To capture this effect, a saturated incidence form is employed in the cytokine-mediated activation term, where the denominator models mature stem cell-mediated inhibition, with ω representing the scaling coefficient for this inhibitory effect. Suppression of keratinocyte overgrowth by the anti-inflammatory cytokine IL-10 is incorporated via the term $\delta_3 I_{10}(t) K_C(t)$ [91]. Finally, μ_K denotes the apoptosis rate of keratinocytes. It is to be noted that activation effects on $T_A(t)$ and $K_C(t)$ are modeled in relation to cytokine concentrations, while inhibitory effects of regulatory cytokines are incorporated as a multiplicative suppression factor.

7.1.2 Model with Maturation Stages of Stem Cells

Transplantation of healthy stem cells into the affected region can induce their differentiation, ultimately maturing into $S_M(t)$. These mature stem cells possess immunomodulatory properties, enabling them to regulate the over-activation of T cells and suppress the hyper-proliferation of keratinocytes [103]. In this subsection, we present a comprehensive mathematical model for psoriasis that incorporates the maturation stages of stem cells. The differentiation of undifferentiated epidermal stem cells into mature cells typically proceeds through multiple stages over the course of several weeks. Mathematically, the n-th stage is considered to represent the mature stage, i.e., $S_n(t) = S_M(t)$. However, in psoriasis, the precise differentiation pathway ranges from two to five, but the specific types of cells produced through this process remain unknown and can vary among individuals depending on the immune system's requirements. To account for this variability, initially considered stem cell dynamics involving two compartments: local undifferentiated epidermal stem cells $S_E(t)$ and matured stem cells $S_M(t)$. Due to the uncertainty in the exact number of differentiation steps, we assume that stem cells reach maturity after two stages of differentiation [90]. In this framework, epidermal stem cells $S_E(t)$ differentiate into intermediate transit amplifying cells $S_I(t)$, which ultimately mature into $S_M(t)$. By incorporating these three state variables representing the stem cell maturation process, along with the growth equations (7.1.3)–(7.1.5), the mathematical model for psoriasis, incorporating the regulatory effects of five key cytokines,

can be expressed as

$$\frac{dS_E(t)}{dt} = \Big[\alpha_S\left(1 - \frac{S_E(t)}{S_E^{\max}}\right) - \big[\mu_E - \big(2a_E - 1\big)q_E\big]\Big]S_E(t), \tag{7.1.6a}$$

$$\frac{dS_I(t)}{dt} = \Big[2\big(1 - a_E\big)q_E\Big]S_E(t) - \Big[\mu_I - \big(2a_I - 1\big)q_I\Big]S_I(t), \tag{7.1.6b}$$

$$\frac{dS_M(t)}{dt} = \Big[2\big(1 - a_I\big)q_I\Big]S_I(t) - \mu_M S_M(t), \tag{7.1.6c}$$

$$\frac{dT_A(t)}{dt} = \alpha_T T_A(t)\Big(1 - \frac{T_A(t)}{T_A^{\max}}\Big) + \Big[\zeta_1 T_\alpha(t) + \zeta_2 I_{23}(t)\Big] - \delta_1 I_{10}(t)T_A(t) - \mu_T T_A(t), \tag{7.1.6d}$$

$$\frac{dD_A(t)}{dt} = \alpha_D D_A(t)\Big(1 - \frac{D_A(t)}{D_A^{\max}}\Big) - \delta_2 T_\beta(t)D_A(t) - \mu_D D_A(t), \tag{7.1.6e}$$

$$\frac{dK_C(t)}{dt} = \alpha_K + \left[\frac{\zeta_3 T_\alpha(t) + \zeta_4 T_\beta(t) + \zeta_5 I_{17}(t)}{1 + \omega S_M(t)}\right] - \delta_3 I_{10}(t)K_C(t) - \mu_K K_C(t), \tag{7.1.6f}$$

subject to the initial conditions

$$S_E(0) > 0,\ S_I(0) > 0,\ S_M(0) > 0,\ T_A(0) > 0,\ D_A(0) > 0,\ K_C(0) > 0.$$

7.1.3 Cytokine Dynamics and Quasi-Steady-State Approximation

We now describe the system of ODEs governing the dynamics of the cytokines considered in our model. To simplify the representation of cytokine kinetics, we assume that each cytokine is produced at a constant rate by the respective source cells and degraded at a constant rate over time. Under these assumptions, the cytokine dynamics are given by

$$\begin{aligned}
\frac{dT_\alpha(t)}{dt} &= p_1 T_A(t) + p_2 D_A(t) - d_1 T_\alpha(t), & \frac{dT_\beta(t)}{dt} &= p_3 S_M(t) + p_4 T_A(t) - d_2 T_\beta(t),\\
\frac{dI_{23}(t)}{dt} &= p_5 D_A(t) - d_3 I_{23}(t), & \frac{dI_{17}(t)}{dt} &= p_6 T_A(t) - d_4 I_{17}(t),\\
\frac{dI_{10}(t)}{dt} &= p_7 S_M(t) + p_8 T_A(t) + p_9 K_C(t) - d_5 I_{10}(t).
\end{aligned} \tag{7.1.7}$$

The model parameters are interpreted as follows:

(i) $T_\alpha(t)$ denotes the concentration of the pro-inflammatory cytokine TNF, primarily secreted by activated T cells and dendritic cells (DCs) at rates p_1 and p_2, respectively [54].

(ii) $T_\beta(t)$ denotes the concentration of TGF-β, produced by mature stem cells and activated T cells at rates p_3 and p_4, respectively [54].

(iii) $I_{23}(t)$ denotes the concentration of IL-23, predominantly secreted by activated DCs at a rate p_5 [101].

(iv) $I_{17}(t)$ denotes the concentration of IL-17, secreted by activated T cells at a rate p_6 [104].

(v) $I_{10}(t)$ denotes the concentration of the anti-inflammatory cytokine IL-10, secreted by mature stem cells, activated T cells, and keratinocytes at rates p_7, p_8, and p_9, respectively [104]. This cytokine plays a regulatory role in suppressing excessive T cell activation and keratinocyte proliferation.

(vi) The parameters d_i $(i = 1, 2, \ldots, 5)$ represent the clearance rates of the respective cytokines.

Biologically, cytokines act on a faster timescale (hours to a few days), while cell growth and decay occur more slowly (days to weeks). This difference in timescales supports the use of quasi-steady-state approximation (QSSA) for cytokine dynamics [105]. All rates are written in day^{-1} units to maintain dimensional accuracy and consistency in simulations. QSSA reduces the model size and simplifies computations, though in numerical results both cell and cytokine profiles are shown for clarity. Under this assumption

$$\frac{dT_\alpha(t)}{dt} \approx 0, \quad \frac{dT_\beta(t)}{dt} \approx 0, \quad \frac{dI_{23}(t)}{dt} \approx 0, \quad \frac{dI_{17}(t)}{dt} \approx 0, \quad \frac{dI_{10}(t)}{dt} \approx 0. \tag{7.1.8}$$

This gives the following algebraic expressions

$$\begin{aligned} T_\alpha(t) &\approx \frac{p_1}{d_1}T_A(t) + \frac{p_2}{d_1}D_A(t), & T_\beta(t) &\approx \frac{p_3}{d_2}S_M(t) + \frac{p_4}{d_2}T_A(t), \\ I_{23}(t) &\approx \frac{p_5}{d_3}D_A(t), & I_{17}(t) &\approx \frac{p_6}{d_4}T_A(t), \\ I_{10}(t) &\approx \frac{p_7}{d_5}S_M(t) + \frac{p_8}{d_5}T_A(t) + \frac{p_9}{d_5}K_C(t). \end{aligned} \tag{7.1.9}$$

Substituting the above-mentioned expressions into system (7.1.6) yields the complete mathematical model

$$\frac{dS_E(t)}{dt} = \Big[\alpha_S\left(1 - \frac{S_E(t)}{S_E^{\max}}\right) - \big[\mu_E - \big(2a_E - 1\big)q_E\big]\Big]S_E(t), \tag{7.1.10a}$$

$$\frac{dS_I(t)}{dt} = \Big[2\big(1 - a_E\big)q_E\Big]S_E(t) - \Big[\mu_I - \big(2a_I - 1\big)q_I\Big]S_I(t), \tag{7.1.10b}$$

$$\frac{dS_M(t)}{dt} = \Big[2\big(1 - a_I\big)q_I\Big]S_I(t) - \mu_M S_M(t), \tag{7.1.10c}$$

$$\frac{dT_A(t)}{dt} = \alpha_T T_A(t)\left(1 - \frac{T_A(t)}{T_A^{\max}}\right) + \kappa_1 T_A(t) + \kappa_2 D_A(t) - \Big[\xi_1 S_M(t) + \xi_2 T_A(t) + \xi_3 K_C(t) + \mu_T\Big]T_A(t), \tag{7.1.10d}$$

$$\frac{dD_A(t)}{dt} = \alpha_D D_A(t)\left(1 - \frac{D_A(t)}{D_A^{\max}}\right) - \Big[\xi_4 S_M(t) + \xi_5 T_A(t) + \mu_D\Big]D_A(t), \tag{7.1.10e}$$

$$\frac{dK_C(t)}{dt} = \alpha_K + \left[\frac{\kappa_3 S_M(t) + \kappa_4 T_A(t) + \kappa_5 D_A(t)}{1 + \omega S_M(t)}\right] - \Big[\xi_6 S_M(t) + \xi_7 T_A(t) + \xi_8 K_C(t) + \mu_K\Big]K_C(t). \tag{7.1.10f}$$

The coefficients are given by

$$\kappa_1 = \frac{p_1\zeta_1}{d_1},\ \kappa_2 = \left(\frac{p_2\zeta_1}{d_1} + \frac{p_5\zeta_2}{d_3}\right),\ \kappa_3 = \frac{p_3\zeta_4}{d_2},\ \kappa_4 = \left(\frac{p_1\zeta_3}{d_1} + \frac{p_4\zeta_4}{d_2} + \frac{p_6\zeta_5}{d_4}\right),\ \kappa_5 = \frac{p_2\zeta_3}{d_1};$$
$$\xi_1 = \frac{p_7\delta_1}{d_5},\ \xi_2 = \frac{p_8\delta_1}{d_5},\ \xi_3 = \frac{p_9\delta_1}{d_5},\ \xi_4 = \frac{p_3\delta_2}{d_2},\ \xi_5 = \frac{p_4\delta_2}{d_2},\ \xi_6 = \frac{p_7\delta_3}{d_5},\ \xi_7 = \frac{p_8\delta_3}{d_5},\ \xi_8 = \frac{p_9\delta_3}{d_5}. \tag{7.1.11}$$

The system (7.1.10) is subject to the following positive initial conditions

$$S_E(0) > 0,\ S_I(0) > 0,\ S_M(0) > 0,\ T_A(0) > 0,\ D_A(0) > 0,\ K_C(0) > 0. \tag{7.1.12}$$

Variable	Description	Unit	Initial Value	Reference
$S_E(t)$	Population of epidermal stem cells	cells/mm^3	50	[41]
$S_I(t)$	Population of intermediate stem cells	cells/mm^3	25	[41]
$S_M(t)$	Mature stem cell population	cells/mm^3	25	assumed
$T_A(t)$	Activated T cell population	cells/mm^3	20	[106]
$D_A(t)$	Activated dendritic cell population	cells/mm^3	20	[106]
$K_C(t)$	Keratinocyte population	cells/mm^3	100	[54]
$T_\alpha(t)$	Concentration of TNF	pg/mm^3	5	[106]
$T_\beta(t)$	Concentration of TGF-β	pg/mm^3	3	assumed
$I_{23}(t)$	Concentration of interleukin-23 (IL-23)	pg/mm^3	2	assumed
$I_{17}(t)$	Concentration of interleukin-17 (IL-17)	pg/mm^3	1	[106]
$I_{10}(t)$	Concentration of interleukin-10 (IL-10)	pg/mm^3	1	assumed

Table 7.1: Description of the model variables, their corresponding units, initial values used in the numerical simulations, and supporting references.

7.2 Mathematical Properties of the Model

To ensure the mathematical model is well-posed and epidemiologically feasible, in this section we have studied the positivity and boundedness of the complete model populations, the existence criterion of the interior equilibrium point, and its local stability analysis for the system (7.1.10).

7.2.1 Positivity of the Invariant Region and Boundedness

In this subsection, we have discussed the positivity of the solutions and boundedness properties of our proposed system (7.1.10). Now, we prove the following theorem, which guarantees the positivity of the solutions of system.

Theorem 7.2.1 *If the initial condition satisfies* $(S_E(0), S_I(0), S_M(0), T_A(0), D_A(0), K_C(0))^{\mathrm{T}} \in \mathrm{Int}(\mathbb{R}^6_+)$*, then all solutions of the system* (7.1.10) *remain positive for all* $t > 0$.

Proof. Define the variables as $X_1(t) = S_E(t)$, $X_2(t) = S_I(t)$, $X_3(t) = S_M(t)$, $X_4(t) = T_A(t)$, $X_5(t) = D_A(t)$, and $X_6(t) = K_C(t)$. The system (7.1.10) can then be rewritten in vector form as

$$\frac{dX(t)}{dt} = \Gamma\big[X(t)\big], \text{ where } X(t) = \big[X_1, X_2, X_3, X_4, X_5, X_6\big]^T, \ \Gamma = \big[\Gamma_1, \Gamma_2, \Gamma_3, \Gamma_4, \Gamma_5, \Gamma_6\big]^T. \tag{7.2.1}$$

Here, Γ_i $(i = 1, \ldots, 6)$ denote the right-hand sides of the corresponding equations in system (7.1.10). We observe that

$$\Gamma_i(X)|_{X_i=0,\ X\in\mathbb{R}^6_+} \geq 0 \quad \text{for all } i = 1, \ldots, 6. \tag{7.2.2}$$

This condition means that the vector field $\Gamma(X)$ is either inward or tangent to the boundary of the positive octant $\mathbb{R}^6_+$ whenever any $X_i = 0$. By Nagumo's theorem [62], the solutions remain in $\mathbb{R}^6_+$ for all $t > 0$. Thus, if $X(0) \in \text{Int}(\mathbb{R}^6_+)$, then $X(t) \in \mathbb{R}^6_+$ for all $t > 0$, showing that $\mathbb{R}^6_+$ is positively invariant for system (7.1.10).

It is essential to determine the bounds of all model variables in the system (7.1.10) over time. This ensures that the system remains biologically meaningful and mathematically well-posed. Before proving the boundedness of the solution of the system, we cite the following lemma [35].

Lemma 7.2.1 *Let $P(t)$ be a differentiable function satisfying the inequality*

$$\frac{dP(t)}{dt} < R - Q(\varphi)P(t), \tag{7.2.3}$$

where R is a positive constant and $Q(\varphi)$ is a positive function that is independent of P and t. Then, if $P(0) < R/Q(\varphi)$, it follows that

$$P(t) < \frac{R}{Q(\varphi)} \quad \textit{for all } t > 0. \tag{7.2.4}$$

The following theorem demonstrates the invariant region Δ where the solutions of system (7.1.10) are bounded. We have used the above-mentioned lemma (7.2.1), to prove this theorem.

Theorem 7.2.2 *All solutions of the system (7.1.10) enter into the region $\Delta \subseteq \mathbb{R}^6_+$ and are ultimately bounded within that region. Specifically,*

$$\Delta = \left\{ \big(S_E, S_I, S_M, T_A, D_A, K_C\big)^T \in \mathbb{R}^6_+ : \begin{array}{l} 0 < S_E(t) \leq H_1,\ 0 < S_I(t) \leq H_2,\ 0 < S_M(t) \leq H_3, \\ 0 < T_A(t) \leq H_4,\ 0 < D_A(t) \leq H_5,\ 0 < K_C(t) \leq H_6 \end{array} \right\},$$

where the upper bounds H_i $(i = 1, \ldots, 6)$ are defined as

$$H_1 = \frac{\alpha_S S_E^{\max}}{4m_E},\ H_2 = \frac{\alpha_S l_E S_E^{\max}}{4m_E m_I},\ H_3 = \frac{\alpha_S l_E l_I S_E^{\max}}{4m_E m_I \mu_M},$$
$$H_4 = \frac{\alpha_T \mu_D T_A^{\max} + \alpha_D \kappa_2 D_A^{\max}}{4\mu_D(\mu_T - \kappa_1)},\ H_5 = \frac{\alpha_D D_A^{\max}}{4\mu_D},\ H_6 = \frac{\alpha_K}{\mu_K} + \left[\frac{\kappa_3 H_3 + \kappa_4 H_4 + \kappa_5 H_5}{\mu_K(1 + \omega S_M^{\min})}\right].$$

The solutions retain their biological significance for all $t > 0$.

Proof. From equation (7.1.10a), the logistic growth term attains a maximum value at $S_E = \frac{S_E^{\max}}{2}$, giving an upper bound

$$\frac{dS_E(t)}{dt} \leq \frac{\alpha_S S_E^{\max}}{4} - m_E S_E(t), \quad \text{where } m_E = \mu_E - (2a_E - 1)q_E > 0.$$

Solving the above inequality for large t, we obtain

$$\therefore \limsup_{t\to\infty} S_E(t) \leq \frac{\alpha_S S_E^{\max}}{4m_E} =: H_1. \tag{7.2.5}$$

Using the bound of $S_E(t)$, from the equation (7.1.10b), we get

$$\frac{dS_I(t)}{dt} \leq \frac{\alpha_S l_E S_E^{\max}}{4m_E} - m_I S_I(t), \quad \text{where } l_E = 2(1 - a_E)q_E > 0,\ m_I = \mu_I - (2a_I - 1)q_I > 0.$$

$$\therefore \limsup_{t\to\infty} S_I(t) \leq \frac{\alpha_S l_E S_E^{\max}}{4m_E m_I} =: H_2. \tag{7.2.6}$$

Similarly, from the equation (7.1.10c)

$$\frac{dS_M(t)}{dt} \leq \frac{\alpha_S l_E l_I S_E^{\max}}{4m_E m_I} - \mu_M S_M(t), \quad \text{where } l_I = 2(1 - a_I)q_I > 0,$$

$$\therefore \limsup_{t\to\infty} S_M(t) \leq \frac{\alpha_S l_E l_I S_E^{\max}}{4m_E m_I \mu_M} =: H_3. \tag{7.2.7}$$

From the equation (7.1.10e), neglecting second-order negative terms

$$\frac{dD_A(t)}{dt} \leq \frac{\alpha_D D_A^{\max}}{4} - \mu_D D_A(t).$$

$$\therefore \limsup_{t\to\infty} D_A(t) \leq \frac{\alpha_D D_A^{\max}}{4\mu_D} =: H_5. \tag{7.2.8}$$

Substituting this into the equation (7.1.10d) gives

$$\frac{dT_A(t)}{dt} \leq \frac{\alpha_T T_A^{\max}}{4} + \frac{\alpha_D \kappa_2 D_A^{\max}}{4\mu_D} - (\mu_T - \kappa_1)T_A(t), \quad \text{with } \mu_T > \kappa_1,$$

$$\therefore \limsup_{t\to\infty} T_A(t) \leq \frac{\alpha_T \mu_D T_A^{\max} + \alpha_D \kappa_2 D_A^{\max}}{4\mu_D(\mu_T - \kappa_1)} =: H_4. \tag{7.2.9}$$

For the equation (7.1.10f), applying bounds H_3, H_4, H_5, and using the minimal value

$S_M^{\min} > 0$, we get

$$\frac{dK_C(t)}{dt} \leq \alpha_K + \frac{\kappa_3 H_3 + \kappa_4 H_4 + \kappa_5 H_5}{1 + \omega S_M^{\min}} - \mu_K K_C(t),$$

$$\therefore \limsup_{t\to\infty} K_C(t) \leq \frac{\alpha_K}{\mu_K} + \left[\frac{\kappa_3 H_3 + \kappa_4 H_4 + \kappa_5 H_5}{\mu_K(1 + \omega S_M^{\min})}\right] =: H_6. \tag{7.2.10}$$

Thus, all variables are bounded by constants H_i, and the region Δ is positively invariant. Moreover, the following conditions in (7.2.11) confirm that trajectories re-enter and remain in the interior of Δ for all $t > 0$. Hence, Δ is a positive invariant and absorbing set for system (7.1.10).

$$\begin{aligned} &\left.\frac{dS_E}{dt}\right|_{\partial\Delta} < 0, \quad \left.\frac{dS_I}{dt}\right|_{\partial\Delta} < 0, \quad \left.\frac{dS_M}{dt}\right|_{\partial\Delta} < 0, \\ &\left.\frac{dT_A}{dt}\right|_{\partial\Delta} < 0, \quad \left.\frac{dD_A}{dt}\right|_{\partial\Delta} < 0, \quad \left.\frac{dK_C}{dt}\right|_{\partial\Delta} < 0. \end{aligned} \tag{7.2.11}$$

7.2.2 Existence and Local Stability of Interior Equilibrium

We analyze the local stability of the interior equilibrium point $E^*(S_E^*, S_I^*, S_M^*, T_A^*, D_A^*, K_C^*)$. From the equations (7.1.10a)–(7.1.10c), we can easily determine the values of the first three populations.

$$S_E^* = S_E^{\max}\left[1 - \frac{\mu_E - (2a_E - 1)q_E}{\alpha_S}\right] = S_E^{\max}\left[1 - \frac{m_E}{\alpha_S}\right], \tag{7.2.12a}$$

$$S_I^* = \frac{2(1 - a_E)q_E}{\mu_I - (2a_I - 1)q_I} \cdot S_E^* = \frac{l_E S_E^{\max}}{m_I}\left[1 - \frac{m_E}{\alpha_S}\right], \tag{7.2.12b}$$

$$S_M^* = \frac{2(1 - a_I)q_I}{\mu_M} \cdot S_I^* = \frac{l_E l_I S_E^{\max}}{m_I \mu_M}\left[1 - \frac{m_E}{\alpha_S}\right]. \tag{7.2.12c}$$

The necessary condition for the feasibility of S_E^*, S_I^*, and S_M^* is given by $\alpha_S > m_E$. From equations (7.1.10d) and (7.1.10e), we can determine the values of D_A^* and K_C^* in terms of T_A^*.

$$D_A^* = \left(\frac{D_A^{\max}}{\alpha_D}\right)\left[\rho_D - \xi_5 T_A^*\right], \tag{7.2.13a}$$

$$K_C^* = \frac{1}{\xi_3}\left[\rho_T + \kappa_2\left(\frac{D_A^*}{T_A^*}\right) - \left(\frac{\alpha_T}{T_A^{\max}} + \xi_2\right) T_A^*\right], \tag{7.2.13b}$$

where $\rho_D = \alpha_D - \mu_D - \xi_4 S_M^*$ and $\rho_T = \alpha_T + \kappa_1 - \mu_T - \xi_1 S_M^*$.

Substituting these values given by the system of equations (7.2.12) and (7.2.13) in the equation (7.1.10f), we arrive at a polynomial equation in T_A^* of degree four.

$$\sigma_1 T_A^{*4} + \sigma_2 T_A^{*3} + \sigma_3 T_A^{*2} + \sigma_4 T_A^* + \sigma_5 = 0. \tag{7.2.14}$$

The coefficients are given by

$$\begin{aligned}
\sigma_1 &= \left(\frac{\alpha_T}{T_A^{\max}} + \xi_2\right)\left[\xi_8\left(\frac{\alpha_T}{T_A^{\max}} + \xi_2\right) - \xi_3\xi_7\right], \\
\sigma_2 &= \frac{\kappa_5\xi_3^2\xi_5 D_A^{\max}}{\alpha_D(1+\omega S_M^*)} + \left[\xi_3\xi_7 - 2\xi_8\left(\frac{\alpha_T}{T_A^{\max}} + \xi_2\right)\right]\left(\rho_T - \frac{D_A^{\max}\kappa_2\xi_5}{\alpha_D}\right) \\
&\quad - \xi_3\left(\xi_6 S_M^* + \mu_K\right)\left(\frac{\alpha_T}{T_A^{\max}} + \xi_2\right) - \frac{\kappa_4\xi_3^2}{1+\omega S_M^*}, \\
\sigma_3 &= \xi_8\left(\rho_T - \frac{D_A^{\max}\kappa_2\xi_5}{\alpha_D}\right)^2 + \xi_3\left(\xi_6 S_M^* + \mu_K\right)\left(\rho_T - \frac{D_A^{\max}\kappa_2\xi_5}{\alpha_D}\right) \\
&\quad + \frac{\rho_D D_A^{\max}\kappa_2}{\alpha_D}\left[\xi_3\xi_7 - 2\xi_8\left(\frac{\alpha_T}{T_A^{\max}} + \xi_2\right)\right] - \rho_K\xi_3^2, \\
\sigma_4 &= \frac{\rho_D D_A^{\max}\kappa_2}{\alpha_D}\left[\xi_3\left(\xi_6 S_M^* + \mu_K\right) + 2\xi_8\left(\rho_T - \frac{D_A^{\max}\kappa_2\xi_5}{\alpha_D}\right)\right], \\
\sigma_5 &= \xi_8\left(\frac{\rho_D D_A^{\max}\kappa_2}{\alpha_D}\right)^2.
\end{aligned}$$

If the conditions $\xi_3\xi_7 > 2\xi_8\left(\frac{\alpha_T}{T_A^{\max}} + \xi_2\right)$ and $\rho_T > D_A^{\max}\kappa_2\xi_5/\alpha_D$ are satisfied, then it follows that $\sigma_1 < 0$, $\sigma_4 > 0$, and $\sigma_5 > 0$. Consequently, by Descartes' rule of signs, the existence of a positive root of the polynomial (7.2.14) depends solely on the signs of σ_2 and σ_3. Four cases can thus be distinguished

(a) If $\sigma_2 > 0$ and $\sigma_3 > 0$, then one positive real root exists.

(b) If $\sigma_2 < 0$ and $\sigma_3 < 0$, then a positive real root also exists.

(c) If $\sigma_2 > 0$ and $\sigma_3 < 0$, then either one or three positive real roots may occur.

(d) If $\sigma_2 < 0$ and $\sigma_3 > 0$, then exactly one positive real root exists.

Thus, polynomial (7.2.14) always possesses at least one positive root. Therefore, for the existence of the interior equilibrium point E^*, we state the following lemma.

Lemma 7.2.2 *The system (7.1.10) possesses an interior equilibrium point if the following conditions are satisfied*

$$(i)\ \alpha_S > m_E, \qquad (ii)\ \rho_D > \xi_5 T_A^*, \qquad (iii)\ \rho_T > \frac{D_A^{\max}\kappa_2\xi_5}{\alpha_D},$$

$$(iv)\ \xi_3\xi_7 > 2\xi_8\left(\frac{\alpha_T}{T_A^{\max}} + \xi_2\right), \quad (v)\ \rho_T + \kappa_2\left(\frac{D_A^*}{T_A^*}\right) > \left(\frac{\alpha_T}{T_A^{\max}} + \xi_2\right)T_A^*.$$

We now analyze the stability of the interior equilibrium point E^*. The Jacobian matrix

V evaluated at E^* can be decomposed into block matrices

$$V_1 = \begin{pmatrix} -\frac{\alpha_S S_E^*}{S_E^{\max}} & 0 & 0 \\ l_E & -m_I & 0 \\ 0 & l_I & -\mu_M \end{pmatrix},$$

$$V_2 = \begin{pmatrix} -\left(\frac{\alpha_T T_A^*}{T_A^{\max}} + \frac{\kappa_2 D_A^*}{T_A^*} + \xi_2 T_A^*\right) & \kappa_2 & -\xi_3 T_A^* \\ -\xi_5 D_A^* & -\frac{\alpha_D D_A^*}{D_A^{\max}} & 0 \\ \frac{\kappa_4}{1+\omega S_M^*} - \xi_7 K_C^* & \frac{\kappa_5}{1+\omega S_M^*} & -(\xi_6 S_M^* + \xi_7 T_A^* + 2\xi_8 K_C^* + \mu_K) \end{pmatrix}.$$

The block matrix V_1 admits three negative eigenvalues

$$-\frac{\alpha_S S_E^*}{S_E^{\max}},\ -m_I,\ \text{and}\ -\mu_M.$$

The characteristic equation of the other block matrix V_2 is given by

$$\mathcal{Y}(\varrho) \equiv \varrho^3 + \mathcal{C}_1 \varrho^2 + \mathcal{C}_2 \varrho + \mathcal{C}_3 = 0, \tag{7.2.15}$$

where the coefficients are

$$\begin{aligned}
\mathcal{C}_1 &= \frac{\alpha_T T_A^*}{T_A^{\max}} + \frac{\alpha_D D_A^*}{D_A^{\max}} + \frac{\kappa_2 D_A^*}{T_A^*} + (\xi_2 + \xi_7) T_A^* + \xi_6 S_M^* + 2\xi_8 K_C^* + \mu_K, \\
\mathcal{C}_2 &= \left(\frac{\alpha_T T_A^*}{T_A^{\max}} + \frac{\alpha_D D_A^*}{D_A^{\max}} + \frac{\kappa_2 D_A^*}{T_A^*} + \xi_2 T_A^*\right)(\xi_6 S_M^* + \xi_7 T_A^* + 2\xi_8 K_C^* + \mu_K) \\
&\quad + \xi_3 T_A^* \left(\frac{\kappa_4}{1+\omega S_M^*} - \xi_7 K_C^*\right) + \frac{\alpha_D D_A^*}{D_A^{\max}} \left(\frac{\alpha_T T_A^*}{T_A^{\max}} + \frac{\kappa_2 D_A^*}{T_A^*} + \xi_2 T_A^*\right) + \kappa_2 \xi_5 D_A^*, \\
\mathcal{C}_3 &= (\xi_6 S_M^* + \xi_7 T_A^* + 2\xi_8 K_C^* + \mu_K) \left[\frac{\alpha_D D_A^*}{D_A^{\max}} \left(\frac{\alpha_T T_A^*}{T_A^{\max}} + \frac{\kappa_2 D_A^*}{T_A^*} + \xi_2 T_A^*\right) + \kappa_2 \xi_5 D_A^*\right] \\
&\quad + \xi_3 T_A^* \left[\frac{\alpha_D D_A^*}{D_A^{\max}} \left(\frac{\kappa_4}{1+\omega S_M^*} - \xi_7 K_C^*\right) - \frac{\kappa_5 \xi_5 D_A^*}{1+\omega S_M^*}\right].
\end{aligned}$$

The local stability of the interior equilibrium E^* is determined by the eigenvalues of the Jacobian matrix V evaluated at E^*. Stability requires all eigenvalues to be negative or to have negative real parts. Since the eigenvalues of V_1 are negative, the stability of E^* depends solely on the eigenvalues of V_2, i.e., on the roots of the characteristic equation (7.2.15). According to the Routh–Hurwitz criterion [63], the equation (7.2.15) has three roots with negative real parts if $\mathcal{C}_1 > 0$, $\mathcal{C}_3 > 0$, and $\mathcal{C}_1\mathcal{C}_2 - \mathcal{C}_3 > 0$. Computing $(\mathcal{C}_1\mathcal{C}_2 - \mathcal{C}_3)$ and express the stability condition through the following lemma.

Lemma 7.2.3 *The interior equilibrium E^* is locally asymptotically stable if*

$$\frac{\kappa_4}{1+\omega S_M^*} > \xi_7 K_C^* + \frac{\kappa_5 \xi_5 D_A^{\max}}{\alpha_D (1+\omega S_M^*)}. \tag{7.2.16}$$

Remark 7.2.1 *The stability analysis highlights the role of specific system parameters in determining the long-term dynamics of psoriasis. In particular, the stability condition of our*

system reveals that parameters associated with TNF inhibition and stem cell–secreted cytokine effects exert a critical influence on system stability. Mathematically, variations in these parameters can shift the eigenvalue spectrum of the Jacobian, thereby altering the equilibrium behavior. Biologically, this reflects how therapeutic modulation of cytokine pathways can determine whether the disease dynamics remain stable or progress toward instability. In the following section, we analyze the Hopf bifurcation corresponding to these parameters.

7.2.3 Hopf bifurcation Analysis of the Interior Equilibrium

Hopf bifurcation describes a critical transition in system dynamics, identifying the shift from a stable interior equilibrium to sustained periodic oscillations or vice versa. It occurs in a system at the equilibrium if the characteristic equation has two purely imaginary roots at that state, while all other roots are either negative real or have negative real parts. In this study, the system (7.1.10) exhibits Hopf bifurcation at the interior equilibrium E^* if the third-degree equation (7.2.15) possesses two purely imaginary roots. Here we have considered $\lambda \in \mathbb{R}$ as the bifurcation parameter of the system (7.1.10).

Let $\Psi : (o, \infty) \to \mathbb{R}$ be the continuously differentiable function defined as

$$\Psi(\lambda) = \mathcal{C}_1(\lambda)\mathcal{C}_2(\lambda) - \mathcal{C}_3(\lambda). \tag{7.2.17}$$

The system (7.1.10) undergoes the Hopf bifurcation, if there exist $\lambda^* \in (0, \infty)$ within the spectrum $\mathcal{C}(\lambda) = \{\varrho : \mathcal{Y}(\varrho) = 0\}$ of the characteristic equation (7.2.15), where a pair of complex eigenvalues $\varrho(\lambda^*)$ and $\bar{\varrho}(\lambda^*)$ comply with the following conditions

$$Re[\varrho(\lambda^*)] = 0, \quad Im[\varrho(\lambda^*)] > 0. \tag{7.2.18}$$

Moreover, the following transversality conditions must be satisfied

$$\frac{dRe(\varrho_i(\lambda))}{d\lambda}\bigg|_{\lambda=\lambda^*} \neq 0 \quad \text{for} \quad i = 1, 2. \tag{7.2.19}$$

Theorem 7.2.3 *The interior equilibrium E^* of system (7.1.10) undergoes Hopf bifurcation at $\lambda = \lambda^*$ if and only if the following conditions hold*

$$(i)\ \ \mathcal{C}_1(\lambda^*) > 0, \mathcal{C}_3(\lambda^*) > 0, \ \ (ii)\ \ \Psi(\lambda^*) = 0, \ \ (iii)\ \mathcal{C}_3'(\lambda^*) - \mathcal{C}_1'(\lambda^*)\mathcal{C}_2(\lambda^*) - \mathcal{C}_1(\lambda^*)\mathcal{C}_2'(\lambda^*) \neq 0.$$

Proof. Let a critical value λ^* of the bifurcation parameter λ exist so that the conditions (i)-(ii) hold. Using the conditions (ii), the third-degree equation (7.2.15) can be written in the following form

$$\left[\varrho(\lambda^*) + C_1(\lambda^*)\right]\left[\varrho^2(\lambda^*) + C_2(\lambda^*)\right] = 0. \tag{7.2.20}$$

The roots of the equation (7.2.20) are, $\varrho_1(\lambda^*) = -C_1(\lambda^*)$, $\varrho_2(\lambda^*) = i\sqrt{C_2(\lambda^*)}$ and $\varrho_3(\lambda^*) = -i\sqrt{C_2(\lambda^*)}$. According to the first condition (i), $\varrho_1(\lambda^*)$ is negative real root and another two roots $\varrho_2(\lambda^*)$, $\varrho_3(\lambda^*)$ are purely imaginary roots. Now we verify the transversality condition (7.2.19) for the existence of Hopf bifurcation at $\lambda = \lambda^*$. Substituting

$\varrho_i(\lambda) = \vartheta_1(\lambda) \pm \vartheta_2(\lambda)$ in the equation (7.2.15) and differentiating, we obtained

$$\mathcal{K}(\lambda)(\vartheta_1^{'}(\lambda) + \vartheta_2^{'}(\lambda)) + \mathcal{L}(\lambda) = 0, \tag{7.2.21a}$$
$$\mathcal{M}(\lambda)(\vartheta_1^{'}(\lambda) - \vartheta_2^{'}(\lambda)) + \mathcal{N}(\lambda) = 0, \tag{7.2.21b}$$

where the values of $\mathcal{K}(\lambda), \mathcal{L}(\lambda), \mathcal{M}(\lambda)$ and $\mathcal{N}(\lambda)$ are as follows

$$\begin{aligned} \mathcal{K}(\lambda) &= 3(\vartheta_1 + \vartheta_2)^2 + 2C_1(\vartheta_1 + \vartheta_2) + C_2, \quad \mathcal{L}(\lambda) = (\vartheta_1 + \vartheta_2)^2 C_1^{'} + (\vartheta_1 + \vartheta_2)C_2^{'}, \\ \mathcal{M}(\lambda) &= 3(\vartheta_1 - \vartheta_2)^2 + 2C_1(\vartheta_1 - \vartheta_2) + C_2, \quad \mathcal{N}(\lambda) = (\vartheta_1 - \vartheta_2)^2 C_1^{'} + (\vartheta_1 - \vartheta_2)C_2^{'}. \end{aligned} \tag{7.2.22}$$

Now, solving equations (7.2.21a) and (7.2.21b) for the value of $\vartheta_1^{'}(\lambda)$, we obtained

$$\begin{aligned} \left.\frac{dRe(\varrho_i(\lambda))}{d\lambda}\right|_{\lambda=\lambda^*} &= \left.\vartheta_1^{'}(\lambda)\right|_{\lambda=\lambda^*} \\ &= -\frac{\mathcal{K}(\lambda^*)\mathcal{N}(\lambda^*) + \mathcal{L}(\lambda^*)\mathcal{M}(\lambda^*)}{2\mathcal{K}(\lambda^*)\mathcal{M}(\lambda^*)} \\ &= \frac{\mathcal{C}_3^{'}(\lambda^*) - \mathcal{C}_1^{'}(\lambda^*)\mathcal{C}_2(\lambda^*) - \mathcal{C}_1(\lambda^*)\mathcal{C}_2^{'}(\lambda^*)}{2\left[C_1^2(\lambda^*) + C_2^2(\lambda^*)\right]}. \end{aligned} \tag{7.2.23}$$

Since, $2\left[C_1^2(\lambda^*) + C_2^2(\lambda^*)\right] > 0$ always, therefore from the equation (7.2.23), we can say that

$$\left.\frac{dRe(\varrho_i(\lambda))}{d\lambda}\right|_{\lambda=\lambda^*} \neq 0 \quad \text{holds, if} \quad \mathcal{C}_3^{'}(\lambda^*) - \mathcal{C}_1^{'}(\lambda^*)\mathcal{C}_2(\lambda^*) - \mathcal{C}_1(\lambda^*)\mathcal{C}_2^{'}(\lambda^*) \neq 0. \tag{7.2.24}$$

Thus, Hopf bifurcation occurs in the system (7.1.10) at the critical value $\lambda = \lambda^*$ around the interior equilibrium E^*.

Remark 7.2.2 *Hopf bifurcation (HB) analysis characterizes the transition between a stable equilibrium and periodic oscillations of the interior equilibrium E^*. After applying the QSSA, the cell compartments exhibit several negative quadratic terms that capture the feedback from anti-inflammatory responses. This feedback mechanism provides a mathematical explanation for the emergence of oscillatory behavior in the system. When the strength of this negative feedback is reduced, the stabilizing effect is lost, leading to destabilization of the equilibrium. Moreover, from the stability condition, we observed that the system's stability depends on key biological parameters. To capture this dependence, we performed HB with respect to a general bifurcating parameter λ, without considering any fixed parameter. We have numerically demonstrated the HB for two biologically relevant parameters: ζ_3 (the TNF-driven up-regulatory effect on keratinocytes) and p_7 (anti-inflammatory cytokine production from mature stem cells), highlighting their importance in the context of therapeutic controls. The bifurcation with respect to ζ_3 demonstrates that increasing its value, the system transitions into oscillatory behavior, indicating the emergence of TNF inhibition. In contrast, the bifurcation with respect to p_7 shows that higher values stabilize the system, corresponding to low inflammation and emphasizing the therapeutic potential of stem cell–mediated cytokine modulation. Collectively, these findings demonstrate how bifurcation analysis can inform the*

identification of therapeutic targets and guide the design of effective control strategies for psoriasis.

7.3 The Model with Biologic Inhibitor

In light of the bifurcation with respect to ζ_3, we observed that increasing its value, the system transitions into oscillatory behavior. This reflects the destabilizing effect of TNF-mediated keratinocyte up-regulation and indicates the emergence of TNF inhibition. Thus here in this section, we investigate the effects of biologic therapy, specifically the TNF inhibitor, on the key system populations $T_A(t)$ and $K_C(t)$ within an impulsive control framework. We explicitly note the equations where the effects of TNF are incorporated and subsequently modified under inhibition. Only these equations are restated here, since they directly involve TNF or its inhibitory effect. The remaining cellular compartments in system (7.1.6) and the cytokine dynamics described by system (7.1.7) remain unaltered and are indirectly coupled through the QSSA relations (7.1.8) and (7.1.9). Furthermore, we numerically demonstrate the consequences of TNF inhibition on the downstream cytokine profiles, thereby highlighting the therapeutic impact.

$$\begin{aligned}
\frac{dT_A(t)}{dt} &= \alpha_T T_A(t)\Big(1-\frac{T_A(t)}{T_A^{\max}}\Big)+\Big[\zeta_1\Big(\frac{F_{50}}{F_{50}+F(t)}\Big)T_\alpha(t)+\zeta_2 I_{23}(t)\Big]-\delta_1 I_{10}(t)T_A(t)-\mu_T T_A(t),\\
\frac{dK_C(t)}{dt} &= \alpha_K+\left[\frac{\zeta_3\Big(\frac{F_{50}}{F_{50}+F(t)}\Big)T_\alpha(t)+\zeta_4 T_\beta(t)+\zeta_5 I_{17}(t)}{1+\omega S_M(t)}\right]-\delta_3 I_{10}(t)K_C(t)-\mu_K K_C(t).
\end{aligned} \tag{7.3.1}$$

Here, we introduce a hill-type inhibition function, $F_{50}/\big(F_{50}+F(t)\big)$, to modify the parameters ζ_1 and ζ_3, which represent the TNF-mediated up-regulation of T cells and keratinocytes, respectively. Incorporation of these inhibition terms reflects the suppressive effects of biologic agents on the respective immune pathways, according to experimental observations [95]. The parameter F_{50} denotes the concentrations of TNF inhibitor required to achieve a reduction of 50% in the up-regulation effects. The temporal dynamics of drug concentrations, $F(t)$, are governed by the following equations

$$\frac{dF(t)}{dt} = -rF(t)\,, \qquad \text{when } \ t \neq t_k \tag{7.3.2a}$$

$$F(t_k^+) = F(t_k^-) + F_c\,, \quad \text{when } \ t = t_k \ \ (k = 1, 2, \cdots, n). \tag{7.3.2b}$$

The clearance rate of the TNF inhibitor is represented by r. The concentration $F(t_k^-)$ denotes the levels of these inhibitors immediately before the administration of the k-th dose, while $F(t_k^+)$ represents the concentrations immediately after dosing. F_c corresponds to the fixed doses of TNF inhibitor administered at each impulsive time point $t = t_k$, for $k = 1, 2, \cdots, n$.

The use of impulsive differential equations to model drug adherence introduces perturbations to the internal steady state of the system, leading to periodic solutions that exhibit

discontinuities at discrete time points. Notably, equations (7.3.1) and (7.3.2) indicate that these discontinuities occur exclusively in the drug concentration profiles, while the other system variables remain continuous. In the absence of treatment, that is, when $F(t) = 0$ the system reduces to its original form as described in system (7.1.6). We assume that the drugs are administered at uniform time intervals, with $\vartheta = t_{k+1} - t_k$ denoting the fixed dosing period. For time t in the interval $t_k < t < t_{k+1}$, the system evolves according to: $F(t) = F(t_k^+)e^{-r(t-t_k)}$. Using recursion relations at the moment of impulses, we derived the left and right ends of the impulsive periodic orbits and we obtained

$$F(t_{k+1}^-) = \frac{F_c e^{-r\vartheta}}{1 - e^{-r\vartheta}}, \quad F(t_{k+1}^+) = \frac{F_c}{1 - e^{-r\vartheta}} \quad (\text{as } k \to \infty) \tag{7.3.3}$$

Here, we do not present the detailed analytical derivation of the periodic orbit's stability. Instead, we focus on numerically illustrating the impact of impulsive drug administration on the dynamics of the system populations. Figure 7.7 illustrates the behavior of the system variables and associated cytokine profiles both before and after treatment under the influence of impulsive control with TNF inhibition. A detailed explanation of the figure is provided in the Numerical Simulation section.

7.4 Impulsive Cell-Replacement Strategy

Stem cell-based therapies are widely utilized for the prevention and treatment of various diseases, often requiring multiple infusions of stem cells. Clinicians assess therapeutic effects after each administration, with the number of infusions determined by the severity of the disease and the factors of each patient [91]. These repeated infusions introduce time-dependent discontinuities in the system that can be analytically modeled using an impulsive approach.

In the case of psoriasis, dysregulation of local epidermal stem cells leads to their infiltration into the keratinocyte pool, resulting in a decrease in the concentration of $S_E(t)$ as well as in mature stem cell $S_M(t)$ concentration. Moreover, the differentiation potential of these local stem cells and their immunomodulatory functions deteriorate over time. When biologic drug fail to achieve complete disease eradication, exhibit significant side effects, or cause frequent relapse after discontinuation of treatment, stem cell replacement therapy may serve as a viable alternative. In particular, umbilical cord-derived stem cells are increasingly favored due to their regenerative potential and their ability to restore immune homeostasis without long-term adverse effects [22].

7.4.1 Dynamics of the Impulsive Model

The following model investigates the periodic infusions of epidermal stem cells, which supplement or replace the dysregulated local epidermal stem cell population, denoted as $S_E(t)$, through mathematical analysis. Furthermore, the impact of the impulsive stem cell replacement strategy on the remaining cell populations is examined numerically (see the **Numerical Simulation** section). The dynamics of this replacement process are described using impulsive differential equations, which provide a framework for analyzing the effects of periodic

stem cell administration.

$$
\begin{aligned}
\frac{dS_E(t)}{dt} &= \alpha_S S_E(t)\Big(1-\frac{S_E(t)}{S_E^{max}}\Big) - m_E S_E(t), \;\; t \neq t_k \\
\frac{dS_I(t)}{dt} &= l_E S_E(t) - m_I S_I(t), \\
\frac{dS_M(t)}{dt} &= l_I S_I - \mu_M S_M(t), \\
\frac{dT_A(t)}{dt} &= \alpha_T T_A(t)\Big(1-\frac{T_A(t)}{T_A^{max}}\Big) + \kappa_1 T_A(t) + \kappa_2 D_A(t) \\
&\quad - \Big[\xi_1 S_M(t) + \xi_2 T_A(t) + \xi_3 K_C(t) + \mu_T\Big] T_A(t), \\
\frac{dD_A(t)}{dt} &= \alpha_D D_A(t)\left(1-\frac{D_A(t)}{D_A^{\max}}\right) - \Big[\xi_4 S_M(t) + \xi_5 T_A(t) + \mu_D\Big] D_A(t), \\
\frac{dK_C(t)}{dt} &= \alpha_K + \left[\frac{\kappa_3 S_M(t) + \kappa_4 T_A(t) + \kappa_5 D_A(t)}{1+\omega S_M(t)}\right] \\
&\quad - \Big[\xi_6 S_M(t) + \xi_7 T_A(t) + \xi_8 K_C(t) + \mu_K\Big] K_C(t), \\
S_E(t_k^+) &= S_E(t_k^-) + d, \;\; t = t_k
\end{aligned}
\tag{7.4.1}
$$

where $m_E = \mu_E - (2a_E - 1)q_E$, $m_I = \mu_I - (2a_I - 1)q_I$, $l_E = 2(1-a_E)q_E$ and $l_I = 2(1-a_I)q_I$. $S_E(t_k^-)$ and $S_E(t_k^+)$ represent the concentration of epidermal stem cell (S_E) population just before and after $t = t_k$. d represents the average doses of health epidermal stem cells administered in the system at a fixed time interval $\tau = t_{k+1} - t_k$, where $k = 1, 2, \cdots$.

Let us assume that the initial number of epidermal stem cells present before the first impulse is S_E^0. Before the first dose of stem cells, it can be written as $S_E(t_1^-) = S_E^0$. Consider the first equation of the system (7.4.1) and we get

$$
\frac{dS_E(t)}{dt} = \alpha_S S_E(t)\Big(1-\frac{S_E(t)}{S_E^{max}}\Big) - m_E S_E(t) \leq \frac{\alpha_S S_E^{max}}{4} - m_E S_E(t). \tag{7.4.2}
$$

Using the inequality as an equation to find the density of $S_E(t)$ after each administration

$$
S_E(t) = \frac{\alpha_S S_E^{max}}{4m_E} + \left(S_E(t_k^+) - \frac{\alpha_S S_E^{max}}{4m_E}\right) e^{-m_E(t-t_k)}. \tag{7.4.3}
$$

Therefore, we obtain

$$
\begin{aligned}
S_E(t_1^-) &= S_E^0, \\
S_E(t_1^+) &= S_E(t_1^-) + d \\
&= S_E^0 + d, \\
S_E(t_2^-) &= \frac{\alpha_S S_E^{max}}{4m_E} + \left(S_E(t_1^+) - \frac{\alpha_S S_E^{max}}{4m_E}\right) e^{-m_E(t_2-t_1)} \\
&= \frac{\alpha_S S_E^{max}}{4m_E} + \left(S_E^0 - \frac{\alpha_S S_E^{max}}{4m_E}\right) e^{-m_E(t_2-t_1)} + d e^{-m_E(t_2-t_1)},
\end{aligned}
$$

$$
\begin{aligned}
S_E(t_2^+) &= S_E(t_2^-) + d \\
&= \frac{\alpha_S S_E^{max}}{4m_E} + \left(S_E^0 - \frac{\alpha_S S_E^{max}}{4m_E}\right) e^{-m_E(t_2-t_1)} + d\left(1 + e^{-m_E(t_2-t_1)}\right), \\
&\vdots \\
S_E(t_n^-) &= \frac{\alpha_S S_E^{max}}{4m_E} + \left(S_E^0 - \frac{\alpha_S S_E^{max}}{4m_E}\right) e^{-nm_E\tau} + d\left(1 + e^{-m_E\tau} + e^{-2m_E\tau} + ... + e^{-(n-1)m_E\tau}\right) e^{-m_E\tau} \\
&= \frac{\alpha_S S_E^{max}}{4m_E} + \left(S_E^0 - \frac{\alpha_S S_E^{max}}{4m_E}\right) e^{-nm_E\tau} + de^{-m_E\tau}\left(\frac{1 - e^{-nm_E\tau}}{1 - e^{-m_E\tau}}\right), \\
S_E(t_n^+) &= S_E(t_n^-) + d \\
&= \frac{\alpha_S S_E^{max}}{4m_E} + \left(S_E^0 - \frac{\alpha_S S_E^{max}}{4m_E}\right) e^{-nm_E\tau} + d\left(\frac{1 - e^{-(n+1)m_E\tau}}{1 - e^{-m_E\tau}}\right).
\end{aligned}
\tag{7.4.4}
$$

As $n \to \infty$, we have

$$
\lim_{n\to\infty} S_E(t_n^-) = \frac{\alpha_S S_E^{max}}{4m_E} + \frac{de^{-m_E\tau}}{1 - e^{-m_E\tau}} \quad \text{and} \quad \lim_{n\to\infty} S_E(t_n^+) = \frac{\alpha_S S_E^{max}}{4m_E} + \frac{d}{1 - e^{-m_E\tau}}. \tag{7.4.5}
$$

Therefore, the impulsive periodic orbit epidermal stem cell (S_E) is given by

$$
\frac{\alpha_S S_E^{max}}{4m_E} + \frac{de^{-m_E\tau}}{1 - e^{-m_E\tau}} \leq \mathcal{S}_E^* \leq \frac{\alpha_S S_E^{max}}{4m_E} + \frac{d}{1 - e^{-m_E\tau}}. \tag{7.4.6}
$$

For the impulsive periodic orbit epidermal stem cell (S_E), the impulsive system (7.4.1) has a solution denoted by $\bar{E}^*$, which we refer to as the equilibrium-like periodic orbit. In the subsequent section, we perform a stability analysis of this equilibrium-like periodic orbit.

7.4.2 Stability of the Equilibrium-Like Periodic Orbit

Assessing the periodic stability of the system under impulsive effects is crucial for understanding its long-term population dynamics. In this study, Floquet's theory [36] is employed to predict the system's long-term periodic behavior by analyzing the stability of equilibrium-like periodic orbits ($\bar{E}^*$). Examining the Floquet multipliers of the monodromy matrix, it is possible to determine whether $\bar{E}^*$ is stable or not. From a biological perspective, the stability of $\bar{E}^*$ indicates that stem cell therapy effectively regulates psoriasis. Conversely, instability suggests the need to adjust the dose amount and dosing intervals of stem cell replacement therapy for achieving effective disease control.

The impulsive system (7.4.1) possesses an equilibrium-like periodic orbit, denoted by $\bar{E}^* = (\mathcal{S}_E^*, \mathcal{S}_I^*, \mathcal{S}_M^*, \mathcal{T}_A^*, \mathcal{D}_A^*, \mathcal{K}_C^*)$. To analyze the stability of the periodic solution $\bar{E}^*$, we introduce perturbation in each component of the periodic orbit.

$$
\begin{aligned}
&S_E(t) = \mathcal{S}_E^* + \epsilon_1(t), \quad S_I(t) = \mathcal{S}_I^* + \epsilon_2(t), \quad S_M(t) = \mathcal{S}_M^* + \epsilon_3(t), \\
&T_A(t) = \mathcal{T}_A^* + \epsilon_4(t), \quad D_A(t) = \mathcal{D}_A^* + \epsilon_5(t), \quad K_C(t) = \mathcal{K}_C^* + \epsilon_6(t), \\
&\text{where } \epsilon_i << 1, \quad i = 1, 2, \cdots, 6.
\end{aligned}
\tag{7.4.7}
$$

Substituting these into the system (7.4.1), we have the corresponding linear system of

equations

$$\frac{d\epsilon_1(t)}{dt} = -(\alpha_S + m_E)\epsilon_1(t), \tag{7.4.8a}$$
$$\frac{d\epsilon_2(t)}{dt} = l_E\epsilon_1(t) - m_I\epsilon_2(t), \tag{7.4.8b}$$
$$\frac{d\epsilon_3(t)}{dt} = l_I\epsilon_2(t) - \mu_M\epsilon_3(t), \tag{7.4.8c}$$
$$\frac{d\epsilon_4(t)}{dt} = -\xi_1\mathcal{T}_A^*\epsilon_3(t) - A_1\epsilon_4(t) + \kappa_2\epsilon_5(t) - \xi_3\mathcal{T}_A^*\epsilon_6(t), \tag{7.4.8d}$$
$$\frac{d\epsilon_5(t)}{dt} = -\xi_4\mathcal{D}_A^*\epsilon_3(t) - \xi_5\mathcal{D}_A^*\epsilon_4(t) - A_2\epsilon_5(t), \tag{7.4.8e}$$
$$\frac{d\epsilon_6(t)}{dt} = -A_3\epsilon_3(t) + A_4\epsilon_4(t) + A_5\epsilon_5(t) - A_6\epsilon_6(t), \tag{7.4.8f}$$

where the coefficients are

$$\begin{aligned}
A_1 &= \alpha_T\Big(2\frac{\mathcal{T}_A^*}{T_A^{max}} - 1\Big) - \kappa_1 + \xi_1\mathcal{S}_M^* + 2\xi_2\mathcal{T}_A^* + \xi_3\mathcal{K}_C^* + \mu_T,\\
A_2 &= \alpha_D\Big(2\frac{\mathcal{D}_A^*}{D_A^{max}} - 1\Big) + \xi_4\mathcal{S}_M^* + \xi_5\mathcal{T}_A^* + \mu_D,\\
A_3 &= \xi_6\mathcal{K}_C^* + \frac{\omega(\kappa_3\mathcal{S}_M^* + \kappa_4\mathcal{T}_A^* + \kappa_5\mathcal{D}_5^*) - \kappa_3}{1 + \omega\mathcal{S}_M^*},\\
A_4 &= \frac{\kappa_4}{1 + \omega\mathcal{S}_M^*} - \xi_7\mathcal{K}_C^*, \quad A_5 = \frac{\kappa_5}{1 + \omega\mathcal{S}_M^*}.\\
A_6 &= \xi_8\mathcal{K}_C^* + \xi_6\mathcal{S}_M^* + \xi_7\mathcal{T}_A^* + \xi_8\mathcal{D}_A^* + \mu_K,
\end{aligned}$$

Rewrite the system (7.4.8) in matrix notation to solve it

$$\frac{d}{dt}\begin{pmatrix}\epsilon_1(t)\\ \epsilon_2(t)\\ \epsilon_3(t)\\ \epsilon_4(t)\\ \epsilon_5(t)\\ \epsilon_6(t)\end{pmatrix} = \begin{pmatrix}-(\alpha_S + m_E) & 0 & 0 & 0 & 0 & 0\\ l_E & -m_I & 0 & 0 & 0 & 0\\ 0 & l_I & -\mu_M & 0 & 0 & 0\\ 0 & 0 & -\xi_1\mathcal{T}_A^* & -A_1 & \kappa_2 & -\xi_3\mathcal{T}_A^*\\ 0 & 0 & -\xi_4\mathcal{D}_A^* & -\xi_5\mathcal{D}_A^* & -A_2 & 0\\ 0 & 0 & -A_3 & A_4 & A_5 & -A_6\end{pmatrix}\begin{pmatrix}\epsilon_1(t)\\ \epsilon_2(t)\\ \epsilon_3(t)\\ \epsilon_4(t)\\ \epsilon_5(t)\\ \epsilon_6(t)\end{pmatrix}. \tag{7.4.9}$$

The corresponding monodromy matrix is given by considering the eigenvectors of the above fundamental matrix and taking the initial conditions of each column vectors of the identity matrix of order six (I_6). As a result, the monodromy matrix takes the form

$$\mathcal{M} = \begin{pmatrix}J_{11} & 0 & 0 & 0 & 0 & 0\\ J_{21} & J_{22} & 0 & 0 & 0 & 0\\ 0 & J_{32} & J_{33} & 0 & 0 & 0\\ 0 & 0 & J_{43} & J_{44} & J_{45} & J_{46}\\ 0 & 0 & J_{53} & J_{54} & J_{55} & 0\\ 0 & 0 & J_{63} & J_{64} & J_{65} & J_{66}\end{pmatrix}.$$

The coefficient of the monodromy matrix are given by

$$J_{11} = \exp\Big(\int_0^\tau -(\alpha_S + m_E)dt\Big), \quad J_{21} = \exp\Big(\int_0^\tau l_E dt\Big), \quad J_{22} = \exp\Big(\int_0^\tau -m_I dt\Big),$$
$$J_{32} = \exp\Big(\int_0^\tau l_I dt\Big), \quad J_{33} = \exp\Big(\int_0^\tau -\mu_M dt\Big), \quad J_{43} = \exp\Big(\int_0^\tau -\xi_1 \mathcal{T}_A^* dt\Big),$$
$$J_{44} = \exp\Big(\int_0^\tau -A_1 dt\Big), \quad J_{45} = \exp\Big(\int_0^\tau \kappa_2 dt\Big), \quad J_{46} = \exp\Big(\int_0^\tau -\xi_3 \mathcal{T}_A^* dt\Big),$$
$$J_{53} = exp\Big(\int_0^\tau -\xi_4 \mathcal{D}_A^* dt\Big), \quad J_{54} = \exp\Big(\int_0^\tau -\xi_5 \mathcal{D}_A^* dt\Big), \quad J_{55} = \exp\Big(\int_0^\tau -A_2 dt\Big),$$
$$J_{63} = \exp\Big(\int_0^\tau -A_3 dt\Big), \quad J_{64} = \exp\Big(\int_0^\tau A_4 dt\Big), \quad J_{65} = \exp\Big(\int_0^\tau A_5 dt\Big),$$
$$J_{66} = \exp\Big(\int_0^\tau -A_6 dt\Big).$$

Decompose the monodromy matrix into four different block-matrices and we have

$$\mathcal{M}_1 = \begin{pmatrix} J_{11} & 0 & 0 \\ J_{21} & J_{22} & 0 \\ 0 & J_{32} & J_{33} \end{pmatrix}, \mathcal{M}_2 = \begin{pmatrix} 0 & 0 & J_{43} \\ 0 & 0 & J_{53} \\ 0 & 0 & J_{63} \end{pmatrix}, \mathcal{M}_3 = \begin{pmatrix} J_{44} & J_{45} & J_{46} \\ J_{54} & J_{55} & 0 \\ J_{64} & J_{65} & J_{66} \end{pmatrix}, O = \begin{pmatrix} 0 & 0 & 0 \\ 0 & 0 & 0 \\ 0 & 0 & 0 \end{pmatrix}.$$

Floquet's theory states that, the periodic orbit $\bar{E}^*$ is asymptotically stable if the absolute value of all the eigenvalues of monodromy matrix $\mathcal{M}$ are less than unity. Since eigenvalues of the matrix $\mathcal{M}_1$ are $|J_{11}| < 1$, $|J_{22}| < 1$, and $|J_{33}| < 1$, therefore the stability of $\bar{E}^*$ depends on the eigenvalues of matrix $\mathcal{M}_3$. The characteristic equation corresponding to the matrix $\mathcal{M}_3$ as follows

$$x^3 + \Lambda_1 x^2 + \Lambda_2 x + \Lambda_3 = 0, \tag{7.4.10}$$

where the coefficients are given by

$$\Lambda_1 = -(J_{44} + J_{55} + J_{66}), \quad \Lambda_2 = J_{44}J_{55} - J_{45}J_{54} + J_{55}J_{66} + J_{44}J_{66} - J_{46}J_{64},$$
$$\Lambda_3 = -J_{44}J_{55}J_{66} + J_{45}J_{54}J_{66} - J_{46}(J_{54}J_{65} - J_{55}J_{64}).$$

The equilibrium-like periodic orbit $\bar{E}^* = (\mathcal{S}_E^*, \mathcal{S}_I^*, \mathcal{S}_M^*, \mathcal{T}_A^*, \mathcal{D}_A^*, \mathcal{K}_C^*)$ is asymptotically stable if all the roots of the characteristic equation (7.4.10) have absolute values less than one. According to the Jury's condition [107], this stability is ensured if the following condition holds.

$$|\Lambda_1 + \Lambda_3| < 1 + \Lambda_2, \quad |\Lambda_3| < 1, \quad \text{and} \quad |\Lambda_2 - \Lambda_1\Lambda_3| < |1 - \Lambda_3^2|. \tag{7.4.11}$$

Remark 7.4.1 *The conditions outlined above provide the mathematical criteria for assessing the stability of impulse-driven periodic orbits in the system. The associated Floquet multipliers determine whether perturbations around the periodic solution decay or grow. This reflects whether stem cell regulation sustains homeostasis or drives disease oscillations.*

Parameter	Biological description	Value	Unit	Source
α_S	Proliferation rate of epidermal stem cells	0.8	day^{-1}	[41]
$S_E^{\max}$	Carrying capacity of epidermal stem cells	1000	cells/mm^3	[41]
a_E	Self renewal percentage of epidermal stem cells	0.55	dimensionless	[98]
q_E	Division rate of epidermal stem cells	0.3	day^{-1}	[93]
μ_E	Apoptosis rate of epidermal stem cells	0.125	day^{-1}	[90]
a_I	Self renewal percentage of intermediate differentiated cells	0.35	dimensionless	[90]
q_I	Division rate of intermediate differentiated cells	0.6	day^{-1}	[108]
μ_I	Apoptosis rate of intermediate differentiated cells	0.053	day^{-1}	[93]
μ_M	Apoptosis rate of mature stem cells	0.9	day^{-1}	[100]
α_T	Proliferation rate of activated T cells	0.12	day^{-1}	[52]
$T_A^{\max}$	Carrying capacity of activated T cells	1000	cells/mm^3	[109]
ζ_1	TNF activation effect on activated T cells	0.06	cells/(pg·day)	[106]
ζ_2	IL-23 activation effect on activated T cells	0.07	cells/(pg·day)	[106]
δ_1	Inhibition rate of activated T cells by IL-10	0.003	mm^3/(pg·day)	[110]
μ_T	Apoptosis rate of activated T cells	0.02	day^{-1}	[106]
α_D	Proliferation rate of activated dendritic cells	0.12	day^{-1}	[42]
$D_A^{\max}$	Carrying capacity of activated dendritic cells	1000	cells/mm^3	[106]
δ_2	Inhibition rate of dendritic cells by TGF-β	0.004	mm^3/(pg·day)	[54]
μ_D	Apoptosis rate of activated dendritic cells	0.02	day^{-1}	[106]
α_K	Basal production rate of keratinocytes	0.6	cells/(mm^3·day)	[54]
ζ_3	Up-regulatory effect on keratinocytes by TNF	0.2	cells/(pg·day)	[106]
ζ_4	Up-regulatory effect on keratinocytes by TGF-β	0.2	cells/(pg·day)	[52]
ζ_5	Up-regulatory effect on keratinocytes by IL-17	0.2	cells/(pg·day)	assumed
ω	Inhibition scaling coefficient of MSC-mediated suppression of keratinocyte up-regulation	0.01	mm^3/cell	assumed
δ_3	Inhibition rate of keratinocytes by IL-10	0.001	mm^3/(pg·day)	[54]
μ_K	Apoptosis rate of keratinocytes	0.02	day^{-1}	[52]

Table 7.2: The list of parameters associated with the main model, along with their biological descriptions, units, and their assigned values used in the numerical simulations is provided. To ensure biological feasibility, some parameters were inferred from various literature sources, while the remaining parameters were assumed to support the model's behavior.

7.5 Numerical Simulations

To validate and substantiate the analytical findings, it is crucial to exhibit numerical experiments. In this section, we illustrate the dynamics of the proposed model through a series of numerical simulations that highlight baseline disease progression, the emergence of oscillatory behavior, the effects of biologic therapies, and the impact of impulsive stem-cell infusions. Parameter values are taken from Tables 7.2 and 7.3, with initial conditions specified in Table 7.1. The following descriptions summarize the principal observations from each figure and outline the numerical setup used for each simulation.

Parameter	Description	Value	Unit	Source
p_1	TNF secretion by T cells	0.08	pg/(cell·day)	[111]
p_2	TNF secretion by dendritic cells	0.08	pg/(cell·day)	[54]
p_3	TGF-β secretion by mature stem cells	0.03	pg/(cell·day)	assumed
p_4	TGF-β secretion by T cells	0.04	pg/(cell·day)	[54]
p_5	IL-23 secretion by dendritic cells	0.08	pg/(cell·day)	[106]
p_6	IL-17 secretion by T cells	0.06	pg/(cell·day)	[106]
p_7	IL-10 secretion by mature stem cells	0.005	pg/(cell·day)	assumed
p_8	IL-10 secretion by T cells	0.003	pg/(cell·day)	[110]
p_9	IL-10 secretion by keratinocytes	0.003	pg/(cell·day)	[54]
d_1	TNF clearance rate	0.1	day^{-1}	[111]
d_2	TGF-β clearance rate	0.2	day^{-1}	[112]
d_3	IL-23 clearance rate	0.08	day^{-1}	[106]
d_4	IL-17 clearance rate	0.07	day^{-1}	[106]
d_5	IL-10 clearance rate	0.04	day^{-1}	[110]

Table 7.3: Parameter description of the cytokine equations, along with their descriptions, units, and assigned values used in the numerical simulations, are provided.

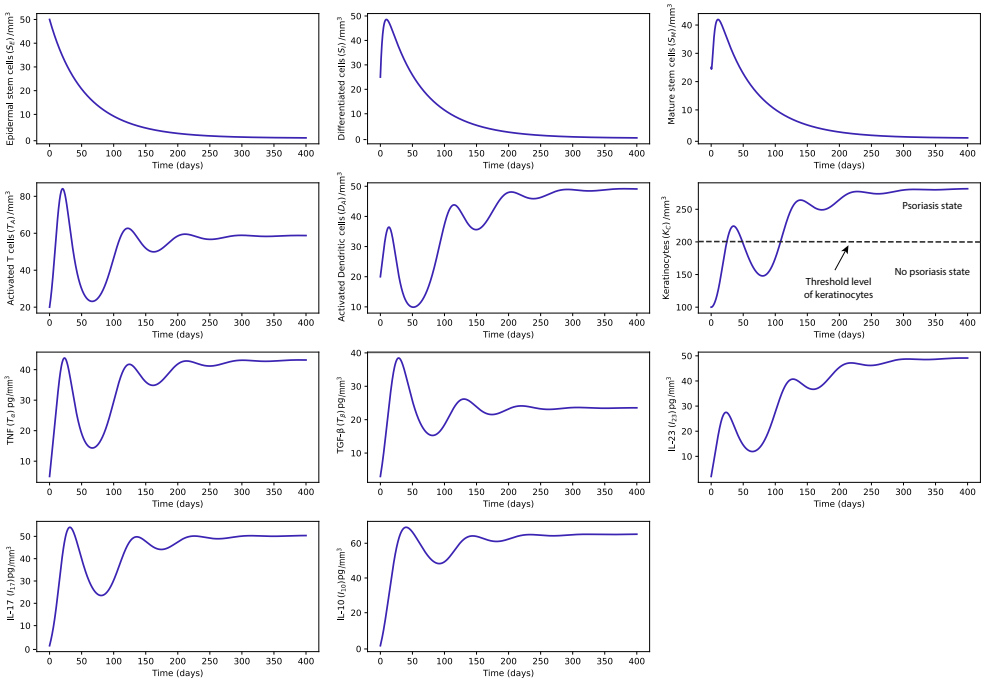

Figure 7.2: During disease progression, epidermal, intermediate, and mature stem cells decline, losing immunomodulatory control, while immune cells and cytokines remain elevated with initial oscillations before stabilizing at E^*. Parameters from Tables 7.2–7.3 and initial conditions from Table 7.1 generate the time-series of system (7.1.10), capturing psoriatic dynamics across compartments.

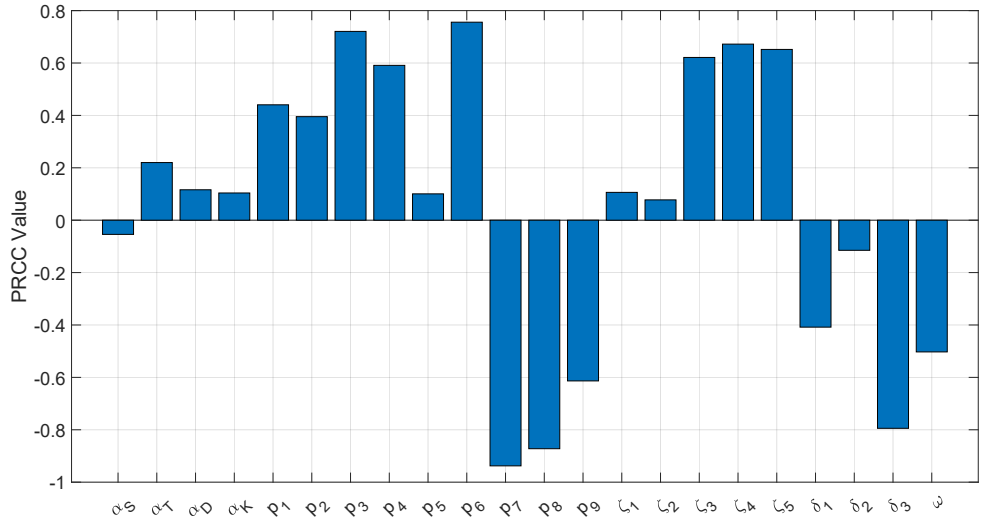

Figure 7.3: Global sensitivity analysis using Latin Hypercube Sampling and PRCCs highlights key parameters influencing keratinocyte dynamics. Parameters p_7, p_8, p_9, ζ_5, δ_3, and ω exhibit strong negative correlations with the keratinocyte population, whereas p_1, p_2, p_3, p_4, p_6, ζ_2, ζ_3, and ζ_4 show positive correlations. These results identify biologically relevant parameters that serve as potential therapeutic targets.

Epidermal, intermediate, and mature stem cell densities decline markedly during untreated disease progression, accompanied by sustained elevation of activated immune cells and pro-inflammatory cytokines; transient oscillations are observed before the system reaches to an interior equilibrium E^* (see Figure 7.2). These time series solutions capture the psoriatic dynamics across all modeled cell and cytokine populations. According to our consideration of the psoriasis state, a persistent elevation of keratinocyte density ($K_C(t) > \hat{K}_C$), together with sustained increases in key pro-inflammatory cytokines (TNF, IL-23, etc.) and activated immune cell populations $T_A(t)$ and $D_A(t)$ beyond their homeostatic levels. Throughout the numerical simulations, we mark only the keratinocyte threshold $\hat{K}_C$, with densities below it representing the non-psoriatic state and densities above it indicating the psoriatic state. It should be noted that this represents a hypothetical example of the use of the model, considered primarily for the purpose of treatment optimization.

The sensitivity analysis revealed that keratinocyte dynamics are strongly modulated by both pro-inflammatory and anti-inflammatory pathways. Specifically, parameters such as p_7 (anti-inflammatory cytokine production from mature stem cells) and ω (stem cell inhibition scaling coefficient) demonstrated the strongest negative correlations, suggesting their importance in counteracting excessive keratinocyte proliferation. In contrast, parameters like ζ_3 (TNF-driven keratinocyte up-regulation) and p_1–p_4 (cytokine production from activated immune cells) showed positive correlations, highlighting their role in amplifying inflammation. These insights not only identify sensitive nodes in the psoriatic network but also point toward effective therapeutic targets (see Figure 7.3). To further explore the impact of these sensitive parameters, Hopf bifurcation analyses with respect to p_7 and ζ_3 are presented in Figures 7.5

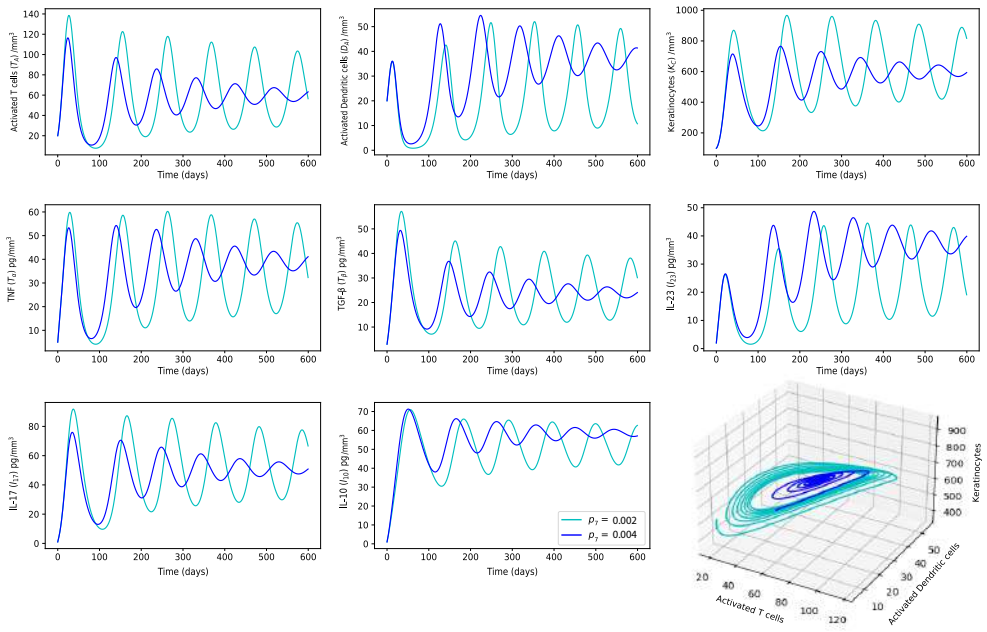

Figure 7.4: An increase in the IL-10 secretion by mature stem cells (p_7) reduces the amplitude of oscillations in activated immune cells, keratinocytes, and cytokine profiles, stabilizing the system toward equilibrium. Time-series plots for two values of p_7 (0.002 and 0.004) illustrate the reduction in oscillatory amplitude, with corresponding limit cycles in the 3D phase space (activated T cells, activated dendritic cells, keratinocytes) shown in distinct colors.

and 7.6.

The model exhibits sustained oscillations when the negative feedback mediated by the anti-inflammatory cytokine IL-10 is weakened. This feedback arises from IL-10 secretion by mature stem cells. Varying the secretion parameter p_7 reveals that decreasing p_7 below a critical threshold destabilizes the steady state and induces a limit cycle: lower values of p_7 yield larger amplitude oscillations, whereas higher values damp oscillations and restore equilibrium. For illustration, we present simulations at two representative values of p_7 (0.002 and 0.004), and the corresponding limit cycles are shown to illustrate this behavior in the 3D phase space with respect to activated T cells, dendritic cells, and keratinocytes (see Figure 7.4).

Sensitivity analysis with respect to keratinocyte population identified the strongest negative correlation for parameter p_7, representing anti-inflammatory cytokine (IL-10) production from mature stem cells. This motivated the choice of p_7 as a bifurcation parameter. A supercritical Hopf bifurcation occurs as p_7 crosses a numerically determined threshold: higher values of p_7 stabilize the equilibrium, while lower values induce sustained oscillations in activated T cells, dendritic cells, keratinocytes, and cytokines. This transition highlights the stabilizing influence of IL-10 feedback on disease dynamics, suggesting that enhanced IL-10 production corresponds to a low-inflammation state (Figure 7.5).

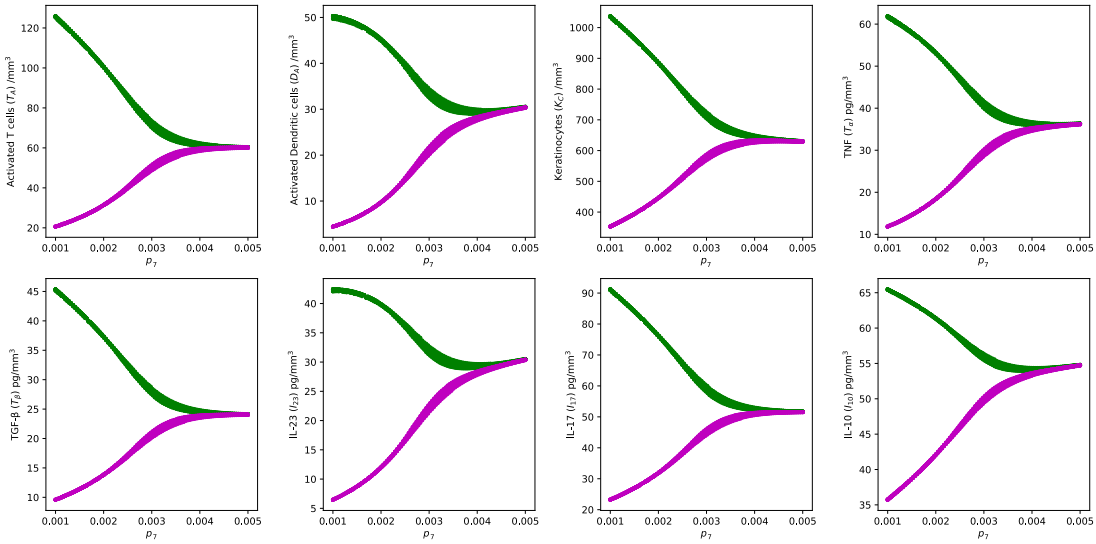

Figure 7.5: Increasing p_7 stabilizes the system, while decreasing it beyond a threshold induces sustained oscillations in immune cells and cytokines. The Hopf bifurcation for $p_7 \in [0.001, 0.005]$, representing IL-10 secretion by mature stem cells, shows the transition from stable equilibrium to periodic solution, highlighting the role of IL-10 in immune balance.

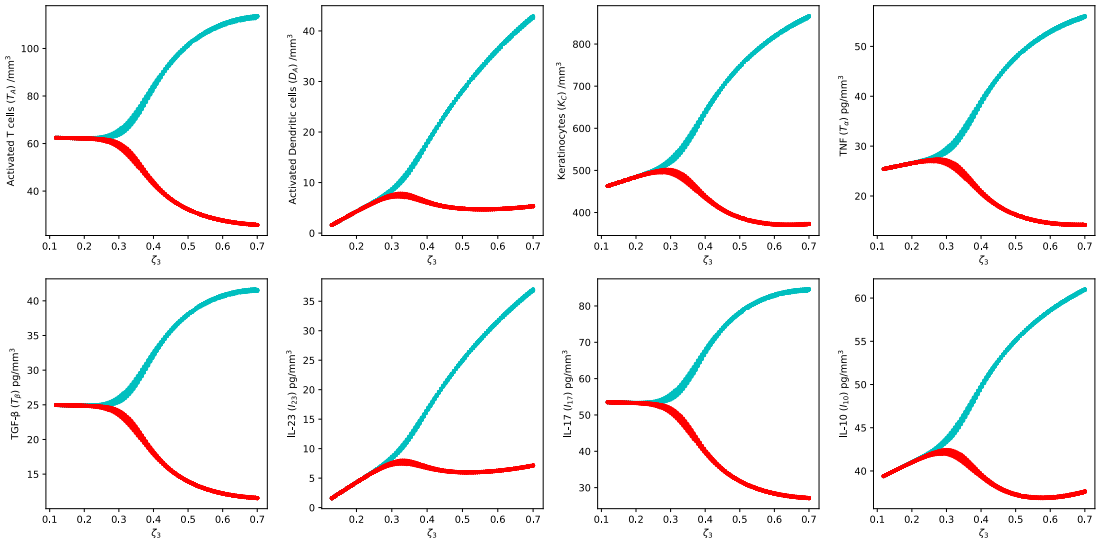

Figure 7.6: Increasing ζ_3, the TNF-driven keratinocyte up-regulation parameter, destabilizes the steady state and induces oscillations corresponding to recurrent inflammatory flares. The Hopf bifurcation for $\zeta_3 \in [0.1, 0.7]$ highlights the transition between low-inflammation equilibrium and sustained oscillatory dynamics, underscoring the role of TNF signaling in psoriasis progression.

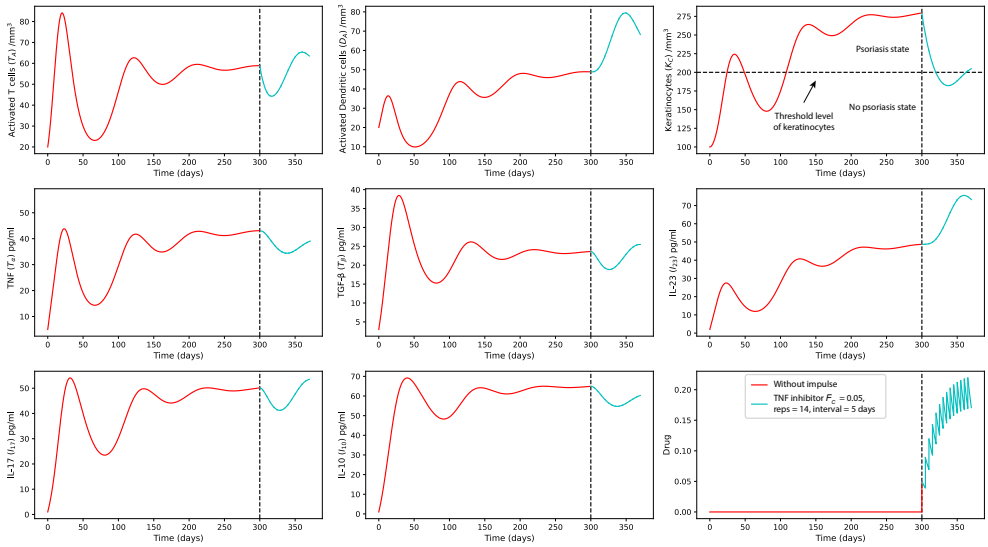

Figure 7.7: Impulsive TNF inhibition starting at day 300 with 14 doses (5 days apart) gives only partial and temporary reduction in keratinocytes and cytokines. Red curves show the untreated baseline, while cyan curves show TNF inhibition from equations (7.3.1) and (7.1.7). Keratinocytes drop below the healthy threshold $\hat{K_C}$ but rebound, and TNF rises again during drug-free intervals.

From the sensitivity, ζ_3 (TNF-driven keratinocyte up-regulation) emerged as one of the most positively correlated parameters, highlighting its role in amplifying the inflammation. Which allowed us to choose ζ_3 as a bifurcating parameter. As the value of ζ_3 increases, the system transitions from a stable equilibrium to sustained oscillations, biologically reflecting inflammatory flares in psoriasis. The bifurcation computed for $\zeta_3 \in [0.1, 0.7]$ identifies the threshold of this transition and underscores the emergence of TNF inhibition as a therapeutic mechanism (see Figure 7.6).

To investigate therapeutic intervention, we simulated the impulsive administration of TNF inhibitors beginning at day 300. The regimen consists of 14 impulses with $F_C = 0.05$, administered every 5 days, covering a total duration of 70 days. We perform this simulation considering the system (7.3.1) through the impulsive differential equations (7.3.2). The simulations reveal that while keratinocyte and TNF concentrations initially decline, the reduction is incomplete and transient. Keratinocytes temporarily fall below the normal threshold before recovering, and TNF levels resume rising during drug-free intervals (Figure 7.7). This destabilizing trend is mirrored in activated T cell dynamics, whereas activated dendritic cells and IL-23 concentrations remain largely unaffected or even increase following treatment. These results are consistent with the clinical observation that inflammation often re-emerges after treatment discontinuation, particularly in severe cases [113].

To assess the therapeutic potential of stem cell transplantation, we modeled the impulsive infusion of healthy stem cells from an external source beginning at day 340. The intervention consistently reduced activated immune cell, keratinocyte, and pro-inflammatory cytokine levels, while simultaneously increasing stem cell densities and slightly elevating anti-

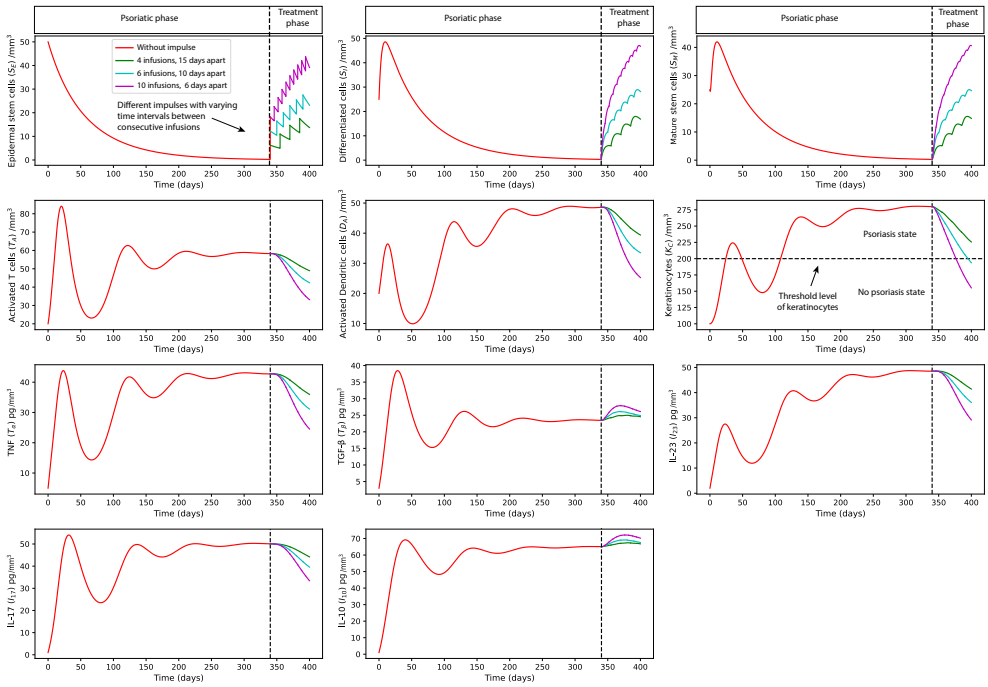

Figure 7.8: Impulsive infusion of healthy stem cells from day 340 lowers activated immune cells, keratinocytes, and pro-inflammatory cytokines, while increasing stem cells and anti-inflammatory cytokines. Simulations with 4, 6, and 10 infusions (spaced 15, 10, and 6 days apart) show that more frequent dosing causes stronger keratinocyte reduction (even below $\hat{K_C}$) and greater suppression of inflammation.

inflammatory cytokines such as IL-10 and TGF-β. Three regimens were compared: 4, 6, and 10 infusions spaced 15, 10, and 6 days apart, respectively, keeping the total simulation duration fixed at 60 days and the dose constant at 6 cells/mm^3 per infusion (Figure 7.8). The results indicate that shorter dosing intervals with more frequent infusions yield the strongest therapeutic impact. In particular, keratinocyte density dropped below the healthy threshold under the 10-impulse regimen, accompanied by marked reductions in activated T cells, dendritic cells, TNF, IL-23, and IL-17. These findings suggest that distributing the treatment into multiple smaller infusions is more effective than delivering the same total dose in fewer, widely spaced administrations.

To investigate the dose–response of stem cell infusion therapy, we simulated six impulsive infusions administered at 10-day intervals, beginning at day 340 and continuing for a total of 60 days. Three per-infusion doses were compared: 2, 4, and 6 cells/mm^3 (see Figure 7.9). All regimens produced declining trends in keratinocyte density, activated immune cells, and pro-inflammatory cytokines. However, only the highest dose of 6 cells/mm^3 successfully reduced keratinocyte density below the healthy threshold, indicating remission-like behavior in the model. Based on the considered model and from the simulation, lower doses (2 and 4 cells/mm^3) were insufficient to achieve full suppression and allowed residual inflammation to persist. These findings highlight the importance of both sufficient total stem cell input

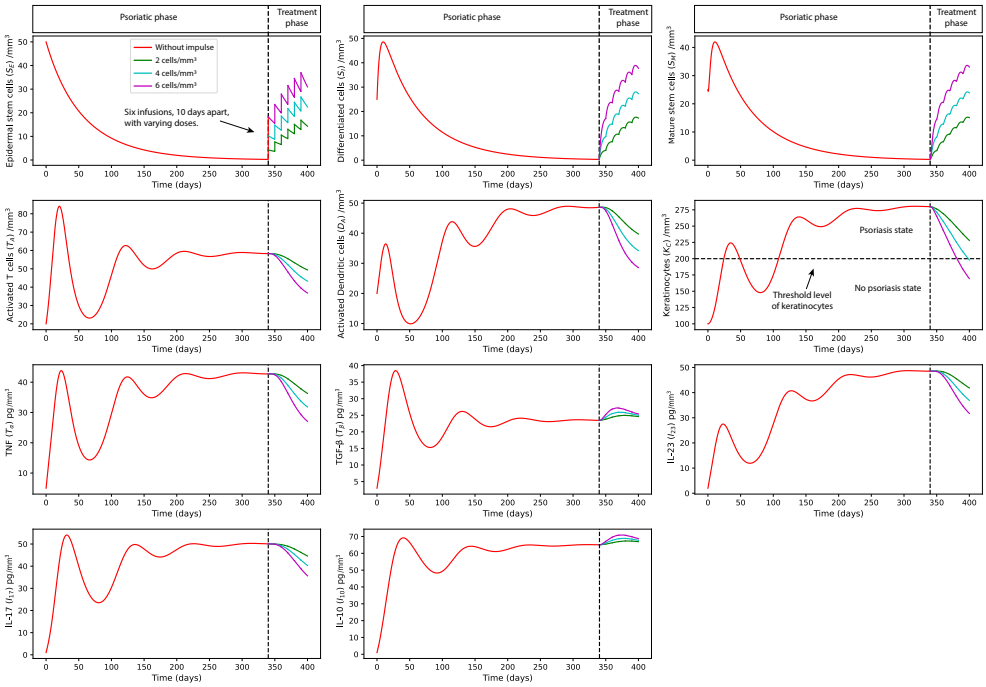

Figure 7.9: Dose–response effect of impulsive stem cell infusion on psoriasis dynamics. Simulations from day 340 with six infusions (10-day intervals over 60 days) show that only the highest dose (6 cells/mm^3) reduces keratinocytes below $\hat{K}_C$, while lower doses (2 and 4 cells/mm^3) give partial reductions. Pro-inflammatory cytokines decline in parallel, highlighting the importance of both dose and schedule for therapeutic efficacy.

and appropriate dosing schedules in achieving robust and sustained therapeutic outcomes.

Collectively, the simulations highlight three main insights. First, enhanced TNF-driven keratinocyte growth and reduced anti-inflammatory feedback (low p_7) can trigger oscillations via a Hopf bifurcation, amplifying inflammation. Second, transient TNF inhibitor therapy provides only partial and temporary relief, with disease activity rebounding after discontinuation. Third, impulsive infusion of healthy stem cells ensures sustained suppression of immune activation and keratinocyte proliferation when dose and schedule are optimized. These results emphasize the potential of stem cell therapy to modulate immune dysregulation in severe psoriasis and restore cytokine balance.

7.6 Discussion and Conclusion

In this chapter, we formulated a mathematical model of psoriasis that includes stem-cell differentiation ($S_E \to S_I \to S_M$), immune cells (activated T cells and dendritic cells), keratinocytes, and important cytokines (TNF, TGF-β, IL-23, IL-17, IL-10). To make the model simple, we used the quasi-steady-state approximation (QSSA) for cytokines and studied the interactions between cells and cytokines. With suitable initial values and parameters, we ana-

lyzed the system for disease dynamics, oscillations, and treatments. We proved that the model gives bounded solutions and studied stability of the equilibrium using the Routh–Hurwitz condition. Sensitivity and bifurcation studies showed that more TNF activity (ζ_3) or less IL-10 production from stem cells (p_7) can produce flare-like oscillations, while stronger IL-10 feedback makes the system stable. Numerical tests of treatments showed that TNF inhibitor reduces TNF and keratinocytes only for a short time, but stem-cell infusion can give long-term control if the dose and timing are proper. We also found that giving stem cells at shorter intervals and in higher doses increases IL-10 and TGF-β, helping to reach a healthy state. The mathematical results, proved using Floquet theory, showed when the periodic behavior from impulsive stem-cell therapy remains stable. Overall, these results show that psoriasis dynamics depend on the balance between pro- and anti-inflammatory signals, and suggest that stem cell therapy may provide better long-term control of severe psoriasis.

In the final chapter of this thesis, we outline future research directions and introduce a mathematical model for psoriasis. The model captures the inflammatory role of psoriatic stem cells and their differentiated progeny, which interact with major immune cell populations through cytokine-mediated signaling.

Chapter 8

Future Direction

The present thesis explores stem cell therapy as an alternative to existing biologic treatments for psoriasis through mathematical modeling. The study highlights how stem cells may help control abnormal immune responses and reduce the effects of inflammatory cytokines. The proposed models show the interactions between stem cells, immune cells, and cytokines, and how these regulate long-term immune responses. While the models provide a simplified view of the biological system, psoriasis remains a multifactorial disease with several interacting cells and signaling molecules. In particular, the influence of local inflammatory stem cells within psoriatic lesions is not fully addressed. Since these cells play a key role in disease initiation and progression, new models have been proposed for future research.

In this final *Chapter*, we discuss the directions for future research. Future studies may focus on developing more robust models by incorporating additional immune cell types, different stages of stem cell differentiation, and broader cytokine networks. With modern mathematical and computational tools, one can extend the current work to gain deeper and more refined results. For instance, incorporating psoriatic stem cell activity into the model can provide better insights into disease progression. A clear distinction between healthy stem cells and psoriatic stem cells, along with their immune modulation pathways, may help explain psoriasis dynamics more accurately.

8.0.1 Mathematical Model

For future research, we develop a mathematical model that incorporates two major immune cells, three skin cells, and four key cytokines as populations, each of which plays a significant role in maintaining the chronic inflammatory environment observed in psoriatic lesions. A detailed description of the model parameters is presented in Table 8.1. The concentrations of the model variables at any given time t are denoted as follows:

$P_{SC}(t)$: Stem Cells, $P_{TA}(t)$: Transit Amplifying Cells, $P_{TC}(t)$: Activated T Cells,
$P_{DC}(t)$: Activated Dendritic Cells, $P_{KG}(t)$: Keratinocytes, $T_{\alpha}(t)$: TNF-α,
$I_{23}(t)$: Interleukin-23 (IL-23), $I_{17}(t)$: Interleukin-17 (IL-17), $I_{10}(t)$: Interleukin-10 (IL-10).

Parameter	Definition of parameter
α_{SC}	SC self-proliferation rate constant
$P_{SC}^{\max}$	SC growth capacity
η_S	Symmetric SC division rate constant
η_A	Asymmetric SC division rate constant
α_{TA}	TA cell accumulation rate constant
α_{TC}	T cell accumulation rate constant
α_{DC}	Dendritic cell accumulation rate constant
α_{KG}	Keratinocyte self-proliferation rate constant
β_1	T cell activation rate constant via cytokine IL-23
β_2	Dendritic cell activation rate constant via cytokine IL-17
β_3	Keratinocyte growth activation rate constant through TNF-α
β_4	Keratinocyte growth activation rate constant through IL-17
γ_1	T cell deactivation rate constant through cytokine IL-10
γ_2	Keratinocyte growth deactivation rate constant through cytokine IL-10
ξ_1	Keratinocyte growth production rate constant by SC
ξ_2	Keratinocyte growth production rate constant by TA cell
δ	Infiltration rate constant by inflammatory T cell and DC interactions
λ_{SC}	Basal apoptosis rate constant of SC
λ_{TA}	Basal apoptosis rate constant of TA cells
λ_{TC}	Sum of inherent mortality and apoptosis rate constant of T cell
λ_{DC}	Sum of natural mortality and apoptosis rate constant of DC
λ_{KG}	Sum of natural mortality and degradation rate constant of KG
ζ_1	TNF-α production rate constant by T cells
ζ_2	IL-23 production rate constant by dendritic cells
ζ_3	IL-17 production rate constant by T cells
ζ_4	IL-10 production rate constant by T cells
ζ_5	IL-10 production rate constant by Keratinocytes
μ_1	TNF-α degradation rate constant
μ_2	IL-23 degradation rate constant
μ_3	IL-17 degradation rate constant
μ_4	IL-10 degradation rate constant

Table 8.1: Descriptions of the model parameters along with their corresponding biological interpretations.

The governing equations are:

$$\begin{aligned}
\frac{dP_{SC}(t)}{dt} &= \left[\alpha_{SC}\Big(1-\frac{P_{SC}(t)}{P_{SC}^{\max}}\Big)-\eta_s-\lambda_{SC}\right]P_{SC}(t),\\
\frac{dP_{TA}(t)}{dt} &= \alpha_{TA}+(\eta_A+2\eta_S)P_{SC}(t)-\lambda_{TA}P_{TA}(t),\\
\frac{dP_{TC}(t)}{dt} &= \alpha_{TC}+\big[\beta_1 I_{23}(t)-\gamma_1 I_{10}(t)\big]P_{TC}(t)-\lambda_{TC}P_{TC}(t),\\
\frac{dP_{DC}(t)}{dt} &= \alpha_{DC}+\beta_2 I_{17}(t)P_{DC}(t)-\lambda_{DC}P_{DC}(t),\\
\frac{dP_{KG}(t)}{dt} &= \alpha_{KG}+\big[\beta_3 T_\alpha(t)+\beta_4 I_{17}(t)-\gamma_2 I_{10}(t)\big]\big[\xi_1 P_{SC}(t)+\xi_2 P_{TA}(t)\big]\\
&\quad +\delta P_{TC}(t)P_{DC}(t)-\lambda_{KG}P_{KG}(t),
\end{aligned} \tag{8.0.1}$$

with cytokine dynamics:

$$\begin{aligned} \frac{dT_\alpha(t)}{dt} &= \zeta_1 P_{TC}(t) - \mu_1 T_\alpha(t), \quad \frac{dI_{23}(t)}{dt} = \zeta_2 P_{DC}(t) - \mu_2 I_{23}(t), \\ \frac{dI_{17}(t)}{dt} &= \zeta_3 P_{TC}(t) - \mu_3 I_{17}(t), \quad \frac{dI_{10}(t)}{dt} = \zeta_4 P_{TC}(t) + \zeta_5 P_{KG}(t) - \mu_4 I_{10}(t). \end{aligned} \tag{8.0.2}$$

8.1 Objectives for Future Work

The key objectives for future are:

1. To perform parameter estimation for better model validation.
2. To use individualized patient data (weekly PASI scores before and after UV treatment) for model fitting and study how stochasticity influences system behavior.
3. To introduce stochastic noise into key parameters that regulate psoriatic inflammation and analyze its role using stochastic approaches.
4. To investigate therapeutic interventions (e.g., biologics or stem cell therapy) under modified impulsive control strategies.

Bibliography

[1] Dalia Saleh and Ahmed Tawfik. Stem cell-based therapies in psoriasis: current status and future directions. *Stem Cell Reviews and Reports*, 14(5):734–741, 2018.

[2] Rosa Parisi, Deborah PM Symmons, Christopher EM Griffiths, Darren M Ashcroft, et al. Global epidemiology of psoriasis: a systematic review of incidence and prevalence. *Journal of Investigative Dermatology*, 133(2):377–385, 2013.

[3] C.E. Griffiths and J.N. Barker. Pathogenesis and clinical features of psoriasis. *Lancet*, 370:263–271, 2007.

[4] J.M. Gelfand, R.S. Stern, and T. et al. Nijsten. Epidemiology of psoriasis: results from a population-based study. *JAMA*, 293(6):731–735, 2005.

[5] F.O. Nestle, D.H. Kaplan, and J. Barker. Psoriasis. *New England Journal of Medicine*, 361:496–509, 2009.

[6] W.H. Boehncke and M.P. Schön. Psoriasis. *Lancet*, 386(9997):983–994, 2015.

[7] N.N. et al. Mehta. Association of psoriasis with cardiovascular risk factors and metabolic syndrome. *JAMA*, 303:573–581, 2010.

[8] World Health Organization. Global report on psoriasis. https://apps.who.int/iris/handle/10665/204417, 2016.

[9] M.A. Lowes, M. Suarez-Fariñas, and J.G. Krueger. Pathogenesis of psoriasis: current concepts. *Journal of Investigative Dermatology*, 134(2):231–241, 2014.

[10] Antonio Di Cesare, Paola Di Meglio, and Frank O Nestle. Il-17 and il-22 in psoriasis: a tale of two cytokines. *Expert review of clinical immunology*, 5(3):301–312, 2009.

[11] Emma Fitch, Eleanor Harper, Kamil Skorupa, and et al. Pathogenesis of psoriasis: recent insights on the role of adaptive and innate immunity. *Clinical Reviews in Allergy & Immunology*, 51(2):164–178, 2016.

[12] Cristina Albanesi, Stefania Madonna, Paolo Gisondi, and Giampiero Girolomoni. The interplay between keratinocytes and immune cells in the pathogenesis of psoriasis. *Frontiers in Immunology*, 9:1549, 2018.

[13] Frank O. Nestle and et al. Plasmacytoid predendritic cells initiate psoriasis through interferon-α production. *Journal of Experimental Medicine*, 202(1):135–143, 2005.

[14] Jeong Eun Kim and James G Krueger. T-cell subsets in psoriasis: an update. *Seminars in Immunopathology*, 36(4):365–371, 2014.

[15] A Gröne. Keratinocytes and cytokines. *Veterinary immunology and immunopathology*, 88(1-2):1–12, 2002.

[16] Steven R. Feldman. Phototherapy in the age of biologics. *Journal of the American Academy of Dermatology*, 53(3):S130–S134, 2005.

[17] Christopher E.M. Griffiths and Christina M. Clark. A systematic review of treatments for severe psoriasis. *Health Technology Assessment*, 11(1):1–125, 2007.

[18] Alice B. Gottlieb and Alan Menter. Topical therapies for psoriasis. *Dermatologic Therapy*, 22(1):40–46, 2009.

[19] Neil N. Mehta and et al. Biologic therapy in psoriasis: an update on mechanisms of action. *Journal of Clinical and Aesthetic Dermatology*, 10(7):12–22, 2017.

[20] Y. et al. Wang. Mesenchymal stem cell-based immunomodulation: properties and clinical application. *Stem Cells International*, 2014:1–9, 2014.

[21] Imran Ullah, Raghavendra Baregundi Subbarao, and Gyu Jin Rho. Human mesenchymal stem cells-current trends and future prospective. *Bioscience reports*, 35(2):e00191, 2015.

[22] Lamei Cheng, Siqi Wang, Cong Peng, Xiao Zou, Chao Yang, Hua Mei, Chuang Li, Xian Su, Na Xiao, Qi Ouyang, et al. Human umbilical cord mesenchymal stem cells for psoriasis: a phase 1/2a, single-arm study. *Signal Transduction and Targeted Therapy*, 7(1):263, 2022.

[23] Jack K Hale. Retarded functional differential equations: basic theory. In *Theory of functional differential equations*, pages 36–56. Springer, 1977.

[24] Vangipuram Lakshmikantham, Pavel S Simeonov, et al. *Theory of impulsive differential equations*, volume 6. World scientific, 1989.

[25] Clark Robinson. *Dynamical systems: stability, symbolic dynamics, and chaos*. CRC press, 1998.

[26] Jack K Hale and Hüseyin Koçak. *Dynamics and bifurcations*, volume 3. Springer Science & Business Media, 2012.

[27] M Caputo. Elasticit'a e dissipazione. 1965.

[28] Michele Caputo and Mauro Fabrizio. A new definition of fractional derivative without singular kernel. *Progress in Fractional Differentiation & Applications*, 1(2):73–85, 2015.

[29] Abdon Atangana and Dumitru Baleanu. New fractional derivatives with nonlocal and non-singular kernel: theory and application to heat transfer model. *arXiv preprint arXiv:1602.03408*, 2016.

[30] Shigui Ruan, Dongmei Xiao, and John C Beier. On the delayed ross–macdonald model for malaria transmission. *Bulletin of mathematical biology*, 70(4):1098–1114, 2008.

[31] Fahad Al Basir. A multi-delay model for pest control with awareness induced interventions—hopf bifurcation and optimal control analysis. *International Journal of Biomathematics*, 13(06):2050047, 2020.

[32] Nigar Ali and Gul Zaman. Optimal control of double delayed hiv-1 infection model of fighting a virus with another virus. *Computational Methods for Differential Equations*, 9(3):874–885, 2021.

[33] LS Pontryagin. Mathematical theory of optimal processes, english edn, 1987.

[34] V.D. Mil'man and A.D. Myshkis. On the stability of motion in the presence of impulses. *Siberian Mathematical Journal*, 1:233–237, 1960.

[35] Robert J Smith and LM Wahl. Distinct effects of protease and reverse transcriptase inhibition in an immunological model of hiv-1 infection with impulsive drug effects. *Bulletin of Mathematical Biology*, 66:1259–1283, 2004.

[36] Christopher A Klausmeier. Floquet theory: a useful tool for understanding nonequilibrium dynamics. *Theoretical Ecology*, 1:153–161, 2008.

[37] Nicholas J Savill, Richard Weller, and Jonathan A Sherratt. Mathematical modelling of nitric oxide regulation of rete peg formation in psoriasis. *Journal of theoretical biology*, 214(1):1–16, 2002.

[38] Brian L Diffey. Towards optimal regimens for the uvb phototherapy of psoriasis: A mathematical model. *Acta dermato-venereologica*, 84(4), 2004.

[39] MV Laptev and NK Nikulin. A mathematical model of paracrine regulation of the proliferative activity of epidermis with the participation of t lymphocytes. *Biophysics*, 55:305–316, 2010.

[40] Abhirup Datta and Priti Kumar Roy. T-cell proliferation on immunopathogenic mechanism of psoriasis: a control based theoretical approach. *Control and Cybernetics*, 42(2):365–386, 2013.

[41] Hong Zhang, Wenhong Hou, Laurence Henrot, Sylvianne Schnebert, Marc Dumas, Catherine Heusèle, and Jin Yang. Modelling epidermis homoeostasis and psoriasis pathogenesis. *Journal of The Royal Society Interface*, 12(103):20141071, 2015.

[42] Harshal B Oza, Rakesh Pandey, Daniel Roper, Yusur Al-Nuaimi, Sarah K Spurgeon, and Marc Goodfellow. Modelling and finite-time stability analysis of psoriasis pathogenesis. *International Journal of Control*, 90(8):1664–1677, 2017.

[43] Priti Kumar Roy, Amit Kumar Roy, Evgenii N Khailov, Fahad Al Basir, and Ellina V Grigorieva. A model of the optimal immunotherapy of psoriasis by introducing il-10 and il-22 inhibitors. *Journal of Biological Systems*, 28(03):609–639, 2020.

[44] Tae-Hoon Shin, Hyung-Sik Kim, Soon Won Choi, and Kyung-Sun Kang. Mesenchymal stem cell therapy for inflammatory skin diseases: clinical potential and mode of action. *International journal of molecular sciences*, 18(2):244, 2017.

[45] Danni Yao, Shuyan Ye, Ziyang He, Yu Huang, Jingwen Deng, Zehuai Wen, Xinsheng Chen, Hongyi Li, Qin Han, Hao Deng, et al. Adipose-derived mesenchymal stem cells (ad-mscs) in the treatment for psoriasis: results of a single-arm pilot trial. *Annals of Translational Medicine*, 9(22), 2021.

[46] Hu Chen, Jing-Wen Niu, Hong-Mei Ning, Xin Pan, Xiao-Bin Li, Yu Li, Dan-Hong Wang, Liang-Ding Hu, Hong-Xia Sheng, Man Xu, et al. Treatment of psoriasis with mesenchymal stem cells. *The American journal of medicine*, 129(3):e13–e14, 2016.

[47] Kristin Comella, Michelle Parlo, Rosemary Daly, and Kellie Dominessy. First-in-man intravenous implantation of stromal vascular fraction in psoriasis: a case study. *International Medical Case Reports Journal*, pages 59–64, 2018.

[48] Rajasekar Seetharaman, Anjum Mahmood, Prashant Kshatriya, Divyang Patel, and Anand Srivastava. Mesenchymal stem cell conditioned media ameliorate psoriasis vulgaris: a case study. *Case Reports in Dermatological Medicine*, 2019(1):8309103, 2019.

[49] Mehmet Can Ugur and Füsun Gediz. Evaluation of patients diagnosed with psoriasis and multiple myeloma after autologous stem cell transplantation. *Transfusion and Apheresis Science*, 60(4):103137, 2021.

[50] Amir Bajouri, Dorsa Dayani, Anoushe Taj Sharghi, Shahedeh Karimi, Maryam Niknejadi, Kasra Moeinabadi Bidgoli, Hoda Madani, Fatemeh Abbasi Kakroodi, Tina Blourieh, Sura Mardpour, et al. Subcutaneous injection of allogeneic adipose-derived mesenchymal stromal cells in psoriasis plaques: clinical trial phase i. *Cell Journal (Yakhteh)*, 25(6):363, 2023.

[51] Sean D Doherty, Abby Van Voorhees, Mark G Lebwohl, Neil J Korman, Melodie S Young, and Sylvia Hsu. National psoriasis foundation consensus statement on screening for latent tuberculosis infection in patients with psoriasis treated with systemic and biologic agents. *Journal of the American Academy of Dermatology*, 59(2):209–217, 2008.

[52] Amit Kumar Roy, Mark Nelson, and Priti Kumar Roy. A control-based mathematical study on psoriasis dynamics with special emphasis on il- 21 and ifn- γ interaction network. *Mathematical Methods in the Applied Sciences*, 44(17):13403–13420, 2021.

[53] Amit Kumar Roy, Fahad Al Basir, Priti Kumar Roy, and Amar Nath Chatterjee. A model analysis to measure the adherence of etanercept and fezakinumab therapy for

the treatment of psoriasis. *Nonlinear Analysis: Modelling and Control*, 27(3):513–533, 2022.

[54] Amit Kumar Roy, Fahad Al Basir, and Priti Kumar Roy. A vivid cytokines interaction model on psoriasis with the effect of impulse biologic (tnf- α inhibitor) therapy. *Journal of Theoretical Biology*, 474:63–77, 2019.

[55] Mark Aleksandrovich Krasnoselskii. The operator of translation along the trajectories of differential equations. *(No Title)*, 1968.

[56] G Birkhoff and GC Rota. Ordinary differential equation, ginn and co, 1982.

[57] Jie Lou and Robert J Smith. Modelling the effects of adherence to the hiv fusion inhibitor enfuvirtide. *Journal of theoretical biology*, 268(1):1–13, 2011.

[58] Liangyu Lin and Liming Du. The role of secreted factors in stem cells-mediated immune regulation. *Cellular immunology*, 326:24–32, 2018.

[59] Yu Han, Xuezhou Li, Yanbo Zhang, Yuping Han, Fei Chang, and Jianxun Ding. Mesenchymal stem cells for regenerative medicine. *Cells*, 8(8):886, 2019.

[60] Yuli Zhang, Jianjun Yan, Zhengjun Li, Juan Zheng, and Qing Sun. Exosomes derived from human umbilical cord mesenchymal stem cells alleviate psoriasis-like skin inflammation. *Journal of Interferon & Cytokine Research*, 42(1):8–18, 2022.

[61] Mark F Pittenger, Dennis E Discher, Bruno M Péault, Donald G Phinney, Joshua M Hare, and Arnold I Caplan. Mesenchymal stem cell perspective: cell biology to clinical progress. *NPJ Regenerative medicine*, 4(1):22, 2019.

[62] Mitio Nagumo. Über die lage der integralkurven gewöhnlicher differentialgleichungen. *Proceedings of the Physico-Mathematical Society of Japan. 3rd Series*, 24:551–559, 1942.

[63] Edmund X DeJesus and Charles Kaufman. Routh-hurwitz criterion in the examination of eigenvalues of a system of nonlinear ordinary differential equations. *Physical Review A*, 35(12):5288, 1987.

[64] Heinz Schättler and Urszula Ledzewicz. Optimal control for mathematical models of cancer therapies. *An application of geometric methods*, 2015.

[65] José García Otero, Arturo Alvarez-Arenas Alcami, and Juan Belmonte-Beitia. Dynamics and analysis of a mathematical model of neuroblastoma treated with celyvir. *Applied Mathematical Modelling*, 110:131–148, 2022.

[66] Amit Kumar Roy, Priti Kumar Roy, and Ellina Grigorieva. Mathematical insights on psoriasis regulation: Role of th1 and th2 cells. *Mathematical Biosciences & Engineering*, 15(3):717–738, 2017.

[67] Anne-Marie Tobin and Brian Kirby. Tnfα inhibitors in the treatment of psoriasis and psoriatic arthritis. *BioDrugs*, 19:47–57, 2005.

[68] Andrea Saltelli, Stefano Tarantola, and KP-S Chan. A quantitative model-independent method for global sensitivity analysis of model output. *Technometrics*, 41(1):39–56, 1999.

[69] Subhankar Kushary, Xianbing Cao, Tushar Ghosh, and Priti Kumar Roy. A mathematical insight to control the disease psoriasis using mesenchymal stem cell transplantation with a biologic inhibitor. *Scientific Reports*, 14(1):21897, 2024.

[70] Bapan Ghosh. Fractional order modeling of ecological and epidemiological systems: ambiguities and challenges. *The Journal of Analysis*, 33:341–366, 2025.

[71] Debdeep Roy and Bapan Ghosh. Dimensionally homogeneous fractional order rosenzweig–macarthur model: a new perspective of paradox of enrichment and harvesting. *Nonlinear Dynamics*, 112(20):18137–18161, 2024.

[72] IL Correa-Escudero, JF Gómez-Aguilar, MG López-López, VM Alvarado-Martínez, and D Baleanu. Correcting dimensional mismatch in fractional models with power, exponential and proportional kernel: Application to electrical systems. *Results in Physics*, 40:105867, 2022.

[73] Mark Aleksandrovich Krasnosel'skii. Two remarks on the method of successive approximations. *Uspekhi matematicheskikh nauk*, 10(1):123–127, 1955.

[74] S.M. Ulam. Problems in modern mathematics. 2004.

[75] A.A. Kilbas, H.M. Srivastava, and J.J. Trujillo. Theory and applications of fractional differential equations. 2006.

[76] Wendell H Fleming and Raymond W Rishel. *Deterministic and stochastic optimal control*, volume 1. Springer Science & Business Media, 2012.

[77] I Ameen, Dumitru Baleanu, and Hegagi Mohamed Ali. An efficient algorithm for solving the fractional optimal control of sirv epidemic model with a combination of vaccination and treatment. *Chaos, Solitons & Fractals*, 137:109892, 2020.

[78] Xia Yang, Lansun Chen, and Jufang Chen. Permanence and positive periodic solution for the single-species nonautonomous delay diffusive models. *Computers & Mathematics with Applications*, 32(4):109–116, 1996.

[79] Marek Bodnar. The nonnegativity of solutions of delay differential equations. *Applied Mathematics Letters*, 13(6):91–95, 2000.

[80] Bruce Anderson, Jeffrey Jackson, and Meera Sitharam. Descartes' rule of signs revisited. *The American Mathematical Monthly*, 105(5):447–451, 1998.

[81] Dimitri Breda, Stefano Maset, and Rossana Vermiglio. Pseudospectral approximation of eigenvalues of derivative operators with non-local boundary conditions. *Applied numerical mathematics*, 56(3-4):318–331, 2006.

[82] Jorge L Moiola and Guanrong Chen. *Hopf bifurcation analysis: a frequency domain approach*, volume 15. World Scientific, 1996.

[83] Laurenz Göllmann and Helmut Maurer. Theory and applications of optimal control problems with multiple time-delays. *Journal of Industrial & Management Optimization*, 10(2), 2014.

[84] Subhankar Kushary, Priti Kumar Roy, and Xianbing Cao. Introducing msc therapy to inhibit t h 1 and t h 17 mediated cytokines: A mathematical study to regulate psoriasis. In *International Conference on Mathematical Analysis and Application in Modeling*, pages 87–101. Springer, 2023.

[85] Teklebirhan Abraha, Fahad Al Basir, Legesse Lemecha Obsu, and Delfim FM Torres. Pest control using farming awareness: Impact of time delays and optimal use of biopesticides. *Chaos, Solitons & Fractals*, 146:110869, 2021.

[86] Priti Kumar Roy and Abhirup Datta. Negative feedback control may regulate cytokines effect during growth of keratinocytes in the chronic plaque of psoriasis: A mathematical study. *International Journal of Applied Mathematics*, 25(2):233–254, 2012.

[87] Rakesh Pandey, Yusur Al-Nuaimi, Rajiv Kumar Mishra, Sarah K Spurgeon, and Marc Goodfellow. Role of subnetworks mediated by tnf α, il-23/il-17 and il-15 in a network involved in the pathogenesis of psoriasis. *Scientific Reports*, 11(1):2204, 2021.

[88] Ellina Grigorieva and Evgenii Khailov. Chattering and its approximation in control of psoriasis treatment. *Discrete & Continuous Dynamical Systems-Series B*, 24(5), 2019.

[89] ECVMV Beretta, Vincenzo Capasso, and Nadya Morozova. Mathematical modelling of cancer stem cells populationbehavior. *Mathematical Modelling of Natural Phenomena*, 7(1):279–305, 2012.

[90] Przemysław Rafał Paździorek. Mathematical model of stem cell differentiation and tissue regeneration with stochastic noise. *Bulletin of mathematical biology*, 76:1642–1669, 2014.

[91] SM Lwin, JA Snowden, and CEM Griffiths. The promise and challenges of cell therapy for psoriasis. *British Journal of Dermatology*, 185(5):887–898, 2021.

[92] Thomas Stiehl and Anna Marciniak-Czochra. Characterization of stem cells using mathematical models of multistage cell lineages. *Mathematical and Computer Modelling*, 53(7-8):1505–1517, 2011.

[93] Anna Marciniak-Czochra, Thomas Stiehl, Anthony D Ho, Willi Jäger, and Wolfgang Wagner. Modeling of asymmetric cell division in hematopoietic stem cells—regulation of self-renewal is essential for efficient repopulation. *Stem cells and development*, 18(3):377–386, 2009.

[94] Chang-Hyun Kim, Chi-Yeon Lim, Ju-Hee Lee, Keun Cheon Kim, Ji Yeon Ahn, and Eun Ju Lee. Human embryonic stem cells-derived mesenchymal stem cells reduce the symptom of psoriasis in imiquimod-induced skin model. *Tissue engineering and regenerative medicine*, 16:93–102, 2019.

[95] Theresa Benezeder and Peter Wolf. Resolution of plaque-type psoriasis: what is left behind (and reinitiates the disease). In *Seminars in Immunopathology*, volume 41, pages 633–644. Springer, 2019.

[96] Paul Glendinning. *Stability, instability and chaos: an introduction to the theory of nonlinear differential equations*. Cambridge university press, 1994.

[97] Helmut Lütkepohl. *New introduction to multiple time series analysis*. Springer Science & Business Media, 2005.

[98] Frederik Ziebell, Ana Martin-Villalba, and Anna Marciniak-Czochra. Mathematical modelling of adult hippocampal neurogenesis: effects of altered stem cell dynamics on cell counts and bromodeoxyuridine-labelled cells. *Journal of The Royal Society Interface*, 11(94):20140144, 2014.

[99] Iqra Batool and Naim Bajcinca. Well-posedness of a coupled pde–ode model of stem cell lineage involving homeostatic regulation. *Results in Applied Mathematics*, 9:100135, 2021.

[100] Suzanne L Weekes, Brian Barker, Sarah Bober, Karina Cisneros, Justina Cline, Amanda Thompson, Lynn Hlatky, Philip Hahnfeldt, and Heiko Enderling. A multi-compartment mathematical model of cancer stem cell-driven tumor growth dynamics. *Bulletin of mathematical biology*, 76:1762–1782, 2014.

[101] Michelle A Lowes, Mayte Suarez-Farinas, and James G Krueger. Immunology of psoriasis. *Annual review of immunology*, 32(1):227–255, 2014.

[102] Yun Sang Lee, Shyam Kishor Sah, Ji Hyun Lee, Kwang-Won Seo, Kyung-Sun Kang, and Tae-Yoon Kim. Human umbilical cord blood-derived mesenchymal stem cells ameliorate psoriasis-like skin inflammation in mice. *Biochemistry and Biophysics Reports*, 9:281–288, 2017.

[103] Li-Tzu Wang, Chiao-Hsuan Ting, Men-Luh Yen, Ko-Jiunn Liu, Huey-Kang Sytwu, Kenneth K Wu, and B Linju Yen. Human mesenchymal stem cells (mscs) for treatment towards immune-and inflammation-mediated diseases: review of current clinical trials. *Journal of biomedical science*, 23:1–13, 2016.

[104] Na Song, Martijn Scholtemeijer, and Khalid Shah. Mesenchymal stem cell immunomodulation: mechanisms and therapeutic potential. *Trends in pharmacological sciences*, 41(9):653–664, 2020.

[105] Lee A Segel and Marshall Slemrod. The quasi-steady-state assumption: a case study in perturbation. *SIAM review*, 31(3):446–477, 1989.

[106] Fedor Shmarov, Graham R Smith, Sophie C Weatherhead, Nick J Reynolds, and Paolo Zuliani. Individualised computational modelling of immune mediated disease onset, flare and clearance in psoriasis. *PLOS Computational Biology*, 18(9):e1010267, 2022.

[107] A Sen and D Mukhejee. Study of stability of a discrete two-predators and one prey model. *Int. J. Contemp. Math. Sciences*, 6(13):637–646, 2011.

[108] Gerald D Weinstein, Jerry L McCullough, and Priscilla A Ross. Cell kinetic basis for pathophysiology of psoriasis. *Journal of Investigative Dermatology*, 85(6):579–583, 1985.

[109] Wing-Cheong Lo, Razvan I Arsenescu, and Avner Friedman. Mathematical model of the roles of t cells in inflammatory bowel disease. *Bulletin of mathematical biology*, 75(9):1417–1433, 2013.

[110] Yuri Kogan, Zvia Agur, and Moran Elishmereni. A mathematical model for the immunotherapeutic control of the th1/th2 imbalance in melanoma. *Discrete and Continuous Dynamical Systems-B*, 18(4):1017–1030, 2013.

[111] Xi Chen, Xiling Jiang, Rajitha Doddareddy, Brian Geist, Thomas McIntosh, William J Jusko, Honghui Zhou, and Weirong Wang. Development and translational application of a minimal physiologically based pharmacokinetic model for a monoclonal antibody against interleukin 23 (il-23) in il-23-induced psoriasis-like mice. *Journal of Pharmacology and Experimental Therapeutics*, 365(1):140–155, 2018.

[112] Paula K Denman, DL Sean McElwain, Damien G Harkin, and Zee Upton. Mathematical modelling of aerosolised skin grafts incorporating keratinocyte clonal subtypes. *Bulletin of mathematical biology*, 69:157–179, 2007.

[113] Gabrielle Brown, Eva Wang, Monica Huynh, Mackenzie Wehner, Rebecca Matro, Eleni Linos, Wilson Liao, and Anna Haemel. Tumor necrosis factor-α inhibitor-induced psoriasis: systematic review of clinical features, histopathological findings, and management experience. *Journal of the American Academy of Dermatology*, 76(2):334–341, 2017.

List of Publications

1. **Subhankar Kushary**, Priti Kumar Roy, and Xianbing Cao, "Introducing MSC Therapy to Inhibit Th_1 and Th_{17} Mediated Cytokines: A Mathematical Study to Regulate Psoriasis.", International Conference on Mathematical Analysis and Application in Modeling, pp. 87-101. (2023): Springer Nature Singapore.
   DOI: https://doi.org/10.1007/978-981-97-9194-1_7.

2. **Subhankar Kushary**, Xianbing Cao, Tushar Ghosh, and Priti Kumar Roy, "A mathematical insight to control the disease psoriasis using mesenchymal stem cell transplantation with a biologic inhibitor", Scientific Reports 14, no.1 (2024): 21897.
   DOI: https://doi.org/10.1038/s41598-024-71251-3.

3. **Subhankar Kushary**, Tushar Ghosh, Oluwole Daniel Makinde, Xue-Zhi Li, and Priti Kumar Roy, "Stem Cell Based Fractional-Order Dynamical Model of Psoriasis: A Mathematical Study", Jambura J. Biomath, vol.6, no.3, pp. 200–221, 2025,
   DOI: https://doi.org/10.37905/jjbm.v6i3.33134.

List of Communicated Works

1. Xianbing Cao, **Subhankar Kushary**, Tushar Ghosh, Fahad Al Basir, and Priti Kumar Roy, "A Mathematical Study for Psoriasis Transmission with Immune-Mediated Time Delays and Optimal Control Strategies", (*Communicated*)

2. Priti Kumar Roy, **Subhankar Kushary**, Tushar Ghosh, and Stacey R. Smith?, "Can Impulsive Stem Cell Therapy Stabilise Periodicity in a Psoriasis Model?", (*Communicated*)

3. **Subhankar Kushary**, Tushar Ghosh, and Priti kumar Roy, "Impulsive Stem Cell Transplantation to Modulate Psoriasis: Insights of Complex Cytokine Network", (*Communicated*)

– – – – – – – – –